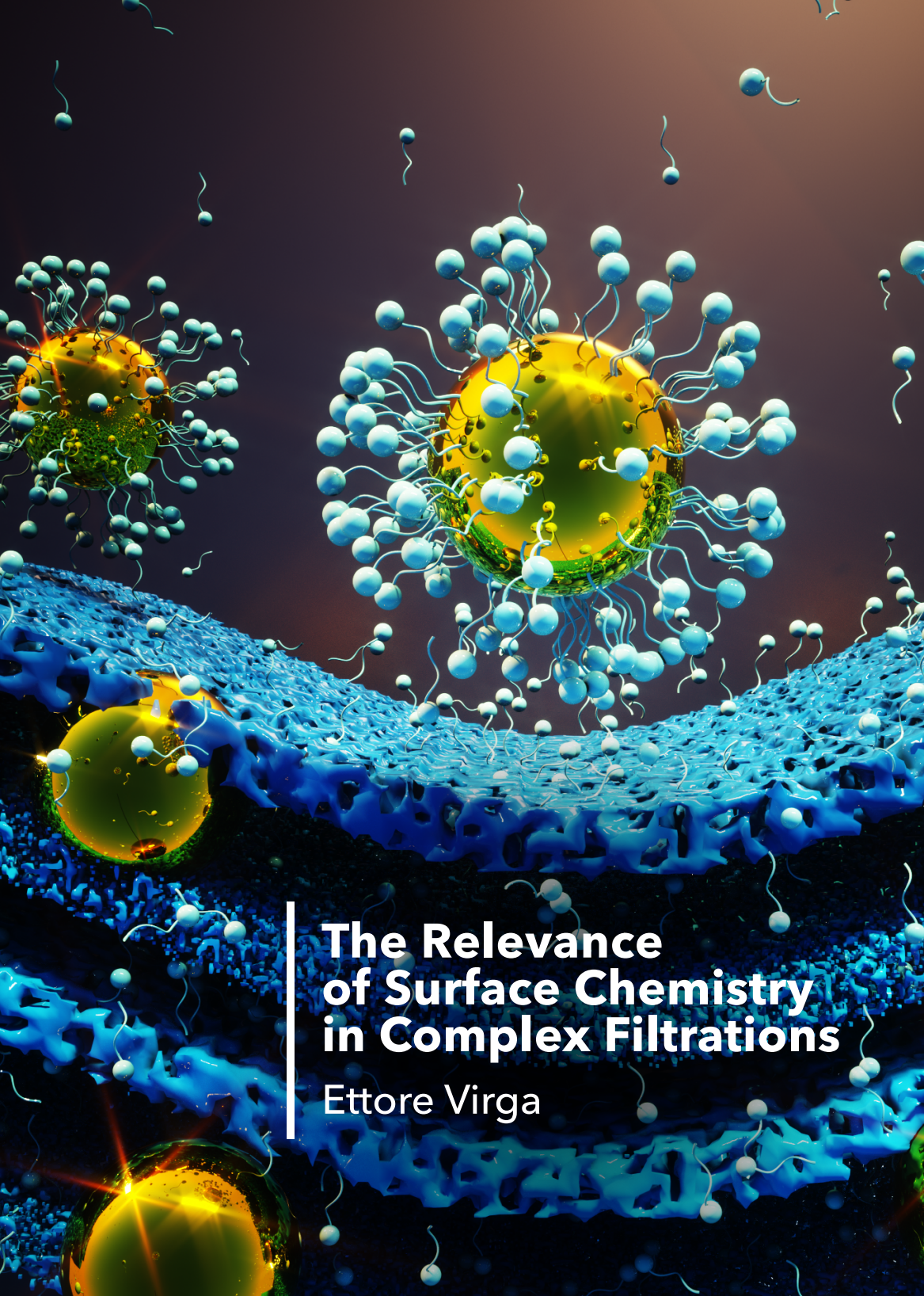

The Relevance of Surface Chemistry in Complex Filtrations

Ettore Virga

The Relevance of Surface Chemistry in Complex Filtrations

Ettore Virga

University of Twente

Graduation committee

Chairman	Prof. dr. J. L. Herek	University of Twente
Promotor	Prof. dr. ir. W. M. de Vos	University of Twente
Copromotor	Dr. ir. P. M. Biesheuvel	Wetsus
Other members	Dr. ir. D. Fernandez Rivas	University of Twente
	Dr. S. J. A. de Beer	University of Twente
	Prof. dr. ir. H.D.W. Roesink	University of Twente
	Prof. dr. ing. A. Van der Wal	Wageningen University
	Prof. dr. R.W. Field	Northumbria University

The work described in this thesis was performed in the Membrane Science and Technology cluster at the Mesa+ Institute for Nanotechnology at the University of Twente and in the cooperation framework of Wetsus, European Centre of Excellence for Sustainable Water Technology (www.wetsus.eu). Wetsus is co-funded by the Dutch Ministry of Economic Affairs and Ministry of Infrastructure and Environment, the Province of Fryslân and the Northern Netherlands Provinces. The author would like to thank the participants of the research theme Concentrates for the fruitful discussions and their financial support.

The Relevance of Surface Chemistry in Complex Filtrations
ISBN: 978-90-365-5217-2
DOI: 10.3990/1.9789036552172
URL: https://doi.org/10.3990/1.9789036552172
Cover design by Ella Maru Studio
Typeset in LaTeXusing Overleaf

The Relevance of Surface Chemistry in Complex Filtrations

DISSERTATION

to obtain
the degree of doctor at the University of Twente,
on the authority of the rector magnificus,
Prof. dr. A. Veldkamp,
on account of the decision of the graduation committee,
to be publicly defended
on Friday, September 17th, 2021 at 15:00

by

Ettore Virga
Born on September 9th, 1993
in Palermo, Italy

This dissertation has been approved by the promotor:

Prof. dr. ir. W. M. de Vos

and the copromotor:

Dr. ir. P. M. Biesheuvel

To all the Scientists who fight for a more sustainable and united world

Contents

1
Introduction°

°Adapted from publication: Elif N. Durmaz* & Sevil Sahin* & **Ettore Virga***, Sissi J. A. de Beer, Louis C. P. M. de Smet, and Wiebe M. de Vos, *Polyelectrolytes as Building Blocks for Next-Generation Membranes with Advanced Functionalities*, ACS Applied Polymer Materials **2021**. *These authors contributed equally.

1.1 The urgent need for water treatment and reuse

Access to clean water is essential for human life, not only as drinking water or water for irrigation, but also for livestock, energy and manufacturing [1]. However, in many areas around the world, clean water is scarce and does not meet its demand in terms of quality and/or quantity for such essential use. Water scarcity is widely considered as one of the largest global risks for the coming decades [2]. Especially, as water scarcity is only expected to grow due to growing global population and economy, thereby increasing demand for animal products and biofuels [3]. Moreover, climate change will affect the availability, quality and quantity of water for basic human needs, threatening the human right access to water and sanitation for potentially billions of people [2]. The described water scarcity crisis emphasizes the urgent need for effective water management. An important way to do so is to look differently at the many complex wastewater streams that result from human endeavours. Rather than seeing these waste streams as problematic due to their ecological impact, we should start to see them as valuable sources for water [1, 4, 5]. Critical in achieving this are separation methods that effectively remove pollutants to bring the water to the quality desired for re-use.

1.1.1 Produced Water as Water for Reuse

Many industrial water streams can be difficult to treat and reuse due to their high complexity and varied composition. Produced water (PW), a massive water stream produced during Oil&Gas (O&G) extraction, is a prime example of these complex streams, as it is rich in a wide range of variable contaminants that make its treatment highly challenging. The major contaminants that need to be removed to allow its reuse are oil and grease, salts, BTEX compounds (benzene, toluene, ethylbenzene, and xylenes), PAHs (polyaromatic hydrocarbons), organic acids, and chemical additives used for improved extraction [6]. Such a complex waste stream cannot be treated with a single separation technology, and already such wastewaters are often treated by combining several separation techniques. However, due to increasingly strict legislation regarding PW discharge and reuse (e.g. in agriculture), it is expected that PW will require further polishing treatments to meet stricter specifications [7].

While several factors, such as salinity, oil concentration, pH, dispersed solids etc., are dependent on the reservoir location and lifetime [8], other contaminants vary with the specific extraction process and the chemicals employed. Surfactants are one of the chemicals added during oil and gas extraction to in-

crease oil recovery from the reservoir, and to protect equipment (e.g. corrosion inhibitors). While surfactants improve the oil extraction and recovery from the reservoir, they pose a further challenge in PW treatment. Indeed, surfactants stabilize oil in water by creating oil-water (O/W) emulsions where the smallest and more stable oil droplets (<10 µm) cannot be removed by conventional separation techniques such as hydrocyclones, gas flotation, adsorption, and media filtration [9–11].

Membranes, ranging from microfiltration (MF) to reverse osmosis (RO), have been proven to be extremely effective in the removal of such small and stable droplets, providing higher quality effluents with a series of advantages in terms of environmental impact, space requirements and automated operation when compared to traditional methods [12]. Moreover, dense membranes such as NF and RO, can also remove dissolved pollutants and allow (partial) desalination. Table 1.1 shows applicability, advantages and current issues of the principal membrane technologies, i.e. MF, ultrafiltration (UF), nanofiltration (NF), and RO.

Table 1.1: Comparison of produced water membrane treatment technologies. Sources: [10, 13, 14]

Membrane Technology	Application	Strong points	Issues
Ceramic MF/UF	Applied when high chemical and physical stability is required. Reject suspended solids, colloids, bacteria, viruses.	Stable and easy to clean. Remove suspended solids. Require little pre-treatment.	Periodic cleaning required. Irreversible fouling in presence of large amounts of iron. Post-treatment needed for water reuse as several contaminants can pass through.
Polymeric MF/UF	Applicable for saline and total dissolved solids (TDS) rich water. Reject suspended solids, colloids, bacteria, viruses.	Cheaper membrane materials. Remove suspended solids, require little pre-treatment. Wide range of chemistry available.	Periodic cleaning required, lower materials stability, post-treatment needed for water reuse as several contaminants may pass through.
NF	Reject great part of divalent and multivalent ions as well as large dissolved organics, allowing the passage of monovalent ions.	Removes most major contaminants from PW including multivalent ions	Sensitive to organic and inorganic fouling, pre-treatment required, low stability at high temperatures.
RO	Reject nearly all ionic species and dissolved organics.	Desalinates and removes all major contaminants from PW	Highly sensitive to organic and inorganic fouling, extensive pre-treatment required. Low stability at high temperatures. Water remineralization maybe needed depending on the specific reuse. Require high applied pressures.

While membranes are certainly promising for PW treatment, one of the

main challenges all membranes have to face is membrane fouling [15, 16]. Foulants can adsorb at the membrane surface and inside its pores, and consequently reduce the flux of permeating water during filtration. This phenomenon causes an increase in operating costs [16] and the need for more frequent chemical cleanings [17], which can affect the membrane stability and performance over time [18]. Additionally, the presence of a fouling layer can substantially impact the separation quality of the filtration [19–21]. Membrane fouling is a complex phenomenon, that lies at the boundary between physics and chemistry. Both physical (e.g. permeation drag, shear forces) and chemical factors (e.g. hydrophobic interactions, ions binding effects), are important actors in the interaction between membranes and their foulants [22].

1.2 The complexity of PW treatment with membranes

In the filtration of solid particles, the size of the particles with respect to membrane pore opening will determine their rejection, allowing full retention when the particles are larger than the membrane pores. Meanwhile, in O/W emulsions, such as PW, the selectivity towards the oil droplets is mainly related to the interfacial forces at the oil-water interface [23]. This means that even if the droplet is bigger than the membrane pore size, it can pass through the membrane if the pressure is high enough to overcome the interfacial forces, as shown in Figure 1.1. Here the interfacial tension of the oil droplet and its interaction with the membrane surfaces become the critical parameters, as they determines how easily the droplet can deform to fit through the pore. This constitutes a problem for membranes with relatively big pore size, such as MF and UF, where the the interfacial forces can easily be overcome by the operating pressure that drives the separation.

PW treatment with membranes is quite complex, not only because oil can permeate through the membrane and therefore affect the permeate quality, but also because of the complex droplet-surfactant-membrane interactions that underlay membrane fouling. Usually fouling mechanisms can be categorised in 4 different processes, as shown in Figure 1.2 A-D, that can take place sequentially or simultaneously.

In complete pore blocking (Fig.1.2A), the pore is blocked by a large particle, blocking the water passage. In standard blocking (Fig.1.2B), small particles deposit inside the pores walls, narrowing the passage area, and therefore lowering the flux. In intermediate blocking (Fig.1.2C), a layer of particles or

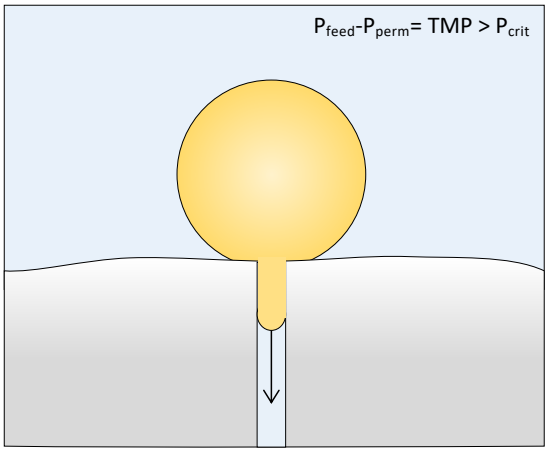

Figure 1.1: Illustration of oil droplet breaking through a membrane pore.

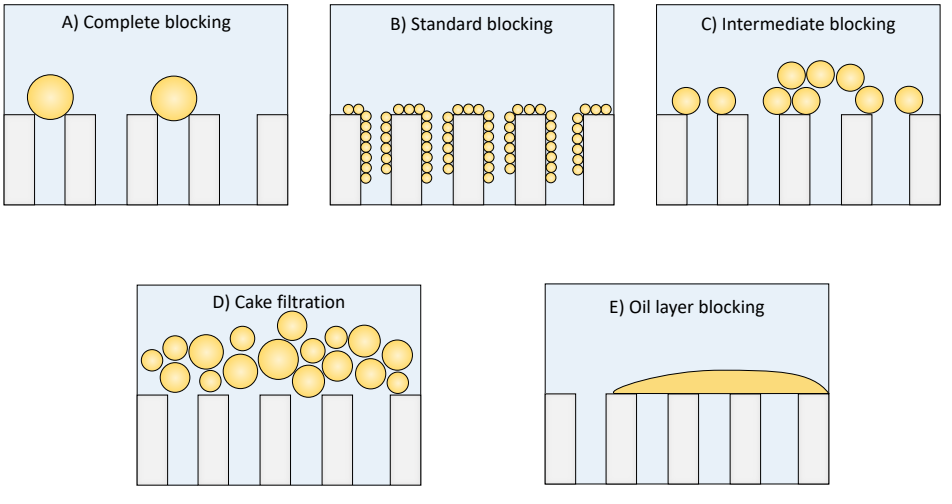

Figure 1.2: Illustration of the main fouling mechanisms in PW treatment.

droplets is builds up on the surface and narrows the pore entrances. Finally, in cake filtration (Fig.1.2D) the formation of a layer of particles or droplets on the surface of the membrane creates an additional resistance to the passage of water.

Additionally to the 4 fouling mechanisms previously described (Fig. 1.2A-D), in PW treatment another fouling mechanism, see Figure 1.2E, can take place. This mechanism, so-called oil layer blocking, occurs only when the particles or droplets can coalesce at the membrane surface and form a continuous oil layer that affects not only the permeation of water but also the membrane clean-ability [10]. Therefore, the fact that oil droplets can even interact at the membrane surface, and there deform and even coalesce, makes filtration of PW quite complex and fouling more persistent.

Next to oil droplets and solid particles, several of the organic compounds present in PW, such as dissolved organics (e.g. BTEX) and surfactants, can also easily lead to fouling [11, 24]. Physicochemical interactions between these organic molecules and the membrane surface can lead to adsorption, which is considered the main mechanism for organic membrane fouling [25].

1.3 The role of surface chemistry in membrane fouling

Surface chemistry plays a crucial role in membrane fouling [26, 27]. As fouling is a phenomenon that occurs at the feed-membrane interface, both membrane and foulants surface properties, such a surface charge, chemistry and hydrophilicity, play a critical role in the eventual formation of the fouling layer. While, fouling is certainly also dependent on the exact process conditions, including the flux, cross-flow velocity and the recovery, it is important to first focus on the interfacial aspects.

As surface interactions are critical in PW treatment with membranes, surface chemistry plays a key role, and therefore a good control over both the surface chemistry of the emulsion and the surface chemistry of the membrane can substantially alleviate fouling.

1.3.1 O/W emulsion chemistry

Surfactants are a component of PW that requires special attention in the case of PW treatment with membranes, as they are responsible for the stability of the emulsion and as they can interact in several ways with the membrane [10].

Surfactants are mostly organic molecules with a hydrophilic head group and a hydrophobic tail that allow for the molecular adsorption at the oil-water interface. The hydrophilic head group of a surfactant molecule is usually anionic, cationic, non-ionic or zwitterionic in nature [10]. Therefore, surfactants not only stabilize oil droplets in water by absorbing at their oil-water interface, but subsequently they also determine the chemistry and charge of oil droplets, allowing for a great deal of control over the chemistry of the O/W emulsions.

Surfactants not only change the chemistry and charge of the oil droplets but additionally they lower the oil-water interfacial tension (IFT), which allows oil droplets to become more deformable, making it for example easier for them to squeeze through the membrane pores. An increase in surfactant concentration leads to lower IFT, and thus an increase in oil droplet deformability and probability of permeation. For charged surfactants, the salt concentration will also play a large role in determining the IFT. At higher salinities, more surfactants can adsorb at the oil water interface, due to screening of their charged head-groups, further lowering the IFT.

But, one of the main characteristics of a surfactant, the critical micelle concentration (CMC), should also be taken into account. The CMC is the concentration of surfactants above which micelles form and all additional surfactants added to the system will form micelles. As the IFT is related to the free surfactant concentration is solution, the IFT will decrease strongly with the concentration of the surfactant below CMC, while it becomes almost constant above the CMC.

So far we have discussed how the surfactants interact with the oil-water interface, but certainly surfactants can also adsorb at the membrane-water interface. While the extent of membrane fouling by charged surfactants is mainly related to electrostatic interactions [28], for nonionic surfactants it seems to be related to the membrane hydrophilicity and pore size [29]. Researchers have therefore suggested that in order to minimize fouling it is recommended to use membranes with a more hydrophilic, smoother surface, and the same charge as the fouling agents [30, 31]. However, the role of surfactant chemistry relative to different membrane surfaces remains still unclear, especially in PW treatment, and needs further investigation. Indeed, adsorption of surfactants to the membrane surface could change the interfacial properties of the membrane and thereby its ability to retain oil and its propensity to fouling.

1.3.2 Layer-by-layer assembly to control membrane chemistry

A much investigated approach to reduce membrane fouling is to minimize the attractive interactions between the surface of the membrane and the foulants contained in the feed [32, 33]. For this reason, surface modification of existing membranes is considered an effective tool to reduce foulant-membrane interactions and indeed to design low fouling membranes [34–36].

An easy way to control the membrane surface chemistry, and at the same time its separation properties, is the so called Layer-by-Layer (LbL) technique [37–40]. Already in 1997, Decher demonstrated that the alternating exposure of a charged surface to positive and negative polyelectrolyte solutions, allows for LbL deposition of thin films of polyelectrolytes, so-called polyelectrolyte multilayers (PEMs) [41].

In particular, in the last 10 years, the knowledge on LbL assembly of PEMs on porous supports has been translated into the application [42] and production of very relevant commercial membranes with advanced separation properties and functionalities [43]. PEM coatings allow for a nanometer control over the membrane active layer thickness and chemistry [44, 45]. In particular, the availability of different polyelectrolytes as building blocks [41, 46], as well as coating conditions (e.g., salinity [47, 48] and pH [49, 50]) provide thin films with engineered functionality for multiple membrane applications, such as ion selectivity [51], fouling control [52], stability to harsh wastewaters [53], removal of contaminants from water [54, 55], and responsiveness [56].

As one of the main advantages of polyelectrolyte multilayer coating is the great deal of control over membrane surface chemistry, it in turn may also help in the fight against membrane fouling. For such dense membranes, fouling can even be more complex to investigate, since the interactions that lead to fouling take place at the nanoscale, both in and on the active separation layer [15, 30]. As PEM-based membranes show quite promising results for future innovative application, it is therefore interesting to see how these membranes deal with treatment of challenging wastewaters, such as O/W emulsions, as illustrated in Figure 1.3, especially regarding their fouling behaviour.

1.4 Scope of this Thesis

The effective treatment of complex industrial wastestreams such as PW is important to ensure clean water. Membranes can play a key role in this process, but membrane fouling remains a major problem. We propose that surface

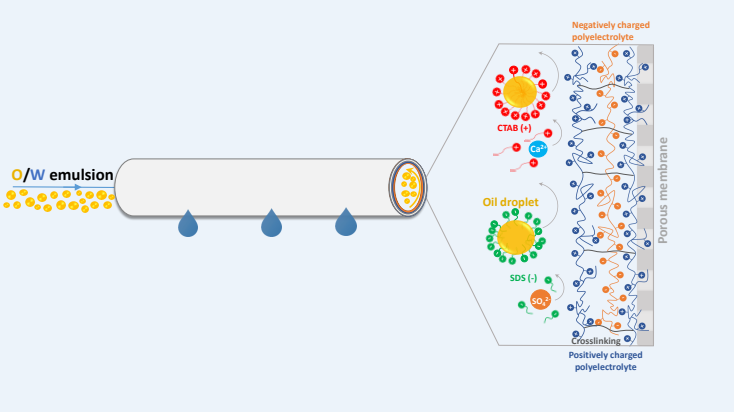

Figure 1.3: Illustration of a hollow fiber membrane coated with PEM filtering an oil-in-water emulsion.

chemistry plays a key role here, and that control over the surface chemistry of the emulsion and the membrane can substantially alleviate fouling.

As surface interactions are critical in PW treatment with **Porous Membranes**, it is important to control the surface chemistry of the major fouling agent, the oil droplets, by carefully choosing its stabilizer, i.e. the surfactant. In **Chapter 2**, we study the relation between surfactant type and the effect of the ionic strength on membrane fouling during UF of artificial produced water emulsions. In **Chapter 3**, we investigate membrane fouling and oil retention of artificial PW stabilized with a cationic, anionic, zwitterionic or nonionic surfactant, at various surfactant and salt concentrations, with a focus on the role of IFT for a Silicon Carbide (SiC) MF membrane. In **Chapter 4**, we compare the experimental data of the previous chapters with a newly designed quantitative model which allows predictions for flux decline during MF and UF based treatment of PW. By modelling pore blocking in terms of membrane contact angle and cake layer via mass balances that also involve an erosion flux, we get insights on how membrane fouling occurs as a function of membrane type, surfactants used and salinity of the feed stream.

On the other hand, polyelectrolyte multilayers allow a very nice approach to control the membrane properties of **Dense Membranes**, including the membrane surface chemistry. In **Chapter 5** we explore the stability of polyelectrolyte multilayers toward different types of surfactant, initially on model surfaces and then on hollow fiber membranes, to make stable PEM coatings to apply on hollow fiber support membranes with the aim of creating hollow

fiber NF membranes to treat PW. In **Chapter 6**, we investigate the effect of membrane surface chemistry on fouling in surface water treatment for polyelectrolyte multilayer based NF membranes. The polyelectrolyte multilayer approach allows us to prepare three membranes with the same active separation layer, but with a difference in surface chemistry, i.e. nearly uncharged crosslinked, strongly negative and zwitterionic. In **Chapter 7**, we investigate the effect of surface chemistry on fouling of NF membranes based on PEM, during the treatment of artificial produced water. To this end, oil-in-water (O/W) emulsions stabilized with four different surfactants (anionic, cationic, zwitterionic and non-ionic) were treated with PEM-based NF membranes having the same multilayer, but different top layer polymer chemistry, nearly uncharged, strongly negative, zwitterionic, and negative hydrophobic.

Interfacial Phenomena are determinant in different fields, from membrane filtration to the design of energy harvesters. As in NF, where multivalent ions can bind to the membrane and modify its surface charge to allow charge reversal, in **Chapter 8**, we consider the adsorption of divalent ions in the polyamide (PA) active layer of commercial NF membranes and describe how this adsorption process affects the membrane charge and its ions rejection. In **Chapter 9**, we present, and validate with experiments, a novel theory to predict the contact angle of water on amphoteric surfaces, as a function of pH and ionic strength. Here, our theory suggests the possibility of a novel responsive membrane design, based on aphoteric groups, for wastewater treatment. In **Chapter 10**, we present a novel mechanism to harvest energy from mechanical fluctuations by using coiled carbon nanotube yarns coated with polyelectrolyte gels.

Finally, in **Chapter 11**, with the obtained knowledge from the different chapters, the main outcomes of this thesis are revisited, and the future challenges of PEM-based membranes for PW treatment and other applications are addressed.

References

[1] M. van Vliet, M. Flörke, and Y. Wada, "Quality matters for water scarcity", Nature Geoscience **10** (2017).

[2] U. W. W. A. Programme, "The united nations world water development report 2020: water and climate change", (2020).

[3] A. Hoekstra, “Water scarcity challenges to business”, Nature Climate Change **4** (2014).

[4] M. van Vliet, E. Jones, M. Flörke, W. Franssen, N. Hanasaki, Y. Wada, and J. Yearsley, “Global water scarcity including surface water quality and expansions of clean water technologies”, Environmental Research Letters **16**, 024020 (2021).

[5] C. Tortajada, “Contributions of recycled wastewater to clean water and sanitation sustainable development goals”, (2020).

[6] S. Jiménez, M. Micó, M. Arnaldos, F. Medina, and S. Contreras, “State of the art of produced water treatment”, Chemosphere **192**, 186–208 (2018).

[7] G. L. Ghurye, D. Mishra, and L. Lucas, “Thermal desalination of produced wateran analysis of the partitioning of constituents into product streams and its implications for beneficial use outside the oamp;g industry”, Water **13** (2021).

[8] A. Fakhrul-Razi, A. Pendashteh, L. C. Abdullah, D. R. A. Biak, S. S. Madaeni, and Z. Z. Abidin, “Review of technologies for oil and gas produced water treatment”, Journal of Hazardous Materials **170**, 530 – 551 (2009).

[9] M. Cheryan and N. Rajagopalan, “Membrane processing of oily streams. wastewater treatment and waste reduction”, Journal of Membrane Science **151**, 13 – 28 (1998).

[10] J. Dickhout, J. Moreno, P. Biesheuvel, L. Boels, R. Lammertink, and W. de Vos, “Produced water treatment by membranes: A review from a colloidal perspective”, Journal of Colloid and Interface Science **487**, 523–534 (2017).

[11] E. Tummons, Q. Han, H. J. Tanudjaja, C. A. Hejase, J. W. Chew, and V. V. Tarabara, “Membrane fouling by emulsified oil: A review”, Separation and Purification Technology **248**, 116919 (2020).

[12] H. J. Tanudjaja, C. A. Hejase, V. V. Tarabara, A. G. Fane, and J. W. Chew, “Membrane-based separation for oily wastewater: A practical perspective”, Water Research **156**, 347 – 365 (2019).

[13] E. T. Igunnu and G. Z. Chen, “Produced water treatment technologies”, International Journal of Low-Carbon Technologies **9**, 157–177 (2012).

[14] S. Munirasu, M. A. Haija, and F. Banat, "Use of membrane technology for oil field and refinery produced water treatmenta review", Process Safety and Environmental Protection **100**, 183–202 (2016).

[15] A. Mohammad, Y. Teow, W. Ang, Y. Chung, D. Oatley-Radcliffe, and N. Hilal, "Nanofiltration membranes review: Recent advances and future prospects", Desalination **356**, 226 – 254 (2015), state-of-the-Art Reviews in Desalination.

[16] W. Guo, H.-H. Ngo, and J. Li, "A mini-review on membrane fouling", Bioresource Technology **122**, 27 – 34 (2012), membrane Bioreactors (MBRs): State-of-Art and Future.

[17] N. Porcelli and S. Judd, "Chemical cleaning of potable water membranes: A review", Separation and Purification Technology **71**, 137 – 143 (2010).

[18] X. Shi, G. Tal, N. P. Hankins, and V. Gitis, "Fouling and cleaning of ultrafiltration membranes: A review", Journal of Water Process Engineering **1**, 121 – 138 (2014).

[19] C. Bellona, M. Marts, and J. E. Drewes, "The effect of organic membrane fouling on the properties and rejection characteristics of nanofiltration membranes", Separation and Purification Technology **74**, 44 – 54 (2010).

[20] F. Kramer, R. Shang, L. Rietveld, and S. Heijman, "Influence of ph, multivalent counter ions, and membrane fouling on phosphate retention during ceramic nanofiltration", Separation and Purification Technology **227**, 115675 (2019).

[21] Y. ying Zhao, X. mao Wang, H. wei Yang, and Y. feng F. Xie, "Effects of organic fouling and cleaning on the retention of pharmaceutically active compounds by ceramic nanofiltration membranes", Journal of Membrane Science **563**, 734 – 742 (2018).

[22] W. Zhang and B. Dong, "Effects of physical and chemical aspects on membrane fouling and cleaning using interfacial free energy analysis in forward osmosis", Environmental Science and Pollution Research **25**, 21555–21567 (2018).

[23] A. Salama, "Coalescence of an oil droplet with a permeating one over a membrane surface: Conditions of permeation, recoil, and pinning", Langmuir **37**, 3672–3684 (2021), pMID: 33734691.

[24] S. Alzahrani and A. W. Mohammad, "Challenges and trends in membrane technology implementation for produced water treatment: A review", Journal of Water Process Engineering **4**, 107 – 133 (2014).

[25] L. Braeken, B. Van der Bruggen, and C. Vandecasteele, "Flux decline in nanofiltration due to adsorption of dissolved organic compounds: model prediction of time dependency", The Journal of Physical Chemistry B **110**, 2957–2962 (2006), pMID: 16471907.

[26] M. F. A. Goosen, S. S. Sablani, H. AlHinai, S. AlObeidani, R. AlBelushi, and D. Jackson, "Fouling of reverse osmosis and ultrafiltration membranes: A critical review", Separation Science and Technology **39**, 2261–2297 (2005).

[27] I. Ibrar, O. Naji, A. Sharif, A. Malekizadeh, A. Al Hawari, A. Alhathal Alanezi, and A. Altaee, "A review of fouling mechanisms, control strategies and real-time fouling monitoring techniques in forward osmosis", Water **11**, 695 (2019).

[28] K. Boussu, C. Kindts, C. Vandecasteele, and B. Van der Bruggen, "Surfactant fouling of nanofiltration membranes: Measurements and mechanisms", ChemPhysChem **8**, 1836–1845 (2007).

[29] G. Cornelis, K. Boussu, B. Van der Bruggen, I. Devreese, and C. Vandecasteele, "Nanofiltration of nonionic surfactants: effect of the molecular weight cutoff and contact angle on flux behavior", Industrial & Engineering Chemistry Research **44**, 7652–7658 (2005).

[30] B. Van der Bruggen, M. Mänttäri, and M. Nyström, "Drawbacks of applying nanofiltration and how to avoid them: A review", Separation and Purification Technology **63**, 251–263 (2008).

[31] D. Zhao and S. Yu, "A review of recent advance in fouling mitigation of nf/ro membranes in water treatment: pretreatment, membrane modification, and chemical cleaning", Desalination and Water Treatment **55**, 870–891 (2015).

[32] L. Upadhyaya, X. Qian, and S. R. Wickramasinghe, "Chemical modification of membrane surfaceoverview", Current Opinion in Chemical Engineering **20**, 13 – 18 (2018), nanotechnology / Separation Engineering.

[33] Y.-R. Chang, Y.-J. Lee, and D.-J. Lee, "Membrane fouling during water or wastewater treatments: Current research updated", Journal of the Taiwan Institute of Chemical Engineers **94**, 88 – 96 (2019).

[34] G.-d. Kang and Y.-m. Cao, "Development of antifouling reverse osmosis membranes for water treatment: A review", Water research **46**, 584–600 (2011).

[35] S. M. J. Zaidi, K. A. Mauritz, and M. K. Hassan, *Membrane Surface Modification and Functionalization*, 391–416 (Springer International Publishing, Cham) (2019).

[36] S. P. Nunes, "Can fouling in membranes be ever defeated?", Current Opinion in Chemical Engineering **28**, 90 – 95 (2020).

[37] J. Saqib and I. H. Aljundi, "Membrane fouling and modification using surface treatment and layer-by-layer assembly of polyelectrolytes: State-of-the-art review", Journal of Water Process Engineering **11**, 68 – 87 (2016).

[38] F. Crespilho, V. Zucolotto, and O. Oliveira, "Electrochemistry of layer-by-layer films: a review", International Journal of Electrochemical Science **1** (2006).

[39] W. Jin, A. Toutianoush, and B. Tieke, "Use of polyelectrolyte layer-by-layer assemblies as nanofiltration and reverse osmosis membranes", Langmuir **19**, 2550–2553 (2003).

[40] V. A. Izumrudov, B. K. Mussabayeva, and K. B. Murzagulova, "Polyelectrolyte multilayers: preparation and applications", Russian Chemical Reviews **87**, 192–200 (2018).

[41] G. Decher, "Fuzzy nanoassemblies: Toward layered polymeric multicomposites", Science **277**, 1232–1237 (1997).

[42] X. Li, C. Liu, and B. Van der Bruggen, "Polyelectrolytes self-assembly: versatile membrane fabrication strategy", J. Mater. Chem. A **8**, 20870–20896 (2020).

[43] N. Joseph, P. Ahmadiannamini, R. Hoogenboom, and I. F. J. Vankelecom, "Layer-by-layer preparation of polyelectrolyte multilayer membranes for separation", Polym. Chem. **5**, 1817–1831 (2014).

[44] A. R. Esker, C. Mengel, and G. Wegner, "Ultrathin films of a polyelectrolyte with layered architecture", Science **280**, 892–895 (1998).

[45] J. J. Richardson, M. Björnmalm, and F. Caruso, "Technology-driven layer-by-layer assembly of nanofilms", Science **348** (2015).

[46] L. Ouyang, R. Malaisamy, and M. L. Bruening, "Multilayer polyelectrolyte films as nanofiltration membranes for separating monovalent and divalent cations", Journal of Membrane Science **310**, 76–84 (2008).

[47] J. de Grooth, R. Oborný, J. Potreck, K. Nijmeijer, and W. M. de Vos, "The role of ionic strength and oddeven effects on the properties of polyelectrolyte multilayer nanofiltration membranes", Journal of Membrane Science **475**, 311 – 319 (2015).

[48] R. M. DuChanois, R. Epsztein, J. A. Trivedi, and M. Elimelech, "Controlling pore structure of polyelectrolyte multilayer nanofiltration membranes by tuning polyelectrolyte-salt interactions", Journal of Membrane Science **581**, 413–420 (2019).

[49] S. Ilyas, R. English, P. Aimar, J.-F. Lahitte, and W. M. de Vos, "Preparation of multifunctional hollow fiber nanofiltration membranes by dynamic assembly of weak polyelectrolyte multilayers", Colloids and Surfaces A: Physicochemical and Engineering Aspects **533**, 286 – 295 (2017).

[50] L. Y. Ng, A. W. Mohammad, and C. Y. Ng, "A review on nanofiltration membrane fabrication and modification using polyelectrolytes: Effective ways to develop membrane selective barriers and rejection capability", Advances in Colloid and Interface Science **197-198**, 85 – 107 (2013).

[51] C. Cheng, A. Yaroshchuk, and M. L. Bruening, "Fundamentals of selective ion transport through multilayer polyelectrolyte membranes", Langmuir **29**, 1885–1892 (2013), pMID: 23317152.

[52] P. Ahmadiannamini, M. L. Bruening, and V. V. Tarabara, "Sacrificial polyelectrolyte multilayer coatings as an approach to membrane fouling control: Disassembly and regeneration mechanisms", Journal of Membrane Science **491**, 149–158 (2015).

[53] M. Elshof, W. de Vos, J. de Grooth, and N. Benes, "On the long-term ph stability of polyelectrolyte multilayer nanofiltration membranes", Journal of Membrane Science **615**, 118532 (2020).

[54] P. N. Chandra and K. Usha, "Removal of atrazine herbicide from water by polyelectrolyte multilayer membranes", Materials Today: Proceedings **41**, 622–627 (2021), international Conference on Energy and Environment.

[55] Y. Wang, I. Zucker, C. Boo, and M. Elimelech, "Removal of emerging wastewater organic contaminants by polyelectrolyte multilayer nanofiltration membranes with tailored selectivity", ACS ES&T Engineering **1**, 404–414 (2021).

[56] W. Yuan, G.-M. Weng, J. Lipton, C. M. Li, P. R. Van Tassel, and A. D. Taylor, "Weak polyelectrolyte-based multilayers via layer-by-layer assembly: Approaches, properties, and applications", Advances in Colloid and Interface Science **282**, 102200 (2020).

Part I

Porous Membranes

2

Surfactant Specific Ionic Strength Effects on Membrane Fouling during Produced Water Treatment°

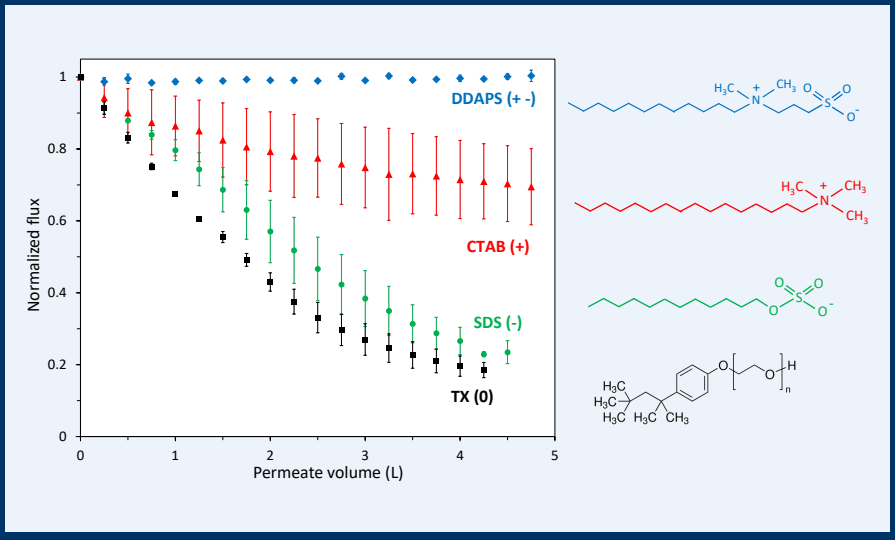

°Published as: Janneke M.Dickhout* & **Ettore Virga***, Rob G. H. Lammertink, and Wiebe M. de Vos, *Surfactant specific ionic strength effects on membrane fouling during produced water treatment*, Journal of Colloid and Interface Science **2019**, *556*, 12-23. *These authors contributed equally.

Abstract

Membrane filtration is a technique that can be successfully applied to remove oil from stable oil-in-water emulsions. This is especially interesting for the re-use of produced water (PW), a water stream stemming from the petrochemical industry, which contains dispersed oil, surface-active components and often has a high ionic strength. Due to the complexity of this emulsion, membrane fouling by produced water is more severe and less understood than membrane fouling by more simple oil-in-water emulsions. In this work, we study the relation between surfactant type and the effect of the ionic strength on membrane filtration of an artificial produced water emulsion. As surfactants, we use anionic sodium dodecyl sulphate (SDS), cationic hexadecyltrimethylammonium bromide (CTAB), nonionic Triton ™ X-100 (TX) and zwitterionic N-dodecyl-N,N-dimethyl-3-ammonio-1-propanesulfonate (DDAPS), at various ionic strengths (1, 10, 100 mM NaCl). Filtration experiments on a regenerated cellulose ultrafiltration (UF) membrane showed a pronounced effect of the ionic strength for the charged surfactants SDS and CTAB, although the nature of the effect was quite different. For anionic SDS, an increasing ionic strength leads to less droplet-droplet repulsion, allowing a denser cake layer to form, resulting in a much more pronounced flux decline. CTAB, on the other hand leads to a lower interfacial tension than observed for SDS, and thus more deformable oil droplets. At high ionic strength, increased surfactant adsorption leads to such a low oil-water surface tension that the oil droplets can permeate through the much smaller membrane pores. For the non-ionic surfactant TX, no clear effect of the ionic strength was observed, but the flux decline is very high compared to the other surfactants. For the zwitterionic surfactant DDAPS, the flux decline was found to be very low and even decreased with increasing ionic strength, suggesting that membrane fouling decreases with increasing ionic strength. Especially promising is that at lower surfactant concentration (0.1 CMC) and high ionic strength no flux decline was observed, while a high oil retention (85%) was obtained.

From our results, it becomes clear that the type of the surfactant used is crucial for a successful application of membrane filtration for PW treatment, especially at high ionic strengths. In addition, they point out that the application of zwitterionic surfactants can be highly beneficial for PW treatment with membranes.

2.1 Introduction

Membrane filtration is an increasingly important technique for the treatment of a wide spectrum of waste waters from a large variety of sources [1–6]. Membranes are, for example, used for municipal waste water treatment in combination with bioreactors [7], and in the food industry both in the processes themselves [1, 8] and as waste water treatment for factory effluents [9, 10]. Moreover, membrane filtration is used to remove harmful chemicals and particles, such as heavy metals or oil and grease, from industrial waste streams. Treating these wastewaters sufficiently brings the water to such quality that it also allows its re-use, thereby decreasing the fresh water demand. This large variety of applications and feed streams means that membrane filtration has to be tailored to each specific process. The membrane material, process parameters and pretreatment, all influence the performance of the membrane system and therefore have to be carefully chosen. This is especially important, as virtually all membrane processes suffer from fouling, the building up of retained material on the feed side of the membrane [6]. In membrane fouling, the foulant adhesion/deposition is a thermodynamic mechanism based on energy balance principles [11] that can cause filtration resistances driven by chemical potential differences [12, 13]. Fouling blocks the pores, builds into a cake layer and thereby reduces the membrane flux and increases operational costs. In some cases, however, this cake layer on top of the membrane forms a new active layer and improves the filtration characteristics of the membrane [14].

A current focus area of membrane science is the use of membranes to treat the challenging water stream of so-called produced water (PW), a very large water stream that stems from the petrochemical industry and has the potential to act as a substantial source of water for re-use. Quite some research has now shown that PW can be effectively treated using membrane filtration, but that membrane fouling remains a critical problem [6, 15]. PW contains dissolved and dispersed hydrocarbons, salts, heavy metals and solid particles, as well as production chemicals. Before this water can be re-used or disposed, those components have to be removed. For example, to meet the OSPAR regulations dispersed oil in PW discharges should not exceed a concentration of 30 mg/L [16]. The dispersed oil can be removed largely by conventional techniques such as gas flotation, adsorption, evaporation and hydrocyclones, but the smallest oil droplets with a size <10 μm are less efficiently removed by these techniques [17]. Membrane filtration can remove those droplets, but, as mentioned, the fouling of the membrane by these oil droplets is often severe.

Moreover, the membrane fouling by produced water is typically more severe than membrane fouling by many other oil-in-water emulsions such as food emulsions or other industrial waste waters containing oils [18]. One parameter that widely changes from source to source is salinity [6], highly affected by the geochemistry of the reservoir [19]. Therefore, ionic strength is an important parameter to investigate. A high salinity can have a detrimental effect of the stability of the stabilized oil droplets, which in turn can lead to more detrimental fouling [20]. It is good to mention that produced water is a stream with varying properties. The composition of produced water changes from well to well but also over the lifetime of an oil reservoir [21]. Therefore, there is no universally applicable solution or method for all sources of produced water.

In order to control membrane fouling by produced water, it is important to understand the interaction of the oil droplets with the membrane surface. Here the presence of surfactants is believed to play a key role. The surfactant adsorbs to the oil-water interface of the droplets, but also often adsorbs to the membrane surface. The surfactant will thus determine much of the interactions between droplet and membrane surface, and naturally the droplet-droplet interactions. Since PW contains such a variety in components, it is important to understand what the influence of each component is on the membrane fouling, but also how one component might affect the fouling propensity of another component. For example, the effective stabilization of an oil droplet by a charged surfactant will be strongly influenced by the ionic strength, while for an uncharged surfactant the ionic strength might play only a small role.

In literature, many examples of oil-water separation with membranes can be found, as well as studies on the kinetics of fouling. Here, we will discuss a few examples in which the influence of emulsion components or process parameters was studied systematically. Li *et al.* developed a cellulose ultrafiltration (UF) hollow fiber membrane for oil-water separation [22]. They chose cellulose for its high resistance against swelling from organic compounds and its hydrophilic nature. The retention was 99% for an emulsion of machine oil in water while showing only minimal fouling, showing the potential for this membrane material. Lipp *et al.* also tested a cellulose membrane for oil-in-water emulsion separation. Their emulsion contained a mixture of oil and surface-active components [23]. They found evidence of coalescence in the cake layer, and proposed a loss of surfactant to the permeate due to this coalescence, thereby changing the properties of the cake layer, making it more dense. Out of a range of membranes, however, the regenerated cellulose membrane showed excellent oil rejection and flux recovery after cleaning. Lu *et al.* studied the

filtration of oil-in-water emulsions with three different surfactants on a ceramic membrane [24]. Interestingly enough, they found that an emulsion with surfactant oppositely charged to the membrane surface charge showed less irreversible fouling than a surfactant with similar charge. They attributed this effect to the adsorption of surfactant molecules to the surface and the inside of the membrane pores, hindering the entrance of oil into the membrane. The exact mechanism however was not understood well and requires further investigation. Singh *et al.* studied the influence of the ionic strength on membrane fouling during aqueous filtration of silica particles [25]. They found that the fouling potential of the feed water was linearly related to the double layer thickness. In their experiments and model, a 10-fold increase in ionic strength had the same effect as a 2-fold increase in colloid concentration of the feed.

What becomes apparent from the discussed studies, is that the effect of many parameters, such as type of surfactant, type of membrane surface, ionic strength etc., have received prior interest. However, all studies look at just a single parameter at the same time, while it is clear that a parameter such as surfactant type, could strongly influence the effect for the ionic strength. In this work, we chose four different model surfactants with different properties. We used an anionic, cationic, nonionic and zwitterionic surfactant and compare their behavior when used in membrane filtration experiments. In addition, we varied the salt concentration of the feed emulsion to study the effect of ionic strength on membrane fouling, and how that is affected by the type of surfactant. The emulsions used in this study are synthetic model emulsions with carefully chosen components, so we are able to control the properties of the emulsions.

2.1.1 Theory

Here we provide the theoretical background that is the basis for all interpretation of the experimental data. After prolonged filtration of oily waste water, we expect that the membrane fouling will be dominated by a cake layer formed on the membrane surface [26, 27]. Therefore we study the effect of increasing ionic strength on membrane fouling by oil-in-water emulsions stabilized by four different surfactants. Since the properties, and especially the charge of the head group of those surfactants are different, we expect to see an influence on the formed cake layer and thus the observed flux decline. Here we link the expected properties of the cake layer, described by the Kozeny-Carman term, to the DLVO theory. We also discuss the critical pressure required to push an oil droplet through a membrane pore.

The resistance of a cake layer on the membrane can be described by the Kozeny-Carman term

$$R_c = \frac{150 l_c (1-\varepsilon_c)^2}{D_v^2 \varepsilon_c^3}, \tag{2.1}$$

where l_c is the thickness of the cake layer, ε_c the porosity of the cake layer and D_v the effective diameter of the oil droplets [28]. This resistance is heavily dependent on the porosity ε_c of the cake layer, and therefore of the interaction between the droplets in the cake layer. As shown in previous work [29], the pores in a cake layer of monodisperse particles are not effective in rejecting oil droplets based on pore size, as the pores in the layer are larger than the membrane pores.

At fixed oil concentrations, droplet sizes, crossflow velocities and initial fluxes, the properties of the cake layer will to a large extend be governed by droplet-droplet interactions. The interaction between two colloidal particles, in our case oil droplets, can be described by the DLVO theory. This theory adds the attractive interaction energy V_A and the repulsive interaction energy V_R in the total potential V_T

$$V_T = V_A + V_R. \tag{2.2}$$

It is possible to extend the DLVO by including a hydration energy term [30]. However, since this goes beyond the scope of this manuscript, we refer to the classical DLVO theory. The attractive van der Waals potential, caused by the alignment of dipoles in adjacent molecules, can be found by calculating the interaction of one atom in a droplet with all the atoms in a second droplet, leading to a long-range interaction. When the particle separation distance h is small compared to the droplet radius a ($h << 2a$), the potential V_A, expressed in J, is given by

$$V_A = -\frac{Aa}{12h} \tag{2.3}$$

where A is the Hamaker constant, which depends on the polarizability of the droplet material. Thus, the attractive potential between two oil droplets is inversely dependent of the separation distance between the droplets. While the used surfactant will have some influence on the attractive van der Waals potential, it will be dominated by the droplets bulk material. The surfactant type and the ionic strength will therefore have limited influence on the attractive interaction between droplets.

The electrostatic repulsion is an important stabilizing factor in oil-in-water emulsions. When the oil droplets carry a surface charge, the repulsion will prevent collision between the droplets. For short distances h, the electrostatic repulsion V_R, also expressed in J, can be written as

$$V_R = 2\pi\epsilon_0\epsilon_r a\psi_\delta^2 \exp(-\kappa h) \tag{2.4}$$

where ψ_δ is the surface potential of the oil droplet. This electrostatic repulsion is dependent on the thickness of the electrostatic double layer (EDL) or the Debye length ($1/\kappa$, expressed in m), which is given by

$$\kappa^{-1} = \sqrt{\frac{\epsilon_r\epsilon_0 k_B T}{2N_A e^2 I}} \tag{2.5}$$

where ϵ_0 is the permittivity of vacuum, ϵ_r the dielectric constant of the medium, k_B is the Boltzmann constant, T is the absolute temperature, N_A Avogadro's number, e the elementary charge and I the ionic strength of the emulsion.

The total interaction energy V_T, as stated in Eq. (2.2), results in a potential curve with a maximum which has to be overcome for droplets to come in close contact. As can be seen from Eqs. (2.4)-(2.5), the repulsive force is dependent on the ionic strength of the emulsion. At increasing ionic strength, the repulsive forces between charged droplets decreases, allowing the droplets to come into much closer contact, or even to coalesce. At higher ionic strength more surfactant will adsorb to the droplet surfaces, thereby increasing the surface charge density. The screening effect of salt that lowers the electrostatic repulsion between droplets is, however, stronger than the increased repulsion due to the additional surfactant on the surface [31].

Droplets stabilized by nonionic surfactants however do not carry a surface charge. They stabilize the oil droplets by steric hindrance of a large hydrophilic head group [32]. As this interaction is not charge based, the ionic strength will have little effect on the strength of steric stabilization.

Zwitterionic surfactants stabilize by hydration of the head group. In contrast to charged surfactants, the water molecules around the head group are ordered in the same manner as in the bulk phase of water instead of reordering the water around the single charge of an ionic surfactant [33]. In this unperturbed state, the water molecules around the zwitterionic group are in a H-bonded structure, which takes a considerable amount of energy to disturb.

When a cake layer is formed on the membrane surface, we expect that the repulsive forces between oil droplets with charged surfactants contribute to

the porosity of the cake layer. Because the surface charge of the droplets and the resulting electrostatic repulsion, we expect a more open cake layer and less flux decline. However, at increasing ionic strength, the electrostatic repulsion decreases and the cake layer is expected to become more dense because of electrostatic screening of the surface charge. For nonionic and zwitterionic surfactants, which suffer less from electrostatic screening, we expect that increasing the ionic strength has a less pronounced effect on the flux decline. For these surfactants especially the steric repulsion and head group hydration will dominate. It is important to mention that for zwitterionic surfactants, the hydration of the headgroup typically does depend on the ionic strength. At higher ionic strength, the headgroup will be more hydrated and a larger repulsion could follow. So for zwitterionic surfactants, a higher ionic strength might even lead to a more open cake layer and thus a lower flux decline [34].

Apart from the membrane flux, a key membrane performance parameter in PW treatment is the retention of oil droplets. While in this study the membrane pores are much smaller than the oil droplets, oil droplets can deform to flow through the pore if the applied pressure is large enough. The critical pressure difference P_{crit} (in bar) at which oil transport through the membrane starts to occur can be estimated by:

$$P_{crit} = -\frac{\gamma O_p \cos\theta}{A_p} \tag{2.6}$$

where γ is the interfacial tension between the oil and the aqueous phase, O_p the circumference of the pore, θ the advancing contact angle of the droplet on the surface and A_p the surface area of the membrane pore. As can be seen, a key parameter here is the oil-water interfacial tension. For charged surfactants the interfacial tension is a function of the ionic strength. The higher the ionic strength, the lower the repulsion between headgroups, allowing more surfactant molecules to adsorb at the oil-water interface. Ideally, the contact angle used to calculate the critical pressure should be measured on a smooth polymer film, to exclude any effects of roughness. Here we used the contact angle on a rougher surface (the membrane) as in the previous works no significant difference in contact angle was observed between the cellulose membrane and a spincoated cellulose film [35]. The adsorbed amount of surfactant at the oil droplet surface Γ_s (expressed in mol/m^2), at constant temperature T and pressure p, can be derived from the interfacial tension γ via

$$\Gamma_s = -\frac{C}{RT}\left(\frac{\delta\gamma}{\delta C}\right)_{T,p} \tag{2.7}$$

where R is the ideal gas constant, and C is the surfactant concentration. For charged surfactants, a higher ionic strength leads to a lower interfacial tension, and as a consequence it lowers the critical pressure at which the oil droplets can be pushed through the membrane. For non-ionic and zwitterionic surfactants this effect is not expected.

2.2 Materials and methods

2.2.1 Materials

For preparation of the emulsions, we used DI water, sodium dodecyl sulfate (SDS, Sigma Aldrich, ACS reagent, 99.0%), hexadecyltrimethylammonium bromide (CTAB, Sigma Aldrich, for molecular biology, 99%), Triton ™ X-100 (TX, Sigma Aldrich, laboratory grade), N-dodecyl-N,N-dimethyl-3-ammonio-1-propanesulfonate (DDAPS, 97.0% (dried material, CHN)), n-hexadecane (Merck Schuchardt 99.0%) as the oil, Coumarin 6/ Neeliglow Yellow 196 (Neelikon) as fluorescent dye, and sodium chloride (NaCl, VWR, 100%). The membrane used was a regenerated cellulose UF membrane with a pore size of 500kDa (Microdyn Nadir UC500T). All chemicals were used without further purification steps.

2.2.2 Emulsion preparation and characterization

To detect the amount of oil that permeates through the membrane, the hexadecane was colored with a dye. As fluorescent dyes bleach over time, the colored oil was prepared freshly before each experiment. Approximately 5 mg of the dye powder was put in a test tube together with 8 mL of n-hexadecane and put in an ultrasonic bath for 10 minutes. Afterwards, the oil was filtered over a Millipore 0.45 μm filter to remove any solid particles left.

To ensure all emulsions have the same characteristics, a stock emulsion was prepared, which was then further diluted to obtain the desired salt and surfactant concentration. The surfactant concentrations were all chosen to be at or below the CMC, but high enough to ensure a stable emulsion and a reproducible droplet size distribution. The stock emulsions were prepared by dissolving a surfactant (463 mg/L SDS; 346 mg/L CTAB; 298 mg/L TX; 100.6, 201.2 or 1006 mg/L DDAPS) in 1 L of DI water in a Duran® bottle (Duran 21801545) by mixing with a dispersing mixer (IKA® T25 digital Ultra-Turrax with S25N 18G element) for 2 minutes at 14,000 rpm. Then, 2 g of colored oil was injected near the mixer head and mixed for 10 minutes at

14,000 rpm. The stock emulsion was diluted to contain 100 mg/L hexadecane and the desired surfactant and NaCl concentration to make up 20L of feed emulsion. The particle size distribution was determined with a DIPA 2000 - Particle Analyzer (Prolyse). The mean droplet size in the diluted emulsions was 4 μm, with a rather broad distribution in droplet sizes ($\pm$3) and was constant for all conditions. In this work no zeta potentials were obtained of the emulsions. For similar surfactant concentrations and ionic strength, oil-in-water emulsions are known to be strongly negatively charged for SDS (zeta potentials of -110 to -120 mV [36, 37]), strongly positively charged for CTAB ($\sim$+85 mV [37, 38]), slightly negative for TX (from -20 to -5 mV [39]) and negatively charged for DDAPS (from -35 to -45 mV [40]). Regenerated cellulose membranes are known to be negatively charged (zeta potentials of -8 to -25 mV [41–43]).

2.2.3 Membrane filtration

The membrane filtration experiments were performed using an OSMO-inspector crossflow membrane filtration system built by Con-Vergence. A fresh membrane sheet was used for each experiment. The membrane was mounted in a flat sheet crossflow membrane cell with an effective surface of 240 cm^2, using a feed spacer with a thickness of 700 μm, a filament angle of 90° and a maze size of 2.5 $\times$ 2.5 mm. The volume and density of the feed and permeate streams were measured by Bronkhorst M15 mass flow meters. The 20 L glass feed bottle was constantly stirred to prevent creaming of the feed. Both concentrate and permeate were recycled to the feed bottle to ensure a consistent feed quality. Before mounting the membrane, it was soaked in DI water overnight to remove production chemicals and glycerine from the membrane. Then, the clean water flux was measured. A membrane filtration experiment consisted of filtering for 3 hours at a TMP of 1 bar and a flow rate of 48 kg/h, which corresponds to a crossflow velocity of 0.2 m/s. This crossflow velocity corresponds to laminar Reynolds (Re$\sim$220) making it possible to neglect droplets break up due to shear stress in our system [44]. The permeate flux was constantly monitored. To clean the membrane, the cell was flushed with DI water for 1h without applied transmembrane pressure, then a backflush with DI water of 3 minutes at 0.2 bar, and then another flush. After the cleaning, the clean water flux was measured again to determine the flux recovery. Each experiment was repeated at least two times and an average and standard deviation were taken on the basis of these data.

2.2.4 Permeate analysis

The oil retention for SDS based emulsions was measured by liquid-liquid extraction of the permeate and subsequent HPLC analysis as described in previous work [29]. For the other surfactants, the fluorescent dye method was used, because the presence of surfactants often caused excessive foaming, hindering the extraction. We repeated the fluorescence method for SDS based emulsions and found good agreement with the results obtain by extraction.
The oil retention R (%) is defined as

$$R = \left(1 - \frac{F_p}{F_f}\right) \tag{2.8}$$

where F_p and F_f are the oil concentrations in the permeate and the feed respectively. Therefore, we took a concentrate and permeate sample at the same time and used those for analysis. The concentrate with fluorescent oil was used to make a calibration line. The permeate was subsequently measured on the same sample plate to determine the oil concentration in the permeate using this calibration line. The fluorescence of the samples was measured in a Perkin Elmer Victor3 Multilabel Plate Reader, using a protocol for Fluorescein (465nm/510nm, 1.0s). The dilutions for the calibration line and permeate were injected in threefold in a 96-hole well plate. The volume of liquid in one hole was 200 μL. As shown in previous studies [29], the rejection of oil does not change significantly over the course of the experiment, therefore we took the permeate sample only once, after 2 hours of filtration.

2.2.5 Contact angle and interfacial tension measurements

Both types of measurements were performed on a contact angle and contour analysis instrument (Dataphysics OCA 35). The contact angle measurements were performed in captive bubble mode, where a droplet of colored n-hexadecane is captured under a piece of membrane in the aqueous solution with surfactant and salt. The interfacial tension measurements were performed with the pendant droplet technique [29, 45], where a droplet of aqueous solution with surfactant and salt is suspended in colored n-hexadecane in a cuvette. Image analysis of the droplet shapes from both contact angle and interfacial tension measurements was performed with the software provided with the measuring instrument, taking into account the density of the media. These experiments were repeated at least two times, and average and standard deviations were obtained from these data.

2.3 Results

In this section, we will first discuss background data on the contact angle and interfacial tensions for four different surfactant types, at three different salt concentrations. Membrane performance data regarding flux decline over time, oil retention and flux recovery after cleaning are then discussed per surfactant type.

2.3.1 Interfacial tension

The interfacial tension was measured using the pendant droplet technique, where a droplet of aqueous solution is suspended in a cuvette filled with colored oil. The results are plotted in Figure 2.1. It is immediately apparent that the four different surfactants show different behavior.
SDS, the anionic surfactant, provides the highest oil-water interfacial tension at low ionic strength. At 1 mM NaCl, the interfacial tension is 18.2 ± 5 mN/m, decreasing to 12.4 ± 0.5 mN/m for 10 mM NaCl and 2.3 ± 0.2 mN/m for 100 mM NaCl. This strong dependence on the ionic strength indicates that the adsorbed amount of surfactant depends on the ionic strength. Upon increasing the ionic strength, the charge of the head groups is screened, allowing more surfactant molecules to adsorb to the droplet surface, leading to a lower interfacial tension.
CTAB, the cationic surfactant, shows the lowest interfacial tensions of the four. CTAB has the longest carbon tail of all surfactants studied here, leading to a higher adsorbed amount and thus a lower interfacial tension. At 1 mM NaCl, the interfacial tension is 1.9 ± 0.3 mN/m, lowering to 0.4 ± 0.1 mN/m and 0.3 ± 0.1 mN/m for 10 and 100 mM respectively. These last two values are not accurate because the pendant droplet technique is not appropriate to study such low interfacial tensions. There is a clear decrease in interfacial tension between 1 and 10 mM however, so we can assume that we have a similar situation as with SDS, where the screening of charges at the head group of the surfactant molecules allows more surfactant molecules to adsorb, leading to a lower interfacial tension at higher ionic strengths. Based on this data we cannot confirm that this trend continues from 10 mM to 100 mM of salt, but this would be expected.
As expected, for TX-100, the non-ionic surfactant, an increase in ionic strength does not influence the adsorption of surfactant to the droplet surface very much. The interfacial tensions for 1, 10 and 100 mM are 6.7 ± 0.6 mN/m, 8.0 ± 0.1 mN/m and 7.8 ± 0.1 mN/m respectively. The small variation in

interfacial tension could be caused by small changes in the solvent quality for the polyethylene oxide tail of TX upon the addition of salt.
The interfacial tension of DDAPS stabilized droplets also does not change significantly with increasing salt concentration. The interfacial tension is 2.5 ± 0.1 mN/m, 2.4 ± 0.1 mN/m and 2.4 ± 0.1 mN/m for 1, 10 and 100 mM respectively. As was the case with CTAB, these values are in a regime that is hard to measure accurately using the pedant drop technique. The head groups of DDAPS are neutral as a whole, but do have a positive and a negative charge on their head groups [34].

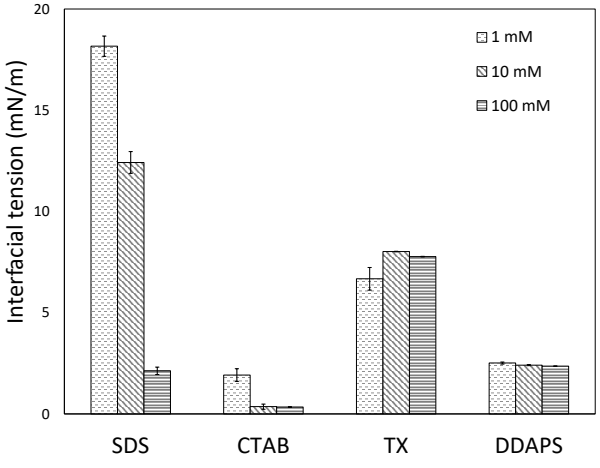

Figure 2.1: The interfacial tension of the water/oil interface for four different surfactants and three different salt concentrations as indicated.

2.3.2 Contact angle

The contact angle was obtained from a captured droplet of colored hexadecane under the membrane in a cuvette filled with the aqueous phase. The results are shown in Figure 2.2. For all surfactants and ionic strenghts, there is a rather high contact angle, here indicating a rather hydrophilic surface and thus little spreading of the oil droplet.
For SDS, the contact angles are 150 ± 0.5, 140 ± 0.5 and 131 ± 4 for 1, 10 and 100 mM. There seems to be a slight decreasing trend, indicating increased hydrophobic interactions. Due to the dissociation of OH groups on the cel-

lulose surface it is slightly negatively charged. At higher ionic strengths, the negatively charged droplet might interact more favourably with the negative membrane surface, allowing more spreading of the oil droplet. For CTAB we see a slighty increasing contact angle at increasing ionic strength. The contact angles measured are 148 ± 2, 149 ± 2 and 151 ± 1 for 1, 10 and 100 mM NaCl respectively. This might indicate an increase in hydrophilic interactions. The cationic surfactant CTAB will adsorb to the negatively charged cellulose. A higher ionic strength could lead to more CTAB adsorption and to the observed slight change in contact angle.

For TX, there is no influence on the contact angle, as the measured values are 148 ± 0.4, 149 ± 0.4 and 149 ± 0.2 for 1, 10 and 100 mM respectively. This is in line with expectations. Because TX has no charge, we also do not expect an influence of the ionic strength.

Similar behavior is observed for DDAPS. The contact angle was 150 ± 2, 152 ±1 and 151 ± 1 for 1, 10 and 100 mM respectively. Just as with TX, we expected no significant influence of the ionic strength on the contact angle, as the head group has no net charge.

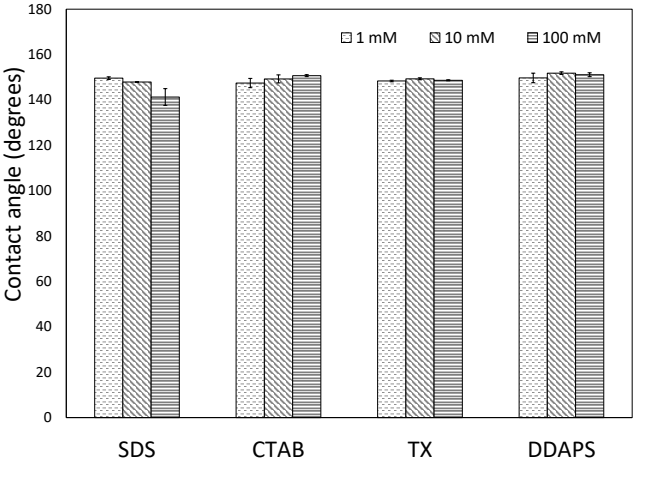

Figure 2.2: The contact angle of an oil droplet trapped under the membrane surface in the aqueous phase, for four different surfactants and three different salt concentrations as indicated

2.3.3 SDS stabilized emulsions

An emulsion with 100 ppm hexadecane, 463 mg/L SDS and 1, 10 and 100 mM NaCl was filtered in a crossflow membrane filtration system using a regenerated cellulose membrane. The crossflow velocity was 0.2 m/s and the transmembrane pressure was kept constant at 1 bar. The flux decline as a function of permeate volume is plotted in Figure 2.3. At 1 mM NaCl, the flux decline is gradual, and after three hours of filtration the flux decline reached 50 ± 3% of the initial flux. At 10 mM NaCl, the initial flux decline is very steep, after which the flux decline becomes more gradual. At the end of the experiment, the flux had dropped to 37 ±6% of the original flux. At 100 mM NaCl, the flux first declines quite fast, and then slows down, reaching a permeate flux of 23 ± 3% of the initial flux at the end of the experiment. From these results, it is clear that increasing the ionic strength has a strong influence on the flux decline, where a higher ionic strength gives more membrane fouling. The initial flux decline is associated with the direct adsorption of oil droplets to the membrane, whereas the more gradual flux decline later on in the experiment is associated with the formation of a cake layer [29]. During cake layer formation, however, the interaction between oil droplets dominates. For 1 and 100 mM NaCl, the flux decline follows a similar trend, whereas the flux decline at 10 mM shows a much steeper initial decline. This suggests there is a different fouling mechanism dominating the initial flux decline.

The flux recovery of the membrane was measured after a cleaning procedure including a forward flush, backwash and another forward flush of the membrane cell. The results are given in Table 2.1. At higher salt concentrations, the flux recovery increases, although we observed that the degree of fouling increases. Two possible mechanisms may be able to explain this observation. Firstly, we expect the cake layer formed on the surface to become denser at high ionic strengths, as a consequence of screening of the charged surfactants at the oil droplets interfaces. A denser cake layer might be easier to remove as a whole, hence the increase in flux recovery at high ionic strengths. In literature, it was observed that larger particles and aggregates are indeed more prone to detach from a cake layer [46]. The second explanation is that at higher ionic strength, more surfactants are adsorbed to the droplet interface, as discussed above. Upon flushing with pure water, the salt and surfactant are diluted and removed from the cake layer, which can have a destabilizing effect. However, because the initial concentration of surfactant was higher at high ionic strengths, the droplets might stay stable for a longer period of time, allowing for easier cleaning.

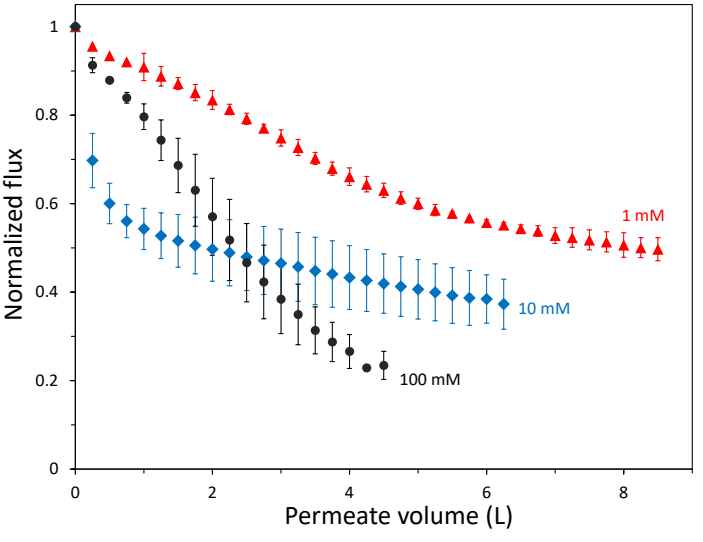

Figure 2.3: Flux decline of SDS stabilized emulsions at a crossflow velocity of 0.2 m/s and a transmembrane pressure of 1 bar. Error bars represent standard deviation after duplicates.

The oil retention for SDS stabilized emulsions is between 90 and 95% for all ionic strengths. High retentions were expected based on the theoretical critical pressure (Eq. (2.6)) required to push an oil droplet through the membrane. This was calculated on the basis of the data previously shown and it is for all three ionic strengths predicted to be above the applied pressure of 1 bar. This means that the small amount of oil found in the permeate is probably made up of the smallest droplets present in the feed stream passing through the largest pores in the membrane.

2.3.4 CTAB stabilized emulsions

The same experimental conditions were used to filter an emulsion containing 100 ppm oil, 346 mg/L CTAB and 1, 10 or 100 mM NaCl. The flux decline upon filtration of CTAB-stabilized emulsions is plotted in Figure 2.4. It is immediately apparent that the behavior is different from the results obtained with SDS-stabilized emulsions. The flux decline is much lower for CTAB-stabilized emulsions, reaching a value of 80 ± 2% for 1 mM NaCl, 84 ± 1% for 10 mM NaCl and 70 ± 10% for 100 mM NaCl after three hours of filtration.

Salt concentration (mM)	Flux recovery (%)	Oil retention (%)	Critical pressure (bar)
1	74 ± 8	93 ± 5	10.5
10	78 ± 5	94.5 ± 2.5	7.0
100	95 ± 8	90 ± 6	1.1

Table 2.1: Flux recovery, oil retention and critical pressure at 48 kg/h and 1 bar TMP for SDS stabilized emulsions.The theoretical critical pressure was calculated using Eq. (2.6), and data from section 2.3.1 and 2.3.2. The error margin on the flux recovery is an approximation, as the membrane broke during cleaning after several experiments.

The flux decline is gradual for all three ionic strengths and seems to approach a steady value at the end of the filtration experiment.
The flux recovery of CTAB shows no clear trend with increasing ionic strength (Table 2.2). The values measured for the different experiments vary quite strong even for repetitions, suggesting that removal of this cake layer is sensitive to slight variations in the experiments. We do see however, that at 100 mM NaCl, the flux recovery is high in all measurements. We also see, that for this ionic strength the oil retention is very low as almost all oil passes through the membrane. This means that there is simply not a lot of oil left on the feed side to form a cake layer, possibly also allowing easier cleaning. When we calculate the theoretical critical pressure required to push these CTAB-stabilized oil droplets through the membrane, it is clear that only at 1 mM NaCl we are above the critical pressure. At 10 and 100 mM NaCl, oil would be expected to permeate through the membrane. While this is clearly the case for 100 mM NaCl, the oil retention at 10 mM however is still 89%, despite being filtered above the critical pressure. It seems that with the theoretical critical pressure, as calculated with Eq. (2.6), we can explain the observed trends. At the same time, it cannot perfectly predict at which ionic strength oil will permeate.

2.3.5 TX stabilized emulsions

The flux decline of emulsions stabilized with the nonionic surfactant TX at three different salt concentrations is plotted in Figure 2.5. As expected, the increase in ionic strength has little influence on the flux decline. After three hours of filtration, the flux has decreased to 23 ± 1% for 1 mM NaCl, 30 ± 4% for 10 mM NaCl and 26 ± 12% for 10 mM NaCl. The nonionic head groups

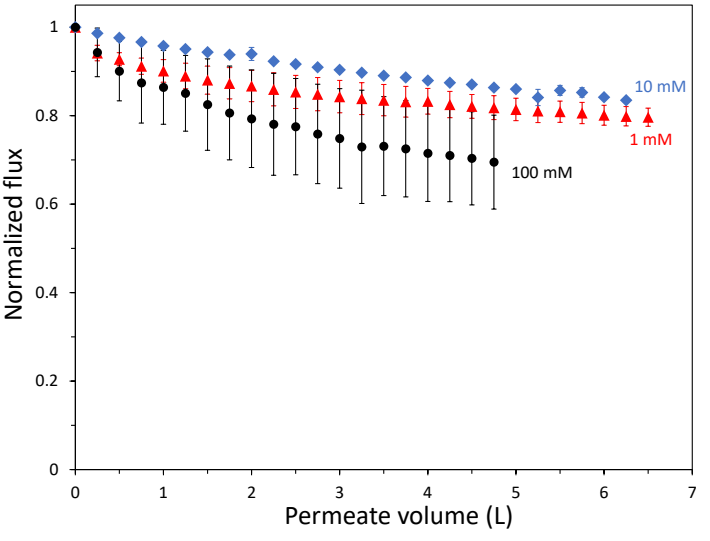

Figure 2.4: Flux decline of CTAB stabilized emulsions at a crossflow velocity of 0.2 m/s and a transmembrane pressure of 1 bar. Error bars represent standard deviation after duplicates.

Salt concentration(mM)	Flux recovery (%)	Oil retention (%)	Critical pressure (bar)
1	90 ± 9	95	1.1
10	82 ± 10	89	0.2
100	91 ± 2	3	0.2

Table 2.2: Flux recovery, oil retention and critical pressure at 48 kg/h and 1 bar TMP for CTAB stabilized emulsions.

on the droplet surface do not give a surface charge, so there is no electrostatic repulsion between the droplets. This leads to a dense cake layer and therefore more resistance.

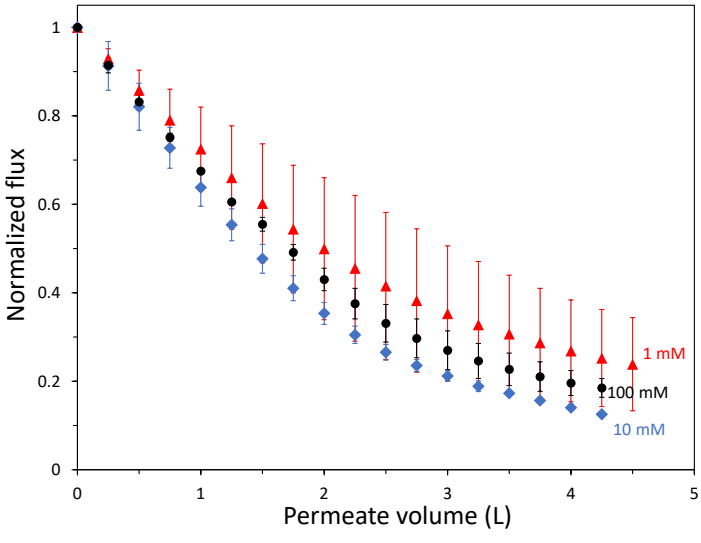

Figure 2.5: Flux decline of TX stabilized emulsions

The flush recovery for the membrane after filtering TX-stabilized emulsion is in all cases around 80% (Table 2.3). This indicates that there is a substantial amount of irreversible fouling. This can be due to a cake layer that is hard to remove, or the fouling takes place in the pores of the membrane in addition to the formation of a cake layer on the surface. The oil retention for TX-stabilized emulsion is below 80% for all ionic strengths (Table 2.3). The calculated critical pressure is however higher than the applied pressure, suggesting that oil passes through the pores by another mechanism. At sufficient high shear forces, droplets can break up and pass through the membrane [44]. Since oil can pass through the membrane and the flux recovery after forward and back washing is relatively low, the irreversible fouling of the membrane might take place primarily inside of the pores.

2.3.6 DDAPS stabilized emulsions

Finally, we studied the flux decline upon filtration of an emulsion stabilized by the zwitterionic DDAPS. Surprisingly, this surfactant has not been studied

Salt concentration (mM)	Flux recovery (%)	Oil retention (%)	Critical pressure (bar)
1	78 ± 11	77 ± 1	3.8
10	80 ± 1	69 ± 4	4.6
100	79 ± 11	74 ± 12	4.5

Table 2.3: Flux recovery, oil retention and critical pressure at 48 kg/h and 1 bar TMP for TX stabilized emulsions.

as much as the other three surfactants, while the anti-fouling properties attributed to zwitterionic species might make it very relevant for this challenging application. The head group of a zwitterionic surfactant has no net charge, but a positively and a negatively charged moiety. Because of this, it is capable of forming a hydrated layer around the head group. Therefore, we expect it to have excellent antifouling properties, because hydrophobic interactions will be hindered [47]. The flux decline of the membrane filtration experiment at three different salt concentrations is given in Figure 2.6. The flux decline after 3 hours of filtration is 81 ± 7% for 1 mM NaCl, 97 ± 2% for 10 mM NaCl and 95 ± 1% for 100 mM NaCl. Especially for the higher ionic strengths, the flux decline is so low that either no cake layer forms on the surface, or the cake layer is extremely open. We also noted that the flux decline decreased at increasing ionic strength. This is is line with expectations, as we expect that the stabilizing effect of DDAPS increases with increasing ionic strength [34].

The flux recovery after forward flushing and backwashing is given in Table **??**. For all ionic strengths the flux recovery is above 96%, which indicates excellent cleanability. Since there was virtually no flux decline, there is probably not a lot of fouling to remove. The oil retention for DDAPS stabilized emulsions at CMC is also given in Table **??**. The oil retention decreases with increasing ionic strength, but it is not completely clear why. There is no evidence from the interfacial tension data that the oil droplets become more deformable at higher ionic strength, neither does the predicted critical pressure change.

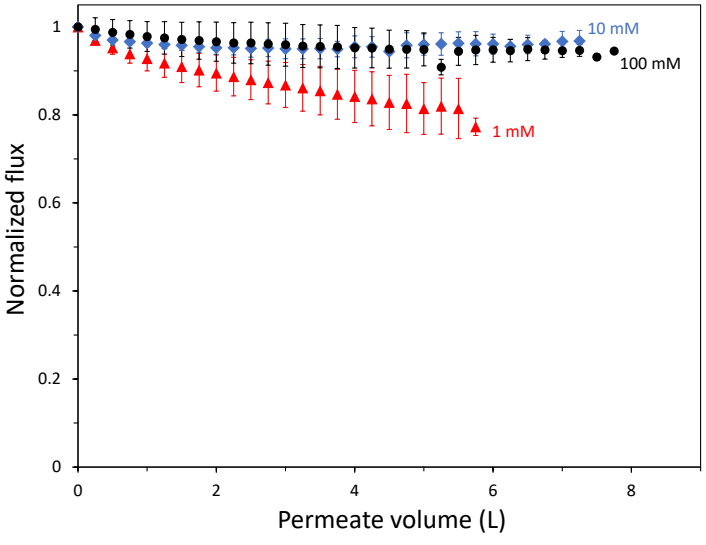

Figure 2.6: Flux decline of DDAPS stabilized emulsions

Salt concentration (mM)	Flux recovery (%)	Oil retention (%)	Critical pressure (bar)
1	98 ± 2	78 ± 6	1.4
10	96 ± 1	70 ± 20	1.4
100	98 ± 2	44 ± 6	1.4

Table 2.4: Flux recovery, oil retention and critical pressure at 48 kg/h and 1 bar TMP for DDAPS stabilized emulsions.

The low fouling propensity of the zwitterionic surfactants at high salt concentration is very promising, but the oil retention is much too low. For this reason we further studied the effect of surfactant concentration on both flux decline and oil retention. In Figure 2.7, we show flux decline curves for zwitterionic surfactant concentrations of 0.1, 0.2 and 1 times CMC at 100 mM NaCl, while in Table 2.5 we show flux recovery and oil retention. Decreasing the surfactant concentration to 0.2 CMC translates into a slightly higher flux decline, but strongly increases the oil retention (85 ± 6%, Table 2.5). At lower surfactant concentration the oil droplets are less deformable due to a higher interfacial tension (10.5 and 14.1 mN/m respectively for 0.2 and 0.1

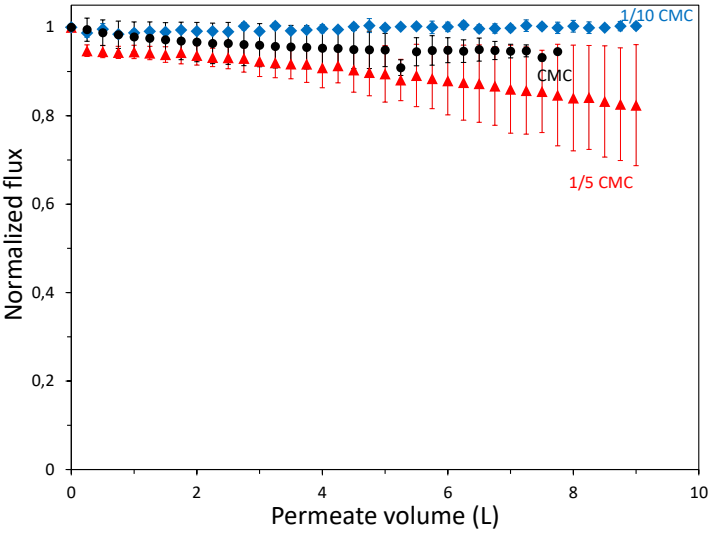

Figure 2.7: Flux decline of DDAPS stabilized emulsions as a function of surfactant concentration

times CMC). If we further lower the surfactant concentration to 1/10 CMC, we observe no flux decline over the timescale of our experiment, retaining a high oil retention (85%).

Surfactant concentration (CMC)	Flux recovery (%)	Oil retention (%)	Critical pressure (bar)
0.1	100 ± 0	85 ± 0	8.1
0.2	99 ± 1	85 ± 6	6.0
1	98 ± 2	44 ± 6	1.4

Table 2.5: Flux recovery and oil retention at 48 kg/h and 1 bar TMP for DDAPS stabilized emulsions.

2.4 Discussion

In the previous section, we showed results of the membrane filtration of emulsions stabilized with four different surfactants and at 3 different ionic

strengths. In our theory section (2.1.1), we stated that according to the DLVO theory and the Kozeny-Carman term, we expect that charged surfactants show a change in flux decline with increased ionic strength due to a changing porosity of the cake layer. A higher ionic strength is expected to lead to a lower porosity of the cake layer and thus a higher flux decline. For SDS, an anionic surfactant, this effect was very pronounced, as at higher ionic strength the flux decline was much more severe. For CTAB however, a cationic surfactant, the effect was less pronounced. At higher ionic strength, the oil permeation increased substantially, especially at 100 mM (only 3% oil retention). With more oil permeating, less oil will remain as a fouling layer. The oil permeating, especially at high ionic strength, is in line with the very low interfacial tension (and thus low critical pressure) of CTAB stabilized oil droplets. For surfactants without a head group charge, we expected no or little effect of changing the ionic strength on membrane fouling and flux decline. Indeed for the non-ionic surfactant TX and the zwitterionic surfactant DDAPS, the observations in membrane filtration were different from those observed for CTAB and SDS. Changing the ionic strength did not have a large effect on the flux decline for both TX and DDAPS, although for DDAPS the flux decline was lower at the higher ionic strengths. The extent of flux decline, however, was very different for these surfactants. Whereas TX stabilized emulsions showed a very strong flux decline, DDAPS stabilized emulsions showed almost none. We propose that this has to do with the different stabilizing mechanisms of the head groups. TX stabilizes by steric hindrance by a long non-ionic head group. As this is a short range interaction (compared to ionic interactions) this leads to a cake layer with a rather low porosity and thus a high flux decline. DDAPS however is a zwitterionic surfactant. The positive and negative moieties on the head group are capable of forming a hydration layer around the oil droplets, providing a very strong inter droplet repulsion. With very low flux declines, especially at higher ionic strengths, it seems that the high repulsion is even able to prevent a cake layer from forming. Such behaviour is in line with the excellent anti-fouling properties normally attributed to zwitterionic headgroups and zwitterionic polymers, especially at increasing ionic strength [33, 47]. Furthermore, by tuning the surfactant concentration it is possible to achieve excellent performance. At a low DDAPS concentration, 0.1 CMC, we observed no flux decline and good oil retention (85%), even at high ionic strength.

As our results show, the type of surfactant can have a large influence on the fouling potential of otherwise identical oil-in-water emulsions. Moreover, the

effects of ionic strength are different, depending on the exact type and especially charge of the surfactant. Where charged surfactants stabilize emulsions well because of their electrostatic repulsion, factors such as interfacial tension or interactions with the membrane surface definitely play an important role too in determining its appropriateness for membrane filtration and should be considered in the choice of surfactant. Especially at high salt concentrations, often found in produced waters, the use of charged surfactants can either lead to more fouling or to the passing of oil through the membrane. Nonionic surfactants, which are far less influenced by a high salt concentration, did however also not show desirable behavior. Because of a lack of electrostatic repulsion and their short range steric interactions the cake layer becomes far too dense, leading to a high flux decline. The zwitterionic surfactant DDAPS showed excellent performances due to its hydration layer, with no flux decline and 85% oil retention at the highest ionic strength tested (100 mM) and at 0.1 CMC. The zwitterionic headgroup chemistry allows for such low fouling performances while the higher interfacial tension, due to the lower surfactant concentration, maybe responsible for the higher oil retention. These results make DDAPS especially promising for successful treatment of oily waste waters at high salinity, while they are also capable of replacing the surfactants currently used for enhanced oil recovery [48].

2.5 Conclusion

In this work, we studied membrane fouling by artificial oily waste water for four different surfactant types, all at varying ionic strength. In this way, we demonstrate clearly that the effects of ionic strength on performance parameters such as flux decline, oil rejection and flux recovery after cleaning, are strongly linked to the type of surfactant used. For the anionic SDS, oil is retained well, but the flux decline is much stronger at higher ionic strength. Prolonged filtration leads to the formation of a cake layer at the membrane surface, as shown in previous works [23, 24, 29]. We hypothesise that, at low ionic strength, strong electrostatic repulsion between SDS stabilized oil droplets leads to the formation of an open cake layer and a relatively low flux decline. But at higher ionic strength the electrostatic repulsion is reduced, leading to denser cake layers and higher flux declines. For the cationic surfactant CTAB, much lower flux reductions are observed including a less pronounced effect of the ionic strength compared to SDS. For CTAB the oil-water

interfacial tension at high salt is so low, that the oil droplets can be pushed through the membrane. While at 1 mM of NaCl, 95% of oil is retained, at 100 mM of NaCl, only 3% of oil is retained. For charged surfactants, a high ionic strength can thus lead to denser cake layers, but can also lead to a drop in oil retention. As expected, the effect of ionic strength for the non-ionic surfactant TX, and the zwitterionic DDAPS, are small compared to the effects observed for CTAB and SDS. Still the extend of fouling differs greatly. For TX the flux decline is large (around 80% for all ionic strengths), while for DDAPS low flux decline was observed, especially at higher ionic strengths ($>$ 10 mM), with no flux decline at 0.1 CMC and 100 mM NaCl. The highly hydrated nature of the zwitterionic headgroup makes this surfactant type especially promising for successful oily streams filtration. We see a bright future for zwitterionic surfactants in enhanced oil recovery, but more study needs to be carried out.

References

[1] G. Daufin, J.-P. Escudier, H. Carrère, S. Bérot, L. Fillaudeau, and M. Decloux, "Recent and Emerging Applications of Membrane Processes in the Food and Dairy Industry", Food and Bioproducts Processing **79**, 89–102 (2001).

[2] B. Van Der Bruggen, C. Vandecasteele, T. Van Gestel, W. Doyen, and R. Leysen, "A review of pressure-driven membrane processes in wastewater treatment and drinking water production", Environmental Progress **22**, 46–56 (2003).

[3] W.-J. Lau and A. Ismail, "Polymeric nanofiltration membranes for textile dye wastewater treatment: Preparation, performance evaluation, transport modelling, and fouling control a review", Desalination **245**, 321–348 (2009).

[4] Y. Zhu, D. Wang, L. Jiang, and J. Jin, "Recent progress in developing advanced membranes for emulsified oil/water separation", NPG Asia Materials **6**, 1–11 (2014).

[5] S. O. Ganiyu, E. D. van Hullebusch, M. Cretin, G. Esposito, and M. A. Oturan, "Coupling of membrane filtration and advanced oxidation processes for removal of pharmaceutical residues: A critical review", Separation and Purification Technology **156**, 891–914 (2015).

[6] J. Dickhout, J. Moreno, P. Biesheuvel, L. Boels, R. Lammertink, and W. de Vos, "Produced water treatment by membranes: A review from a colloidal perspective", Journal of Colloid and Interface Science (2016).

[7] N. S. A. Mutamim, Z. Z. Noor, M. A. A. Hassan, and G. Olsson, "Application of membrane bioreactor technology in treating high strength industrial wastewater: a performance review", Desalination **305**, 1–11 (2012).

[8] A. Ambrosi, N. S. M. Cardozo, and I. C. Tessaro, "Membrane Separation Processes for the Beer Industry: a Review and State of the Art", Food and Bioprocess Technology **7**, 921–936 (2014).

[9] T. Mohammadi and A. Esmaeelifar, "Wastewater treatment of a vegetable oil factory by a hybrid ultrafiltration-activated carbon process", Journal of Membrane Science **254**, 129–137 (2005).

[10] A. Cassano, R. Molinari, M. Romano, and E. Drioli, "Treatment of aqueous effluents of the leather industry by membrane processes: A review", Journal of Membrane Science **181**, 111–126 (2001).

[11] J. Teng, M. Zhang, K.-T. Leung, J. Chen, H. Hong, H. Lin, and B.-Q. Liao, "A unified thermodynamic mechanism underlying fouling behaviors of soluble microbial products (smps) in a membrane bioreactor", Water Research **149**, 477 – 487 (2019).

[12] J. Chen, M. Zhang, F. Li, L. Qian, H. Lin, L. Yang, X. Wu, X. Zhou, Y. He, and B.-Q. Liao, "Membrane fouling in a membrane bioreactor: High filtration resistance of gel layer and its underlying mechanism", Water Research **102**, 82 – 89 (2016).

[13] M. Zhang, H. Hong, H. Lin, L. Shen, H. Yu, G. Ma, J. Chen, and B.-Q. Liao, "Mechanistic insights into alginate fouling caused by calcium ions based on terahertz time-domain spectra analyses and dft calculations", Water Research **129**, 337 – 346 (2018).

[14] K. W. Trzaskus, W. M. de Vos, A. Kemperman, and K. Nijmeijer, "Towards controlled fouling and rejection in dead-end microfiltration of nanoparticles Role of electrostatic interactions", Journal of Membrane Science **496**, 174–184 (2015).

[15] S. Alzahrani and A. W. Mohammad, "Challenges and trends in membrane technology implementation for produced water treatment: A review", Journal of Water Process Engineering **4**, 107–133 (2014).

[16] T. Bakke, J. Klungsøyr, and S. Sanni, "Environmental impacts of produced water and drilling waste discharges from the norwegian offshore petroleum industry", Marine Environmental Research **92**, 154 – 169 (2013).

[17] A. Fakhru'l-Razi, A. Pendashteh, L. C. Abdullah, D. R. A. Biak, S. S. Madaeni, and Z. Z. Abidin, "Review of technologies for oil and gas produced water treatment.", Journal of hazardous materials **170**, 530–51 (2009).

[18] B. Chakrabarty, A. Ghoshal, and M. Purkait, "Cross-flow ultrafiltration of stable oil-in-water emulsion using polysulfone membranes", Chemical Engineering Journal **165**, 447–456 (2010).

[19] B. Alley, R. John, and C. James W, "Chemical and physical characterization of produced waters from conventional and unconventional fossil fuel resources", Chemosphere **85**, 74 – 82 (2011).

[20] J. Dickhout, M. Kleijn, and W. M. Lammertink, Rob G.H.and Vos, "Adhesion of emulsified oil droplets to hydrophilic and hydrophobic surfaces - effect of surfactant charge, surfactant concentration and ionic strength", Soft Matter **14** (2018).

[21] U. W.R. Siagian, S. Widodo, K. Khoiruddin, A. Wardani, and I. G. Wenten, "Oilfield produced water reuse and reinjection with membrane", MATEC Web of Conferences **156**, 08005 (2018).

[22] H.-J. Li, Y.-M. Cao, J.-J. Qin, X.-M. Jie, T.-H. Wang, J.-H. Liu, and Q. Yuan, "Development and characterization of anti-fouling cellulose hollow fiber UF membranes for oilwater separation", Journal of Membrane Science **279**, 328–335 (2006).

[23] P. Lipp, C. Lee, A. Fane, and C. Fell, "A fundamental study of the ultrafiltration of oil-water emulsions", Journal of Membrane Science **36**, 161–177 (1988).

[24] D. Lu, T. Zhang, and J. Ma, "Ceramic Membrane Fouling during Ultrafiltration of Oil/Water Emulsions: Roles Played by Stabilization Surfactants of Oil Droplets", Environmental Science & Technology **49**, 4235–4244 (2015).

[25] G. Singh and L. Song, "Quantifying the effect of ionic strength on colloidal fouling potential in membrane filtration", Journal of Colloid and Interface Science **284**, 630–638 (2005).

[26] L. Song, "Flux decline in crossflow microfiltration and ultrafiltration: mechanisms and modeling of membrane fouling", Journal of Membrane Science **139**, 183–200 (1998).

[27] F. Wang and V. V. Tarabara, "Pore blocking mechanisms during early stages of membrane fouling by colloids", Journal of Colloid and Interface Science **328**, 464–469 (2008).

[28] J. D. Seader, E. J. Henley, and J. Wiley, *Separation process principles*, 2 edition (John Wiley & Sons) (2006).

[29] J. Dickhout and W. M. Lammertink, Rob G.H.and Vos, "Adhesion of emulsified oil droplets to hydrophilic and hydrophobic surfaces - effect of surfactant charge, surfactant concentration and ionic strength", Colloids and Interfaces **3**, 9 (2019).

[30] H. Yotsumoto and R.-H. Yoon, "Application of extended dlvo theory: I. stability of rutile suspensions", Journal of Colloid and Interface Science **157**, 426 – 433 (1993).

[31] P. Ghosh and M. Banik, "Effects of Salts Containing Mono-, Di-, and Trivalent Ions on Electrical and Rheological Properties of Oil-Water Interface in Presence of Cationic Surfactant: Importance in the Stability of Oil-in-Water Emulsions", Journal of Dispersion Science and Technology **35**, 471–481 (2014).

[32] C.-M. Chen, C.-H. Lu, C.-H. Chang, Y.-M. Yang, and J.-R. Maa, "Influence of pH on the stability of oil-in-water emulsions stabilized by a splittable surfactant", Colloids and Surfaces A: Physicochemical and Engineering Aspects **170**, 173–179 (2000).

[33] J. B. Schlenoff, "Zwitteration: coating surfaces with zwitterionic functionality to reduce nonspecific adsorption.", Langmuir : the ACS journal of surfaces and colloids **30**, 9625–36 (2014).

[34] D. Schulz, D. Peiffer, P. Agarwal, J. Larabee, J. Kaladas, L. Soni, B. Handwerker, and R. Garner, "Phase behaviour and solution properties of sulphobetaine polymers", Polymer **27**, 1734–1742 (1986).

[35] J. M. Dickhout, R. G. H. Lammertink, and W. M. de Vos, "Membrane filtration of anionic surfactant stabilized emulsions: Effect of ionic strength on fouling and droplet adhesion", Colloids and Interfaces **3** (2019).

[36] J. Li, D. Mcclements, and L. Mclandsborough, "Interaction between emulsion droplets and escherichia coli cells", Journal of Food Science **66**, 570–657 (2006).

[37] R. Vácha, S. W. Rick, P. Jungwirth, A. G. F. de Beer, H. B. de Aguiar, J.-S. Samson, and S. Roke, "The orientation and charge of water at the hydrophobic oil dropletwater interface", Journal of the American Chemical Society **133**, 10204–10210 (2011), pMID: 21568343.

[38] K. B. Medrzycka, "The effect of particle concentration on zeta potential in extremely dilute solutions", Colloid and Polymer Science **269**, 85–90 (1991).

[39] H. Zhong, L. Yang, G. Zeng, M. L. Brusseau, Y. Wang, Y. Li, Z. Liu, X. Yuan, and F. Tan, "Aggregate-based sub-cmc solubilization of hexadecane by surfactants", RSC Adv. **5**, 78142–78149 (2015).

[40] S. R. Varade and P. Ghosh, "Foaming in aqueous solutions of zwitterionic surfactant: Effects of oil and salts", Journal of Dispersion Science and Technology **38**, 1770–1784 (2017).

[41] P. R. Babu and V. Gaikar, "Membrane characteristics as determinant in fouling of uf membranes", Separation and Purification Technology **24**, 23 – 34 (2001).

[42] J. Shao, J. Hou, and H. Song, "Comparison of humic acid rejection and flux decline during filtration with negatively charged and uncharged ultrafiltration membranes", Water Research **45**, 473 – 482 (2011).

[43] T. Puspasari, N. Pradeep, and K.-V. Peinemann, "Crosslinked cellulose thin film composite nanofiltration membranes with zero salt rejection", Journal of Membrane Science **491**, 132 – 137 (2015).

[44] T. Darvishzadeh and N. V. Priezjev, "Effects of crossflow velocity and transmembrane pressure on microfiltration of oil-in-water emulsions", Journal of Membrane Science **423-424**, 468–476 (2012).

[45] H. Bazyar, N. van de Beek, and R. G. H. Lammertink, "Liquid-infused membranes with oil-in-water emulsions", Langmuir **0**, null (0), pMID: 31241957.

[46] J. Altmann and S. Ripperger, "Particle deposition and layer formation at the crossflow microfiltration", Journal of Membrane Science **124**, 119–128 (1997).

[47] J. de Grooth, M. Dong, W. M. de Vos, and K. Nijmeijer, "Building Polyzwitterion-Based Multilayers for Responsive Membranes", Langmuir **30**, 5152–5161 (2014).

[48] H. Yarveicy and A. Javaheri, "Application of Lauryl Betaine in enhanced oil recovery: A comparative study in micromodel", Petroleum (2017).

3

Surfactant-dependent Critical Interfacial Tension in Silicon Carbide Membranes for Produced Water Treatment°

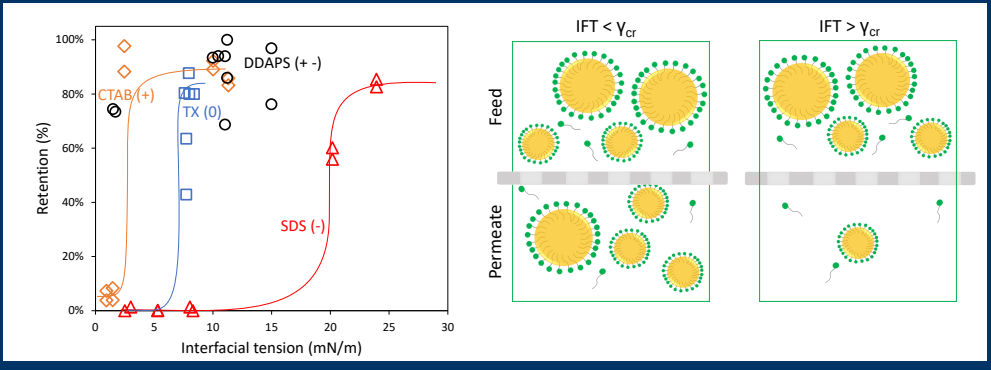

°Published as: **Ettore Virga**, Bernard Bos, P. M. Biesheuvel, Arian Nijmeijer, and Wiebe M. de Vos, *Surfactant-dependent critical interfacial tension in silicon carbide membranes for produced water treatment*, Journal of Colloid and Interface Science **2020**, *571*, 222-231.

Abstract

During fossil oil extraction, a complex water stream known as produced water (PW), is co-extracted. Membrane treatment makes PW re-use possible, but fouling and oil permeation remain major challenges. In this work, membrane fouling and oil retention of Synthetic PW stabilized with a cationic, anionic, zwitterionic or nonionic surfactant, were studied at various surfactant and salt concentrations. We discuss our results in the framework of the Young-Laplace (YL) equation, which predicts for a given membrane, pressure and oil-membrane contact angle, a critical interfacial tension (IFT) below which oil permeation should occur. We observe such a transition from high to low oil retention with decreasing IFT for the anionic (SDS), cationic (CTAB) and non-ionic (TX) surfactant, but at significantly higher critical IFTs than predicted by YL. On the other side, for the zwitterionic DDAPS we do not observe a drop in oil retention, even at the lowest IFT. The discrepancy between our findings and the critical IFT predicted by YL can be explained by the difference between the measured contact angle and the effective contact angle at the wall of the membrane pores. This leads to a surfactant-dependent critical IFT. Additionally, our results point out that zwitterionic surfactants even at the lowest IFT did not present a critical IFT and exhibited low fouling and low oil permeation.

3.1 Introduction

During the extraction of oil, for each volume of oil an average of three volumes of water are co-extracted [1]. This water is known as produced water (PW). It stems not only from natural well water, but also from water used to improve the extraction [2]. With the ongoing population growth and increased environmental stress, water treatment and re-use are becoming a necessity, especially in areas where water is already scarce.

PW is a very challenging water stream to treat due to its variable composition. Salinity, oil concentration, pH, dispersed solids and many other factors, may vary drastically from one location to another [3] and also change with well lifetime. Surfactants, added during oil and gas extraction to increase oil recovery from reservoirs, and to protect equipment (e.g. corrosion inhibitors), pose a further challenge to PW treatment. Surfactants stabilize the oil-water emulsion by creating smaller and more stable oil droplets (<10 μm), which makes separation by conventional methods, such as hydrocyclones and dissolved air flotation, much harder. These droplets can, however, be removed by membrane filtration [4].

Independent of the type, all membranes will eventually suffer from fouling [5]. This can be due to scaling, biofilm growth or in the case of oil-in-water emulsions, such as PW, the formation of an oil layer on top of the membrane surface and in its pores [6]. Fouling results in a decreased permeability, which in some cases may be hardly reversible. The type and extent of fouling depends on the water characteristics, membrane type and operational conditions. Because of their chemical and temperature resistance, ceramic membranes can be cleaned with much harsher chemicals and hot fluids, which can remove fouling without affecting the chemical stability of the membrane. In particular, SiC membranes are increasingly used in the treatment of oily waste waters [7–10]. The suitability of SiC as a membrane material is mainly based on its high water permeability, due to its high porosity and hydrophilicity.

When using membranes for filtration of oil-in-water emulsions, surfactant chemistry plays a crucial role in membrane fouling [11–13]. Surfactants not only stabilize oil droplets in water by absorbing at the oil-water interface, but subsequently they also determine the chemistry and charge of oil droplets. In a recent work, we investigated the effect of surfactant type and ionic strength on membrane fouling [14]. In particular, we found that the used surfactant is crucial in determining the extend and type of membrane fouling, especially at high ionic strengths. While fouling can be critical in determining the successful application of membrane filtration, it can be clear that also the permeation

of oil is such a critical parameter. Unfortunately, clear understanding of oil permeation for the different surfactants and under different conditions is still missing. Surfactants not only change the chemistry and charge of the oil droplets but an added effect is that they low the oil-water interfacial tension (IFT), which allows oil droplets to be more deformable and easily squeeze through the membrane pores. In this work, we use ionic strength, surfactant type and concentration to control and manipulate the IFT. This approach allows us to study the IFT influence on oil permeation through the pores of the membrane during the filtration of oil-in-water emulsions, such as PW. We compare and discuss our results in the framework of the Young-Laplace equation, which predicts, for a given pressure and membrane, a critical IFT below which oil permeation occurs.

3.1.1 Theory

In membrane fouling by oil-in-water emulsions, the interactions that take place at the oil-water-membrane interface(s) play a crucial role. Due to these interactions, the oil can adhere to the membrane surface, determining different degrees of fouling. Hydrophilic surfaces are less prone to fouling by organic compounds because the hydrophilic surface is covered by a thin layer of water molecules loosely bound by hydrogen bonding [12]. A good indication of the hydrophilicity of a membrane is given by the contact angle θ between the water phase and the membrane surface. This is described by Young's equation,

$$\gamma_{om} = \gamma_{wm} + \gamma_{ow} \cos\theta, \tag{3.1}$$

where γ_{om} (mN/m) is the oil-membrane interfacial tension, γ_{wm} (mN/m) the water-membrane interfacial tension and γ_{ow} (mN/m) the oil-water interfacial tension. Young's equation is, however, based on the assumption that the surface is smooth, clean and that no chemical reactions take place.

In the case of oil-in-water emulsions stabilized with surfactants, the amount of surfactants adsorbed at the oil-water interface affects the IFT. A measure of the amount of moles of surfactant per droplet surface area is given by the surface excess Γ (mol/m^2), described as

$$\Gamma = -\frac{1}{RT}\frac{\partial \gamma_{ow}}{\partial \ln C}, \tag{3.2}$$

where R is the ideal gas constant, T the absolute temperature, C (mol/m^3) the surfactant concentration. This equation comes from the Gibbs adsorption isotherm and Γ is roughly equal to the areal concentration of the surfactants

at the oil-water interface. However, this is true for relatively high surfactant concentrations in the bulk.

From Equation (3.2), we can see that an increase in surfactant concentration leads to lower IFT, and thus an increase in oil droplet deformability. This is very relevant to the case of an oil droplet permeating through a membrane pore. Effectively, oil droplets require less energy to change their shape and to squeeze through pores smaller than the droplet size compared to a situation where less or no surfactant is used. The pressure at which the droplets go into and through the pores is the so-called critical entry pressure (P_{cr}, bar) [15]. It can be calculated with the Young-Laplace (YL) equation,

$$P_{cr} = -\frac{\gamma_{ow} c_p \cos\theta}{A_p}, \tag{3.3}$$

with c_p (m) being the circumference of the pore, A_p (m^2) the surface area of the pore and θ (°) the contact angle of the oil droplet with the membrane. The presence of surfactants can affect the contact angle, since surfactants may adsorb at the membrane-liquid interface and change the oil-membrane interaction. Equation (3.3) is valid for a liquid layer, i.e. for a oil droplet-membrane interface where the size of the membrane pore is very small compared with the droplet size. Since the ratio of the droplet and membrane pore size is in our case very large (>10), no correction is needed for Eq. (3.3) [16].

We performed all experiments at constant transmembrane pressure (ΔP = 0.1 bar). Therefore, we can rewrite Equation (3.3) and we can calculate a critical interfacial tension γ_{cr} for our membrane, as a function of the contact angle θ between the oil droplet and the membrane in water

$$\gamma_{cr} = -\frac{A_p \Delta P}{c_p \cos\theta}. \tag{3.4}$$

If the interfacial tension is the dominant parameter influencing oil retention, we expect oil permeation at or below γ_{cr}.

3.2 Experimental Section

3.2.1 Materials

For the preparation of synthetic PWs, we used DI water, sodium dodecyl sulfate (SDS, anionic, Sigma Aldrich, ACS reagent, 99.0%), hexadecyltrimethylammonium bromide (CTAB, cationic, Sigma Aldrich, for molecular biology,

99%), Triton ™ X-100 (TX, nonionic, Sigma Aldrich, laboratory grade), N-dodecyl-N,N-dimethyl-3-ammonio-1-propanesulfonate (DDAPS, zwitterionic, 97.0% (dried material, CHN)), n-hexadecane (Merck Schuchardt 99.0%) as the oil, Coumarin 6/ Neeliglow Yellow 196 (Neelikon) as fluorescent dye, and sodium chloride (NaCl, VWR, 100%). The membrane is a CoMem© asymmetric silicon carbide (SiC) membrane of which characteristics are given in table 3.1. All chemicals were used without further purification steps.

Carrier material	Silicon carbide (SiC)
Selective membrane material	Silicon carbide (SiC)
Channels	31
Single channel diameter	3 mm
Membrane area	0.09 m^2
Nominal pore size	150 nm*
Typical flux at 25°C at 1 bar (non-fouled)	3000 $Lm^{-2}h^{-1}$

Table 3.1: CoMem© asymmetric silicon carbide (SiC) ultrafiltration membrane characteristics. *Pore size analysis reported in Appendix A.

3.2.2 Emulsion preparation and characterization

We prepared artificial produced water emulsions following the protocol of our previous work [14]. PW is an oil-in-water emulsion, where the oily phase is dispersed in the aqueous phase, stabilized by corrosion inhibitors, biocides and extraction enhancers, which act as surfactants [12]. For this reason, we made each synthetic produced water by dispersing oil droplets of n-hexadecane in water using surfactants as stabilizers.

Since PW is a complex stream, it can be difficult to mimic. Usually anionic surfactants (such as SDS) or blends of different surfactants are used in enhanced oil recovery (EOR) to achieve a low IFT and therefore improve the extraction of oil from the well [17]. But surfactants are present in PW also as corrosion inhibitors and biocides and even as natural surfactants. This complex mixture of surfactants would not allow a more fundamental study of PW as proposed in this work. For this reason, rather than using mixtures of surfactants, in our work we make artificial PW with a single surfactant. While the zwitterionic surfactant (DDAPS) that we use in our study was less explored, all the other surfactants selected (SDS, CTAB and TX) are commonly employed as model surfactants to mimic PW [17–19].

To detect the amount of oil that permeates through the membrane, we added a fluorescent dye to n-hexadecane. As fluorescent dyes bleach over time, we prepared the colored oil freshly before each experiment. We first put approximately 5 mg of the dye powder in a test tube together with 8 mL of n-hexadecane, later we placed the tube in an ultrasonic bath for 10 minutes. Afterwards, we filtered the oil with a Millipore 0.45 μm filter to remove any remaining solid particles.

To ensure all emulsions have the same characteristics, we prepared a stock emulsion, which we then further diluted to obtain the desired salt (1, 10 or 100 mM) and surfactant concentration. The surfactant concentrations were all chosen to be 0.1, 0.2 and 1 times the critical micelle concentration (CMC) value in absence of salt. We prepared the stock emulsions by dissolving a surfactant (239.1, 478.2 or 2391 mg/L SDS; 34.6, 69.2 or 346 mg/L CTAB; 14.4, 28.8 or 144 mg/L TX; 100.6, 201.2 or 1006 mg/L DDAPS) in 1 L of DI water in a Duran® bottle (Duran 21801545) by mixing with a dispersing mixer (IKA® T25 digital Ultra-Turrax with S25N 18G element) for 4 minutes at 14,000 rpm. Then, we injected 2 g of colored oil near the mixer head and mixed for 10 minutes at 14,000 rpm. For the filtration experiment, we diluted the prepared 1 L of emulsion with DI water in a 20 L tank in order to end up with a 100 ppm n-hexadecane solution and the desired surfactant and NaCl concentration. This method is proven to make emulsions with a mean droplet size of 5 μm and distributed between 1 and 9 μm [14]. In this work no zeta potentials were obtained of the emulsions. For similar surfactant concentrations and ionic strength, oil-in-water emulsions are known to be strongly negatively charged for SDS (zeta potentials of -110 to -120 mV [20, 21]), strongly positively charged for CTAB ($\sim$+85 mV [21, 22]), slightly negative for TX (from -20 to -5 mV [23]) and negatively charged for DDAPS (from -35 to -45 mV [24]). SiC membranes are known to be strongly negatively charged (zeta potentials of -20 to -35 mV [11, 25]) at neutral pH, at which all experiments were performed .

3.2.3 Membrane filtration

Filtration experiments were performed by using an OSMO-inspector cross flow membrane filtration system supplied by Convergence. The feed, permeate and concentrate flows are measured by Bronkhorst M15 mass flow meters. The emulsion is continuously stirred to minimize any creaming which was aided by recycling of the concentrate and permeate back into the 20 L feed bottle. Before each experiment the clean water flux was measured. The cleaning of the

ceramic membrane is done with acid and base and extensive DI water flushing. Each experiment is performed at least twice and all data points are reported. A membrane filtration experiment consisted of filtering for 3 hours at a ΔP of 0.1 bar and a flow rate of 60 kg/h, which corresponds to a crossflow velocity (CFV) of 7.6 cm/s (Re∼230). The SiC membranes that we used have a really high permeate flux/bar (3000 LMH/bar) and for this reason a relatively low pressure, such as 0.1 bar, already provides a high flux. The flux is the most relevant factor in fouling as it determines the transport of foulants towards the membrane surface. The permeability was constantly monitored. The low CFV (7.6 cm/s) was chosen to stimulate fouling, allowing for efficient fouling experiments. In a real PW treatment process, one would choose a higher CFV to allow shear to reduce and slow down membrane fouling.

3.2.4 Permeate analysis

We measured the oil retention by using a fluorescent dye method already reported in previous works [6, 14]. The oil retention R (%) is defined as

$$R = 1 - \frac{C_p}{C_f} \tag{3.5}$$

where C_p and C_f are the oil concentrations (ppm) in the permeate and the feed respectively. Therefore, we took a feed and permeate sample at the same time and used those for analysis. We used the feed with fluorescent oil to make a calibration line. Subsequently we measured the fluorescence of the permeate on the same sample plate and determine the oil concentration in the permeate using the calibration line. We measured the fluorescence of the samples in a Perkin Elmer Victor3 Multilabel Plate Reader, using a protocol for Fluorescein (465 nm/510 nm, 1.0 s). The dilutions for the calibration line and permeate were injected in threefold in a 96-hole well plate. The volume of liquid in one hole was 200 μL. We took a permeate sample every 30 min during a filtration experiment.

3.2.5 Cleanability

The ability to clean membranes, called cleanability (CA), is given by:

$$CA = \frac{J_{AC}}{J_0} \tag{3.6}$$

where J_{AC} (LMH/bar) is the permeability after cleaning and J_0 the permeability of a completely clean membrane. Since pressure can slightly change

during the experiments the fluxes are corrected with the actual trans membrane pressure, giving the membrane permeability (LMH/bar).

We determined two different cleanabilities. The first one, water cleanability, is based on the water flux after 15 min forward flushing ($\Delta P = 0.5$ bar), 15 min backwashing and 15 min forward flushing ($\Delta P = 0.5$ bar), all with DI water. The second one, chemical cleanability, is instead based on the flux after the procedure that follows. The membrane was first flushed for 30 min with a 15 g/L NaOH solution at 85°C and $\Delta P = 0.5$ bar, then for 30 min with DI water at room temperature and $\Delta P = 0.5$ bar, later backwashed for 30 min with DI water at room temperature, and finally flushed again for 30 min with DI water at room temperature and $\Delta P = 0.5$ bar. This procedure was then repeated but starting with a 15 min membrane flush with a 10 mL/L HNO3 solution at 50°C and $\Delta P = 0.5$ bar, instead of NaOH solution flush.

Before starting a new experiment, we made sure the water permeability was the same as the clean membrane water permeability (CWP). If the flux, after the cleaning procedures reported above, differed from the CWP, the membrane module was opened and the membrane cleaned with abundant water, pressurized air and ethanol, until the initial CWP was recovered.

3.2.6 Contact angle and interfacial tension measurements

Both types of measurements were performed on a contact angle and contour analysis instrument (Dataphysics OCA 35). The contact angle measurements were performed in captive bubble mode, where a droplet of colored hexadecane is captured under a SiC membrane slice in the aqueous solution with the desired surfactant concentration and salt. The interfacial tension measurements were instead performed with the pendant droplet technique, where a droplet of solution, made of water, salt and surfactant, was suspended in n-hexadecane from a stainless steel needle of 1.65 mm in diameter, which directly acted as a scale bar for the calculations. Image analysis of the droplet shapes for both contact angle and interfacial tension were performed with the apparatus software, which makes use of Young-Laplace fitting. For each type of synthetic PW the measurement was taken at least 5 times.

3.3 Results and Discussion

In this section, we first discuss the effect of surfactant concentration and ionic strength on the IFT and oil-membrane contact angle. Subsequently, we discuss

membrane performance regarding flux decline over time and oil retention per surfactant type. We finally discuss our results in the framework of the YL equation, where interfacial tension and contact angle can be used to predict the degree of oil-permeation.

3.3.1 Interfacial tension

As discussed in the theory section, the interfacial tension is seen as a key parameter in oil permeation, since it affects the deformability of oil droplets, and thus their potential to squeeze through membrane pores. Different kinds of synthetic PW were prepared in order to study the effect of surfactant type, surfactant concentration and ionic strength. All these parameters influence the interfacial tension at the hexadecane-water interface, albeit not to the same extend for all surfactants. The NaCl concentrations used are 1, 10 and 100 mM, while the surfactant concentrations used are 0.1, 0.2 and 1 times CMC. In Figure 3.1A we show the effect of surfactant concentration on the interfacial tension, while in Figure 3.1B we show the effect of ionic strength.

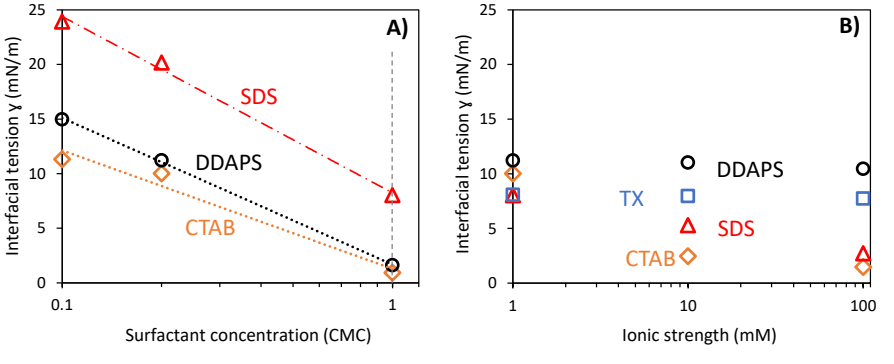

Figure 3.1: Interfacial tension as a function of surfactant concentration (A) at 1 mM NaCl and ionic strength (B) for CTAB (69.2 mg/L, 0.2 CMC), SDS (2391 mg/L, CMC), DDAPS (201.2 mg/L, 0.2 CMC) and TX (144 mg/L, CMC) . With CMC (2391 mg/L for SDS, 346 mg/L for CTAB, 144 mg/L for TX and 1006 mg/L for DDAPS) we indicate the surfactant critical micelle concentration in absence of salt. Symbols represent data points, while lines are based on Eq (2). Error bars were smaller than the markers (standard deviation (SD) $\leq$ 0.6 mN/m, and are for that reason not shown). All the experiments were performed 5 times.

From Figure 3.1A, we can clearly see that the IFT for SDS is higher than CTAB and DDAPS, whose IFTs are instead quite similar. Therefore, CTAB and DDAPS allow for more deformable oil droplets. From Figure 3.1A it is possible to calculate the slope ($\frac{\partial\gamma}{\partial lnC}$), which is normally used to calculate the surface excess Γ, as described by Equation (3.2). The surface excess Γ is defined as the concentration of surfactant molecules at the interface plane, relative to that at a similar plane in the bulk [26]. For the three surfactants, for which the surfactant concentration was changed, namely CTAB, SDS and DDAPS, we calculated this slope, i.e. the effect of surfactant concentration on IFT. The surface excess Γ was estimated to be 1.9 μmol·m^{-2}, 2.8 μmol·m^{-2} and 2.3 μmol·m^{-2}, respectively for CTAB, SDS and DDAPS at CMC.

Next to the effect of surfactant concentration, there is the effect of ionic strength. CTAB has a positive hydrophilic head group while SDS has a negative one. DDAPS has a zwitterionic head group with no net charge, while TX has a nonionic headgroup. As a consequence, the only surfactants for which the IFT is visibly affected by ionic strength are the ones with a net charge, i.e. SDS and CTAB. The lowering of the interfacial tension with ionic strength in this salt concentration range was already reported in previous studies and it is due to the effect of charge screening, reducing the repulsion between the hydrophilic heads of SDS or CTAB increasing the amount of surfactant molecules adsorbed at the oil-water interface [14, 27–29].

3.3.2 Contact angle

The contact angle was obtained from a droplet of colored hexadecane trapped under a SiC membrane in a cuvette filled with the aqueous phase, at the desired surfactant concentration and ionic strength. Contact angle plays a crucial role in oil permeation. A lower value of oil-membrane contact angle translates into lower required pressure to push the oil droplet through the membrane, see YL (Equation (3.3)). The results of contact angle measurements are shown in Figure 3.2. For all surfactants and ionic strenghts, there is a rather high contact angle (>130°), here indicating a rather hydrophilic surface and thus little spreading of the hydrophobic oil droplet. This suggests that rather low IFTs are required for oil to squeeze through the membrane pores. However, the contact angle we measured proves only the colloidal interactions that occur at the outer surface of the membranes. However, since the surface chemistry of the SiC membrane outer surface is the same as that of its pores we do not expect a big discrepancy between macroscopic contact angle and pore interior contact angle. For CTAB we see a slightly decreasing contact angle at

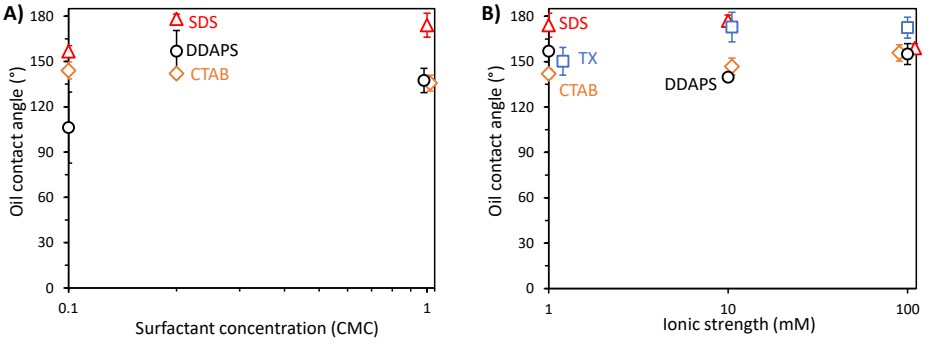

Figure 3.2: Contact angle of oil on a slice of SiC membrane in water solution as a function of surfactant concentration (A) at 1 mM NaCl and ionic strength (B) for CTAB (69.2 mg/L, 0.2 CMC), SDS (2391 mg/L, CMC), DDAPS (201.2 mg/L, 0.2 CMC) and TX (144 mg/L, CMC). With CMC (2391 mg/L for SDS, 346 mg/L for CTAB, 144 mg/L for TX and 1006 mg/L for DDAPS) we indicate the surfactant critical micelle concentration in absence of salt. All the experiments were performed 5 times.

increasing surfactant concentration (from 144°±6 to 136°±5) and a slightly increasing contact angle at increasing ionic strength (from 142°±3 to 156°±5). For SDS, the contact angles slightly increase with increasing surfactant concentration (from 157°±4 to 173°±7), while it slightly decrease at high ionic strength (from 173°±7 to 159°±3). For TX, we do observe little influence on the contact angle at increasing ionic strength. The contact angle is 150°±9 at 1 mM, 172°±8 at 10 mM and 172°±7 at 100 mM. This is confirmed by a previous study, where wettability of charged surfaces was found to increase with ionic strength [30]. However, here the change is little. For DDAPS at 0.1 CMC contact angle was lower than for all the other surfactants (106°±23). With increasing surfactant concentration the contact angle reached similar values to the other surfactants. No clear effect of ionic strength was observed for DDAPS. Overall, the surfactants seem to have little effect on contact angle, and in all cases it remains rather high. This suggests that rather low IFTs are required for oil to permeate the membrane.

3.3.3 CTAB stabilized emulsions

In Figure 3.3, we show the results of fouling studies with emulsions stabilized by the positively charged CTAB. In Figure 3.3A and Figure 3.3B, normalized flux decline curves, and average oil retentions, are displayed as a function of the surfactant concentration and ionic strength, respectively. The respective oil retentions as a function of permeate volume are shown in Appendix A (Figure S5).

CTAB shows a high flux decline for all three surfactant concentration and ionic strengths, as shown in Figure 3.3A and Figure 3.3B. We can explain this behavior by looking at the electrostatic attraction between the negatively charged membrane, based on SiC [11], and the positively charged oil droplets (zeta potential of SiC membrane and CTAB emulsions described in Experimental Section (3.2.2)). This allows severe fouling to build up with limited influence of surfactant concentration and ionic strength. The flux decline is expected to stem from pore blocking, since we do not observe a strong influence of surfactant concentration and ionic strength that would be the main actors of a change in the cake layer resistance [14].

For the oil permeation however, we do see a very strong effect of concentration and ionic strength. At the lower surfactant concentrations we observe a stable high oil retention, but this drops to nearly 15% at the CMC. The same is observed for the ionic strength, high and stable retentions at 1 and 10 mM NaCl, but very low retentions at 100 mM. This sharp transition between high and low oil retention is very much in line with the predictions of YL equation (Equation (3.5)), where oil permeation can occur below a critical interfacial tension. Both increasing the ionic strength, and increasing the surfactant concentration leads to a lower IFT (see figure 3.2). As shown in Appendix A (Figure A.5B and A.5D), the PWs with the lowest interfacial tensions, 0.2 CMC at 100 mM NaCl and CMC at 1 mM show almost no oil retention (from 0 to ∼10%) during filtration. This maybe caused by their low interfacial tensions, respectively 1.47 and 0.94 mN/m. This will be discussed in more detail in section 3.3.7.

3.3.4 SDS stabilized emulsions

In Figure 3.4, we show the results for the emulsions stabilized with negatively charged SDS.

For SDS both the effect of the electrostatic interactions and the interfacial tension are clearly visible in Figure 3.4A. First of all, the decrease in oil reten-

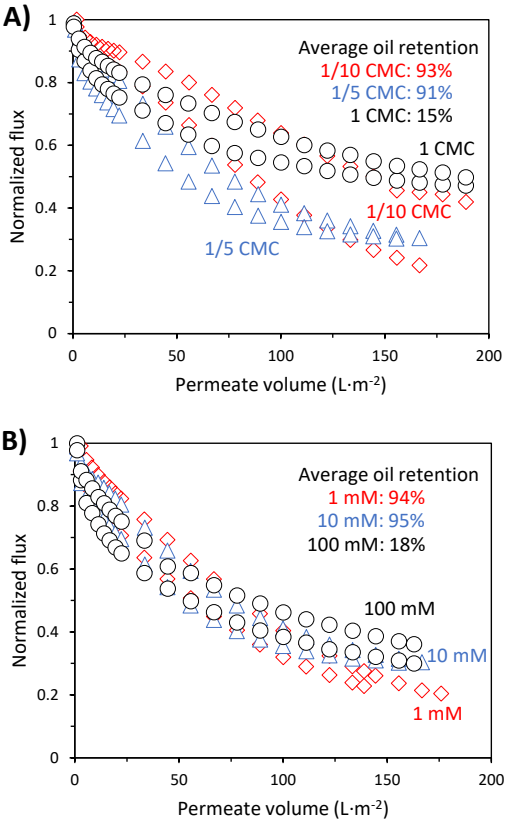

Figure 3.3: Flux decline of CTAB stabilized emulsions and average oil retention at a crossflow velocity of 7.6 cm/s and a transmembrane pressure of 0.1 bar. Flux decline and average oil retention (A) as a function of surfactant concentration at 1 mM NaCl and (B) ionic strength at 0.2 CMC (69.2 mg/L CTAB). CMC = 346 mg/L is the critical micelle concentration for CTAB in absence of salt. All the experiments were performed in duplicate, as shown.

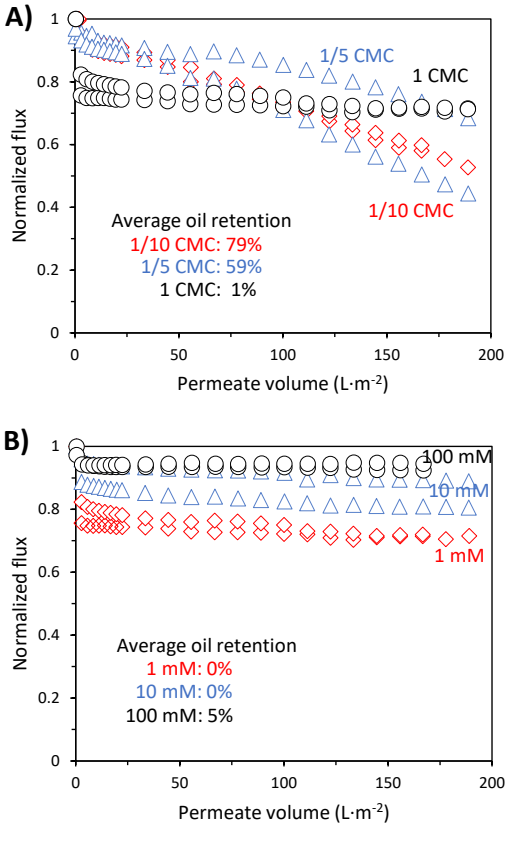

Figure 3.4: Flux decline of SDS stabilized emulsions and average oil retention at a crossflow velocity of 7.6 cm/s and a transmembrane pressure of 0.1 bar. Flux decline and average oil retention (A) as a function of surfactant concentration at 1 mM NaCl and (B) ionic strength at CMC (2391 mg/L SDS). CMC = 2391 mg/L is the critical micelle concentration for SDS in absence of salt. All the experiments were performed in duplicate, as shown.

tion follows the trend of the decrease in interfacial tension, as suggested by the YL equation. This even leads to nearly 0 retention at the CMC. Increasing SDS concentration from 0.1 and 0.2 to 1 time CMC, flux decline becomes less severe, probably due to the high oil permeation. Oil rather than accumulating at the membrane surface and in its pores, goes through the membrane, leading to less fouling. Furthermore, for this type of surfactant, the oil does not strongly adhere to the membrane surface, thus it does not cause a big flux decline and pore blocking, as observed for CTAB even at CMC. While for CTAB we observe a severe flux decline at CMC it does not occur for SDS stabilized emulsions at CMC. This effect may be related to the surface chemistry and charge of the surfactant. Since both membrane (SiC) and SDS are negatively charged (see SiC membrane and SDS emulsions zeta potential in Experimental Section (3.2.2)), the electrostatic interactions that take place at the oil-membrane interface are expected to reduce the oil adhesion.

In Figure 3.4B we show the effect of ionic strength over fouling and average oil retention. In particular, we can see that there is no almost oil retention at all ionic strengths. The experiments are performed at CMC (value in absence of salt) and supposedly, below the critical interfacial tension for SDS . The ionic strength however has only a small effect on the flux decline. This decrease in flux decline with increasing ionic strength can be caused by a decrease in interfacial tension, which we displayed in Figure 3.1B. Indeed, at lower IFT we expect a lower degree of pore blocking, since it becomes easier at low IFTs to push the oil through the membrane. We expect the interfacial tensions to be dominant since the increased charge screening would suggest a denser cake layer, leading to an increase flux decline, which is opposite to our results. Dickhout *et al.* showed the effect of increased ionic strength at lower SDS concentrations, roughly 0.2 CMC, and found an increase in cake layer density though [27]. In our case, the lower interfacial tension makes the oil droplets more deformable and thus easier to squeeze through the membrane, reducing the build up of oil at the membrane surface.

3.3.5 DDAPS stabilized emulsions

In Figure 3.5, we show the results for emulsions stabilized by the zwitterionic DDAPS. The most striking result from Figure 3.5A is the relatively low flux decline for all concentrations of DDAPS, compared to the flux declined of CTAB (Figure 3.3A and 3.3B) and SDS (Figure 3.4A). Furthermore, oil retention is relatively high. From Figure 3.5B we can conclude that ionic strength has an effect on the flux decline, albeit not as clear as for the other ionic surfactants.

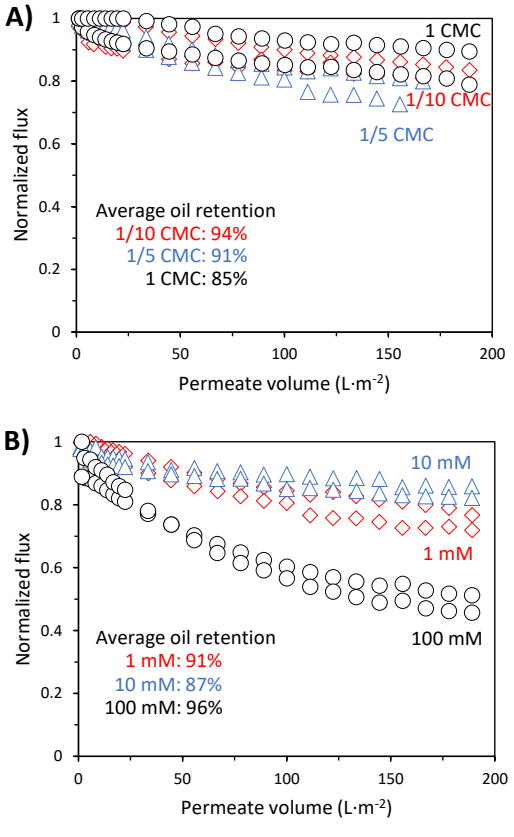

Figure 3.5: Flux decline of DDAPS stabilized emulsions and average oil retention at a crossflow velocity of 7.6 cm/s and a transmembrane pressure of 0.1 bar. Flux decline and average oil retention (A) as a function of surfactant concentration at 1 mM NaCl and (B) ionic strength at 0.2 CMC (201.2 mg/L DDAPS). CMC = 1006 mg/L is the critical micelle concentration for DDAPS in absence of salt. All the experiments were performed in duplicate, as shown.

Figure 3.5C also suggests that there is an optimal ionic strength, 10 mM, at which flux decline is minimized. Oil retention, in contrast to flux decline, does not suffer from any ionic strength related effect and is above 85%, even at the highest ionic strength (100 mM). In contrast to SDS and CTAB, it seems that for DDAPS the critical interfacial tension has not been reached under these conditions.

The excellent hydration of sulfobetaines, such as DDAPS, was already investigated in other studies and showed that almost no rearranging of water molecules was caused by dissolving these zwitterionic molecules [31–34]. Furthermore, for zwitterionic surfactants, in contrast with ionic surfactants, there is no counter ion release, which makes it energetically unfavorable for the DDAPS stabilized oil droplet to adsorb on the charged membrane surface [34]. DDAPS, thanks to its hydration properties, reduces the adhesion of the oil droplets at the membrane surface and even at higher ionic strengths avoids oil permeation. However, flux decline is more severe at 100 mM NaCl.

3.3.6 TX stabilized emulsions

In Figure 3.6, we show the results for the nonionic TX. Here only the ionic strength experiments were performed.

The flux decline results are in close correspondence with those of Dickhout *et al* [14]. Relatively high flux decline, is observed for all ionic strengths. The lack of electrostatic repulsion between the droplets and the membrane, but also between the droplets themselves, causes the rapid formation of a dense cake layer. If droplets adhere at the membrane surface the pore blocking also increases. Since the surfactant is not charged, no salt concentration effects were expected. Still, we do observe a clear effect of the ionic strength on the oil retention. In addition, the membrane seems to behave differently at high ionic strength, showing an increased oil permeation with increasing permeate volumes (SI, Figure S8B). In Figure 3.2 we did observe a small change in IFT for higher ionic strengths, even for the non-ionic TX. It could be that this small change is sufficient to get in IFT values below the critical one. This maybe a reason why here retention drastically changes over time.

3.3.7 Critical interfacial tension, surface chemistry and cleanability

In the previous sections, we discussed the effect of surfactant concentration and ionic strength for each type of surfactant. In Figure 3.7, we show oil

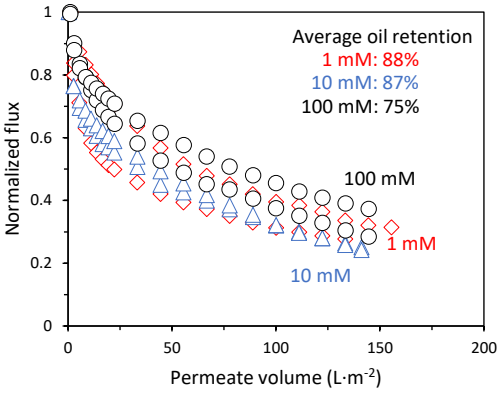

Figure 3.6: Flux decline of TX stabilized emulsions and average oil retention at a crossflow velocity of 7.6 cm/s and a transmembrane pressure of 0.1 bar as a function of ionic strength at CMC (144 mg/L TX). CMC = 144 mg/L is the critical micelle concentration for TX in absence of salt. All the experiments were performed in duplicate, as shown.

retention as a function of IFT for all data collected at different surfactant concentration and ionic strength .

We predicted the critical interfacial tension γ_{cr} by using Equation (3.5), assuming contact angles of $130° \leq \theta \leq 150°$ (see Figure 3.2) and we found a γ_{cr} of 0.37 mN/m$\leq \gamma_{cr} \leq$0.58 mN/m. Based on these calculations we predict a high oil retention for IFT values higher than 0.58 mN/m and low oil retentions below 0.37 mN/m. However, the predicted critical IFT γ_{cr} is very low and all the emulsions tested in this study have a higher IFT. Still, for CTAB, SDS and TX (see Figure 3.7) we observed a clear transition from high to low oil retention with decreasing IFT. These experimentally observed critical IFTs are larger than the predicted one, with a critical IFT value specific to that surfactant. For CTAB, the oil retention drops for IFT values 3 times higher than the predicted critical value, while for SDS, the oil retention drops at IFT values almost 40 times higher than predicted. For the nonionic TX we observe a drop in oil retention from low to high ionic strengths at IFT$\sim$8 mN/m, value 15 times higher than predicted. On the other hand, the zwitterionic DDAPS was the only surfactant that did not show a critical IFT, even at the lowest IFT. If the IFT was the only responsible for oil permeation, we should expect

no differences between oil retentions of different surfactant at similar IFT. Conversely, in Figure 3.7 we do observe several data points with similar IFT but with highly different oil retention.

One would expect that the YL equation (Eq. (3.3)) would not lead to exact predictions for oil breakthrough, but such a big difference was unexpected. As shown in the Experimental Section, we performed contact angle measurements by injecting small droplets of oil under the exact same SiC membrane used in our filtration experiments. In addition, the contact angle measurements were performed in the presence of surfactant and salt, at exactly the same concentrations used in our filtration tests. Therefore, our experiments took into account adsorption of surfactants at the membrane-interface as well as surfactants adsorption at the oil-water interface. Still the very large discrepancy between our findings and the predicted critical IFT clearly indicates a substantial difference between the measured macroscopic contact angle and the effective contact angle at the wall of the membrane pores [15, 35, 36]. This difference would also allow the surfactant-dependent critical IFT as observed by us.

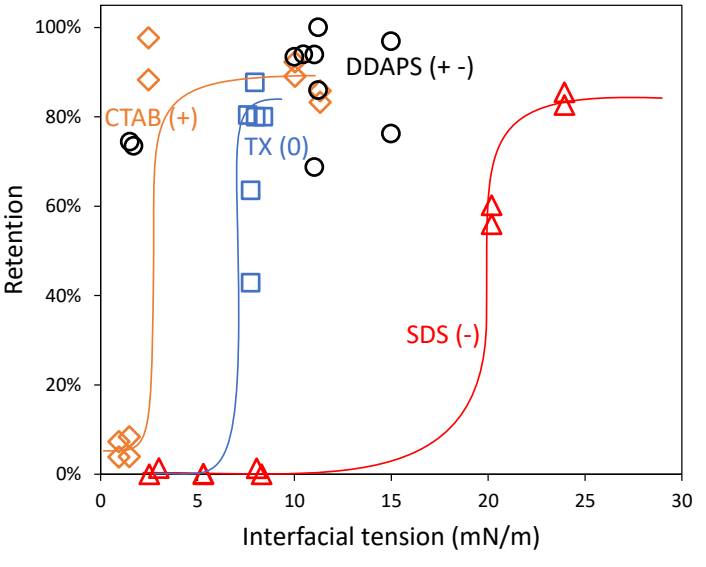

Figure 3.7: Oil retention of CTAB, SDS, DDAPS and TX stabilized emulsions as a function of IFT at a crossflow velocity of 7.6 cm/s and a transmembrane pressure of 0.1 bar. All the experiments were performed in duplicate, as shown.

In Figure 3.8, we show membrane water cleanability and chemical cleanability, as defined in section 3.2.5, as a function of surfactant concentration and ionic strength. For all the surfactants, the water cleanability slightly decreases by increasing surfactant concentration from 0.1 to 0.2 times CMC, while it increases from 0.2 to 1 times CMC (see Figure 3.8A). SDS and DDAPS present a really good water cleanability, probably due to their surface chemistry (zeta potential of these emulsions are described in the Experimental Section (3.2.2)). SDS is negatively charged as the SiC membrane, while DDAPS has a zwitterionic chemistry, well known for its anti-fouling properties [31]. Conversely, CTAB is positively charged , and may strongly interact with the negative SiC membrane (see zeta potential of CTAB emulsions and SiC membrane in Experimental Section (3.2.2)), resulting in poor water cleanability even at the lowest surfactant concentrations. These results are confirmed by adsorption studies of surfactants on model silica surfaces, which have a comparable surface chemistry to SiC [6, 37].

In figure 3.8B, we show the effect of ionic strength on water cleanability. SDS presents 100% flux recovery after cleaning with DI water, at all ionic strengths. For CTAB and TX we observe an increase in water cleanability as a function of ionic strength, while no clear trend is observed for DDAPS.

In Figure 3.8C and 3.8D, we show the effect of chemical cleaning, with acid and base as described in section 3.2.5, as a function of surfactant concentration and ionic strength, respectively. We can clearly see that chemical cleaning helps in recovering almost 100% of the original flux for all the surfactants tested, with exception for CTAB. CTAB fouls the worst and this fouling seems difficult to remove.

The downside of the combination of a charged membrane and a charged surfactant is that ionic surfactants are influenced dramatically by ionic strength increases. This effect is shown by the poor oil retentions of CTAB and SDS at high ionic strength and at CMC, and it is also extensively described in literature [38], where it is shown that the added salt reduces interfacial tension and screens the electrostatic interactions. These effects become evident at the ionic strengths we adopted. Real PW can have even higher ionic strengths (up to 3000 mM [39]) and therefore fouling, and oil permeation, can be worse. Such high ionic strengths lead to several issues, such as fast coalescence of oil droplets and surfactant precipitation, also in real PW. For this reason, and in order to study oil permeation and fouling from a fundamental point of view, in this work we only focus on ionic strengths up to 100 mM. Nonionic surfactants like TX do not show the same dependency on ionic strength but at the

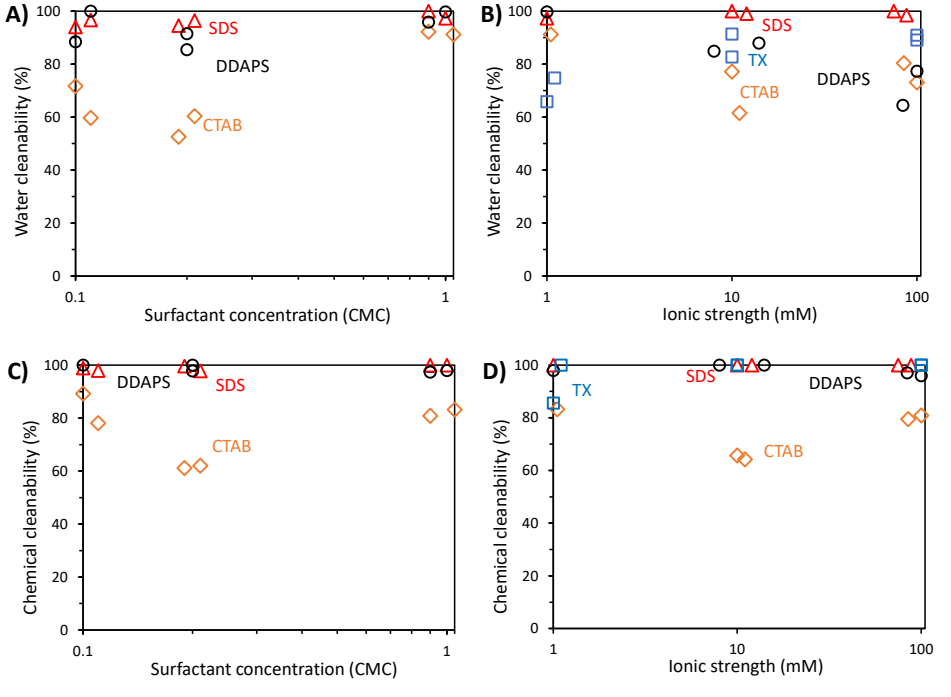

Figure 3.8: Water cleanability and chemical cleanability of CTAB, SDS, DDAPS and TX stabilized emulsions as a function of surfactant concentration (A) (C) and ionic strength (B)(D). With CMC (2391 mg/L for SDS, 346 mg/L for CTAB, 144 mg/L for TX and 1006 mg/L for DDAPS) we indicate the surfactant critical micelle concentration in absence of salt. All the experiments are performed in duplicate, as shown.

same time lack of electrostatic repulsion all together, showing very high flux declines probably due to denser cake layers. Even though the ionic strength does not have the same influence on TX, as with charged surfactants, it is still capable to reduce the oil retention.

Out of the four surfactants used, our results show that DDAPS is the most promising. At the investigated experimental conditions, DDAPS shows excellent retention and maintains a high flux, although it is influenced by a ionic strength increase. This is proved by the increased flux decline at 100 mM NaCl, while switching from 1 to 10 mM we have a lower flux decline. DDAPS gives high flux and high oil retention even at low surfactant concentrations. From a membrane treatment perspective, these results imply that zwitterionic surfactants offer the best characteristics for surfactant based oil recovery.

3.4 Conclusions

In this work, by tuning ionic strength and surfactant concentration of our PW, we controlled the oil-water interfacial tension and investigated its influence on oil breakthrough for a SiC CoMem© membrane. For this, we used synthetic PW, consisting of n-hexadecane stabilized by cationic CTAB, anionic SDS, zwitterionic DDAPS or nonionic TX. Surfactant concentrations studied were 0.1, 0.2 and 1 times CMC, while ionic strengths were 1, 10 and 100 mM NaCl. We discuss our results in the framework of the Young-Laplace equation, which predicts for a given membrane and pressure, a critical interfacial tension γ_{cr} below which oil permeation should occur. We observe such a transition from high to low oil retention with decreasing IFT for the anionic, cationic and nonionic surfactant, but with significantly higher critical IFTs then predicted. For the cationic CTAB, our membrane is performing less well, since oil retention drops for IFT values 3 times higher than the critical one. For the anionic SDS, the oil retention drops for IFT values almost 40 times higher than expected. For the nonionic TX we observe a relative drop in oil retention with increasing ionic strength for IFT values 15 times higher than predicted. On the other hand, the zwitterionic DDAPS was the only surfactant that did not show a critical IFT, even at the lowest IFT. We propose that our simple contact angle measurements do not take into account the complex interactions that occur at the wall of the membrane pores. These surfactants may play a crucial role, and as a consequence, at the pore wall we must expect a contact angle that is different from the one we measured. We can conclude that surfactants stabilized O/W emulsions have a critical IFT highly dependent on the type of

surfactant used. Additionally, our results point out that zwitterionic surfactants, that even at the lowest IFT did not present a critical IFT, are highly interesting for future studies and applications.

References

[1] E. T. Igunnu and G. Z. Chen, "Produced water treatment technologies", International Journal of Low-Carbon Technologies **9**, 157–177 (2014).

[2] B. R. Scanlon, R. C. Reedy, F. Male, and M. Walsh, "Water issues related to transitioning from conventional to unconventional oil production in the permian basin", Environmental Science & Technology **51**, 10903–10912 (2017), pMID: 28876906.

[3] A. Fakhrul-Razi, A. Pendashteh, L. C. Abdullah, D. R. A. Biak, S. S. Madaeni, and Z. Z. Abidin, "Review of technologies for oil and gas produced water treatment", Journal of Hazardous Materials **170**, 530 – 551 (2009).

[4] M. Cheryan and N. Rajagopalan, "Membrane processing of oily streams. wastewater treatment and waste reduction", Journal of Membrane Science **151**, 13 – 28 (1998).

[5] W. Guo, H.-H. Ngo, and J. Li, "A mini-review on membrane fouling", Bioresource Technology **122**, 27 – 34 (2012).

[6] J. M. Dickhout, J. M. Kleijn, R. G. H. Lammertink, and W. M. de Vos, "Adhesion of emulsified oil droplets to hydrophilic and hydrophobic surfaces effect of surfactant charge, surfactant concentration and ionic strength", Soft Matter **14**, 5452–5460 (2018).

[7] M. Fraga, S. Sanches, J. Crespo, and V. Pereira, "Assessment of a new silicon carbide tubular honeycomb membrane for treatment of olive mill wastewaters", Membranes **7**, 12 (2017).

[8] C. Brooks, M. DeCrescente, and D. Scola, "The wetting of silicon carbide surfaces", Journal of Colloid and Interface Science **27**, 772 – 788 (1968).

[9] T. Zsirai, K. Aljaml, H. Qiblawey, M. Al-Marri, A. Ahmed, S. Bach, S. Watson, and S. Judd, "Ceramic membrane filtration of produced water: Impact of membrane module", Separation and Purification Technology **165**, 214–221 (2016).

[10] A. Sadighzadeh, S. Mashayekhan, B. Nedaie, and A. Ghorashi, "Study of sintering temperature on the structure of silicon carbide membrane", Journal of Theoretical and Applied Physics **8**, 169–173 (2014).

[11] D. Abro, P. Dablé, F. Cortez-Salazar, V. Amstutz, and H. Girault, "Characterization of surface state of inert particles : Case of si and sic", Journal of Minerals and Materials Characterization and Engineering **4**, 62–72 (2016).

[12] J. Dickhout, J. Moreno, P. Biesheuvel, L. Boels, R. Lammertink, and W. de Vos, "Produced water treatment by membranes: A review from a colloidal perspective", Journal of Colloid and Interface Science **487**, 523 – 534 (2017).

[13] E. Virga, J. de Grooth, K. vab, and W. M. de Vos, "Stable polyelectrolyte multilayer-based hollow fiber nanofiltration membranes for produced water treatment", ACS Applied Polymer Materials **1**, 2230–2239 (2019).

[14] J. M. Dickhout, E. Virga, R. G. Lammertink, and W. M. de Vos, "Surfactant specific ionic strength effects on membrane fouling during produced water treatment", Journal of Colloid and Interface Science **556**, 12 – 23 (2019).

[15] B.-S. Kim and P. Harriott, "Critical entry pressure for liquids in hydrophobic membranes", Journal of Colloid and Interface Science **115**, 1–8 (1987).

[16] T. Darvishzadeh, V. V. Tarabara, and N. V. Priezjev, "Oil droplet behavior at a pore entrance in the presence of crossflow: Implications for microfiltration of oilwater dispersions", Journal of Membrane Science **447**, 442 – 451 (2013).

[17] A. A. Olajire, "Review of asp eor (alkaline surfactant polymer enhanced oil recovery) technology in the petroleum industry: Prospects and challenges", Energy **77**, 963 – 982 (2014).

[18] M. A. Migahed and A. M. Al-Sabagh, "Beneficial role of surfactants as corrosion inhibitors in petroleum industry: A review article", Chemical Engineering Communications **196**, 1054–1075 (2009).

[19] A. A. Olajire, "Corrosion inhibition of offshore oil and gas production facilities using organic compound inhibitors - a review", Journal of Molecular Liquids **248**, 775 – 808 (2017).

[20] J. Li, D. Mcclements, and L. Mclandsborough, "Interaction between emulsion droplets and escherichia coli cells", Journal of Food Science **66**, 570–657 (2006).

[21] R. Vácha, S. W. Rick, P. Jungwirth, A. G. F. de Beer, H. B. de Aguiar, J.-S. Samson, and S. Roke, "The orientation and charge of water at the hydrophobic oil dropletwater interface", Journal of the American Chemical Society **133**, 10204–10210 (2011), pMID: 21568343.

[22] K. B. Medrzycka, "The effect of particle concentration on zeta potential in extremely dilute solutions", Colloid and Polymer Science **269**, 85–90 (1991).

[23] H. Zhong, L. Yang, G. Zeng, M. L. Brusseau, Y. Wang, Y. Li, Z. Liu, X. Yuan, and F. Tan, "Aggregate-based sub-cmc solubilization of hexadecane by surfactants", RSC Adv. **5**, 78142–78149 (2015).

[24] S. R. Varade and P. Ghosh, "Foaming in aqueous solutions of zwitterionic surfactant: Effects of oil and salts", Journal of Dispersion Science and Technology **38**, 1770–1784 (2017).

[25] J. Binner and Y. Zhang, "Characterization of silicon carbide and silicon powders by xps and zeta potential measurement", Journal of Materials Science Letters **20**, 123–126 (2001).

[26] J. Eastoe, *Surfactant Aggregation and Adsorption at Interfaces*, chapter 4, 50–76 (John Wiley Sons, Ltd) (2009).

[27] J. Dickhout, R. Lammertink, and W. de Vos, "Membrane filtration of anionic surfactant stabilized emulsions: Effect of ionic strength on fouling and droplet adhesion", Colloids and Interfaces **3**, 9 (2019).

[28] K. Wojciechowski, M. Kucharek, W. Wróblewski, and P. Warszyski, "On the origin of the hofmeister effect in anion-selective potentiometric electrodes with tetraalkylammonium salts", Journal of Electroanalytical Chemistry **638**, 204 – 211 (2010).

[29] K. Babu, N. Pal, A. Bera, V. Saxena, and A. Mandal, "Studies on interfacial tension and contact angle of synthesized surfactant and polymeric from castor oil for enhanced oil recovery", Applied Surface Science **353**, 1126 – 1136 (2015).

[30] E. Virga, E. Spruijt, W. M. de Vos, and P. M. Biesheuvel, "Wettability of amphoteric surfaces: The effect of ph and ionic strength on surface ionization and wetting", Langmuir **34**, 15174–15180 (2018), pMID: 30427683.

[31] J. B. Schlenoff, "Zwitteration: Coating surfaces with zwitterionic functionality to reduce nonspecific adsorption", Langmuir **30**, 9625–9636 (2014), pMID: 24754399.

[32] Q. Shao, Y. He, A. D. White, and S. Jiang, "Difference in hydration between carboxybetaine and sulfobetaine", The Journal of Physical Chemistry B **114**, 16625–16631 (2010), pMID: 21086974.

[33] H. Kitano, M. Imai, K. Sudo, and M. Ide, "Hydrogen-bonded network structure of water in aqueous solution of sulfobetaine polymers", The Journal of Physical Chemistry B **106**, 11391–11396 (2002).

[34] Z. G. Estephan, P. S. Schlenoff, and J. B. Schlenoff, "Zwitteration as an alternative to pegylation", Langmuir **27**, 6794–6800 (2011), pMID: 21528934.

[35] M. García-Payo, M. Izquierdo-Gil, and C. Fernández-Pineda, "Wetting study of hydrophobic membranes via liquid entry pressure measurements with aqueous alcohol solutions", Journal of Colloid and Interface Science **230**, 420 – 431 (2000).

[36] G. Racz, S. Kerker, Z. Kovács, G. Vatai, M. Ebrahimi, and P. Czermak, "Theoretical and experimental approaches of liquid entry pressure determination in membrane distillation processes", Periodica Polytechnica Chemical Engineering **58**, 81–91 (2014).

[37] K. W. Trzaskus, S. L. Lee, W. M. de Vos, A. Kemperman, and K. Nijmeijer, "Fouling behavior of silica nanoparticle-surfactant mixtures during constant flux dead-end ultrafiltration", Journal of Colloid and Interface Science **506**, 308 – 318 (2017).

[38] X. Zhu, A. Dudchenko, X. Gu, and D. Jassby, "Surfactant-stabilized oil separation from water using ultrafiltration and nanofiltration", Journal of Membrane Science **529**, 159 – 169 (2017).

[39] S. Jiménez, M. Micó, M. Arnaldos, F. Medina, and S. Contreras, "State of the art of produced water treatment", Chemosphere **192**, 186 – 208 (2018).

4

Theory of Oil Fouling for Microfiltration and Ultrafiltration Membranes in Produced Water Treatment°

°In preparation as: **Ettore Virga**, Robert W. Field, P. M. Biesheuvel, and Wiebe M. de Vos, *Theory of Oil Fouling for Microfiltration and Ultrafiltration Membranes in Produced Water Treatment*, **2021**.

Abstract

Membrane filtration is a powerful method to remove oil from stable oil-in-water emulsions. This is especially attractive for the field of produced water (PW) treatment, where a complex water stream from the Oil&Gas industry, containing dispersed oil, surface-active components and salts, needs to be treated to meet strict environmental standards. Due to the complexity of this emulsion, the existing literature is still missing a mathematical tool that can describe the fouling in a fully quantitative manner on the basis of relevant fouling mechanisms. Such a model would benefit PW treatment with membranes by offering insight in the fouling mechanism, thereby providing clear directions to mitigate fouling. In this work, we present a quantitative model that describes cake layer formation and pore blocking for the typical situation where emulsion oil droplets are much larger than the membrane pore size. Here the degree of pore blocking is determined by the membrane contact angle and the resulting surface coverage, while the cake layer is described by a mass balance and a cake erosion flux. The model is validated by comparison to experimental data from previous works [1, 2] where membrane type, surfactant type and salinity were varied. Most input parameters could be directly taken from the experimental conditions, while only four fitting parameters were required. The experimental data can be well described by the model, using a very limited number of fitting parameters, providing insight into the dominant fouling mechanism. Moreover, where existing models usually assume that pore blocking precedes cake layer formation, here we find that cake layer formation can start and occur while the degree of pore blocking is still increasing, in line with the more dynamic nature of oil droplets filtration.

4.1 Introduction

One of the most difficult technological challenges in the field of environmental technology, with huge environmental impact, is the treatment and reuse of produced water (PW), a massive stream of oily wastewater originated from Oil & Gas (O&G) extraction. Globally, the ratio between the volume of water used per volume of oil extracted is expected to reach a number beyond 10 by 2025 due to the ageing of the wells [3], with over 30 billion of m^3 of produced water estimated for 2020 only [4]. Given the massive worldwide production of PW, the need for better PW treatment is of significant importance, especially in areas where water is already scarce and PW, if well treated, could be immediately reused in industry or agriculture [5].

Membranes have been demonstrated to successfully tackle the challenging separation of oil-in-water (O/W) emulsions like PW, even when the presence of small oil droplets ($<10\mu$m in diameter) makes treatment by other technologies ineffective [6]. Especially microfiltration (MF) and ultrafiltration (UF) membranes have been applied for the treatment of PW, as these membranes can potentially remove a great part of the oil at high water permeability [7–9].

However, the broader use of pressure-driven membranes for produced water treatment is still limited by membrane fouling [6, 10]. For MF and UF, fouling during PW treatment is mainly due to the deposition of oil droplets at the membrane interface, and it is often responsible for substantial flux declines and increases in operating costs. Normally, membrane fouling mechanisms can be grouped into four main categories (complete pore blocking, standard blocking, intermediate blocking, and cake layer formation [6, 7]) that will be later discussed in detail. Understanding and quantifying the mechanisms that lead to oil fouling in PW treatment, including the role of the chemistry of the emulsion and the membrane surface chemistry and pore size, are crucial for designing better membranes and to make more effective use of chemicals and process conditions to mitigate membrane fouling.

Many studies have investigated and tried to model fouling by O/W emulsions, such as PW, for MF and UF membranes. By far the largest part of these studies are based on Hermia's fouling model [11]. For example, Koltuniewicz *et al.* studied, for a variety of membranes, in both dead-end and crossflow experiments, the effect of pressure and crossflow velocity on flux decline [12]. Pan *et al.* prepared a tubular coal-based carbon MF membrane for with uniform pore structure and narrow pore size distribution and then modeled fouling with Hermia's model [13]. Salahi *et al.* employed the model to study the fouling mechanism of the filtration processes of different polymeric membranes

[14]. Abbasi *et al.* synthesized mullite ceramic MF membranes for treatment of oily wastewaters and investigated their fouling mechanisms [15]. Masoudnia *et al.* tested and also modeled fouling for polyvinylidene fluoride membranes under various operating conditions [16] by using Hermia's model. However, while Hermia's model is an excellent empirical model, it is only a qualitative tool as it does not predict fouling a priori but it is limited by a pure fitting. Moreover, an underlying assumption is that the fouling agents act as solids, while emulsion droplets are well known to be able to deform and coalesce.

Recently, other modeling studies focused mainly on oil droplet-membrane interactions. Salama *et al.* identified and modeled two basic mechanisms to explain fouling during oily wastewater filtration, i.e. fouling due to pinning of oil droplets and coalescence of oil droplets [17]. Tanudjaja *et al.* used classical models for colloid interactions, to quantify the foulant-membrane and foulant-foulant interactions [18]. Galvagno *et al.* have shown the existence of different equilibria regions (stable, bistable and unstable) which indicate if an oil droplet will deposit or not on a membrane surface [19]. Darvishzadeh *et al.* estimated analytically the critical permeation pressure from a force balance model that involves the drag force from the flow around the droplet and surface tension forces as well as the pressure variation inside the pore [20]. However, what is still missing in the existing literature is a tool that gives specific insights on the fouling mechanisms based on measurable emulsion (feed) properties (e.g. oil droplet size, oil permeation, oil-membrane contact angle, etc.). Such a model would benefit PW treatment with membranes by offering more insight into the membrane fouling, thereby indicating quantitative solutions to mitigate fouling.

In this work, we present a quantitative but still simple model which predicts flux decline over time in MF and UF systems based on feed and membrane properties. By modelling pore blocking as directly connected to the membrane/oil contact angle and the cake layer via a mass balance limited by an erosion flux, as shown in Figure 4.1, we get insights on how membrane fouling occurs. The model is validated by comparison to experimental data for varying membrane type, surfactant type and salinity of the feed stream. We find good agreement between the model and the experimental data. Moreover, where existing models usually predict that pore blocking precedes cake layer formation, here we find that these mechanisms are expected to occur simultaneously, due to the dynamic nature of the oil droplets.

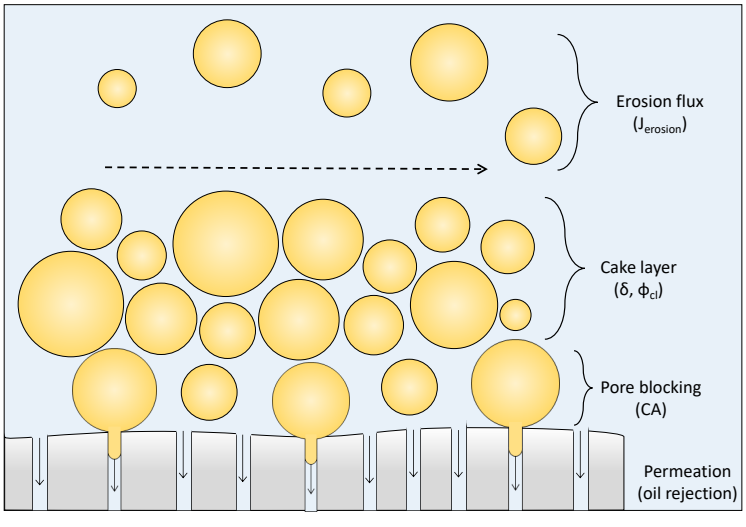

Figure 4.1: Illustration of membrane fouling by oil droplets and main parameters of cake layer, pore blocking, and erosion flux, i.e. erosion flux $J_{erosion}$, cake layer thickness δ, volume fraction of oil in the cake layer ϕ_{cl}, oil-membrane contact angle CA, and oil rejection by the membrane.

4.2 Theory

4.2.1 Fouling mechanisms

Membrane fouling in PW treatment for MF and UF usually refers to the deposition of substances on the membrane surface, such as oil droplets or solid particles. This causes a flux decline of the water phase permeating through the membrane, which indirectly allows us to determine the extent of fouling.

Fouling mechanisms are traditionally categorised into four different processes that can take place: complete pore blocking, standard pore blocking, intermediate blocking and cake layer filtration. In complete pore blocking, the pore is blocked by a large particle and no more water can pass through. In standard blocking, small particles coat the inside of the pores, narrowing the channels and thus lowering the flux. In intermediate blocking, particles build up on top of the membrane surface, narrowing the pore entrances. The fourth process is cake filtration which refers to the formation of a layer of particles on the surface of the membrane. This layer is not impermeable, but adds an additional resistance and sometimes also additional selectivity. Dickhout *et al.* proposed an additional fifth fouling mechanism which might play a role in membrane fouling by PW [7]. In this process, oil droplets are coalescing on the membrane surface, forming a patchy continuous oil layer on the surface.

As the oil droplets In PW are much larger than the membrane pores, in our model we describe fouling only in terms of complete pore blocking and cake layer filtration (processes 1 and 4 mentioned above). Fouling due to coalescence and formation of a continuous oil layer can be modeled as a limiting situation when the cake layer porosity is extremely low. The modelling of the combination of complete pore blocking and cake layer filtration is carefully described in the following sections.

4.2.2 Model hypotheses

In this work, a key assumption is to assume the cake layer porosity as constant, or in other words, of the volume fraction of the droplets that constitute the cake. We assume that in the cake layer we have a fixed volume fraction, which we call ϕ_{CL}, that is relatively constant across the cake. Of course, droplets could be squeezed, so ϕ_{CL} will be depth-dependent. Indeed, when they are deformable, and can be 'squeezed' to a more pancake-like structure, then the following scenario is possible. Namely, that with water flowing through the layer, then deepest in the layer, thus nearest to the membrane, the droplets

will be tightly squeezed, and the porosity (open fraction) in the layer will go down. This reduced porosity will increase the water velocity (in the remaining open space) even more and can lead to even more deformation. Beyond some point droplets will likely coalesce and/or be pushed through the pores of the membrane. These effects related to deformation of the droplets can be significant, especially for relatively large droplets with low surface tensions. If these phenomena do occur, we assume that such deformations take place during the first minutes of filtration. This allows us to assume a cake layer porosity that is constant over time and across the cake.

4.2.3 Equation for complete pore blocking

In this section we derive, to the best of our knowledge, a new formula to describe complete pore blocking by oil droplets, where we correlate the number of blocked pores directly to a measurable physical parameter, the oil-membrane (in water) contact angle.

Due to complete pore blocking, the resistance of the membrane, R_m, will increase with the permeate volume as more and more droplets are transported to the membrane surface. However, we can expect that an oil droplet in contact with the membrane surface will cover more or less pores depending on its affinity for the membrane material. This affinity results in a specific oil-membrane contact angle, CA, in water. For an oil droplet in contact with the membrane surface, the contact area A_{cont} can be expressed by

$$A_{cont} = \pi \left(\frac{d_p}{2} \sin\left(\pi - CA\right) \right)^2 . \tag{4.1}$$

If we consider the pores of the membrane fully blocked for CA<90° (high affinity between oil and membrane) we can then write the the area of the membrane A_{memb} covered because of oil adhesion A_{cov} as

$$A_{cov} = \sin^2\left(\pi - CA\right) \cdot A_{memb}. \tag{4.2}$$

At steady state, when all the oil droplets have been transported to the membrane surface and there is no room for more droplets on top of the same surface, the membrane resistance due to pore blocking will only depend on the contact angle, with $\mathrm{R}_m = \frac{R_0}{1-\sin^2(\pi - CA)}$. A low contact angle allows for more membrane pores to be open. A high affinity between oil droplets and membrane surface translates into lower contact angles and, as droplets spread more over the membrane surface, more pores will be "blocked".

With this in mind, and assuming that the membrane resistance goes exponentially to its steady state value, we can write how the membrane resistance R_m changes with pore blocking by

$$R_m = \frac{R_0}{1 - \sin^2(\pi - CA)} \cdot (1 - \sin^2(\pi - CA) \cdot e^{-\tau_{pb} v}) \tag{4.3}$$

where R_0 (m^{-1}) is the resistance of the clean membrane, CA is the oil contact angle measured for an oil droplet in contact with the membrane surface in water, v (L) is the permeate volume, and τ_{pb} (L^{-1}) a model parameter which indicates how fast the droplets adhere to the membrane surface. The equation is independent of the droplet size.

4.2.4 Equations for Cake Layer Filtration

In this section, we derive a new model for the dynamics of cake layer growth in crossflow filtration relevant for MF/UF of oily wastewaters, such as PW. The new model is here derived for the erosion rate J_{erosion} of a cake layer, i.e. flow rate of oil leaking from the cake layer per unit membrane area. We derive a result that shows how J_{erosion} depends on the thickness δ and water flow rate J_{w} through the membrane at any moment in time. Field et al. previously modified Hermia's expressions to account for a removal term [21, 22] in the calculation of the flux decline. However, we are not aware of an expression for erosion flux similar to the one we derive that can be directly used in a cake layer mass balance and which thereby allows for a self-consistent calculation of the growth of the cake layer and the resulting decline of water flux.

The expression we will derive for J_{erosion} is part of a total model that has two additional equations. These two additional equations are as follows. The first one is an expression for the flow rate J_{w} versus membrane resistance R_{m}, cake layer permeability k, and thickness δ

$$J_w = \frac{\Delta P}{\mu(R_m + k\delta)} \tag{4.4}$$

with ΔP (Pa) the pressure applied across the membrane, $k = \frac{150\delta\phi_{CL}^2}{D_p^2(1-\phi_{CL})^3}$ (m^{-1}) is a permeability parameter that derives from the KozenyCarman equation, ϕ_{cl} the volume fraction of oil in the cake layer, and D_p (m) is the average diameter of the oil droplets. The second equation is a mass balance for the

total amount of material in the cake (e.g. oil droplets)

$$\phi_{cl}\frac{d\delta}{dt} = J_w \cdot (\phi_\infty - \phi_{perm}) - J_{erosion}, \tag{4.5}$$

where ϕ_{cl}, ϕ_∞ and ϕ_{perm} are the volume fractions of oil in the cake layer, in the bulk of the feed, and in the permeate, respectively. For a constant cake layer volume fraction, ϕ_{cl}, this mass balance can be expressed as a time dependence of thickness. This mass balance includes the erosion rate and also advective 'addition' of fresh material into the cake, and 'leakage' of droplets from cake through the membrane to the permeate side.

Though this full model consists of three equations, they can be combined into one long ordinary differential equation (ODE), but for numerical modeling (e.g., using commercial spreadsheet softwares) this is not necessary, and the several required equations can be solved 'side by side'. It is useful to rewrite Eq. (4.5) such that it does not explicitly depend on time, t, but that it depends on the permeated volume, v. Differentiating with respect to the permeate volume v and taking into account that $\frac{dv}{dt} = J_w \cdot A_m$, where A_m (m^2) is the membrane area, we can rewrite Eq. (4.5) to

$$A_m\phi_{cl}\frac{d\delta}{dv} = \phi_\infty - \phi_{perm} - \frac{J_{erosion}}{J_w}. \tag{4.6}$$

In solving this model, we can 'step through time' using an explicit or implicit (Euler) scheme. Interestingly, to arrive at an analytical equation for water flow as function of time t or volume v, actually quite stringent simplifications must be made, and in this paper we will not discuss that research direction. Instead we only present results of the full numerical analysis based on Eqs. (4.3), (4.4), and (4.6). All parameter settings are described in Appendix B, Table B1. We solve the new model dynamically, for a one-dimensional geometry, for a given applied pressure. But in future work, also other simulations are possible where the setpoint for transmembrane pressure is changed (e.g., stepwise), and we follow in time the change of cake layer thickness and flow rate as they respond to the change in pressure. Our mathematical model can describe these situations as well.

The erosion flux serves to limit the growth of the cake layer, i.e., the thicker it gets, the larger will be the erosion flux. Therefore, there will always be a finite cake layer thickness, not growing indefinitely. The erosion flux also depends on the transmembrane water flow rate, J_{w}, because the higher J_{w}, the more it is the case that particles are pushed on one another, i.e., the stronger,

the more resilient, will be the structure, better able to withstand a certain shear force.

How to derive an expression for the erosion flux, J_{erosion}, that depends on water flow rate and on cake layer thickness? The following approach leads to a simple but insightful expression for J_{erosion}. We define coordinate x to start at the membrane surface, directed towards the top of the cake layer, which is located at $x = \delta$, i.e., δ is the cake layer thickness. The model is based on the following approach. At each position in the layer particles (droplets) are 'jammed' into place, i.e., they are more or less strongly 'locked' in place between upper and lower layers. And the more strongly they are locked in place, the less likely will it be for an 'erosion event' to occur, for droplets to make a certain shift in position along one another, similar to layers sliding past one another. This moment of force is proportional the force by which all upper layers push on a certain layer of particles [23]. Here 'upper' refers to all material (droplets) between position x and position δ. The water flowing through the layer pulls on each 'differential layer', dx, by a force that is proportional to J_{w} and is inversely proportional to the cake layer permeability, k. This is Darcy's law. Thus the force acting on the particles at position x equals the pressure drop over the layer on top, due to water flow, i.e.,

$$\text{lock-in force} \propto J_{\text{w}} \left(\delta - x\right) / k \,. \tag{4.7}$$

The next step is to assume that the likelihood, or frequency, of an 'erosion event', a stochastic process, depends by an exponential power on the sum of forces that act on a layer of particles or droplets. One contribution is the shear force that is applied to the cake layer. The fluid that passes the cake layer drags on it by a force that is counteracted by shear stresses that develop inside the cake layer. For a planar cake layer, this stress that is exerted in a direction parallel to the membrane, τ, is independent of depth x, i.e., at each position in the layer the particles are subjected to the same stress, in the direction along the membrane. It is not the case that deeper layers are cushioned somehow from this effect. This statement is the result of a force balance on an elastic layer that is clamped (fixed in space) on one end, and subjected to a shear force on the other end: the stresses in the layer are everywhere the same, independent of depth. This term τ is what drives the erosion process. This tendency to erode can be reduced by the earlier-described moments of force or lock-in effect. These two effects are now combined into an expression for the frequency of an erosion event, which we describe by

$$\mathcal{F} = \exp\left(\tau - \alpha \cdot \left(\delta - x\right) J_{\text{w}}\right) \tag{4.8}$$

where we introduce a factor α, which is inversely proportional to permeability k, multiplied by an unknown factor to translate from force to an 'transition energy' for an erosion event to occur. A similar prefactor could also be placed in front of τ and another one in front of the entire exp-term, but they will ultimately be combined with the unknown τ anyway, so there is no need to add them at this stage.

Thus, the above equation predicts the likelihood of an erosion event at a certain position x. We can assume that the total erosion at that position in the layer, i.e., the relative movement of material past one another, is proportional to this likelihood. And we can assume that the erosion of the full layer, is then given by this term, integrated over the full layer thickness. We then arrive at

$$J_{\text{erosion}} = \int_0^{\delta} \mathcal{F} \mathrm{d}x = \frac{\beta}{\alpha\, J_{\text{w}}} \left(1 - \exp\left(-\alpha \delta J_{\text{w}}\right)\right) \tag{4.9}$$

where $\beta = \exp(-\tau)$. We could have implemented additional prefactors, in the transformation from likelihood to total erosion flux, but these factors all simply end up in β.

For low thickness or low water flow rates, the expression for erosion flux simplifies to

$$J_{\text{erosion}} = \beta \delta \tag{4.10}$$

irrespective of water flow rate. In this limit, there simply is no 'stabilization' at all, and the erosion likelihood is $\exp(\tau)$, equal at all positions in the (thin) layer. Thus, the 'amount of' erosion scales linearly with layer thickness. In any calculation, even at high τ, with this expression for J_{erosion}, the theory predicts there always is a cake layer, with at least a fleetingly small thickness. The other limit is that of a thick layer or large water flow rate, and in that case the erosion flux levels off at $J_{\text{erosion}} = \beta / (\alpha\, J_{\text{w}})$, i.e., now the erosion flux has become independent of thickness, only of water flow rate. In this case, inner layers are so strongly pushed on one another, the likelihood of an erosion event deep in the layer is vanishingly small, and erosion events can only occur in the top of the cake layer, and the more of them, thus more erosion, at low values of the stabilizing force, which is the transmembrane water flow. Because this water flow decreases when the layer grows, the theory will lead to a finite steady-state layer thickness.

This finalizes our explanation of the new expression for J_{erosion} which can be used in the full model for the dynamics of cake layer growth, Eq. (4.6). Note that our calculations make use of the full numerical equation for J_{erosion} of Eq. (4.9), and we do not use any of the simplifications just discussed. However, in

the experimental condition modeled, our results were independent from α (see table B1, Appendix B) and therefore we could have referred to the simplified equation for J_{erosion}, i.e. Eq. (4.10).

4.2.5 Model implementation

In this section we explain how to use and apply the attached spreadsheet model to describe and gain a better understanding of experimental data collected for crossflow filtration of O/W emulsions. For this, it is important that the experimental data are of high quality, and that flux of water through the membrane, J_w, is given as a function of permeate volume. Moreover, the applied pressure, , oil content in both feed and permeate, oil-membrane contact angle in surfactant aqueous solution, CA, and feed emulsion properties, such as droplet size, D_p, and viscosity, μ, need to be measured and provided. We first discuss the measured experimental parameters essential as input to the model calculations, while subsequently we discuss the four fitting parameters that were used to obtain a better understanding of the previously discussed fouling mechanisms.

The measured process and physical parameters from experimental data used to numerically solve Eq. (4.6), and therefore calculate the cake layer thickness δ (m), are the applied pressure (Pa), the membrane surface area A_{memb} (m^2), the feed viscosity μ (Pa·s), the average diameter of the oil droplets D_p (5 $/micro$m [1, 2]), and the oil volume fraction in the retentate, $\phi_\infty - \phi_{perm}$, ratio between oil retention (from our previous work [1, 2]) and density. The experimental parameters that we measured to calculate the membrane resistance due to pore blocking R_m (m^{-1}) via Eq. (4.3) are the oil-membrane contact angle CA (°), reported in Table B1 (Appendix B), and the resistance of the clean membrane R_0 (m^{-1}). In all cases the permeate volume v (L) is variable.

On the other hand, some parameters need to be assumed in order to fit the experimental data. To calculate the membrane resistance due to pore blocking R_m (m^{-1}) the only fitting parameter is τ_{pb} (Eq. (4.3)), which accounts for how fast droplets adhere and block (spread over) the membrane pores. To calculate the cake layer thickness δ (m), three parameters need to be fitted. One is the volume fraction of oil in the cake layer ϕ_{cl}, while the other two are used to calculate the cake erosion flux $J_{erosion}$, and they are α and β (see Eq. (4.6) and Eq. (4.9)).

4.3 Results and Discussion

In this section we compare our model predictions with experimental data from our previous work [1, 2]. We show how our model, described in the previous section, allows for quantitative prediction of membrane fouling as a function of membrane type, surfactant type and feed salinity, and provides an excellent description of the experimental data. The results of our model offer to the reader the opportunity to link quantitatively the main fouling phenomena during filtration of oily wastewater (i.e. pore blocking and cake layer) to experimental evidence of such phenomena for MF/UF systems. The results of this section open up new pathways for membrane fouling understanding, prevention and control.

4.3.1 Effect of membrane type

The type of membrane used during filtration will be quite important in its fouling behaviour. Membrane surface chemistry, roughness, pore size, and charge can all influence the interaction with and retention of oil droplets and thereby fouling [10]. In this work, we modeled the fouling behaviour for two different types of membrane. One is a commercially applied ceramic membrane based on silicon carbide (SiC) [2].The other one is a regenerated cellulose (RC) membrane [1, 24].

Figure 4.2 shows the flux decline for SiC and RC membranes during cross-flow filtration of CTAB-stabilized O/W emulsions with 1 mM NaCl as background salt. Further details on the experimental conditions are reported in our previous work [1, 2], while the model parameters used are reported in Table B1 of Appendix B. The results are expressed in terms of normalized flux as a function of permeate volume per unit of membrane area (L/m^2).

Figure 4.2A shows that indeed surface chemistry plays a crucial role in membrane fouling, as the RC membrane reports a lower flux decline compared to the SiC membrane. While we do observe only a ∼20% flux decline for the RC membrane, fouling is more severe for the SiC membrane with ∼50% flux decline. The model describes the experimental data very well, and can provide us with insights that we cannot simply obtain from pure experimental data, i.e. by only looking at the reported flux decline curves of Figure 4.2A. Figure 4.2B shows the trend of cake layer thickness and areas of the pores blocked (due to pore blocking) by the oil as a function of permeate volume. Pore blocking is the main mechanism responsible for the flux decline, with up to ∼50% of blocked area for SiC membrane and only ∼20% for the RC membrane. This

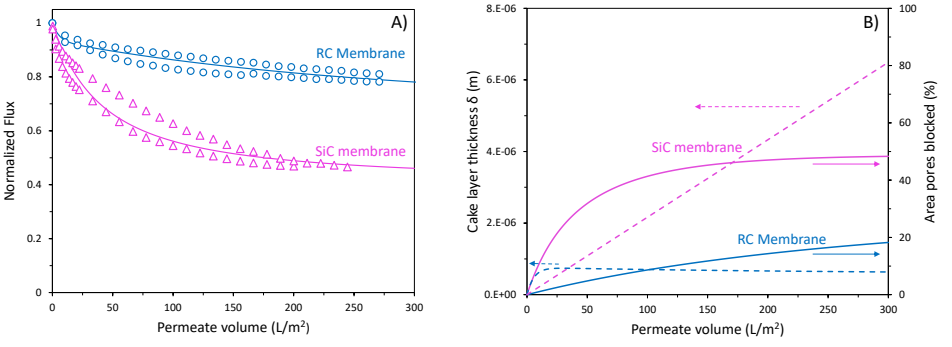

Figure 4.2: A) Flux decline and B) cake layer thickness, δ, and Area of blocked pores (%), for CTAB (345 mg/L, 1 mM NaCl) stabilized emulsions for SiC and regenerated cellulose (RC) membranes. For SiC membrane: pore size = 150 nm, water permeability = 3000 $Lm^{-2}h^{-1}bar^{-1}$, crossflow velocity = 7.6 cm/s, TMP = 0.1 bar. For RC membrane: pore size = 40-80 nm, water permeability = 200 $Lm^{-2}h^{-1}bar^{-1}$, crossflow velocity = 20 cm/s, TMP = 1 bar. Symbols represent data points from our previous experiments [1, 2], while lines are generated by the present model. All the experiments were performed in duplicate, as shown.

is in line in with the values that we observed from the flux decline curves, as the decrease in flux is proportional to the area of the membrane where the pores are blocked. Additionally, our model points out that pore blocking occurs faster for SiC than for the RC membrane. The cake layer remains thin and does not constitute the main resistance to the water flux, we can see that the cake layer thickness is higher for SiC than for the RC membrane, in agreement with the higher crossflow velocity applied in the experiments with the RC membrane. A higher crossflow velocity translates into a higher erosion flux which decreases the thickness of the cake layer. Another reason behind the higher cake layer thickness for SiC can be found in the higher water permeability, and therefore drag force acting on the oil droplets and pushing them to the membrane interface. Overall our model thus confirms that the different fouling behaviour of two membranes with different surface chemistries (by identical emulsions), can be well explained by the way that the oil droplets spread over the membranes surface. SiC has a high negative surface charge, while the emulsion was stabilized by cationic surfactant, likely leading to a lower contact angle compared to the lesser charged RC membrane (Table B1, Appendix B).

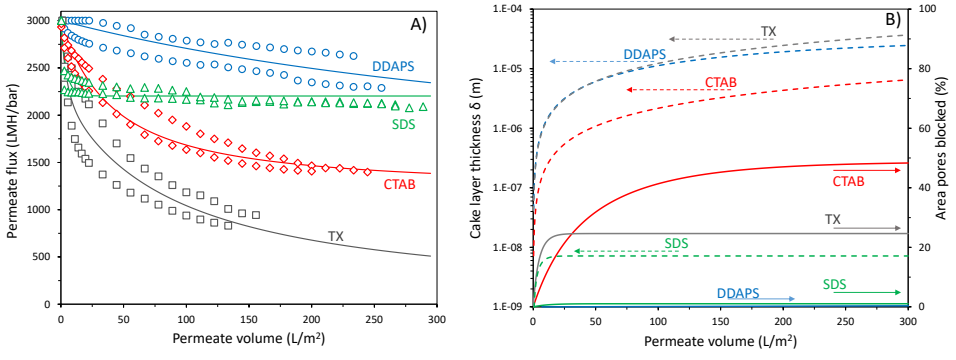

Figure 4.3: A) Flux decline and B) cake layer thickness, δ, and Area of blocked pores (%), for stabilized emulsions filtered by a SiC membrane as a function of surfactant type for SDS (2390 mg/L), CTAB (345 mg/L), DDAPS (1005 mg/L) and TX (145 mg/L) in presence of 1mM NaCl. Pore size = 150 nm, water permeability = 3000 $Lm^{-2}h^{-1}bar^{-1}$, crossflow velocity = 7.6 cm/s, TMP = 0.1 bar. Symbols represent data points from our previous experiments [2], while lines are generated by the present model. All the experiments were performed in duplicate, as shown.

4.3.2 Effect of surfactant type

Surfactants have strong effects on membrane fouling by oily-wastewater, as these molecules adsorb at the oil-water and membrane-water interface, influencing the mutual interaction between the droplets in the fouling layer and as well the membrane surface chemistry [1, 7, 25, 26].

Figure 4.3 shows the effect of surfactant chemistry on flux decline during crossflow filtration with the SiC membrane of surfactant-stabilized O/W emulsions. Anionic SDS, cationic CTAB, zwitterionic DDAPS, and nonionic TX were used to stabilize the emulsions. All the experiments here reported were performed at low salinity (1 mM NaCl) to better show the effect of surfactant chemistry on flux decline. In Figure 4.3A we can observe that nonionic TX fouls the most, while the zwitterionic DDAPS fouls the least. The cationic CTAB fouls more than SDS, in agreement with their respective charges compared to that of anionic membrane.

The model again really well describes the flux decline curves. Moreover, it provides us with interesting results that can help us to better understand the specific fouling mechanisms and reasons hidden behind the observed flux decline. Figure 4.3B shows that while for the cationic CTAB pore blocking is the dominating mechanism, with a ~50% of pores blocked area, for the anionic a rather dense oil layer prevails (~0.93, table B1, Appendix B). On

the other hand, while for DDAPS we do not observe any pore blocking, in line with the known antifouling property of zwitterions, we do observe a relatively thick ($\sim$25μm) cake layer, although with a low resistance and thus a very limited effect on the flux. For TX both fouling mechanisms are quite strong, with around 25% blocked area and highest cake layer thickness $\sim$35μm. Additionally, it is important to that for TX the layer is quite dense. Without charges the oil droplets are likely not as well stabilized by TX as by the other surfactants leading to a dense cake layer and possibly to droplet coalescence.

Finally, we can attribute the high thickness of the cake layer obtained for TX and DDAPS O/W emulsion to the lower erosion flux (see table B1), which is in line with the neutral net charge of these surfactants. It is expected that if surfactants are not charged, the repulsive forces between the surfactants and therefore the droplets are way lower than for charged surfactants. This makes the cake layer more resistant and more difficult to erode, compared to a CTAB or SDS stabilized cake layer where repulsive forces between the droplets dominate as a consequence of the fact that surfactant of same charge (positive or negative) are stabilizing the oil droplets.

Our model thus describes in a very nice way how the fouling mechanisms can change when the emulsion droplets are stabilized by different surfactant types.

4.3.3 Effect of salinity

Salinity is know to have substantial effects on oil droplets stability and membrane fouling, especially in the case of charged surfactants [1, 7, 10, 27]. Figure 4.4 shows the effect of salinity on both SiC and RC membranes for anionic SDS based emulsions. While in the case of SiC an increase in salinity translates into reduced fouling, for the RC membrane it is the opposite. Here the model gives us insights on such behavior.

The main reason for the lower flux decline observed for the SiC membrane is the fact that nearly all the oil passes through the SiC membrane [2], and therefore it does not block the membrane pores or lead to the formation of a cake layer. On the other hand, the oil is mainly retained by the RC membrane, and therefore we do observe both pore blocking and cake layer mechanisms. This difference in oil permeation is mainly due to the fact that the SiC membrane was tested at higher concentrations of SDS (2390 mg/L) than RC membrane (460 mg/L), which translates into higher droplet deformability and therefore increased oil passage.

For the SiC membrane filtrating SDS stabilized emulsions, higher ionic

strengths translate into lower decline of the water flux through the membrane. At higher salinity, the interfacial tension of the droplets becomes even lower further increasing oil permeation and thus reducing the amount of oil that can foul the membrane.

For the RC membrane, where the oil is retained a thicker cake layer is observed for all ionic strengths (∼13-40μm), an some pore blocking is observed, ∼20% of blocked pores area for 1 mM, which then increases to ∼30% for 10 mM, to finally fall to zero for 100 mM. However, it is the cake layer resistance that dominates as the porosity is low. Moreover, the density of the cake layer increases with salinity, again suggesting the presence of a rather dense oil cake layer on top of the membrane. At a higher salinity the charge repulsion between the emulsion droplets will be smaller, allowing a smaller distance between the droplets, moreover coalescence also become much more likely.

To conclude, the model can also provide a good description for for the complex effects on membrane fouling at different salinities. Higher oil permeation with increasing salinity reduces the amount of oil that can foul the membranes as observed for the SiC membrane. For the RC membrane where the oil is well retained the density of the cake layer becomes the key in understanding the increasing fouling at higher salinities, where a reduction in charge repulsion between droplets allows a more compact cake layer.

4.4 Conclusions

In this work, we have presented and validated a new quantitative fouling model able to describe cake layer formation and pore blocking for membrane fouling of porous membranes during PW treatment. The model is used to describe experimental data of previous works [1, 2] where membrane type, surfactant type and salinity of the feed stream were varied. Most input parameters could be directly taken from the experimental conditions, while only four fitting parameters were required. In our model the degree of pore blocking is determined by the membrane contact angle and the resulting surface coverage, while the cake layer is described by a mass balance and a cake erosion flux.

Overall our model confirms that the different fouling behaviour of two membranes with different surface chemistries (by identical emulsions), can be well explained by the way that the oil droplets spread over the membranes surface thereby blocking the membrane pores. Our model also describes in a very nice way how the fouling mechanisms can change when the emulsion droplets are stabilized by different surfactant types, and can provide a good description

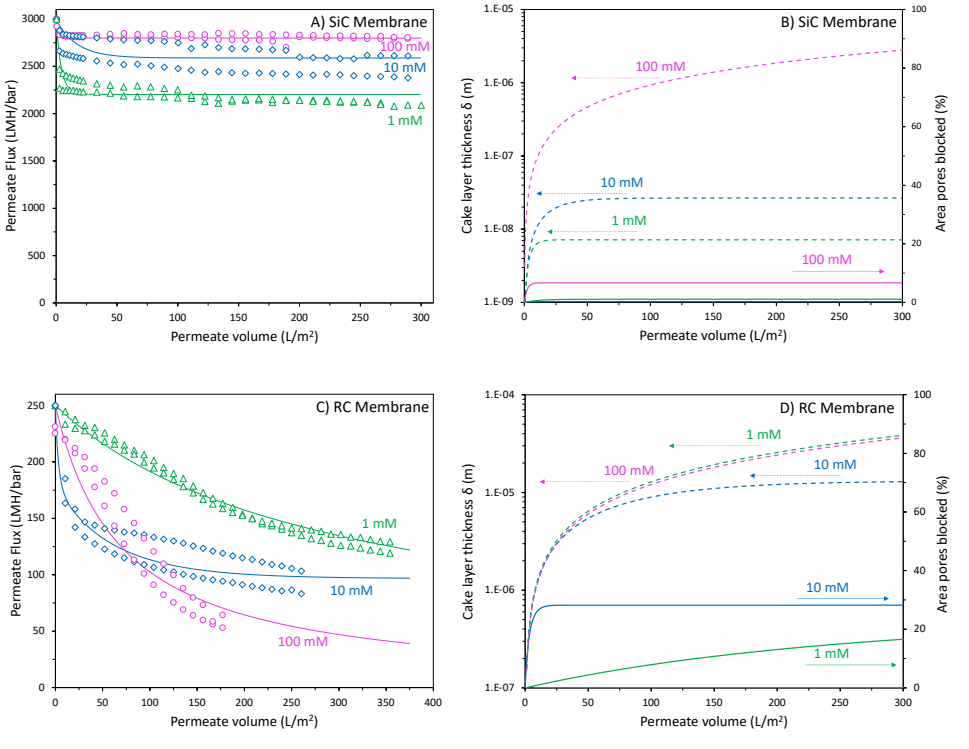

Figure 4.4: Flux decline and cake layer thickness, δ, and Area of blocked pores (%), respectively, of SDS stabilized emulsions for A)B) SiC and C) D) regenerated cellulose (RC) membranes as a function of salinity (1, 10 and 100 mM NaCl). A) and B): pore size = 150 nm, water permeability = 3000 $\mathrm{Lm^{-2}h^{-1}bar^{-1}}$, crossflow velocity = 7.6 cm/s, TMP = 0.1 bar, and 2391 mg/L SDS. C) and D): pore size = 40-80 nm, water permeability = 200 $\mathrm{Lm^{-2}h^{-1}bar^{-1}}$, crossflow velocity = 20 cm/s, TMP = 1 bar, and 463 mg/L SDS. Symbols represent data points from our previous experiments [1, 2], while lines are generated by the present model. All the experiments were performed in duplicate, as shown.

for the complex effects on membrane fouling at different salinities. Higher oil permeation with increasing salinity reduces the amount of oil that can foul the membranes as observed for the SiC membrane. For the RC membrane where the oil is well retained the density of the cake layer becomes a predominant factor in understanding the increasing fouling at higher salinities, where a reduction in charge repulsion between droplets allows a more compact cake layer. These results open up new pathways for membrane fouling understanding, prevention and control.

References

[1] J. M. Dickhout, E. Virga, R. G. Lammertink, and W. M. de Vos, "Surfactant specific ionic strength effects on membrane fouling during produced water treatment", Journal of Colloid and Interface Science **556**, 12–23 (2019).

[2] E. Virga, B. Bos, P. M. Biesheuvel, A. Nijmeijer, and W. M. de Vos, "Surfactant-dependent critical interfacial tension in silicon carbide membranes for produced water treatment", Journal of Colloid and Interface Science **571**, 222–231 (2020).

[3] M. A. Al-Ghouti, M. A. Al-Kaabi, M. Y. Ashfaq, and D. A. Dana, "Produced water characteristics, treatment and reuse: A review", Journal of Water Process Engineering **28**, 222–239 (2019).

[4] A. Echchelh, T. Hess, and R. Sakrabani, "Reusing oil and gas produced water for irrigation of food crops in drylands", Agricultural Water Management **206**, 124–134 (2018).

[5] M. Wenzlick and N. Siefert, "Techno-economic analysis of converting oil gas produced water into valuable resources", Desalination **481**, 114381 (2020).

[6] E. Tummons, Q. Han, H. J. Tanudjaja, C. A. Hejase, J. W. Chew, and V. V. Tarabara, "Membrane fouling by emulsified oil: A review", Separation and Purification Technology **248**, 116919 (2020).

[7] J. Dickhout, J. Moreno, P. M. Biesheuvel, L. Boels, R. Lammertink, and W. M. de Vos, "Produced water treatment by membranes: A review from a colloidal perspective", Journal of Colloid and Interface Science **487**, 523–534 (2017).

[8] M. Ebrahimi, K. S. Ashaghi, L. Engel, D. Willershausen, P. Mund, P. Bolduan, and P. Czermak, "Characterization and application of different ceramic membranes for the oil-field produced water treatment", Desalination **245**, 533–540 (2009), engineering with Membranes 2008.

[9] M. Ebrahimi, D. Willershausen, K. S. Ashaghi, L. Engel, L. Placido, P. Mund, P. Bolduan, and P. Czermak, "Investigations on the use of different ceramic membranes for efficient oil-field produced water treatment", Desalination **250**, 991–996 (2010).

[10] S. Huang, R. H. Ras, and X. Tian, "Antifouling membranes for oily wastewater treatment: Interplay between wetting and membrane fouling", Current Opinion in Colloid Interface Science **36**, 90–109 (2018), wetting and Spreading.

[11] J. Hermia, "Constant pressure blocking filtration law application to powder-law non-newtonian fluid", Trans. Inst. Chem. Eng. **60**, 183–187 (1982).

[12] A. Koltuniewicz, R. Field, and T. Arnot, "Cross-flow and dead-end microfiltration of oily-water emulsion. part i: Experimental study and analysis of flux decline", Journal of Membrane Science **102**, 193–207 (1995), engineering of Membrane Processes II Environmental Applications.

[13] Y. Pan, W. Wang, T. Wang, and P. Yao, "Fabrication of carbon membrane and microfiltration of oil-in-water emulsion: An investigation on fouling mechanisms", Separation and Purification Technology **57**, 388–393 (2007).

[14] A. Salahi, M. Abbasi, and T. Mohammadi, "Permeate flux decline during uf of oily wastewater: Experimental and modeling", Desalination **251**, 153–160 (2010).

[15] M. Abbasi, M. R. Sebzari, A. Salahi, and B. Mirza, "Modeling of membrane fouling and flux decline in microfiltration of oily wastewater using ceramic membranes", Chemical Engineering Communications **199**, 78–93 (2012).

[16] K. Masoudnia, A. Raisi, A. Aroujalian, and M. Fathizadeh, "Treatment of oily wastewaters using the microfiltration process: Effect of operating parameters and membrane fouling study", Separation Science and Technology **48**, 1544–1555 (2013).

[17] A. Salama, "Modeling of flux decline behavior during the filtration of oily-water systems using porous membranes: Effect of pinning of non-permeating oil droplets", Separation and Purification Technology **207**, 240–254 (2018).

[18] H. J. Tanudjaja and J. W. Chew, "Assessment of oil fouling by oil-membrane interaction energy analysis", Journal of Membrane Science **560**, 21–29 (2018).

[19] M. Galvagno and G. Z. Ramon, "Hydrodynamiccolloidal interactions of an oil droplet and a membrane surface", Langmuir **36**, 2858–2864 (2020), pMID: 32101009.

[20] T. Darvishzadeh, B. Bhattarai, and N. V. Priezjev, "The critical pressure for microfiltration of oil-in-water emulsions using slotted-pore membranes", Journal of Membrane Science **563**, 610–616 (2018).

[21] R. Field, D. Wu, J. Howell, and B. Gupta, "Critical flux concept for microfiltration fouling", Journal of Membrane Science **100**, 259 – 272 (1995).

[22] R. W. Field and J. J. Wu, "Modelling of permeability loss in membrane filtration: Re-examination of fundamental fouling equations and their link to critical flux", Desalination **283**, 68–74 (2011), special issue in honour of Professor Tony Fane on his 70th Birthday.

[23] S. Kuiper, C. van Rijn, W. Nijdam, G. Krijnen, and M. Elwenspoek, "Determination of particle-release conditions in microfiltration: a simple single-particle model tested on a model membrane", Journal of Membrane Science **180**, 15–28 (2000).

[24] J. M. Dickhout, R. G. H. Lammertink, and W. M. de Vos, "Membrane filtration of anionic surfactant stabilized emulsions: Effect of ionic strength on fouling and droplet adhesion", Colloids and Interfaces **3** (2019).

[25] D. Lu, T. Zhang, and J. Ma, "Ceramic membrane fouling during ultrafiltration of oil/water emulsions: Roles played by stabilization surfactants of oil droplets", Environmental Science & Technology **49**, 4235–4244 (2015), pMID: 25730119.

[26] T. A. Trinh, Q. Han, Y. Ma, and J. W. Chew, "Microfiltration of oil emulsions stabilized by different surfactants", Journal of Membrane Science **579**, 199–209 (2019).

[27] E. N. Tummons, J. W. Chew, A. G. Fane, and V. V. Tarabara, "Ultrafiltration of saline oil-in-water emulsions stabilized by an anionic surfactant: Effect of surfactant concentration and divalent counterions", Journal of Membrane Science **537**, 384–395 (2017).

Part II

Dense Membranes

5

Stable Polyelectrolyte Multilayer-Based Hollow Fiber Nanofiltration Membranes for Produced Water Treatment°

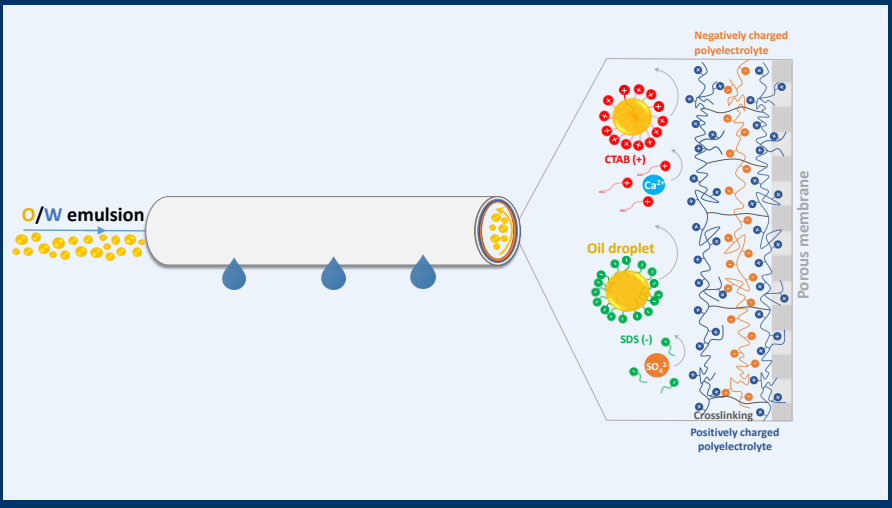

°Published as: **Ettore Virga**, Joris de Grooth, Klara Zvab, and Wiebe M. de Vos, *Stable Polyelectrolyte Multilayer-Based Hollow Fiber Nanofiltration Membranes for Produced Water Treatment*, ACS Applied Polymer Materials **2019**, *1*, 2230-2239.

Abstract

Produced water (PW) constitutes a massive environmental issue due to its huge global production as well as its complexity and toxicity. Membrane technology could, however, convert this complex wastestream into an important source of water for re-use, but new and more efficient membranes are required. In particular, in the last years, polyelectrolyte multilayers established themselves as a very powerful method to prepare hollow fiber based NF membranes, and this membrane type and geometry would be ideal for PW treatment. Unfortunately, the presence of surfactants in PW can affect the stability of polyelectrolyte multilayers. In this work, we investigate the stability of polyelectrolyte multilayers towards different types of surfactant, initially on model surfaces. We find that chemically stable multilayers, such as Poly(diallyldimethylammonium chloride)(PDADMAC)/Poly(sodium 4-styrene sulfonate)(PSS), based only on electrostatic interactions, are substantially desorbed by charged surfactants. For Poly(allylamine hydrochloride)(PAH)/PSS multilayers, however, we demonstrate that chemical crosslinking by glutaraldehyde, leads to surfactant stable layers. These stable PEM coatings can also be applied on hollow fiber support membranes to create hollow fibre NF membranes dedicated for PW treatment. Increased crosslinking time leads to more stable and more selective separation performance. These newly developed membranes were subsequently studied for the treatment of synthetic PW, consisting of freshly prepared oil-in-water emulsions stabilized by Hexadecyltrimethylammonium bromide (CTAB) and Sodium dodecyl sulfate (SDS), in the presence of a mixture of ions. For both types of produced water, the membranes show excellent oil removal ($\sim 100\%$) and organics removal (TOC reduced up to $\sim 97\%$) as well as good divalent ion retentions ($\sim 75\%$ for Ca^{2+} and up to $\sim 80\%$ for SO_4^{2-}). Moreover, we observe a high flux recovery for both emulsions (100% for CTAB and 80% for SDS), with especially for the CTAB emulsion a very low degree of fouling. These stable PEM based hollow fibre membranes thus allow simultaneous de-oiling, removal of small organic molecules, particles, and divalent ions in a single step process, while also demonstrating excellent membrane clean-ability.

5.1 Introduction

Water scarcity is a major global problem, and is expected to only worsen because of world population growth and global warming [1, 2]. One of the essential steps to be taken is to find effective and efficient methods to allow wastewater re-use [3]. In oil producing areas, such as the Middle-East, Africa and the US, a lot of wastewater is produced during oil extraction, counting only in the US already 3.3 million m^3 in 2007 [4]. This so-called produced water (PW) stems from water naturally contained in the well, but also from additional water pumped into the reservoir to facilitate the extraction of oil [5]. Since this process generally results in 3 barrels of wastewater per barrel of oil extracted [6], produced water treatment could be an important source of water for various beneficial re-uses, for example irrigation.

Unfortunately, PW is a very challenging stream to treat; its composition varies widely from one location to another and typically includes dispersed oil, organic and inorganic contaminants, treatment chemicals from the oil production process (e.g. corrosion and scale inhibitors, surfactants, biocides, etc.), produced solids, bacteria, metals and naturally occurring radioactive materials [4, 7]. Currently, PW is treated with a wide variety of physical, chemical and biological techniques in which, hydrocyclones, evaporation and different types of filters are employed [8, 9]. In such large treatment processes, membrane technology is especially interesting as it is one of the few techniques that can successfully remove the smallest (< 10 μm) and most stable oil droplets [10]. For this purpose microfiltration (MF) and especially ultrafiltration (UF) have been shown to be very suitable techniques, with UF also being well suitable to remove small suspended particles and even part of the dissolved hydrocarbons [11]. But membrane technology can do much more. Reverse osmosis (RO) can be used to desalinate produced water and to remove final traces of dispersed and dissolved oil [12]. Unfortunately, the low permeability and high pressure associated with RO, translate into a larger footprint and amount of energy consumed [13]. Here nanofiltration (NF) can be seen as a very interesting alternative. NF membranes can be used at acceptable permeability for de-oiling while simultaneously removing multivalent ions, dissolved organics and part of the monovalent salts [14].

Membrane technology also has clear downsides, and in PW treatment membrane fouling can be considered the most serious problem. In the complex mixture that is produced water, many of its components can foul the membrane leading to very substantial decreases in the flux of treated water. Fouling is especially a problem for RO and NF membranes that, due to their typical

spiral wound configuration, can only deal with relatively clean feed streams. As a result, a very substantial pre-treatment, such as MF or UF, is needed before RO and NF can be applied.

The need for a pre-treatment step excludes the possibility of the proposed one step NF membrane operation to simultaneously de-oil and control the salinity. If, instead, hollow fiber (HF) nanofiltration membranes could be employed, those problems can be overcome because of their ability to withstand much higher fouling loads. This is partly because HF membranes can be cleaned much better by physical cleaning than their spiral wound counterparts [15], e.g. by allowing backwashing at higher pressures [16]. An equally important argument is that HF based membrane modules do not require a spacer, while for spiral wound modules spacer fouling is a much bigger problem than membrane fouling [15].

In the past decade, polyelectrolyte multilayers (PEMs) have really established themselves as a very powerful method to prepare hollow fibre based NF membranes. Moreover, PEMs have significant advantages, that might make them especially well-suited to design membranes for produced water treatment. First of all, NF membranes based on PEMs are highly versatile, as the separation layer properties, such as inner molecular structure and charge, can be controlled by the choice of the polyelectrolytes, the number of layers, the pH and the ionic strength of the coating solution [17, 18]. Thus, it becomes possible to tune the separation performance of these membranes for a specific application or feed stream. A second advantage is the thin separation layer allowing membrane permeabilities to be relatively high compared to commercial NF membranes with comparable separation performance [19, 20]. Finally, polyelectrolyte multilayers coated on top of UF supports, have been shown to be stable both against physical (e.g. backflushing) and chemical cleaning (Hypochlorite (NaOCl)) [16]. In contrast, conventional NF membranes based on polyamide thin film composites showed a significant drop in performance after prolonged exposure to Hypochlorite [21]. It is highly likely that chemical cleaning is a necessity for the treatment of produced water by any membrane type.

But also polyelectrolyte multilayer based membranes have weaknesses. The main challenge for PEM based membranes, especially regarding produced water treatment, is that the multilayer stability can be compromised by the presence of charged organic molecules in the feed stream. In particular, work carried out recently showed that surfactants (naturally present in PW but also added in extra-quantities to inhibit pipe corrosion and to increase oil

recovery) can affect the stability of common PEMs [22]. As polyelectrolyte multilayers are prepared through electrostatic assembly, the major forces involved in keeping those layers together are electrostatic ones. Exposure to wastewater containing surfactant molecules, especially at high salinity, can allow the charged surfactant molecules to complex with the polyelectrolyte layers, thereby compromising the stability of the multilayer.

In recent years, some studies have focused on covalent layer-by-layer films to achieve improved polylectrolyte multilayer stability. Exploiting the chemistry of the chosen polyelectrolytes it becomes possible to make stable multilayers by introducing chemical bonding via chemical crosslinking [23]. Crosslinking of multilayers has been studied before, especially to increase membrane selectivity [24] and sometimes also to increase chemical stability (hypochlorite) [25] as well as stability in extremely saline conditions. Unfortunately, all this previous work has focused on flat sheet membranes, rather than hollow fiber based membranes, where techniques such as UV crosslinking [23, 24] and multilayer spray-assisted assembly [25] cannot be applied.

In this work, we report on the development of PEM based hollow fiber NF membranes specifically for the challenging treatment of produced water. First the focus is on the active layer stability, and we study on model surfaces how two types of multilayer (PDADMAC/PSS and PAH/PSS) are affected by exposure to surfactants with a variety of properties (cationic, anionic, zwitterionic and non-ionic). We then study how different crosslinking approaches, concentration and time can lead to PAH/PSS based PEM coatings stable in surfactant solutions. The effect of crosslinking time is subsequently studied for PEM based hollow fiber NF membranes, where the retention of variety of salts is studied before and after surfactant exposure. Finally, through filtration experiments carried out with synthetic produced water, we demonstrate that hollow fibre based NF membranes are able to simultaneously remove oil droplets, surfactants and divalent ions from the wastestream in a single separation step.

5.2 Experimental procedures

5.2.1 Materials

Poly(allylamine hydrochloride) (PAH, M_w = 50 kDa), poly(sodium 4-styrene sulfonate) (PSS, M_w = 70 kDa), an aqueous solution of 20 wt% poly(diallyldimethylammonium chloride) (PDADMAC, M_w = 400-500 kDa), an aqueous solution of 25 wt% glutaraldehyde (Grade II), N-

methylpyrrolidon and glycerin were purchased from Sigma-Aldrich (The Netherlands). Polyethersulfone (PES) (Ultrason 6020) and SPES (sulfonated polysulfone) were both kindly obtained from BASF (Germany). Sodium dodecyl sulfate (SDS, Sigma-Aldrich), Hexadecyltrimethylammonium bromide (CTAB, Sigma-Aldrich), N-dodecyl-N,Ndimethyl-3-ammonio-1-propanesulfonate (DDAPS, Sigma-Aldrich) and Triton^{TM} X-100 (TX, Sigma-Aldrich) were the four types of surfactant used (Figure 5.1). N-hexadecane (Merck Schuchardt) was used as the oil, Coumarin 6/ Neeliglow Yellow 196 (Neelikon) as fluorescent dye to allow accurate measurements of the oil concentration. All other chemicals were purchased from VWR (The Netherlands).

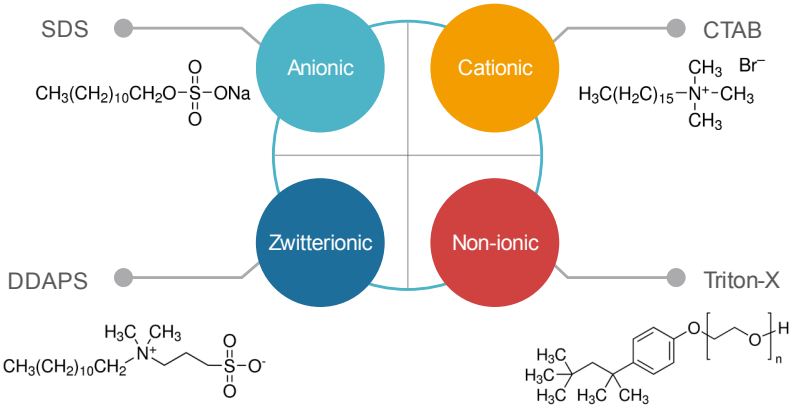

Figure 5.1: Surfactants used in this study: Sodium dodecyl sulfate (SDS), Hexadecyltrimethylammonium bromide (CTAB), N-dodecyl-N,Ndimethyl-3-ammonio-1-propanesulfonate (DDAPS) and Triton^{TM} X-100 (TX)

5.2.2 Polyelectrolyte multilayer coating on SiO_2 Model Surfaces

Silicon wafers were first cleaned with piranha solution, made of a 3:1 mixture of concentrated sulfuric acid (H_2SO_4) with hydrogen peroxide (H_2O_2), in order to remove any organic residues. Then, the wafers were coated via a simple dipcoating procedure. In particular, (PAH/PSS) and (PDADMAC/PSS) multilayers were coated on top of silicon wafers with 84 nm and 121 nm SiO_2

top layers (δ_{SiO_2}) respectively. These SiO_2 layers are required as an optical spacer in reflectometry (see 2.3). For a single bilayer coating, the negatively charged silica wafer was completely immersed in a 0.1 g·l^{-1} polycation solution with 50 mM NaCl. After 15 min, the surfaces were rinsed in a 50 mM NaCl solution for 15 min. To finally complete the bilayer coating, the surfaces were subsequently immersed in a 0.1 g·l^{-1} polyanion solution (pH=5.4) with 50 mM NaCl for 15 min and then rinsed in a 50 mM NaCl solution, again for 15 min. The same procedure was repeated four more times to realize 4.5 and 5.0 bilayers on top of the wafers. Every coating step was executed at room temperature. For crosslinked (PAH/PSS) multilayers, a crosslinking step was added to the procedure written above. In particular, after every PAH coating step, starting from the second bilayer, the wafers were rinsed in 50 mM NaCl and then completely immersed in aqueous solutions with various GA concentrations (2.5, 5, 7.5, 10 and 15 mM) for 15 min at room temperature, keeping the concentration of NaCl to 50 mM. After this step, the wafers were carefully rinsed in 50 mM NaCl for 15 min, and then the PSS layer was applied to complete the bilayer, following the procedure described before. Surfaces coated with 4.5 bilayers (PAH/PSS) at different crosslinking times were realized first via dip coating, and then they were dipped in a 7.5 mM GA solution for different times: 1, 5, 15, 60, 180, and 300 min. In this last approach, membranes were thus crosslinked in a single step, rather than after every PAH step as was done in the first approach.

5.2.3 Reflectometry

The multilayer desorption from silicon wafers, due to the interaction with surfactants, was monitored by means of reflectometry [26]. Cationic (CTAB, 346 mg·l^{-1}), anionic (SDS, 2391 mg·l^{-1}), zwitterionic (DDAPS, 1006 mg·l^{-1}) and non-ionic (TX, 144 mg·l^{-1}) surfactant solutions, approximately at their critical micelle concentration (CMC) and with 5 mM NaCl as background electrolyte, were prepared. These solutions were flushed, under a stagnation point flow, to a silica surface, pre-coated with a PEM (see procedure above), several times, with 5 mM NaCl rinsing step in between, until a steady state desorption was reached. The use of a stagnation point flow cell allows for very well-controlled hydrodynamics during the multilayer desorption. Polarized monochromatic light (HeNe laser, 632.8 nm) hits the wafer around the Brewster angle and is reflected towards the detector. The reflected light is split into its p- and s-polarized components. The ratio between these two components is defined as S (-), and the change in this ratio (ΔS) is directly proportional to the amount

of mass desorbed from the wafer:

$$\Gamma = \frac{\Delta S}{S_0} Q \tag{5.1}$$

where Γ is the amount of mass adsorbed or desorbed from the wafer ($mg \cdot m^{-2}$), S_0 is the starting output signal of the bare silicon wafer (-), and Q is the sensitivity factor for the system ($mg \cdot m^{-2}$). To calculate the sensitivity factor, we used an optical model based on the following values: $\theta = 71°$, $n_{silica} = 1.46$, $\tilde{n}_{silicon} = (3.85, 0.02)$, $n_{H_2O} = 1.33$, $dn/dc_{PDADMAC} = 0.18$ $mL \cdot g^{-1}$, $dn/dc_{PAH} = 0.16$ $mL \cdot g^{-1}$, $dn/dc_{PSS} = 0.18$ $mL \cdot g^{-1}$, $\delta_{SiO_2} = 84$ nm for (PAH/PSS) and 121 nm for (PDADMAC/PSS). The sensitivity factor, Q, obtained to calculate the actual mass desorption for all experiments is 30 $mg \cdot m^{-2}$ for (PAH/PSS) and 40 $mg \cdot m^{-2}$ for (PDADMAC/PSS). Furthermore, we defined the stability of the multilayer as given by

$$PEM_{stability} = \left(1 - \frac{\Gamma_{des}}{m_{tot}}\right) \tag{5.2}$$

where Γ_{des} is the quantity in $mg \cdot m^{-2}$ of PEM desorbed from the wafers and monitored via reflectometry, while m_{tot} is the amount ($mg \cdot m^{-2}$) of PEM contained in the multilayer prior desorption, measured via reflectometry [17]. All experiments were perfomed at least twice.

5.2.4 Membrane Fabrication, Modification and Characterization.

Hollow fiber membranes were produced by a spinning process based on non-solvent induced phase separation. For this, a dope was prepared by mixing 140 g PES, 70 g SPES and 120 g glycerin in 650 g NMP. The clear dope was then filtered through a 5 ţm metallic mesh and deaerated overnight. The hollow fiber membranes were spun by extruding the dope solution through a hollow fiber spinneret at 70°C (see Figure 5.2). A mixture of 10% glycerin in water was used as the bore liquid. After an airgap of 0.3 m, the partly already solidified membrane is immersed in the coagulation bath, containing the water at 60°C. Here the phase inversion is completed. After the coagulation bath, the fiber is fed through a washing bath with water at room temperature. Finally the fiber is collected on an uptake winder.

These hollow fiber membranes are designed for inside-out filtration, having the smallest pores at the inside of the fiber. Scanning electron microscope (SEM) pictures of the membrane are reported in Appendix C (Fig. C1). These

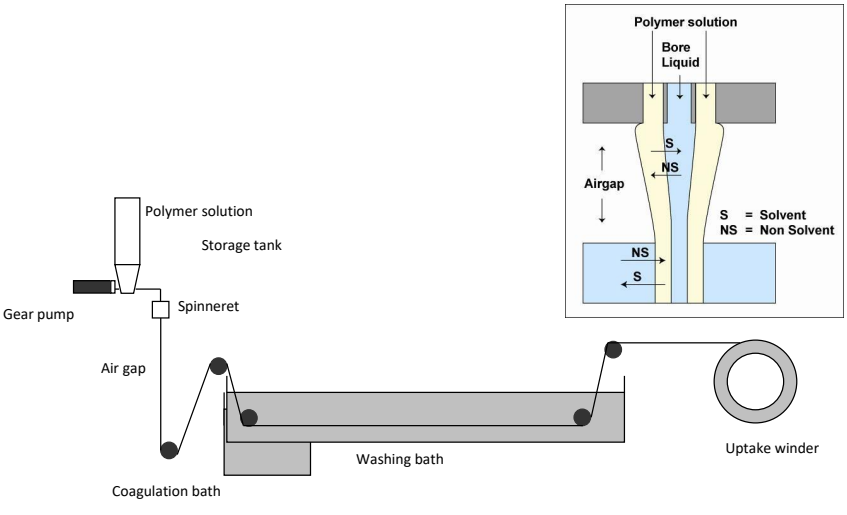

Figure 5.2: Diagram of the spinning setup. The insert shows the non-solvent induced phase separation process in detail.

HF membranes have a water permeability of 150 $L \cdot m^{-2} \cdot h^{-1} \cdot bar^{-1}$, an inner diameter of 0.7 mm and a molecular weight cut-off (MWCO) of 7.5 kDa. The MWCO was determined by using a polyethyleneglycol (PEG) mixture with various molecular weights (6, 10, 20 and 35 kDa) and by analyzing the molecular weight above which a 90% retention is obtained. For this, permeate and retentate samples were analyzed using size exclusion chromatography (SEC). After fabrication, the membranes were stored in demi-water.

Polyelectrolyte multilayers were coated on top of the prepared UF membranes. As we immerse the fibers completely in the coating solution, the deposition of polylectrolyte is not limited to the inner surface of the membrane only and the whole porous structure can be coated by the polyelectrolytes. However, only at the inner surface, where the pores are smallest, does the PEM layer form a dense separation layer on top of the membranes [16–18]. Before proceeding with the coating, we first immersed the fibers for 15 min in a 50 mM NaCl solution. The membranes were then coated via a simple dipcoating procedure. For the bilayer coatings, the fibers were completely immersed in a 0.1 $g \cdot l^{-1}$ PAH solution with 50 mM NaCl at room temperature. After 15 min, the fibers were rinsed in a 50 mM NaCl solution for 15 min. The fibers were subsequently dipped for 15 min in 0.1 $g \cdot l^{-1}$ PSS solution with 50 mM NaCl, and then rinsed for other 15 min in a 50 mM NaCl solution. After this first bilayer, the described procedure was repeated until 4.5 and 5.0 bilayers had been coated on the membranes (taking samples for those two steps). In the case of crosslinked multilayers, fibers coated with 4.5 bilayers were immersed in a 7.5 mM GA solution for 1, 3 and 5 hours, keeping same ionic strenght of the other steps, i.e. 50 mM NaCl. After this crosslinking step, the fibers were rinsed in 50 mM NaCl, and part of them were dipped in a 0.1 $g \cdot l^{-1}$ PSS solution with 50 mM NaCl. This way it was possible to obtain fibers with 4.5 (PAH terminated) and 5.0 (PSS terminated) bilayers at different crosslinking times. After being rinsed in demi-water, all membrane samples were put in a glycerol/water (15/85 wt%) mixture for 4 h and dried overnight under ambient conditions.

For water permeability and ion retention experiments, single PEM-coated fibers were potted in modules with a fiber length of approximately 150 mm. Every module contains only one fiber. The water permeability ($L \cdot m^{-2} \cdot h^{-1} \cdot bar^{-1}$) was calculated by normalizing the measured pure water flux with the trans membrane pressure (TMP). The pure water flux was measured at 20°C with demi-water in a cross-flow configuration at a transmembrane pressure of 3 bar. For the salt retention measurements, a cross-flow

through the fibers was also applied. To reduce the effect of concentration polarization, we set the cross-flow velocity of the feed through the fibers at 1.7 $m \cdot s^{-1}$. This corresponds to a Reynolds number of approximately 1200. The salt concentrations of the feed and permeate were measured with a WTW Cond 3210 conductivity meter. The retention was based on the ratio between the permeate and feed concentrations. All experiments were performed at least in triplicate.

5.2.5 Membrane stability

Single PEM-coated membrane fibers with 4.5 and 5 bilayers of (PAH/PSS), prepared at different crosslinking times (0h, i.e. not crosslinked, 1h, 3h and 5h) were potted in modules with a fiber length of approximately 150 mm. Every module contains only one fiber. After flushing each fiber for three times with alternating SDS and CTAB solutions, (at their CMC, with 5 mM NaCl as background electrolyte), the fibers permeability and ion retention were measured using the same flow and pressure conditions previously described. Each single surfactant flush lasted 5 min. All experiments were performed at least in triplicate.

5.2.6 Artificial produced water: preparation and filtration

To detect the amount of oil that permeates through the membrane, n-hexadecane was colored with a fluorescent dye (Coumarin 6). As fluorescence decays over time, the colored oil was freshly prepared before each experiment. Around 10 mg of the dye powder was added to 8 mL of n-hexadecane and put in an ultrasonic bath for few minutes. Afterwards, the oil was filtered with a Millipore 0.45 μm filter to remove any residual solid particles. To prepare our artificial PW, we follow a procedure set out by Dickhout *et al.* [27]. To ensure all emulsions have the same characteristics, a stock emulsion was prepared under standard conditions, which was then diluted with carefully chosen concentrations to obtain the desired oil, salt and surfactant concentration for the filtration experiments. The surfactant concentrations were all chosen to be approximately at CMC. The stock emulsions were prepared by dissolving a surfactant (346 mg/L CTAB or 2391 mg/L SDS) in 1 L of DI water in a Duranő bottle by mixing with a dispersing mixer (IKAő T25 digital Ultra-Turrax with S25N 18G element) for 4 minutes at 14000 rpm. Then, 2 g of colored oil was injected near the mixer head with a long syringe needle and mixed for 10 minutes at 14000 rpm. The stock emulsion was diluted to contain 1 g/L

n-hexadecane and the desired surfactant and salts concentration to make up 1L of feed emulsion with 1000 mg/L n-hexadecane, 346 mg/L CTAB or 2391 mg/L SDS, 5 mM NaCl, 5 mM $CaCl_2$ and 5 mM Na_2SO_4. Surfactant solutions used for cleaning were prepared the same as the emulsions, but without adding n-hexadecane. In each experiment, the concentrations of surfactant and salts in the rinsing solution were identical to the emulsion used.

For the membrane crossflow filtration experiments, single PEM-coated fibers with 4.5 bilayers were potted in modules with a fiber length of approximately 80 mm. Every module contains only one fiber. The clean water flux of every fiber was measured before filtrating the O/W emulsion. New modules were used for each experiment. The concentrate was recycled to the feed bottle while the permeate was instead collected. Since the permeate flow-rate was small compared to the concentrate flow, this was not expected to affect the feed composition. This was checked by analyzing the feed ion concentration, TOC and oil content at the start and end of some experiments, and indeed negligible changes in feed composition were observed. A membrane filtration experiment consisted of filtering the O/W emulsion for 3 hours at a TMP of 3 bar and a flow-rate of 0.75 kg/h, which corresponds to a cross-flow velocity of 0.55 cm/s and a Reynolds number around 380. The permeate flux was measured between 2 h and 3 h. Samples of the permeate were collected at the same time and their ionic content and TOC were analyzed by ion chromatography (Metrohm Compact IC 761) and by a TOC analyzer (Shimadzu TOC-L) respectively. The oil retention was measured trough a fluorescent dye method already used in previous work [28]. Feed samples were taken at the same time as the permeate samples, and analyzed with same methods. To clean the membranes, the modules were flushed one time with a surfactant rinsing solution for 15 min at a 4 kg/h flow-rate, without applying trans membrane pressure. After cleaning, the water flux was measured again to determine the flux recovery. Each experiment was performed in triplicate.

5.3 Results and Discussion

The results and discussion section is split into three distinct sections. In the first section, we apply model surfaces to study PEM stability against a variety of surfactant types and demonstrate that crosslinking can lead to stable PEM coatings, even in the presence of surfactants. In the next section, we demonstrate this stability also for PEM based hollow fibre NF membranes, where ionic retentions are studied before and after crosslinking. In the final

section we show that with these membranes we can, in a single step, remove surfactants, de-oil and partially desalinate a synthetic PW stream based on a surfactant stabilized O/W emulsion.

5.3.1 Multilayer stability against surfactants

While it is known that surfactants can de-stabilize PEMs [22], much less is known about how different surfactant types affect different types of PEM. Here we study the stability of PEMs adsorbed on model surfaces via optical flow-cell reflectometry. A wafer, pre-coated with a PEM, is exposed several times to a surfactant solution at the CMC until a stable plateau in the desorption is obtained. Examples of these experiments are shown in Figure 5.3, for exposure of a PDADMAC/PSS based PEM to the anionic SDS (A) and the zwitterionic DDAPS (B), the outcomes of which will be discussed in detail below. The desorption plateau is taken after rinsing with a rinsing solution, to ensure that no adsorbed surfactant remains, as indicated in figure 5.3A. All surfactant and rinsing solutions contain 5 mM background electrolyte. Finally the desorbed amount (in $mg{\cdot}m^{-2}$) can be compared to the original amount of multilayer adsorbed on the model surfaces as discussed in section 5.2.3. The stability of the PEM layer is thus defined as the percentage of the remaining mass of the original PEM coating after surfactant exposure.

We first studied the stability of a PEM based on PDADMAC/PSS, a strong polyelectrolyte multilayer couple, really well known in the membrane field for its high chemical stability [16]. In Figure 5.4, we show the PEM stability after exposure to surfactants for PEMs of 4.5 bilayers (terminated with PDADMAC) and 5.0 bilayers (terminated with PSS). Here the stability (%) of the multilayers is reported after exposure to four types of surfactant: anionic (SDS), cationic (CTAB), zwitterionic (DDAPS) and non-ionic (TX). The effect of both a positive and a negative top layer (4.5 and 5.0 bilayers) on the stability was investigated as the charge of the top layer could affect the adsorption of the surfactant and how it interacts with the multilayer.

The results depicted in Figure 5.4, clearly demonstrate that charged surfactants, such as the anionic SDS and the cationic CTAB, compromise the stability of PDADMAC/PSS multilayers significantly. In particular, only 40% of a PDADMAC/PSS multilayer prepared at 50 mM NaCl [17] remains after exposure to SDS, and only 60% remains after exposure to CTAB. On the other hand, surfactants carrying no net charge, such as the zwitterionic DDAPS and the non-ionic TX, do not affect the stability of the multilayer.

It is well known that charged surfactants can interact with oppositely

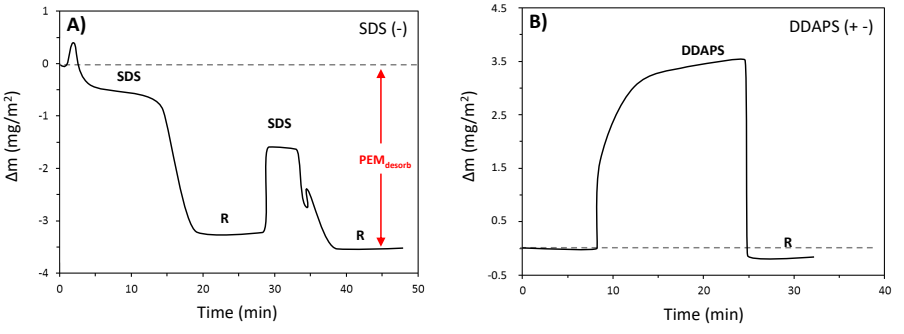

Figure 5.3: Variation in PEM mass (mg/m^2) for a (PDADMAC/PSS) system after flushing with A) SDS and B) DDAPS, at their CMC. Results obtained via reflectometry.

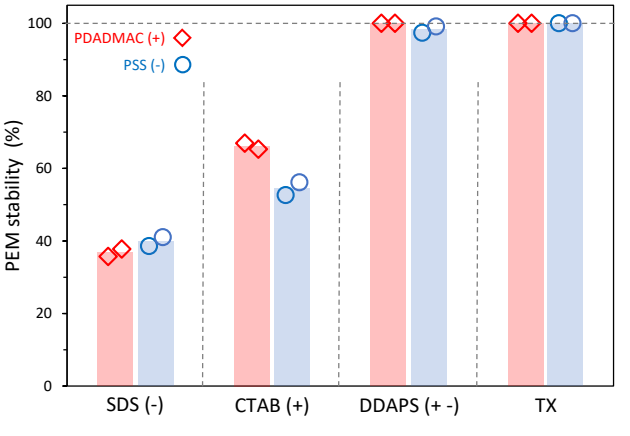

Figure 5.4: Stability (%) of (PDADMAC/PSS) PEM with 4.5 bilayers (red) and 5 bilayers (blue) after flushing with different surfactant solutions (SDS, CTAB, DDAPS and TRITON-X) at their CMC. Results obtained via reflectometry. Points represent single data points, while bars represent the average of these points.

charged polyelectrolytes to form complexes in solution [29]. Polyelectrolyte multilayers are mainly based on electrostatic interactions, which can be supported by other interactions such as hydrogen bonding and hydrophobicity [30]. After the addition of a charged surfactant, the small surfactant molecules can diffuse into the multilayer [22] and screen the electrostatic interactions between the oppositely charged polyelectrolytes. In particular, the cationic CTAB could form a complex with the anionic PSS, while the anionic SDS may complex with the cationic PDADMAC. This results in competitive behaviour, where complexation of the surfactant with one polyelectrolyte weakens and possibly disrupts the polyelectrolyte complexation. We do find that no surfactant can completely desorb the multilayer, thus we expect that if the desorption of one polyelectrolyte is favoured, then a strong charge will build up in the multilayer. For example if negative SDS would desorb the positive PDADMAC, a significant excess of negative charge would form in the multilayer. This excess charge would then prevent more surfactant molecules from approaching the remaining PEM coating.

As PDADMAC/PSS based multilayers are clearly not stable against desorption by charged surfactants, we moved to PSS/PAH based multilayers. PSS/PAH is also a very well studied PEM system known to give dense (low hydration) layers with an excess of positive charge (PAH). Another advantage of this system is that the primairy amine groups of PAH can be crosslinked by application of glutaraldehyde [23]. In Figure 5.5, we show the stability of a PAH/PSS based PEM without crosslinking (0 mM) and after crosslinking with various crosslinker concentrations. Here we crosslinked after every bi-layer coating step and we focus on the stability after exposure to both charged surfactants, SDS and CTAB. The experiments were again performed by using reflectometry. This time, a multilayer coated on top of a silicon wafer, was first exposed to one charged surfactant, and then, after rinsing with 5 mM NaCl, to the other charged surfactant, both at their CMC, for at least three times. If the multilayer was terminated with a cationic PAH layer the experiment started with exposure to the anionic SDS, while for a PEM terminated with anionic PSS the expoure started with cationic CTAB.

From Figure 5.5, it is clear that without crosslinking, also the PAH/PSS system is not stable in surfactant solution, with 85-100 (%) of the layer being removed after consecutive exposure to SDS and CTAB. But even at very low crosslinker concentration, nearly complete stability is observed for all crosslinked layers. These GA concentrations are much lower (and thus safer) [31] compared to the concentrations used by Cho *et al.*(0.25 M - 2.5

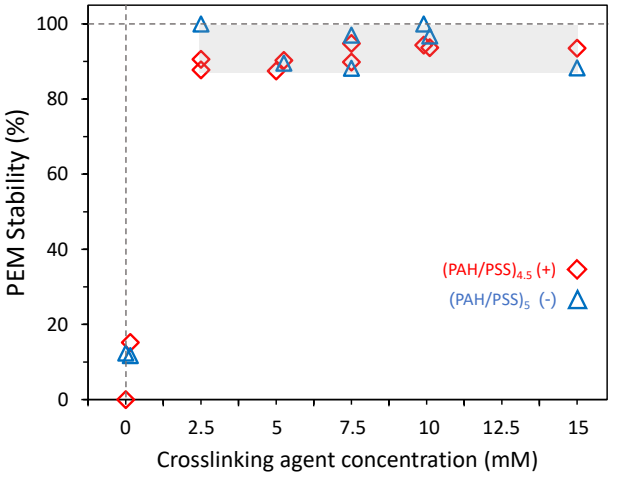

Figure 5.5: Stability (%) as a function of GA concentration of a PAH/PSS based PEM with 4.5 bilayers (orange) or 5.0 bilayers (blue) after flushing with SDS and CTAB solutions at their CMC for three times. These results were obtained by using reflectometry. Points represent single data points.

M) [25]. What might come as a suprise, is that typically no complete stability is observed, and that even at higher crosslinker concentrations some material is desorbed. It is important to remember that only the PAH chains become crosslinked by glutaraldehyde, and some more loosely bound PSS chains, especially from the top layers, could still be desorbed.

The quality of crosslinking can certainly also be affected by the crosslinking time. Since crosslinking after every step (Figure 5.5) may not be needed, it would be very beneficial to do the crosslinking in a single final step. In Figure 5.6, we show the stability of a PAH/PSS multilayer, sequentially exposed to SDS and CTAB, as a function of crosslinking time. Here crosslinking is applied in a single final step with a crosslinker concentration of 7.5 mM and studied using the same optical reflectometry approach.

By looking at Figure 5.6, we can indeed see that, given sufficient crosslinking time, a single crosslinking step works just as well as multiple steps. This is underpinned by the later work performed on membranes (see Figure 5.7 and Figure 5.8). We also conclude that longer crosslinking times lead to more stable layers and more reproducible results.

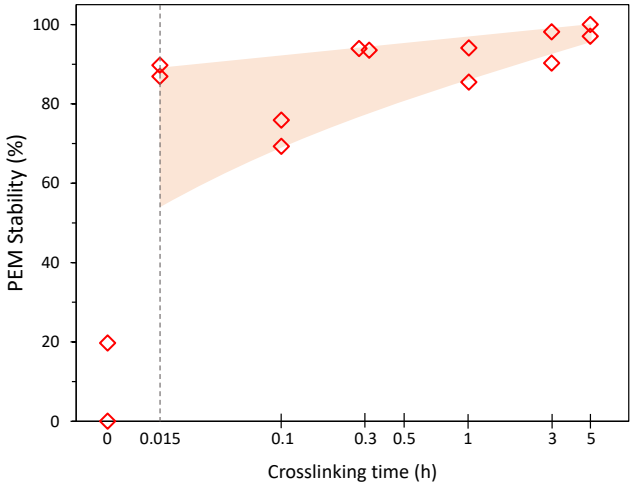

Figure 5.6: Stability (%) as a function of crosslink time for a PAH/PSS based PEM of 4.5 bilayers after flushing with SDS and CTAB solutions at their CMC for three times. These results were obtained by using reflectometry. Points represent single data points.

5.3.2 Stable PEM based NF membranes

In the previous section, we have shown that PAH/PSS based PEM coatings can be made stable by a single crosslinking step at a low crosslinker concentration. Here, we prepared hollow fiber based NF membranes by applying PSS/PAH multilayers on top of negatively charged hollow fiber support membranes. The membranes were coated under identical conditions as the model surfaces, and were subsequently crosslinked for different times, using a safe gluteraldehyde concentration (7.5 mM) [31]. In Figure 5.7, we show the membrane performance for PAH/PSS membranes of 4.5 (7A, PAH terminated) and 5.0 (7B, PSS terminated) bi-layers in thickness. Overall, longer cross-linking times lead to a denser membrane with a lower water permeability and a higher ion retention. Similar effect were observed by Park *et al.* [32]. The increase in retention is especially strong for Na_2SO_4. We expect that here the retention is dominated by the di-valent SO_4^{2-}. Overall PSS/PAH membranes tend to have an excess of positive PAH [25], and a more positive charge would allow more easy permeation of this ion. But crosslinking of glutaraldehyde with the primary amines of PAH can decrease the positive charge and even induce a

negative charge in the membrane [25]. This would lead to a stronger Donnan based repulsion [33] between SO_4^{2-} and the crosslinked membrane, increasing retention significantly.

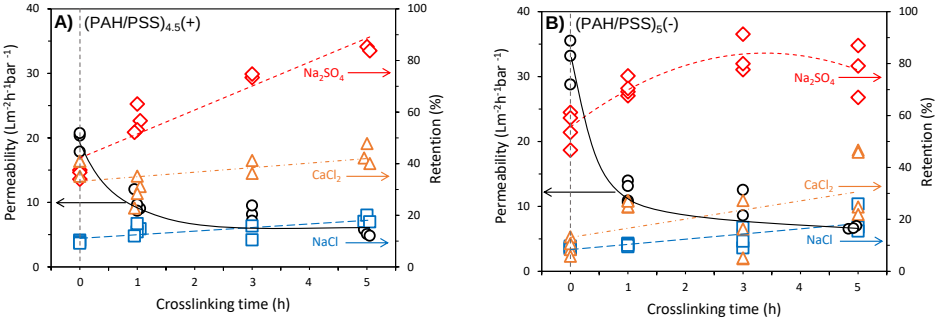

Figure 5.7: Water permeability ($L{\cdot}m^{-2}{\cdot}h^{-1}{\cdot}bar^{-1}$) and retentions (%) of 5 mM $CaCl_2$, NaCl and Na_2SO_4 of membranes coated with $(PAH/PSS)_4$-PAH (A) and $(PAH/PSS)_5$ (B) crosslinked for 0, 1, 3 and 5h with GA. Points represent single data points, while lines represent the average of these points.

5

The stability of these membranes is studied in Figure 5.8. The membranes were consecutively exposed to an anionic and cationic surfactant solutions for at least 3 times, exactly as was done for the model surfaces studied in Figure 5.5 and Figure 5.6. Also here, if the multilayer terminates with a positive top layer the experiment started with SDS flushing, while if the multilayer ended with a negative top layer the experiment started with CTAB. Figure 5.8, shows the retention of (5 mM) $CaCl_2$ and Na_2SO_4 tested and compared with the retentions obtained before the surfactant flush. For the uncrosslinked PEM based membranes (0h), retentions decrease to nearly 0 in line with the substantial desorption observed for PAH/PSS coatings on model surfaces (Figure 5.5). However, with an increase in crosslinking time the reduction in retention decreases, until at 5h of crosslinking really stable performance is observed. Clearly, the stability that was observed at high crosslinking times on model surfaces (Figure 5.6), is also found for PEM based membranes. For shorter crosslinking times for the PAH terminated membrane (8A) we observed a decrease in retention of both Na_2SO_4 and $CaCl_2$. A strange observation is that for shorter crosslinking times for the PSS terminated membrane (8B) Na_2SO_4 retention decreases and $CaCl_2$ retention increases. Most likely the surfactant exposure does remove some of the PSS from the PSS terminated membrane making the layer more positively charged, leading to an increase in $CaCl_2$

retention and a decrease in Na_2SO_4 retention.

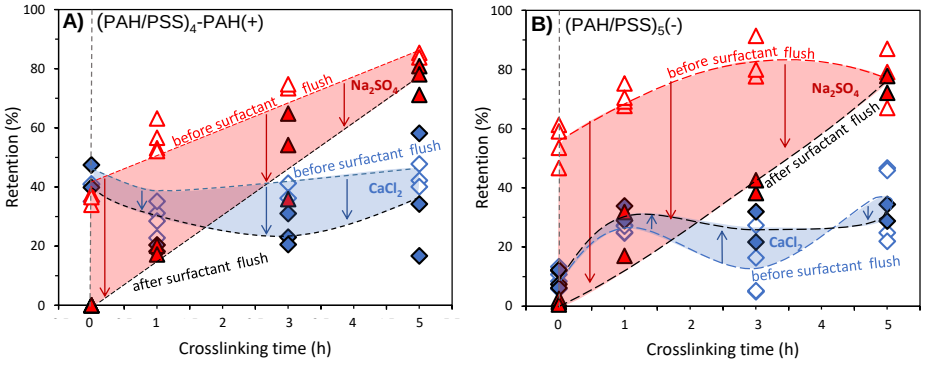

Figure 5.8: Retentions of 5 mM $CaCl_2$ and Na_2SO_4 as a function of crosslinking time for membranes coated with $(PAH/PSS)_4$-PAH (A) and $(PAH/PSS)_5$ (B) before and after three times consecutive rinsing with SDS and CTAB solutions at their CMC. Data are represented by points, while lines represent the average of these points.

5

5.3.3 Produced water treatment

A stable hollow fiber NF membrane would be highly beneficial for produced water treatment, as one could de-oil, and remove particles, small organic molecules (surfactants) and multi-valent ions in a single step. Two artificial produced water emulsions stabilized either by SDS or CTAB, with as oil 1000 ppm n-hexadecane (dropletsize ~5 μm [27]), and 5 mM NaCl, 5 mM $CaCl_2$ and 5 mM Na_2SO_4, were treated in a crossflow system by using HF membranes based on 4.5 bilayers of PAH/PSS crosslinked for 5 hours in 7.5 mM glutaraldehyde. The crossflow velocity was set at 0.55 cm/s and the TMP was kept constant at 3 bar.

In Figure 5.9A, we show the retentions stemming from filtrations using the cationic CTAB as surfactant to stabilize the O/W emulsion. We observe an excellent oil retention (100%), as well as a very high TOC retention (96.5%), implying that also nearly all of the free surfactant molecules are retained. Furthermore, higher Ca^{2+} (75%) and Cl^- (36%) retentions were obtained compared to the retention values obtained for the same ions in conditions were no oil and surfactant were present (Figure 5.7). At the same time, lower SO_4^{2-} retentions than for the pure solutions are observed. This change in retention behaviour likely stems from interaction of the cationic surfactant with the multilayer. This may lead to an increase in Ca^{2+} rejection and a

decrease in SO_4^{2-} retention. The increase in Cl^- retention is a consequence of the electroneutrality principle, if more Ca^{2+} is retained, then also more of it's counterion is retained.

When the anionic SDS is used as surfactant (Figure 5.9B), the membranes still show excellent oil retention (98%), and good TOC retention (83%). This time, we can observe a SO_4^{2-} retention similar to the values obtained without surfactant and previously shown in Figure 5.9, while we have higher Ca^{2+} (73%) retention. SDS is smaller than CTAB. This possibly allows SDS easier diffusion into the multilayer than CTAB, as supported by a lower TOC retention for SDS. Diffusion into and adsorption of SDS to the multilayer not only brings a change in membrane surface charge, but it could also densify the layer, reducing the effective multilayer pore size, thereby also increasing di-valent ion retention.

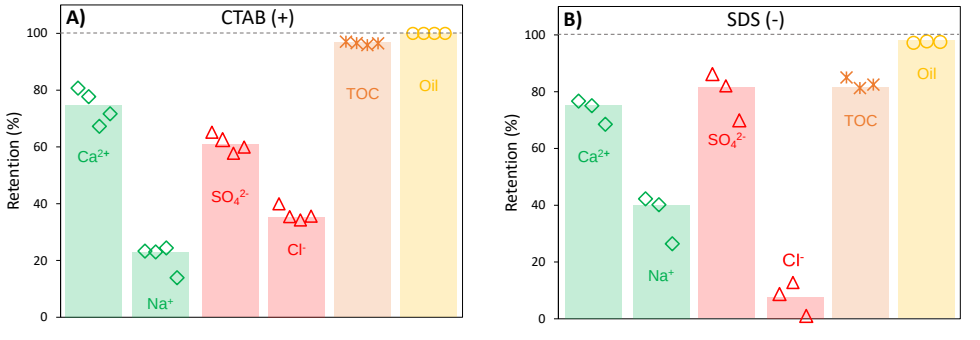

Figure 5.9: Retentions of Ca^{2+}, Na^+, SO_4^{2-}, Cl^-, TOC and oil from membranes coated with $(PAH/PSS)_4$-PAH in experiments performed with O/W emulsions stabilized by A) CTAB and B) SDS. Emulsions were made of 5mM $CaCl_2$, 5 mM NaCl, 5 mM Na_2SO_4, 1000 ppm of n-hexadecane (oil) and surfactant at its CMC. Points represent single data points, while bars represent the average of these points.

Table 1 contains a summary of the results obtained by filtrating artificial PW emulsions with our HF membranes. For CTAB stabilized PW, the membranes showed a low flux decline (just 19%). Furthermore, after cleaning with a CTAB solution at its CMC for 15 min, the membranes were able to completely recover their original flux. This demonstrates that fouling was not severe and that it was 100% reversible. For SDS the situation was a bit different. Flux decline was much higher, reaching a value of 90%. Still, it was

possible to recover 80% of the original flux. The non-reversible part of the fouling could stem from SDS penetrating the PEM layer as discussed above. It is also important to mention that cationic surfactants are good corrosion inhibitors and are much more commonly found in PW than anionic surfactants such as SDS [34]. Overall, these results clearly show that these newly developed membranes would be highly suitable to treat PW stabilized by cationic surfactants, such as CTAB, and would still be suitable to treat PW stabilized by anionic surfactants. The difference in fouling behaviour could stem from the easier diffusion of SDS into the multilayer, as discussed above. In both cases, the membrane clean-ability was extremely good, proving that PEM deposition can lead to surfaces were fouling is less severe and easier to remove. These membranes allow to de-oil, remove most of the surfactants and divalent ions from the wastestream and even some of the monovalent ions in only one step. All these factors together make them highly suitable for treatment of PW.

Surfactant used	Flux after fouling	Flux recovery
CTAB (+)	81 %	100 %
SDS (-)	10 %	80 %

Table 5.1: Remaining membrane flux after fouling and flux recovery after cleaning of the artificial produced water experiments. Emulsions were made of 5mM $CaCl_2$, 5 mM NaCl, 5 mM Na_2SO_4, 1000 mg/L of n-hexadecane (oil) and surfactant at its CMC.

5.4 Conclusions

Membrane technology can be considered a promising technology for PW treatment. By using membranes it becomes possible to convert a complex wastestream, such as PW, into a source of water for re-use. In particular, polyelectrolyte multilayer deposition is one of the methods that established itself as an effective technique to prepare hollow fiber based NF membranes. Hollow fiber membranes can withstand a much higher fouling load compared to their spiral wound counter-parts and would thus be especially promising for PW treatment. Unfortunately, surfactants, naturally present in PW but also added in extra-quantities to inhibit pipe corrosion and to increase oil recovery, can affect the stability of polyelectrolyte multilayers. In this work, we studied

the stability of polyelectrolyte multilayers towards different types of surfactant (anionic, cationic, zwitterionic and non-ionic), and demonstrate that it is possible to produce stable multilayers, resistant towards surfactants, on model surfaces as well as on membranes. This is, however, only true for the crosslinkable PAH/PSS system, and not for chemically stable PDADMAC/PSS system. The effect of crosslinking time for PAH/PSS was also studied for PEM based hollow fiber NF membranes. With increased crosslinking time more stable membranes are produced with better separation properties, but at a lower water permeability. Novel HF membranes based on 4.5 bilayers of PAH/PSS and crosslinked for 5h with a 7.5 mM glutaraldehyde solution, showed excellent stability towards charged surfactants. These membranes were tested with two artificial PW emulsions stabilized either by the cationic CTAB or the anionic SDS. For CTAB stabilized PW, the membranes showed a low flux decline (just 19%) and high surfactant removal (TOC retention 96.5%). Furthermore, after cleaning with a CTAB solution at its CMC the membranes were able to completely recover their original flux. For SDS flux decline was much higher, reaching a value of 90%, and surfactant removal lower (TOC retention 83%). Still, it was possible to recover 80% of the original flux after cleaning with SDS solution at its CMC. SDS is smaller than CTAB and this possibly allows SDS easier diffusion into the multilayer than CTAB, as supported by a lower TOC retention for SDS and its higher flux decline. In both cases, the membranes also showed excellent oil removal ($\sim 100\%$) and divalent ion retention ($\sim 75\%$ for Ca^{2+} and up to $\sim 80\%$ for SO_4^{2-}). In conclusion, these membranes not only show good stability and clean-ability but they also allow de-oiling, and removal of small organic molecules (such as surfactants) and divalent ions in a single step process.

References

[1] P. Gerland *et al.*, "World population stabilization unlikely this century", Science **346**, 234–237 (2014).

[2] M. Springmann, , *et al.*, "Options for keeping the food system within environmental limits", Nature **562**, 519–525 (2018).

[3] M. Kummu *et al.*, "The world's road to water scarcity: Shortage and stress in the 20th century and pathways towards sustainability", Sci. Rep. **6**, 38495 (2016).

[4] B. Alley, R. John, and C. James W, "Chemical and physical characterization of produced waters from conventional and unconventional fossil fuel resources", Chemosphere **85**, 74 – 82 (2011).

[5] B. Scanlon, R. Reedy, F. Male, and M. Walsh, "Water issues related to transitioning from conventional to unconventional oil production in the permian basin", Environ. Sci. Technol. **51**, 10903–10912 (2017).

[6] E. T. Igunnu and G. Z. Chen, "Produced water treatment technologies", Int. J. Low-Carbon Tec. **9**, 157–177 (2014).

[7] U. W.R. Siagian, S. Widodo, K. Khoiruddin, A. Wardani, and I. G. Wenten, "Oilfield produced water reuse and reinjection with membrane", MATEC Web of Conf. **156**, 08005 (2018).

[8] A. Fakhrul-Razi, A. Pendashteh, L. C. Abdullah, D. R. A. Biak, S. S. Madaeni, and Z. Z. Abidin, "Review of technologies for oil and gas produced water treatment", J. Hazard. Mater. **170**, 530 – 551 (2009).

[9] M. Cheryan and N. Rajagopalan, "Membrane processing of oily streams: Wastewater treatment and waste reduction", J. Membrane Sci. **151**, 13–28 (1998).

[10] J. M. Dickhout, J. Moreno, P. M. Biesheuvel, L. Boels, R. G. H. Lammertink, and W. M. de Vos, "Produced water treatment by membranes: A review from a colloidal perspective", J. Colloid Interface Sci. **487**, 523 – 534 (2017).

[11] T. Bilstad and E. Espedal, "Membrane separation of produced water", Wat. Sci. and Tech. **34**, 239 (1996).

[12] G.-d. Kang and Y.-m. Cao, "Development of antifouling reverse osmosis membranes for water treatment: A review", Wat Res. **46**, 584–600 (2011).

[13] D. L. Naidu, S. Saravanan, M. Chidambaram, M. Goel, A. Das, and J. Sarat Chandra Babu, "Nanofiltration in transforming surface water into healthy water: Comparison with reverse osmosis", J. Chem. **2015**, 1–6 (2015).

[14] S. Alzahrani and A. Mohammad, "Challenges and trends in membrane technology implementation for produced water treatment: A review", J. Water Process Eng. **4**, 107–133 (2014).

[15] J. Vrouwenvelder, D. G. von der Schulenburg, J. Kruithof, M. Johns, and M. van Loosdrecht, "Biofouling of spiral-wound nanofiltration and reverse osmosis membranes: A feed spacer problem", Water Res. **43**, 583 – 594 (2009).

[16] J. Grooth, B. Haakmeester, C. Wever, J. Potreck, W. Vos, and K. Nijmeijer, "Long term physical and chemical stability of polyelectrolyte multilayer membranes", J. Membrane Sci. **489**, 153–159 (2015).

[17] J. Grooth, R. Oborny, J. Potreck, K. Nijmeijer, and W. Vos, "The role of ionic strength and oddeven effects on the properties of polyelectrolyte multilayer nanofiltration membranes", J. Membrane Sci. **475**, 311–319 (2015).

[18] S. Ilyas, S. Mehran Abtahi, N. Akkilic, H. Roesink, and W. de Vos, "Weak polyelectrolyte multilayers as tunable separation layers for micropollutant removal by hollow fiber nanofiltration membranes", J. Membrane Sci. **537**, 220–228 (2017).

[19] Y.-L. Ji, B.-X. Gu, Q.-F. An, and C.-J. Gao, "Recent advances in the fabrication of membranes containing ion pairs for nanofiltration processes", Polymers **9**, 715 (2017).

[20] H. Al-Zoubi and W. Omar, "Rejection of salt mixtures from high saline by nanofiltration membranes", Korean J. Chem. Eng. **26**, 799–805 (2009).

[21] Y.-N. Kwon and J. O. Leckie, "Hypochlorite degradation of crosslinked polyamide membranes: Ii. changes in hydrogen bonding behavior and performance", J. Membrane Sci. **282**, 456 – 464 (2006).

[22] J. Kang and L. Dähne, "Strong response of multilayer polyelectrolyte films to cationic surfactants", Langmuir **27**, 4627–4634 (2011), pMID: 21413752.

[23] Q. An, T. Huang, and F. Shi, "Covalent layer-by-layer films: Chemistry, design, and multidisciplinary applications", Chem. Soc. Rev. **47**, 5061–5098 (2018).

[24] P. H. Duong, J. Zuo, and T.-S. Chung, "Highly crosslinked layer-by-layer polyelectrolyte fo membranes: Understanding effects of salt concentration and deposition time on fo performance", J. Membrane Sci. **427**, 411421 (2013).

[25] K. L. Cho, A. J. Hill, F. Caruso, and S. E. Kentish, "Chlorine resistant glutaraldehyde crosslinked polyelectrolyte multilayer membranes for desalination", Adv. Mater. (2015).

[26] J. C. Dijt, M. A. Cohen Stuart, and G. J. Fleer, "Reflectometry as a tool for adsorption studies", Adv. Colloid Interface Sci. **50**, 79–101 (1994).

[27] J. Dickhout, M. Kleijn, R. G H Lammertink, and W. Vos, "Adhesion of emulsified oil droplets to hydrophilic and hydrophobic surfaces - effect of surfactant charge, surfactant concentration and ionic strength", Soft Matter **14**, 5452–5460 (2018).

[28] H. Bazyar, P. Lv, J. Wood, S. Porada, D. Lohse, and R. Lammertink, "Liquidliquid displacement in slippery liquid-infused membranes (slims)", Soft Matter **14**, 1780–1788 (2018).

[29] M. Antonietti, J. Conrad, and A. Thuenemann, "Polyelectrolyte-surfactant complexes: A new type of solid, mesomorphous material", Macromolecules **27**, 6007–6011 (1994).

[30] J. N. Israelachvili, "8 - special interactions: Hydrogen-bonding and hydrophobic and hydrophilic interactions", in *Intermolecular and Surface Forces (Third Edition)*, edited by J. N. Israelachvili, third edition edition, 151 – 167 (Academic Press, Boston) (2011).

[31] T. Takigawa and Y. Endo, "Effects of glutaraldehyde exposure on human health", J. Occup. Health **48**, 75–87 (2006).

[32] J. Park, J. Park, S. H. Kim, J. Cho, and J. Bang, "Desalination membranes from ph-controlled and thermally-crosslinked layer-by-layer assembled multilayers", J. Mater. Chem. **20**, 2085–2091 (2010).

[33] E. Virga, W. M. de Vos, and P. M. Biesheuvel, "Theory of gel expansion to generate electrical energy", EPL **120**, 46002 (2017).

[34] M. Migahed, MRSC and A. Al-Sabagh, "Beneficial role of surfactants as corrosion inhibitors in petroleum industry: A review article", Chem. Eng. Commun. **196**, 1054–1075 (2009).

6

Fouling of Nanofiltration Membranes based on Polyelectrolyte Multilayers: The Effect of a Zwitterionic Final Layer°

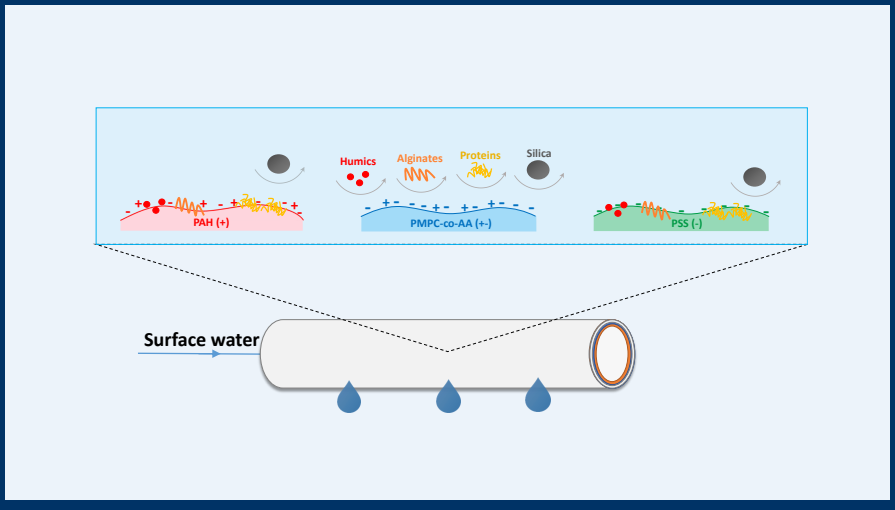

°Published as: **Ettore Virga**, Klara Zvab, and Wiebe M. de Vos, *Fouling of Nanofiltration Membranes based on Polyelectrolyte Multilayers: The Effect of a Zwitterionic Final Layer*, Journal of Membrane Science **2021**, *620*, 118793.

Abstract

In this work, we investigate the effect of membrane surface chemistry on fouling in surface water treatment for polyelectrolyte multilayer based nanofiltration (NF) membranes. The polyelectrolyte multilayer approach allows us to prepare three membranes with the same active separation layer, apart from a difference in surface chemistry: nearly uncharged crosslinked Poly(allylamine hydrochloride) (PAH), strongly negative poly(sodium 4-styrene sulfonate) PSS and zwitterionic poly(2-methacryloyloxyethyl phosphorylcholine-co-acrylic acid) (PMPC-co-AA). Initially, we study foulant adsorption for the three different surfaces (on model interfaces), to demonstrate how a different surface chemistry of the top layer affects the subsequent adsorption of five different model foulants (Humic Acids, Alginates, Silica Nanoparticles, negatively and positively charged Proteins). Subsequently, we study fouling of the same model foulants on our polyelectrolyte multilayer based hollow fiber NF membranes with identical surface chemistry to the model surfaces. Our results show that nearly uncharged crosslinked PAH surface generally fouls more than strongly negatively charged PSS surface. While negative BSA adsorbs better on PSS, probably due to charge regulation. Overall, fouling was mainly driven by electrostatic and acid-base interactions, which led, for both PAH and PSS terminated membranes, to flux decline and changes in selectivity. In contrast, we demonstrate through filtration experiments carried out with synthetic and real surface water, that the bio-inspired zwitterionic phosphatidylcholine surface chemistry exhibits excellent fouling resistance and thus stable performance during filtration.

6.1 Introduction

High quality drinking water is produced worldwide from surface water. This is partly possible thanks to the advances made in membrane filtration. In the last 20 years, membrane filtration has started to replace conventional water treatment techniques, such as coagulation, flocculation, sedimentation, flotation, and sand filtration [1, 2]. This is especially due to their versatility: membranes allow the removal of a wide spectrum of components, ranging from suspended solids (microfiltration) to small organic pollutants and ions (reverse osmosis) [2].

Among the various filtration techniques, nanofiltration (NF) has become an increasingly established technology in surface water treatment [3]. NF allows the removal of humic substances [4, 5], micropollutants [6, 7], heavy metals and salinity [8] from surface water, with a substantially lower energy footprint than reverse osmosis [2, 9].

However, one of the main challenges of membrane filtration is fouling [3, 10]. Membrane fouling is influenced by physical (e.g. permeation drag, shear forces) and chemical factors (e.g. hydrophobic interactions, ions binding effects) [11]. Humic acids, proteins, polysaccharides and solid particles can adsorb at the membrane surface and inside pores, and consequently reduce the flux of treated water. This phenomena leads to an increase in operating costs [10] and the need for membrane chemical cleaning [12], which in turn compromises the membrane stability over time [13]. Moreover, the presence of a fouling layer can have substantial impact on the membrane separation properties [14–16], especially on the retention of charged solutes, by changing the membrane surface charge density [17]. For NF, fouling can even be more complex to investigate , since the interactions that lead to fouling take place at the nanoscale, both in an on the active separation layer [3, 18].

Membrane surface chemistry plays a crucial role in fouling [19, 20]. Membrane fouling is a phenomena that occurs at the water-membrane interface, where foulants-surface interaction takes place [21, 22]. Membrane surface properties, such as surface charge, chemistry and roughness thus become very important [23]. A much investigated approach to reduce membrane fouling is to minimize the attractive interactions between the surface of the membrane and the foulants contained in the feed [24, 25]. For this reason, surface modification of existing membranes is considered an effective tool to reduce foulant-membrane interactions and indeed to design low fouling membranes [26–28].

An easy way to control the membrane surface chemistry and at the same time its separation properties, is the so called Layer-by-Layer (LbL) tech-

nique [29–32]. In LbL, a charged membrane is coated alternately with positive and negative polyelectrolytes, which overcharge the surface of the membrane during every coating step [33]. LbL allows a great deal of control over the properties of the active separation layer, while at the same time it provides large freedom on the choice of membrane surface chemistry [34–36]. This easy technique is proven to increase ion retention [37], selectivity [38, 39], and additionally to reduce membrane fouling [28, 40–42], but it typically leads to a surface with an excess of positive or negative charge [43].

The charge of the membrane surface is a key parameter in the design of low fouling membranes. Since several colloidal materials have a slight negative charge, due to the presence of acid groups (e.g. carboxyl, sulfonic and hydroxil), most commercial membranes are designed with a negative surface charge to reduce fouling [44]. Hydrophilic and negative membranes are less prone to fouling than positive ones, but a zwitterionic chemistry can further enhance membrane low-fouling properties [45–47]. Recently, among a new class of high-flux and fouling resistant zwitterionic-based membranes [48], the effect of different zwitterionic chemistries was investigated, and membranes prepared with 2-methacryloyloxyethyl phosphorylcholine (MPC) showed unprecedented fouling resistance during the filtration of proteins [49].

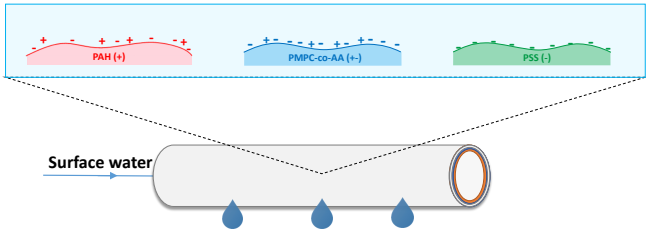

Figure 6.1: Illustration of a hollow fiber membrane with the same multilayer, except from the final adsorbed layer that determines the membrane surface chemistry.

In this work, we investigate the effect of membrane surface chemistry on fouling in surface water treatment for polyelectrolyte multilayer based nanofiltration membranes. Polyelectrolyte multilayers are ideal for such as study, as it is easy to create identical separation layers, with just the final layer having a different surface chemistry. Moreover, these membranes provide highly promising separation properties and thus very relevant membranes. Initially, the focus is on foulant adsorption on polyelectrolyte multilayers pre-

pared on model surfaces to demonstrate how a different surface chemistry of the top layer (nearly uncharged crosslinked Poly(allylamine hydrochloride) (PAH), strongly negative poly(sodium 4-styrene sulfonate) PSS and zwitterionic poly(2-methacryloyloxyethyl phosphorylcholine-co-acrylic acid) (PMPC-co-AA)) affects the subsequent adsorption of five different model foulants (Humic Acids, Alginates, Silica Nanoparticles, negatively and positively charged Proteins). Subsequently, we study fouling of the same model foulants on our PEM based hollow fiber NF membranes with identical surface chemistry to the model surfaces (Figure 6.1). Through filtration experiments carried out with synthetic and real surface water, we demonstrate that especially the zwitterionic surface chemistry, bio-inspired by zwitterionic phosphatidylcholine (PC) headgroups located on cell membranes, exhibits a very low susceptibility to fouling and leads to stable membrane performance.

6.2 Materials and Methods

6.2.1 Chemicals

Poly(allylamine hydrochloride) (PAH, Mw = 50 kDa), poly(sodium 4-styrene sulfonate) (PSS, Mw = 70 kDa), an aqueous solution of 25 wt% glutaraldehyde (GA, Grade II), acrylic acid (AA), 2-methacryloyloxyethyl phosphorylcholine (MPC, 295.27 Da), N-(3-Dimethylaminopropyl)-N-ethylcarbodiimide hydrochloride (EDC), N-Hydroxysuccinimide (NHS), ammonium persulfate ($(NH_4)_2S_2O_8$) and glycerin were purchased from Sigma-Aldrich (The Netherlands). Our model foulants, Alginic acid sodium salt from brown algae (Sodium alginate), Bovine Serum Albumin (BSA, chromatographically purified, $\geq$ 98 %), LUDOX® (AS-30 colloidal silica 30 wt% suspension in H_2O) and Lysozyme (from chicken egg white powder, crystalline 70000 U/mg), were purchased from Sigma-Aldrich (The Netherlands), whereas humic acids (Suwannee River Humic Acid Standard III) were purchased from International Humic Substances Society. Anthracite (1.2 - 2.0 mm) and sand (0.5 1.0 mm), used in the pre-filtration step, were supplied by SIBELCO Filcom B.V. (The Netherlands). A cartridge filter (DGD-2501 Dual-Gradient Polypropylene 25/1 20) was supplied by Pentair (The Netherlands). All other chemicals were purchased from VWR (The Netherlands).

6.2.2 Zwitterionic copolymer synthesis

Even if PMPC-co-AA is not purely zwitterionic [50] (due to the presence of AA groups), in the text we refer to it as zwitterionic. AA was added to the polymer to give a charge excess, needed to build-up the multilayer [51, 52], and allow for chemical crosslinking (via EDC and NHS) to the multilayer.

Our recipe for the synthesis of the zwitterionic PMPC-co-AA copolymer, was adapted from a recipe used for the synthesis of PSBMA [53]. 100 ml of demi water was flushed with nitrogen for 1 hour in a 500 mL Duran® bottle. In this, 5.0 g (16.8 mmol) MPC was dissolved under nitrogen atmosphere and later 2.42 g (33.6 mmol) AA was added. After 1 minute, 0.228 g (1 mmol) $(NH_4)_2S_2O_8$ was added. The mixture was left to react under nitrogen atmosphere at room temperature for 23 hours and then heated up to 50°C and left reacting for 2 hours more. Finally, the mixture was cooled down to room temperature and mixed with 400 mL of Ethanol to precipitate the polymer. The precipitated polymer was washed three times with 50 ml acetone and subsequently dried in a vacuum oven for 2 days. The zwitterionic copolymer was stored under vacuum to prevent water uptake and was used without any purification steps. Using ^{1}H NMR, the monomer distribution was estimated to be approximately 1:2 mole ratio of MPC/acrylic acid (see Figure D.1, Appendix D, for further details). This ratio allows for an adequate polymer charge excess, making the build-up of the multilayer easier.

6.2.3 Model surfaces coating with PEM

Polyelectrolyte solutions were prepared to have a concentration of 0.1 g/L polyelectrolyte dissolved in a 50 mM NaCl solution without pH adjustment (pH∼5.5). Each coating step was performed at room temperature. First, negatively charged SiO_2 wafers were cleaned with piranha solution to remove possible contaminants. Subsequently, the wafers were dipped for 15 minutes in a polycation (PAH in 50 mM NaCl) solution and then rinsed with a 50 mM NaCl aqueous solution for at least 15 minutes to remove any polyelectrolyte not well attached to the surface. To complete the first bilayer, the wafers were then immersed in polyanion (PSS in 50 mM NaCl) solution for 15 minutes. This step was then followed by another rinsing step. The procedure was repeated until the desired number of bilayers was reached. We coated 4.5 bilayers for the nearly uncharged (PAH) terminating layer, 5 bilayers for the negative (PSS) terminating layer. For the zwitterionic top layer, PMPC-co-AA was coated on top of 4.5 bilayers made of PAH/PSS. In addition, the model surfaces were

crosslinked to improve their stability. In case of PAH and PSS as top layers, the surfaces were immersed in a 7.5 mM glutaraldehyde for 5 hours, as described in our previous work [54], while in case of zwitterionic top layer, the wafers were firstly immersed in a 5 mM NHS and a 25 mM EDC solution for 1 hour to crosslink just the top layer [55, 56] and later in a 7.5 mM glutaraldehyde for 5 hours. We apply the same coating procedure on membranes (see paragraph 2.5).

6.2.4 Fouling study on model surfaces via reflectometry

Several compounds are present in typical surface water, including proteins, polysaccharides, humic acids, extracellular polymeric substances and solid particles. These fouling agents tend to adsorb on membrane surfaces and form a gel layer which can significantly promote bacterial growth and cause significant reduction in the flux of treated water [57]. For such a mixture of compounds, fouling can be difficult to study. Here, we have chosen to study five model compounds: negatively and positively charged proteins (i.e. BSA and Lysozyme), Humic Acids from Suwannee River, Alginates from brown algae, and LUDOX® colloidal silica.

We first studied fouling by the five foulants on model surfaces using reflectometry as investigation tool [58]. In order to determine the quantity of fouling agent adsorbed at the surface, we flushed different fouling agents in artificial surface water (with composition 2.92 mM NaCl, 0.57 mM $MgSO_4$, 1.47 mM $CaSO_4$ and 0.3 mM $MgCl_2$, paragraph 2.6) to silica surfaces, previously dip-coated with PEM as described above. After steady state in adsorption is reached, the surfaces rinsed with the same solution without fouling agents. The foulant adsorption/desorption here occours under well control hydrodynamic conditions, thanks to the use of a stagnation point flow cell. A polarized monochromatic light (HeNe laser, 632.8 nm), after hitting the wafer around the Brewster angle, is reflected towards a detector and splits into two polarized components. S (-) is the ratio between the two polarized components, and ΔS the change in this ratio, used calculate the mass of foulant adsorbed or desorbed from the model surface

$$\Gamma = \frac{\Delta S}{S_0} Q. \tag{6.1}$$

where Γ is the quantity of foulant (mg/m^2) which adsorbs or desorbs from the model surface, S_0 is the initial output signal of the model surface (-), and Q is the sensitivity factor (mg/m^2). To calculate Q, we used an optical model based

Fouling agent	dn/dc (mL/g)	Q (mg/m^2)
Lysozyme	0.19 [59]	30
BSA	1.67 [59]	30
Sodium alginate	0.165 [59]	30
LUDOX®	0.06 [60]	90
Humic acids	0.28 [61]	20

Table 6.1: Reflactive index increments (dn/dc) and sensitivity factors for the fouling agents

on the following values: θ=71°, n_{Si}=1.46, $\tilde{n}_{SiO_2}$=(3.85, 0.02), n_{H_2O}=1.33, δ_{SiO_2}=90 nm and refractive index increment dn/dc (mL/g), shown in Table 6.1. The calculated sensitivity factors Q for all fouling agents are also shown in Table 6.1. All experiments were performed at least in duplicate.

6.2.5 Hollow fiber membranes coating

Polyelectrolyte multilayers were coated on sulfonated polysulfone (SPES) hollow fiber membranes with a water permeability of 150 LMH/bar, an inner diameter of 0.7 mm, and a molecular weight cutoff (MWCO) of 7.5 kDa [54]. First, the fibers, stored in fresh water, were immersed in a 50 mM NaCl solution for 2 min at room temperature. Second, the fibers were fully dipped in a 0.1 g/L PAH solution with 50 mM NaCl for 15 min. Later, a rinsing step with a 50 mM NaCl solution followed and, after 15 min, the fibers were immersed in 0.1 g/L PSS solution with 50 mM NaCl (15 min) followed by another rinsing step (50 mM NaCl, 15 min). The described dip coating procedure was repeated until the desired number of bilayers was reached. In the case of PAH and PSS terminated layers, the fibers were crosslinked by immersion in a 7.5 mM GA solution for 5 hours. In the case of zwitterionic terminated layer, the fibers were first immersed in a 5 mM NHS and 25 mM EDC solution for 1 hour, and then dipped in a 7.5 mM glutaraldehyde solution with 50 mM NaCl for 5 hours. After rinsing in demi-water, the membranes were immersed in a solution of glycerol and water (15/85 wt %) for 4 h and left drying overnight at room temperature. Later, each single fiber, coated with PEM, was potted in a module with a fiber length of approximately 170 mm and mounted in our crossflow experimental set-up (Figure S2 and Figure S3, SI), were tested in order to measure water permeability and ion retention. We calculated the water permeability (LMH/bar, Figure S4) as ratio between the pure water

flux and the transmembrane pressure (TMP). Fluxes were measured at room temperature using demi-water at a transmembrane pressure of 3 bar. In order to measure the salt retention, we analyzed the ionic content of the feed and permeate by using ion chromatography (Metrohm Compact IC 761). All experiments were performed at least in triplicate.

6.2.6 Filtration of artificial surface water

In order to investigate the role of the chemistry of the final layer on membrane fouling, we prepared fouling solutions with a 100 mg/L concentration of fouling agent and pH = 6.3-6.5. We dissolved our fouling agents (sodium alginate, BSA, lysozyme, humic acid and LUDOX®, paragraph 2.4) in artificial surface water with the following composition: 2.92 mM NaCl, 0.57 mM $MgSO_4$, 1.47 mM $CaSO_4$ and 0.3 mM $MgCl_2$. This composition reflects the composition of the natural surface water (IJsselmeer, Afsluitdijk, The Netherlands) [62] used in our experiments with real river water (paragraph 2.7). In order to simplify the study, carbonate salts were not added to the artificial surface water. For the membrane crossflow filtration experiments, we use modules with single PEM-coated fibers as described in paragraph 2.5. The clean water flux and ions retention of every fiber was measured before filtration of the fouling agent. We used new modules for each different set of experiments. We recycled the concentrate stream to the feed tank while we collecting the permeate for 1 hour. We checked the pH, ionic concentration and TOC of the feed at every start and end of each experiment, to ensure that no siginificant changes in feed composition occurred, for example due to the used re-cycle. Such changes were never observed.

During the membrane filtration experiments a fouling solution was filtered for 3 hours at a TMP of 3 bar and a flow-rate of 0.75 kg/h (crossflow velocity ∼0.55 cm/s, Reynolds number ∼380). We measured the permeate flux between 2 h and 3 h after the start of the experiment. We collected permeate samples and analyzed their ionic concentration and TOC by ion chromatography (Metrohm Compact IC 761) and a TOC analyzer (Shimadzu TOC-L), respectively. Feed samples were taken before and after each experiment. To clean the membranes, the modules were exposed for 15 min to artificial river water at a 3.75 kg/h flow-rate, without applying TMP. Finally, we measured again the water permeability to calculate the flux recovery. Each experiment was performed at least in triplicate.

	Concentration (mg/L)
Ca^{2+}	52.8 ± 3.2
Na^{+}	81.7 ± 2.8
Mg^{2+}	15 ± 0.6
SO_4^{2-}	68.4 ± 2.6
Cl^{-}	136 ± 5.3
TOC	8.4 ± 1.6

Table 6.2: Composition of the pre-filtered surface water (IJsselmeer, Afsluitdijk, The Netherlands), feed water of the membrane crossflow experiments.

6.2.7 Real surface water filtration

Surface water was collected at the IJsselmeer (Afsluitdijk, The Netherlands) and pre-filtered, first, with a sand filter and, second, with a cartridge filter, in order to remove bigger particles and bacteria, which are not relevant for this study. The sand filter used in the pre-filtration step is based on two medias: anthracite (1.2 - 2.0 mm) and sand (0.5 1.0 mm). Each media has a 50 cm height. After the sand filter, a microfiltration step based on cartridge filter (1-25 μm) was applied to the water stream. The filtered surface water was later stored at 5°C and analyzed before each experiment. Its composition is reported in the table below:

For the membrane crossflow filtration experiments, we use modules with single PEM-coated fibers as described previously (paragraph 2.5). The clean water flux of every fiber was measured before the filtration of surface water. New modules were used for each different set of experiments. We recycled the concentrate to the feed tank and discharged the permeate, on the time scale of the experiment this did not lead to changes in the feed composition. Those small changes were measured and took into account by analyzing the feed pH, ionic content and TOC at the start and end of each experiments, by using average values in the retention calculations. During the membrane filtration experiments the surface water was filtered for 20 hours, again, at a TMP of 3 bar and a flow-rate of 0.75 kg/h (crossflow velocity ∼0.55 cm/s, Reynolds number ∼380). We measured again the permeate flux after 20 h experiment. We collected permeate samples and analyzed their ionic concentration as discussed above. To clean the membranes, the modules were exposed to DI water for 15 min at a 3.75 kg/h flow-rate, without applying transmembrane pressure. Finally, we measured again the water permeability to calculate the flux

recovery. Each experiment was performed at least in triplicate.

6.3 Results and Discussion

This Section is split into three distinct main parts. In the first part, we study the adsorption of model foulants, such as bioproteins (Lysozyme and BSA), standard humic acids, silica nanoparticles (LUDOX®) and alginates, on PEMs prepared on model surfaces with final layers with different charge and surface chemistry. In the second part, we investigate fouling by the same model foulants on hollow fiber membranes coated with identical polyelectrolyte multilayers. Here we investigate how the three different membrane top layers affects fouling in NF and additionally. In the third part, we apply our membranes for real surface water treatment, and analyze our previous results in terms of overall membrane performance and stability.

6.3.1 Foulant adsorption on model surfaces

During membrane operation, the chemistry of the foulants and the membrane surface are key parameters that will determine the extend of adsorption at the membrane surface. Using optical reflectometry, we studied the foulant adsorption on model surfaces pre-coated coated with same PEM, $(PAH/PSS)_{4.5}$, but with different surface chemistries of the final top layer. Each PEM was exposed to a fouling solution until a steady state in foulant adsorption was reached. The steady state in adsorption corresponds to the total amount of foulant adsorbed on the multilayer. In order to determine the amount of irreversible and reversible adsorption for every single fouling agent, the wafer was later flushed with a rinsing solution with the same pH and ion concentration as the fouling solution. This procedure allows to neglect possible effects on the optical signal due to changes in surface zeta potential and ion binding [63–65]. The irreversibility of foulant adsorption on model surfaces is discussed in Appendix D.

In Figure 6.2 we show the adsorption of the five model foulants, previously described, on $(PAH/PSS)_{4.5}$ based PEM with three different top layers: nearly uncharged crosslinked PAH, negatively charged PSS and zwitterionic PMPC-co-AA. The absolute adsorption values are generally small when compared with other results from literature. While Lysozyme adsorption was found to be $\sim$0.9 mg/m^2 and 0.7 mg/m^2, respectively for bare and polystyrene-coated silica surfaces [66, 67], for all the other foulants higher adsorption values are

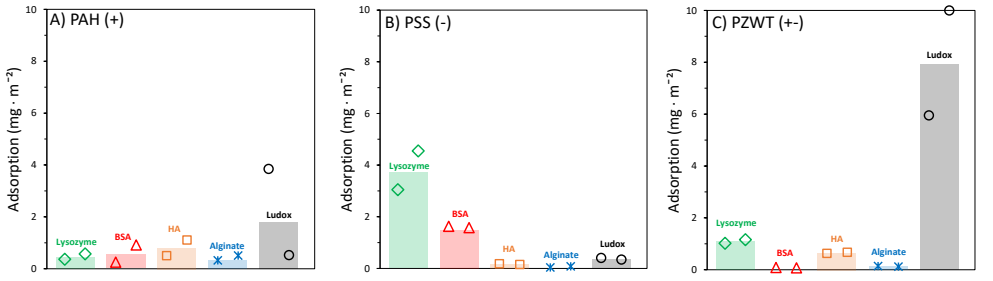

Figure 6.2: Adsorption (mg/m^2) of model fouling agents on model surfaces coated with PAH (A), PSS (B) and PMPC-co-AA (C) top layers. Results obtained via reflectometry. Bars show average values, while markers show data points from all individual measurements.

normally reported in literature. BSA adsorption was found to be ∼10 and 25 mg/m^2, respectively for negatively charged PAA brushes [68] and positively charged PAH terminated multilayers [69]. Also, LUDOX®, Alginate and HA are well known for giving high adsorbed amounts (> 6 mg/m2) especially on positive or neutral surfaces [69–72]

PEMs allow for highly hydrophilic and smooth surfaces[40, 41] which are well known to be less prone to foul [23, 73, 74]. Even if the adsorption values for all the foulants are relatively small, from Figure 6.2 we do observe that electrostatic interactions play a crucial role in foulant adsorption. Negatively charged foulants such as LUDOX®, Alginate and HA adsorb more on nearly uncharged crosslinked PAH (Figure 6.2A), in comparison to the negatively charged PSS (Figure 6.2B). On the other side, positively charged foulants, such as lysozyme, adsorb more on negatively charged PSS top layers.

However, adsorption is not only driven by charge based interactions between top layer and foulant, but Lewis acid-base interactions could also play a crucial role [75]. In Lewis acid-base interactions unpaired electrons are shared among polar surface functional groups (e.g membrane moieties), water molecules, and polar functional groups on the opposing surface or molecule (e.g. foulant) [76].

Negatively charged BSA adsorbs more on the negative PSS top layer (see Figure 6.2B), while negative LUDOX® nanoparticles lead to high adsorbed amounts on the zwitterionic PMPC-co-AA (see Figure 6.2C). BSA may adsorb better on negatively charged PSS due to charge regulation, an effect that

can lead to a charge inversion of the protein [68]. In addition, this adsorption may also be driven by the fact that BSA is a patchy protein, having at pH=6.5 a small region that is positively charged [77]. This region of the protein could complex with the negatively charged PSS [33]. On the other side, LUDOX® nanoparticles may adsorb better on the zwitterionic PMPC-co-AA probably due to hydrogen bond formation between the polymer phosphorylcholine groups and silica hydroxyls [78].

Adsorption is only an indication of how prone a surface is to fouling. Adsorption is not the only mechanism for membrane fouling, but usually foulant-foulant interactions dominate [79]. These interactions, and the constant accumulation of fouling agents at the membrane surface due to permeation, are responsible for the build-up of a cake layer [79, 80].

6.3.2 Effect of foulant chemistry on membrane fouling

The rejection of charged species, such as cations, anions or charged organic molecules, can change due to membrane fouling. During filtration, foulants can adsorb at the membrane surface and pores, changing the original surface chemistry of the membrane. Therefore, fouling could lead to a decrease in water permeability as well as a change in ion and organics retentions, as a consequence of the change in membrane surface chemistry.

In order to monitor fouling for the three different top layers during filtration, first we measure the flux decline of our membranes with pure water and later perform a 3 hours experiment with synthetic surface water containing one of the model foulants. Then, we define as flux decline the ratio between the flux during model foulant filtration and the previously measured flux of pure water. Here, we also measure the ion retentions of clean and fouled membranes, since it helps us in understanding if the surface chemistry of our membrane changed due to the build up of a fouling layer. We finally try to quantify the membrane flux recovery by first flushing the membrane with synthetic surface water without any fouling agent and then measuring again the flux of pure water. We applied this method to all fouling agents: Lysozyme, BSA, LUDOX®, Alginate and HA.

6.3.2.1 Ion retentions for clean membranes

In Figure 6.3, we show ion retentions for clean hollow fiber membranes when synthetic surface water (without addition of foulants) is used. Figure 6.3A, 6.3B and 6.3C respectively show ion retentions for nearly uncharged

crosslinked PAH, negatively charged PSS and zwitterionic PMPC-co-AA top layers. In particular, we show retentions of Ca^{2+}, Na^{+}, Mg^{2+}, SO_4^{2-} and Cl^{-}. For each top layer, we can see that the rejection of ions is probably determined by both Donnan and dielectric exclusion [81]. We show high rejection of sulfate ions, in particular for anionic PSS (Figure 6.3B) and zwitterionic PMPC-co-AA (Figure 6.3C) top layers. All the membranes investigated have a negative zeta potential. In particular, the zeta potentials for PAH, PSS and PMPC-co-AA top layers are respectively -11.8, -37.4 and -24.7 mV (SI, Figure S5). Crosslinking of the weakly cationic primary amines of PAH changes the charge balance in the multilayer, decreasing the positive charge leading to a small negative surface charge [82]. This leads to a stronger Donnan-based repulsion towards SO_4^{2-}, as already shown in previous works [54]. Since membranes with a PAH top layer are overall nearly uncharged, we assume that still some positive PAH moieties are available on the membrane surface. On the other side, PMPC-co-AA membranes are negatively charged, probably due to the residual AA groups.

Still, if the Donnan exclusion mechanism was the only mechanism responsible for ion retention, we would expect lower retentions of Ca^{2+} and Mg^{2+} respect to Na^{+}. But other ions exclusion mechanisms, such as dielectric exclusion [81], can take place in our system. In particular, the dielectric exclusion mechanism may explain why Ca^{2+} and Mg^{2+} have a higher retention than Na^{+}. Ions and polymer moieties polarise their interfaces in water proportionally to their ionic charge. Differences in dielectric constants of the water between bulk solution and membrane separation layer contribute to an exclusion energy, which is proportional to the square of the ion charge [81], higher for divalent ions than monovalent ions [83]. This effect would thus be caused by the inner part of the polyelectrolyte multilayer, indeed leading to quite similar salt retentions for the three membranes where only the final outer layer is different.

6.3.2.2 Filtration of Lysozyme

In Figure 6.4, we show ion retentions and flux decline for crossflow filtration experiments carried out on synthetic surface water with positively charge Lysozyme as a model foulant. Specifically, Figures 6.4A, 6.4B and 6.4C, show ion retentions, as well as lysozyme retention, and flux decline respectively for cationic PAH, anionic PSS and zwitterionic PMPC-co-AA terminated PEM based NF membranes. Flux recovery is discussed together with irreversibility of adsorption in the SI, Figure S6.

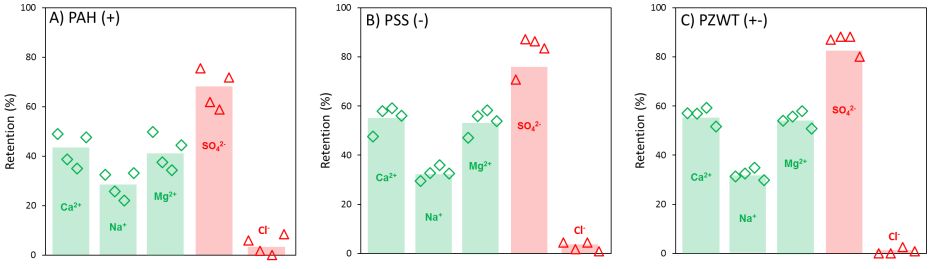

Figure 6.3: Retentions of Ca^{2+}, Na^{+}, Mg^{2+}, SO_4^{2-} and Cl^{-} from membranes coated with A) PAH, B) PSS and C) PMPC-co-AA top layers in experiments performed with synthetic surface water. The synthetic surface water was made of 2.92 mM NaCl, 0.57 mM $MgSO_4$, 1.47 mM $CaSO_4$ and 0.3 mM $MgCl_2$ [62]. Bars show average values, while markers show data points from all individual measurements.

For PAH (Fig.6.4A) and PSS (Fig.6.4B) top layers, we do observe a significant increase in divalent cations retention (Ca^{2+} and Mg^{2+}) compared to Figures 6.3A and 6.3B, respectively. Contrarily, no significant changes in retention are observed for PMPC-co-AA surface chemistry (Figs.6.4C and 6.3C). In addition, Figures 6.4A and 6.4B show ∼30% and ∼45% flux decline, respectively for PAH and PSS top layers, while almost no flux decline is observed for PMPC-co-AA chemistry (Fig.6.4C).

The flux decline observed for PAH and PSS, together with the increased retention in divalent cations, strongly suggest the build-up of a lysozyme fouling layer on top of the membrane surface. Lysozyme is completely retained by the membranes, and since they are positively charged, their adhesion to the membrane surface leads to an increase in Ca^{2+} and Mg^{2+} retention. This change in retention is mainly driven by additional Donnan exclusion effects. Sulphate, SO_4^{2-}, is, however, still highly retained by the membrane, proving that retention is the result of a combination of effects , dielectric exclusion [81] and electroneutrality included.

Lysozyme is positively charged around neutral pH [84] and its adsorption on negative surfaces is mainly driven by electrostatic forces [85]. On negative Silica, lysozyme adsorption changes the zeta potential from negative to positive values [86]. Previous studies have reported high degrees of adsorption and fouling on negatively charged NF and UF membranes[87]. However, lysozyme

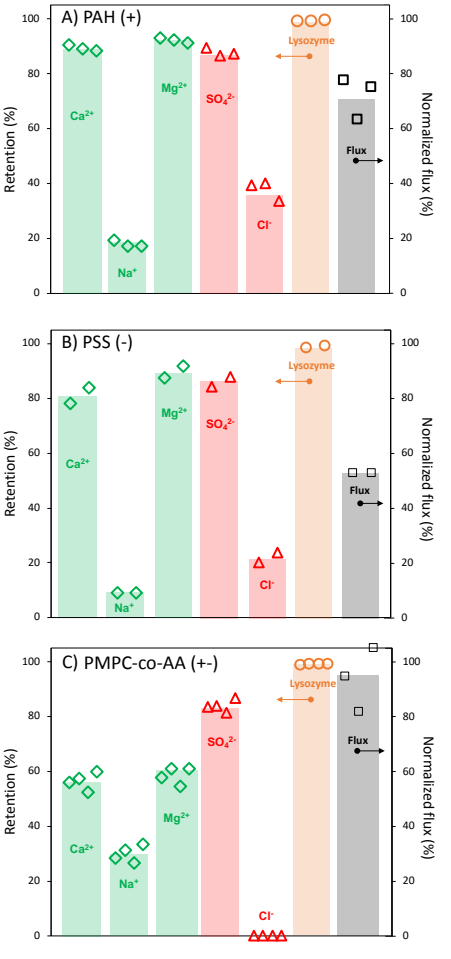

Figure 6.4: Retentions of Ca^{2+}, Na^{+}, Mg^{2+}, SO_4^{2-}, Cl^{-}, Lysozyme and normalized flux (after fouling) for membranes coated with A) PAH, B) PSS and C) PMPC-co-AA top layers in experiments performed with synthetic surface water. The synthetic surface water was made of 2.92 mM NaCl, 0.57 mM $MgSO_4$, 1.47 mM $CaSO_4$, 0.3 mM $MgCl_2$ and 100 mg/L of Lysozyme. Bars show average values, while markers show data points from all individual measurements.

is a small protein, with a molecular weight of ∼14.3 kDa [88]. Lysozyme due to its size cannot diffuse through the membrane and it is thus stopped at the membrane surface where adsorption takes place. Therefore the inner layers will still keep their negative charge.

While a flux decline is observed for PAH fouled by lysozyme, the observed adsorption values (Figure 6.2) were rather low. This could indicate a more dominant role of foulant-foulant interactions in the observed fouling. In reflectometry experiments we do see a small lysozyme adsorption on PMPC-co-AA surfaces (Fig.6.2C), but it does not influence the flux, probably due to the formation of a much more open fouling layer. The high degree of hydration of the zwitterionic moieties leads to a large energy barrier for the protein adsorption [49], preventing the build-up of a dense gel layer on top of the membrane.

6.3.2.3 Filtration of BSA

Figure 6.5 shows the results of our crossflow filtration tests where BSA, as the model foulant, is added to our synthetic surface water. Here, Figures 6.5A, 6.5B and 6.5C, show ion retentions, BSA retention and flux decline respectively for PAH, PSS and PMPC-co-AA top layers.

For PAH (Fig.6.5A) and for PSS (Fig.6.5B) surfaces, we mainly observe a small (∼10%) increase in sulphate SO_4^{2-} retention compared to filtration without foulants (Figures 6.3A and 6.3B). Contrarily, for our polyzwitterionic top layer, made of PMPC-co-AA, we observe almost ∼10% decrease in all divalent ions retention (see Figs. 6.5C and 6.3C). Again, PAH and PSS present flux decline (respectively ∼20% and ∼45%, see Figs. 6.5A and 6.5B), while no flux decline is observed for PMPC-co-AA surface chemistry (Fig.6.5C).

The flux decline, observed for PAH and PSS, suggests that a BSA fouling layer maybe responsible for the increased retention in sulphate. BSA is a relatively big protein (66.5 kDa, bigger than lysozyme) and negatively charged at neutral pH [86]. Adsorption of BSA on PAH and PSS membranes can explain why SO_4^{2-} retention increases (increased Donnan exclusion). In addition, BSA is overall well retained by all our membranes.

Figure 6.5 also shows that BSA fouls PSS membranes more strongly than PAH membranes. This result is in agreement with the adsorption studies we carried out on model surfaces (paragraph 6.3.1, Fig.6.2). Indeed, BSA is a patchy protein, and at the pH of our experiments (∼6.5) it has a small region with positive charge [77] which can complex with negatively charged PSS [33]. As discussed before, BSA may adsorb better, and therefore increase fouling, on PSS rather than PAH, due to charge regulation, that can lead to protein

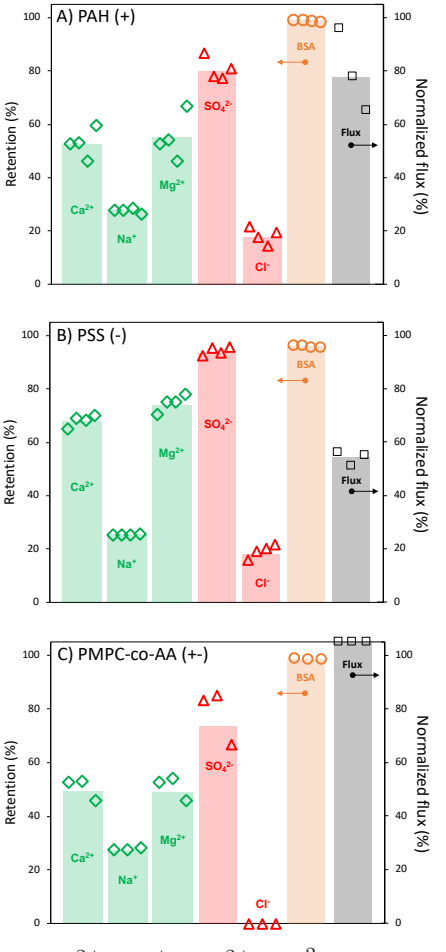

Figure 6.5: Retentions of Ca^{2+}, Na^{+}, Mg^{2+}, SO_4^{2-}, Cl^{-}, BSA and normalized flux (after fouling) for membranes coated with A) PAH, B) PSS and C) PMPC-co-AA top layers in experiments performed with synthetic surface water. The synthetic surface water was made of 2.92 mM NaCl, 0.57 mM $MgSO_4$, 1.47 mM $CaSO_4$, 0.3 mM $MgCl_2$ and 100 mg/L of BSA. Bars show average values, while markers show data points from all individual measurements.

charge inversion [68].

6.3.2.4 Filtration of Humic Acids and Alginates

In Figure 6.6, we show the results obtained for Humic Acids as fouling agent. For PAH (Fig.6.6A) and PMPC-co-AA (Fig.6.6C) we observe ∼10% increase in sulphate SO_4^{2-} retention compared to filtration without foulants (Figures 6.3A). For membranes with PSS top layers, we have no significant changes in ion retentions (Fig.6.6B). PAH shows ∼25% flux decline (Fig.6.6A), PSS ∼15% (Fig.6.6B), but again no flux decline is observed for PMPC-co-AA (Fig.6.6C).

The flux decline, observed for PAH, may suggest the build-up of a HA fouling layer which could increase the retention of sulphate. These HA are a mixture of negatively charged organic molecules, where the charge is mainly due to carboxyl groups [89]. Adsorption of HA on PAH may constitute a negatively charged layer on top which, via Donnan exclusion, increases the retention of SO_4^{2-}. This fouling layer does not clearly influence the retentions for PSS membranes. In addition, HA are ∼100% retained by all our membranes.

Very similar behaviour is observed for Alginates, for which we do not see significant differences in retention for PAH and PSS top layers, while we do note, in both cases, ∼15% flux decline (SI, Figure S7). For both HA and alginates with PSS we observed flux decline but little adsorption (Figure 6.2). This may be due to foulant-foulant interactions which could dominate in the observed fouling. For PMPC-co-AA top layer, we observe ∼10% increase in sulphate retention, but no flux decline (Fig.S6).

Our alginates are acid polysaccharides present in the extracellular matrix of brown algae [90]. The alginate used in this study has a molecular weight distribution from about 12 to about 80 kDa and contains approximate 61% mannuronic acid and 39% guluronic acid [91]. The high carboxylate content gives rise to a high propensity to form cation-stabilized gels, especially with Mg^{2+} and Ca^{2+} [92]. Such a gel layer may cause flux decline in both PAH and PSS membranes. On the other hand, the 2-methacryloyloxyethyl phosphorylcholine (MPC) moiety of our PMPC-co-AA is believed to keep the free water fraction on the top layer surface at a high level [93], which may inhibit the polysaccharides adsorption.

6.3.2.5 Filtration of LUDOX Colloidal Silica

In Figure 6.7, we show the results for LUDOX® colloidal silica. For LUDOX® particles, we do not observe significant differences in retention for all top layers

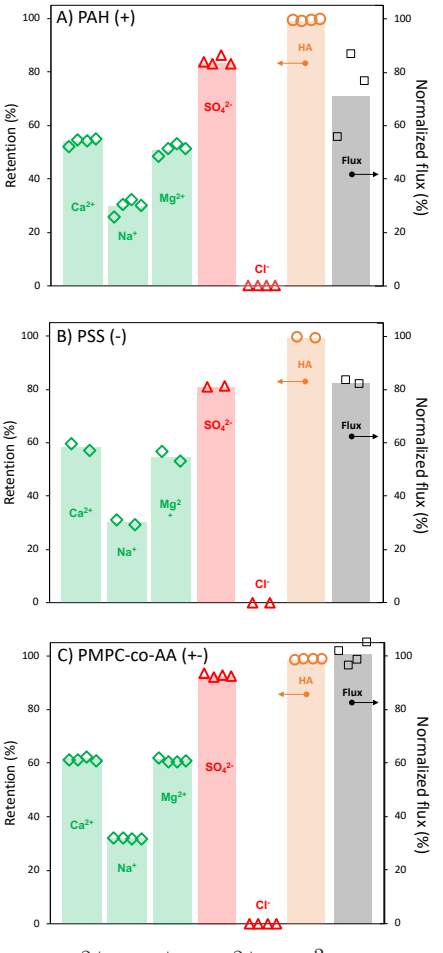

Figure 6.6: Retentions of Ca^{2+}, Na^{+}, Mg^{2+}, SO_4^{2-}, Cl^{-}, HA and normalized flux (after fouling) for membranes coated with A) PAH, B) PSS and C) PMPC-co-AA top layers in experiments performed with synthetic surface water. The synthetic surface water was made of 2.92 mM NaCl, 0.57 mM $MgSO_4$, 1.47 mM $CaSO_4$, 0.3 mM $MgCl_2$ and 100 mg/L of HA. Bars show average values, while markers show data points from all individual measurements.

(Fig.6.7A, Fig.6.7B and Fig.6.7C). However, such a low retention is unexpected relatively to the size of colloidal size (12 nm). We can easily conclude that this result was probably affected by the dissolution of silicon from glassware the permeate analysis. In addition, almost no flux decline is monitored in all cases. This result is no surprise, as colloidal silica is negatively charged, as well as our membranes, and relatively big (12 nm in diameter) compared to the other model foulants. For this reason a dense fouling layer, on top of the membrane surface, is unlikely to be formed. However, in reflectometry we observed significant fouling for top layers, while in our filtration experiments no fouling was observed. Colloidal particles are known to give very open cake layers [94], therefore the resistance of the colloidal silica cake layer is quite low compared to the NF membrane resistance. This can explain why, even if there is expected to be adsorption, colloidal fouling does not significantly affect the NF flux or the separation performance.

6.3.3 Treatment of Real Surface Water and Stability of Membranes Performance

6.3.3.1 Real Surface Water Treatment

A hollow fiber NF membrane with a low-fouling tendency would be highly beneficial for surface water treatment, as one could remove organics and multivalent ions from water at lower energy consumption.

In Figure 6.8, we show ion (Ca^{2+}, Na^{+}, Mg^{2+}, SO_4^{2-}, Cl^{-}) and organics (TOC) retentions for HF membranes with different top layers (PAH, PSS and PMPC-co-AA, respectively Figs. 6.8A, 6.8B and 6.8C). The ion retentions of the three different top layers do not differ significantly from the experiments we carried out with synthetic surface water (Fig. 6.3). Differently, the three membranes present quite different retention values for organics, which do not reflect the experiments carried out with our model foulants. In particular, PAH presents a retention average of ∼40%, PSS ∼0% and PMPC-co-AA ∼70%. No significant flux decline was observed in all three cases.

The similarities between Fig. 6.8 and Fig. 6.3, together with similarities in feeds concentrations, suggest that the retention is not affected by the presence of a fouling layer, which also explains why no flux decline was observed. Differently, organics are able to permeate through the membrane, suggesting that probably the organics in the feed have (in average) a relatively low molecular weight compared to the model foulants that we tested.

The relative organics retention is found to increase in the order PSS < PAH

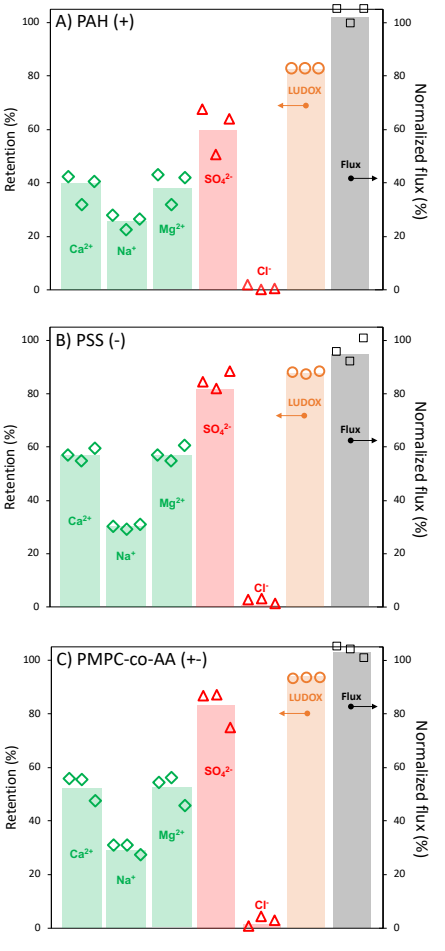

Figure 6.7: Retentions of Ca^{2+}, Na^{+}, Mg^{2+}, SO_4^{2-}, Cl^{-}, LUDOX® and normalized flux (after fouling) for membranes coated with A) PAH, B) PSS and C) top layers in experiments performed with synthetic surface water. The synthetic surface water was made of 2.92 mM NaCl, 0.57 mM $MgSO_4$, 1.47 mM $CaSO_4$, 0.3 mM $MgCl_2$ and 100 mg/L of LUDOX®. Bars show average values, while markers show data points from all individual measurements.

< PMPC-co-AA and can be a consequence of the relative water permeability which, inversely, decreases in the same order PSS > PAH > PMPC-co-AA (11.8, 7.8 and 5.45 LMH/bar, respectively, SI). Membranes terminated with PSS are more permeable to water than PAH membranes, probably due to their higher hydration [95]. On the other side, the PMPC-co-AA membrane is denser, probably due to the additional crosslinking of the carboxyl-amine groups [55, 56]. We can conclude that our zwitterionic surface chemistry performed really well, since it did not exhibit fouling and additionally it retained 70% of the organics in the feed.

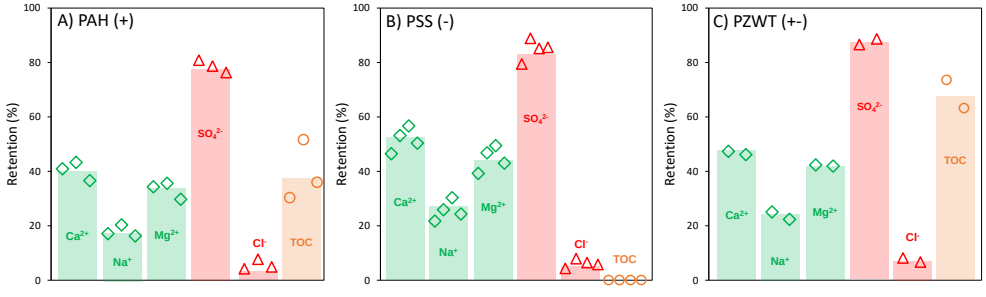

Figure 6.8: Retentions of Ca^{2+}, Na^{+}, Mg^{2+}, SO_4^{2-}, Cl^{-} and TOC from membranes coated with A) PAH, B) PSS and C) PMPC-co-AA top layers in experiments performed with real surface water collected at Afsluitdijk and pre-filtered with sand filter and cartridge filter. Bars show average values, while markers show data points from all individual measurements.

6.3.3.2 Overall Performance stability

Fouling compromises the stability and selectivity of membrane separations [96], as it leads to an increase in hydraulic resistance during filtration, additional energetic costs, and frequent need for chemical cleaning [97]. All these factors lead to a productivity decline in water treatment, which is connected with the decline in permeability and the need to supply additional energy to keep filtration performances constant overtime.

For efficient industrial applications, membranes need to demonstrate stable performances overtime. A stable performance ideally translates into fouling resistant membranes, which ideally allow for a constant water permeability and stable permeate quality. Unfortunately, commercial membranes are usually

charged, and as investigated in section 6.3.2, this charge excess can lead to fouling.

Collecting the results of the experiments shown in section 6.3.2, we studied the performance of our membranes in all our experiments and analyzed their stability. In Figure 6.9, we show the stability of our membranes in terms of normalized flux (Figure 6.9A) and deviation, Δ, in divalent ions retention (Figure 6.9B), i.e. the percentage of deviation in Ca^{2+}, Mg^{2+} and SO_4^{2-} retention. This parameter is calculated for each ion by subtracting the retention of the divalent ion for a clean membrane from the actual retention, and then dividing the result by the clean membrane retention.

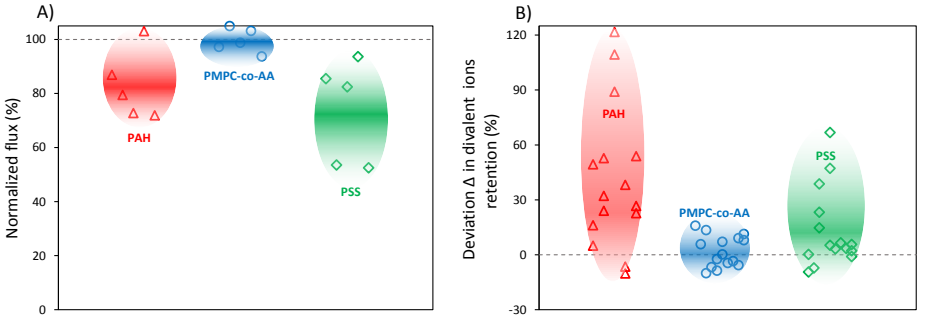

Figure 6.9: Membranes performance, for PAH, PSS and PMPC-co-AA top layer, in terms of A) Normalized flux (%) and B) Deviation Δ in divalent ion retention (%). Markers represent the average of Figs.6.4-6.7 data points, while shapes enclosing these markers darken on the average for each top layer.

From Figure 6.9, we can see how the membrane surface chemistry, the only difference between our membranes, plays a big role both in flux decline and retention properties compared to clean membranes. In Figure 6.9A, we can see that while PAH and PSS top layered membranes show significant flux declines, the zwitterionic top layer allows for stable water fluxes, which is ideal from an industrial perspective. The high fouling resistance of our PMPC-co-AA membrane is mainly related to the preservation of the water structure at the membrane surface-solution interface. The high degree of hydration around the zwitterionic moieties, mainly due to strong electrostatic interactions and hydrogen bonding, leads to a large energy barrier which prevents the adsorption of foulants [49].

On the other side, Figure 6.9B shows how fouling affects the retention prop-

erties of our membranes in terms of divalent ions retention. PAH, due to the formation of fouling layer, increases retention of divalent ions up to 120%, while for PSS the performances a more stable with highest changes around 70 %. Again, the zwitterionic top layers allow for stable performances with way smaller changes in retention, which oscillate around the zero value. This translates into a quality of the permeate constant overtime. We can conclude that, if we look at both parameters, our zwitterionic top layer is highly beneficial since it allows for stable water permeability and permeate quality during filtration, for all five model foulants. Still, future studies could focus on further optimizing the PMPC-co-AA membrane, in particular its water permeability.

During the last decades, thin film composite (TFC) membranes have been extensively used in RO [98] and NF processes [99]. The most commonly used TFC membranes (e.g. produced by Dow Filmetch and Hydronautics) [100] consist of an active polyamide layer deposited on a porous polysulfone support [82]. At neutral pH, TFC membranes have similar zeta potential to our crosslinked PAH membranes [101]. During chemical crosslinking, the primary amines ($pK_a \sim 9$) of our PAH layers convert into imines ($pK_a \sim 4$) giving, at neutral pH, a net negative charge to the membrane [82]. Our PAH terminated membranes thus have a comparable charge, crosslinked structure and a relatively similar chemical structure (imine bonds instead of amide) at the membrane surface as TFC membranes.

For the above reasons we do believe that the finding of our work, especially the results obtained for PAH membranes, are relevant for TFC membranes. Still, other determinant factors, such as membrane roughness and specific acid-base interactions, need to be considered. It is well known that a higher surface roughness, typically associated to TFC membranes, would increase the rate and extent of colloidal fouling [102], while stronger lewis acid-base interactions between membrane and foulant could also worsen membrane fouling.

An important point to make, however, is that polyamide TFC membranes are still commercially available only as flat sheets, as it is quite difficult to make TFC membranes via IP in a hollow fiber configuration [103]. Here, our PEM based membranes have the advantage that hollow fiber manufacturing is very straightforward. In regards to fouling, hollow fiber membranes have the large advantage compared to flat sheet (spiral wound) configurations that spacer fouling is not a problem.

6.4 Conclusions

Charged interfaces, usually present in commercial membranes, have the downside that fouling of oppositely charged components can readily occur. This can increase filtration costs and affect separation selectivity. In this work, we investigated the effect of membranes surface chemistry on fouling during surface water treatment for polyelectrolyte multilayer based nanofiltration membranes. We prepared three membranes with the same active separation layer but a different surface chemistry, including nearly uncharged crosslinked PAH, strongly negatively charged PSS and zwitterionic PMPC-co-AA. Initially, we focused on foulant adsorption for the three differently terminated multilayers on model surfaces to demonstrate how a different surface chemistry of the top layer affects the subsequent adsorption of five different model foulants (Humic Acids, Alginates, Silica Nanoparticles, negatively and positively charged Proteins). Later, we studied fouling of the same model foulants on our polyelectrolyte multilayer based hollow fiber NF membranes with identical surface chemistries to the model surfaces. Generally, the nearly uncharged crosslinked PAH surface chemistry fouls more than the strongly negatively charged PSS. While negative BSA adsorbs better on PSS, probably due to charge regulation. Overall fouling was mainly driven by electrostatic and acid-base interactions, which led, for both nearly uncharged crosslinked PAH and strongly negatively PSS, to flux decline and changes in separation selectivity. Filtration experiments, carried out with synthetic and real surface water, demonstrated that our bio-inspired zwitterionic phosphatidylcholine surface chemistry exhibits excellent fouling resistance and stable performances during filtration. The stable selectivity, and exceptional fouling resistance of these membranes makes them promising not only for surface water treatment but also for bio-molecule separation, and filtration of other feeds with large fouling potential.

References

[1] B. Van Der Bruggen, C. Vandecasteele, T. Van Gestel, W. Doyen, and R. Leysen, “A review of pressure-driven membrane processes in wastewater treatment and drinking water production”, Environmental Progress **22**, 46–56 (2003).

[2] D. M. Warsinger *et al.*, “A review of polymeric membranes and processes for potable water reuse”, Progress in Polymer Science **81**, 209 – 237 (2018).

[3] A. Mohammad, Y. Teow, W. Ang, Y. Chung, D. Oatley-Radcliffe, and N. Hilal, "Nanofiltration membranes review: Recent advances and future prospects", Desalination **356**, 226 – 254 (2015), state-of-the-Art Reviews in Desalination.

[4] A. R. Costa and M. N. de Pinho, "Performance and cost estimation of nanofiltration for surface water treatment in drinking water production", Desalination **196**, 55 – 65 (2006).

[5] R. Bian, Y. Watanabe, N. Tambo, and G. Ozawa, "Removal of humic substances by uf and nf membrane systems", Water Science and Technology **40**, 121 – 129 (1999).

[6] D. M. Reurink, E. te Brinke, I. Achterhuis, H. D. W. Roesink, and W. M. de Vos, "Nafion-based low-hydration polyelectrolyte multilayer membranes for enhanced water purification", ACS Applied Polymer Materials **1**, 2543–2551 (2019).

[7] K. V. Plakas and A. J. Karabelas, "Removal of pesticides from water by nf and ro membranes a review", Desalination **287**, 255 – 265 (2012), special Issue in honour of Professor Takeshi Matsuura on his 75th Birthday.

[8] M. Pontieť, C. Diawara, M. Rumeau, D. Aureau, and P. Hemmery, "Seawater nanofiltration (nf): fiction or reality?", Desalination **158**, 277 – 280 (2003), desalination and the Environment: Fresh Water for All.

[9] L. Naidu, S. Saravanan, C. Manickam, M. Goel, A. Das, and J. Babu, "Nanofiltration in transforming surface water into healthy water: Comparison with reverse osmosis", Journal of Chemistry **2015**, 1–6 (2015).

[10] W. Guo, H.-H. Ngo, and J. Li, "A mini-review on membrane fouling", Bioresource Technology **122**, 27 – 34 (2012), membrane Bioreactors (MBRs): State-of-Art and Future.

[11] W. Zhang and B. Dong, "Effects of physical and chemical aspects on membrane fouling and cleaning using interfacial free energy analysis in forward osmosis", Environmental Science and Pollution Research **25**, 21555–21567 (2018).

[12] N. Porcelli and S. Judd, "Chemical cleaning of potable water membranes: A review", Separation and Purification Technology **71**, 137 – 143 (2010).

[13] X. Shi, G. Tal, N. P. Hankins, and V. Gitis, "Fouling and cleaning of ultrafiltration membranes: A review", Journal of Water Process Engineering **1**, 121 – 138 (2014).

[14] C. Bellona, M. Marts, and J. E. Drewes, "The effect of organic membrane fouling on the properties and rejection characteristics of nanofiltration membranes", Separation and Purification Technology **74**, 44 – 54 (2010).

[15] F. Kramer, R. Shang, L. Rietveld, and S. Heijman, "Influence of ph, multivalent counter ions, and membrane fouling on phosphate retention during ceramic nanofiltration", Separation and Purification Technology **227**, 115675 (2019).

[16] Y. ying Zhao, X. mao Wang, H. wei Yang, and Y. feng F. Xie, "Effects of organic fouling and cleaning on the retention of pharmaceutically active compounds by ceramic nanofiltration membranes", Journal of Membrane Science **563**, 734 – 742 (2018).

[17] L. D. Nghiem and S. Hawkes, "Effects of membrane fouling on the nanofiltration of pharmaceutically active compounds (phacs): Mechanisms and role of membrane pore size", Separation and Purification Technology **57**, 176 – 184 (2007).

[18] B. Van der Bruggen, M. Mänttäri, and M. Nyström, "Drawbacks of applying nanofiltration and how to avoid them: A review", Separation and Purification Technology **63**, 251–263 (2008).

[19] M. F. A. Goosen, S. S. Sablani, H. AlHinai, S. AlObeidani, R. AlBelushi, and D. Jackson, "Fouling of reverse osmosis and ultrafiltration membranes: A critical review", Separation Science and Technology **39**, 2261–2297 (2005).

[20] I. Ibrar, O. Naji, A. Sharif, A. Malekizadeh, A. Al Hawari, A. Alhathal Alanezi, and A. Altaee, "A review of fouling mechanisms, control strategies and real-time fouling monitoring techniques in forward osmosis", Water **11**, 695 (2019).

[21] R. Oliveira, "Understanding adhesion: A means for preventing fouling", Experimental Thermal and Fluid Science **14**, 316 – 322 (1997).

[22] B. He, Y. Ding, J. Wang, Z. Yao, W. Qing, Y. Zhang, F. Liu, and C. Y. Tang, "Sustaining fouling resistant membranes: Membrane fabrication,

characterization and mechanism understanding of demulsification and fouling-resistance", Journal of Membrane Science **581**, 105 – 113 (2019).

[23] D. Norberg, S. Hong, J. Taylor, and Y. Zhao, "Surface characterization and performance evaluation of commercial fouling resistant low-pressure ro membranes", Desalination **202**, 45 – 52 (2007), wastewater Reclamation and Reuse for Sustainability.

[24] L. Upadhyaya, X. Qian, and S. R. Wickramasinghe, "Chemical modification of membrane surfaceoverview", Current Opinion in Chemical Engineering **20**, 13 – 18 (2018), nanotechnology / Separation Engineering.

[25] Y.-R. Chang, Y.-J. Lee, and D.-J. Lee, "Membrane fouling during water or wastewater treatments: Current research updated", Journal of the Taiwan Institute of Chemical Engineers **94**, 88 – 96 (2019).

[26] G.-d. Kang and Y.-m. Cao, "Development of antifouling reverse osmosis membranes for water treatment: A review", Water research **46**, 584–600 (2011).

[27] S. M. J. Zaidi, K. A. Mauritz, and M. K. Hassan, *Membrane Surface Modification and Functionalization*, 391–416 (Springer International Publishing, Cham) (2019).

[28] S. P. Nunes, "Can fouling in membranes be ever defeated?", Current Opinion in Chemical Engineering **28**, 90 – 95 (2020).

[29] J. Saqib and I. H. Aljundi, "Membrane fouling and modification using surface treatment and layer-by-layer assembly of polyelectrolytes: State-of-the-art review", Journal of Water Process Engineering **11**, 68 – 87 (2016).

[30] F. Crespilho, V. Zucolotto, and O. Oliveira, "Electrochemistry of layer-by-layer films: a review", International Journal of Electrochemical Science **1** (2006).

[31] W. Jin, A. Toutianoush, and B. Tieke, "Use of polyelectrolyte layer-by-layer assemblies as nanofiltration and reverse osmosis membranes", Langmuir **19**, 2550–2553 (2003).

[32] V. A. Izumrudov, B. K. Mussabayeva, and K. B. Murzagulova, "Polyelectrolyte multilayers: preparation and applications", Russian Chemical Reviews **87**, 192–200 (2018).

[33] W. M. de Vos and S. Lindhoud, "Overcharging and charge inversion: Finding the correct explanation(s)", Advances in Colloid and Interface Science **274**, 102040 (2019).

[34] L. Y. Ng, A. W. Mohammad, and C. Y. Ng, "A review on nanofiltration membrane fabrication and modification using polyelectrolytes: Effective ways to develop membrane selective barriers and rejection capability", Advances in Colloid and Interface Science **197-198**, 85 – 107 (2013).

[35] N. Joseph, P. Ahmadiannamini, R. Hoogenboom, and I. F. J. Vankelecom, "Layer-by-layer preparation of polyelectrolyte multilayer membranes for separation", Polym. Chem. **5**, 1817–1831 (2014).

[36] J. de Grooth, R. Oborný, J. Potreck, K. Nijmeijer, and W. M. de Vos, "The role of ionic strength and oddeven effects on the properties of polyelectrolyte multilayer nanofiltration membranes", Journal of Membrane Science **475**, 311 – 319 (2015).

[37] D. Menne, J. Kamp, J. E. Wong, and M. Wessling, "Precise tuning of salt retention of backwashable polyelectrolyte multilayer hollow fiber nanofiltration membranes", Journal of Membrane Science **499**, 396 – 405 (2016).

[38] J. J. Harris, J. L. Stair, and M. L. Bruening, "Layered polyelectrolyte films as selective, ultrathin barriers for anion transport", Chemistry of Materials **12**, 1941–1946 (2000).

[39] M. L. Bruening and D. M. Sullivan, "Enhancing the ion-transport selectivity of multilayer polyelectrolyte membranes", Chemistry A European Journal **8**, 3832–3837 (2002).

[40] C. Ba, D. A. Ladner, and J. Economy, "Using polyelectrolyte coatings to improve fouling resistance of a positively charged nanofiltration membrane", Journal of Membrane Science **347**, 250 – 259 (2010).

[41] T. Ishigami, K. Amano, A. Fujii, Y. Ohmukai, E. Kamio, T. Maruyama, and H. Matsuyama, "Fouling reduction of reverse osmosis membrane by surface modification via layer-by-layer assembly", Separation and Purification Technology **99**, 1 – 7 (2012).

[42] F. Fadhillah, A. M. Alghamdi, M. D. Alsubei, and S. A. Aljlil, "Synthesis of protein-fouling-resistance polyelectrolyte multilayered nanofiltration membranes through spin-assisted layer-by-layer assembly", Journal of King Saud University - Engineering Sciences (2020).

[43] D. M. Reurink, J. P. Haven, I. Achterhuis, S. Lindhoud, E. H. D. W. Roesink, and W. M. de Vos, "Annealing of polyelectrolyte multilayers for control over ion permeation", Advanced Materials Interfaces **5**, 1800651 (2018).

[44] R. W. Baker, *Ultrafiltration*, chapter 6, 253–302 (John Wiley Sons, Ltd) (2012).

[45] M. Hadidi and A. L. Zydney, "Fouling behavior of zwitterionic membranes: Impact of electrostatic and hydrophobic interactions", Journal of Membrane Science **452**, 97 – 103 (2014).

[46] J. B. Schlenoff, "Zwitteration: Coating surfaces with zwitterionic functionality to reduce nonspecific adsorption", Langmuir **30**, 9625–9636 (2014), pMID: 24754399.

[47] M. He, K. Gao, L. Zhou, Z. Jiao, M. Wu, J. Cao, X. You, Z. Cai, Y. Su, and Z. Jiang, "Zwitterionic materials for antifouling membrane surface construction", Acta Biomaterialia **40**, 142 – 152 (2016), zwitterionic Materials.

[48] P. Bengani, Y. Kou, and A. Asatekin, "Zwitterionic copolymer self-assembly for fouling resistant, high flux membranes with size-based small molecule selectivity", Journal of Membrane Science **493**, 755 – 765 (2015).

[49] P. Bengani-Lutz, E. Converse, P. Cebe, and A. Asatekin, "Self-assembling zwitterionic copolymers as membrane selective layers with excellent fouling resistance: Effect of zwitterion chemistry", ACS Applied Materials & Interfaces **9**, 20859–20872 (2017), pMID: 28544845.

[50] M. Singh and N. Tarannum, "4 - polyzwitterions", in *Engineering of Biomaterials for Drug Delivery Systems*, edited by A. Parambath, Woodhead Publishing Series in Biomaterials, 69 – 101 (Woodhead Publishing) (2018).

[51] J. B. Schlenoff, H. Ly, and M. Li, "Charge and mass balance in polyelectrolyte multilayers", Journal of the American Chemical Society **120**, 7626–7634 (1998).

[52] P. Lavalle, C. Picart, J. Mutterer, C. Gergely, H. Reiss, J.-C. Voegel, B. Senger, and P. Schaaf, "Modeling the buildup of polyelectrolyte multilayer films having exponential growth", The Journal of Physical Chemistry B **108**, 635–648 (2004).

[53] J. de Grooth, M. Dong, W. M. de Vos, and K. Nijmeijer, "Building polyzwitterion-based multilayers for responsive membranes", Langmuir **30**, 5152–5161 (2014), pMID: 24749944.

[54] E. Virga, J. de Grooth, K. vab, and W. M. de Vos, "Stable polyelectrolyte multilayer-based hollow fiber nanofiltration membranes for produced water treatment", ACS Applied Polymer Materials **1**, 2230–2239 (2019).

[55] K. Nam, T. Kimura, and A. Kishida, "Controlling coupling reaction of edc and nhs for preparation of collagen gels using ethanol/water cosolvents", Macromolecular Bioscience **8**, 32–37 (2008).

[56] M. J. E. Fischer, *Amine Coupling Through EDC/NHS: A Practical Approach*, 55–73 (Humana Press, Totowa, NJ) (2010).

[57] A. Nguyen, S. Azari, and L. Zou, "Coating zwitterionic amino acid l-dopa to increase fouling resistance of forward osmosis membrane", Desalination **312**, 82 – 87 (2013), recent Advances in Forward Osmosis.

[58] J. Dijt, M. Stuart, and G. Fleer, "Reflectometry as a tool for adsorption studies", Advances in Colloid and Interface Science **50**, 79 – 101 (1994).

[59] A. Theisen, *Refractive increment data book for polymer and biomolecular scientists* (Nottingham University Press) (2000).

[60] G. Deeli and J. P. Kratohvil, "Determination of size of small particles by light scattering. experiments on ludox colloidal silica", Kolloid-Zeitschrift **173**, 38–48 (1960).

[61] A. Vermeer, "Interactions between humic acid and hematite and their effects on metal ion speciation", Ph.D. thesis, WUR (1996).

[62] T. Rijnaarts, J. Moreno, M. Saakes, W. Vos, and K. Nijmeijer, "Role of anion exchange membrane fouling in reverse electrodialysis using natural feed waters", Colloids and Surfaces A: Physicochemical and Engineering Aspects **560** (2018).

[63] S.-H. Yoon, C.-H. Lee, K.-J. Kim, and A. G. Fane, "Effect of calcium ion on the fouling of nanofilter by humic acid in drinking water production", Water Research **32**, 2180 – 2186 (1998).

[64] C. Y. Tang, Y.-N. Kwon, and J. O. Leckie, "Fouling of reverse osmosis and nanofiltration membranes by humic acideffects of solution composition and hydrodynamic conditions", Journal of Membrane Science **290**, 86 – 94 (2007).

[65] W.-Y. Ahn, A. G. Kalinichev, and M. M. Clark, "Effects of background cations on the fouling of polyethersulfone membranes by natural organic matter: Experimental and molecular modeling study", Journal of Membrane Science **309**, 128 – 140 (2008).

[66] H. Shirahama, J. Lyklema, and W. Norde, "Comparative protein adsorption in model systems", Journal of Colloid and Interface Science **139**, 177 – 187 (1990).

[67] W. Norde, T. Arai, and H. Shirahama, "Protein adsorption in model systems", Biofouling **4**, 37–51 (1991).

[68] W. de Vos, M. Biesheuvel, A. Keizer, M. Kleijn, and M. Cohen Stuart, "Adsorption of the protein bovine serum albumin in a planar poly(acrylic acid) brush layer as measured by optical reflectometry", Langmuir **24**, 6575–84 (2008).

[69] S. Ilyas, R. English, P. Aimar, J.-F. Lahitte, and W. M. de Vos, "Preparation of multifunctional hollow fiber nanofiltration membranes by dynamic assembly of weak polyelectrolyte multilayers", Colloids and Surfaces A: Physicochemical and Engineering Aspects **533**, 286 – 295 (2017).

[70] D. Xu, C. Hodges, Y. Ding, S. Biggs, A. Brooker, and D. York, "Adsorption kinetics of laponite and ludox silica nanoparticles onto a deposited poly(diallyldimethylammonium chloride) layer measured by a quartz crystal microbalance and optical reflectometry", Langmuir **26**, 18105–18112 (2010), pMID: 21073154.

[71] P. van den Brink, A. Zwijnenburg, G. Smith, H. Temmink, and M. van Loosdrecht, "Effect of free calcium concentration and ionic strength on alginate fouling in cross-flow membrane filtration", Journal of Membrane Science **345**, 207 – 216 (2009).

[72] H. Yamamura, K. Okimoto, K. Kimura, and Y. Watanabe, "Influence of calcium on the evolution of irreversible fouling in microfiltration/ultrafiltration membranes", Journal of Water Supply: Research and Technology-Aqua **56**, 425–434 (2007).

[73] D. Zhao and S. Yu, "A review of recent advance in fouling mitigation of nf/ro membranes in water treatment: pretreatment, membrane modification, and chemical cleaning", Desalination and Water Treatment **55**, 870–891 (2015).

[74] R. Kumar and A. F. Ismail, "Fouling control on microfiltration/ultrafiltration membranes: Effects of morphology, hydrophilicity, and charge", Journal of Applied Polymer Science **132** (2015).

[75] X. Jin, X. Huang, and E. M. Hoek, "Role of specific ion interactions in seawater ro membrane fouling by alginic acid", Environmental Science & Technology **43**, 3580–3587 (2009), pMID: 19544858.

[76] C. J. van Oss (Marcel Dekker, New York) (1994).

[77] E. Seyrek, P. L. Dubin, C. Tribet, and E. A. Gamble, "Ionic strength dependence of protein-polyelectrolyte interactions", Biomacromolecules **4**, 273–282 (2003), pMID: 12625722.

[78] V. V. Murashov and J. Leszczynski, "Adsorption of the phosphate groups on silica hydroxyls: an ab initio study", The Journal of Physical Chemistry A **103**, 1228–1238 (1999).

[79] B. Mi and M. Elimelech, "Chemical and physical aspects of organic fouling of forward osmosis membranes", Journal of Membrane Science **320**, 292 – 302 (2008).

[80] H. Xu, K. Xiao, X. Wang, S. Liang, C. Wei, X. Wen, and X. Huang, "Outlining the roles of membrane-foulant and foulant-foulant interactions in organic fouling during microfiltration and ultrafiltration: A mini-review", Frontiers in Chemistry **8**, 417 (2020).

[81] A. E. Yaroshchuk, "Non-steric mechanisms of nanofiltration: superposition of donnan and dielectric exclusion", Separation and Purification Technology **22-23**, 143 – 158 (2001).

[82] K. L. Cho, A. J. Hill, F. Caruso, and S. E. Kentish, "Chlorine resistant glutaraldehyde crosslinked polyelectrolyte multilayer membranes for desalination", Advanced Materials **27**, 2791–2796 (2015).

[83] S. Bandini and D. Vezzani, "Nanofiltration modeling: the role of dielectric exclusion in membrane characterization", Chemical Engineering Science **58**, 3303 – 3326 (2003).

[84] Y.-N. Wang and C. Y. Tang, "Nanofiltration membrane fouling by oppositely charged macromolecules: Investigation on flux behavior, foulant mass deposition, and solute rejection", Environmental Science & Technology **45**, 8941–8947 (2011), pMID: 21928796.

[85] K. Kubiak-Ossowska and P. A. Mulheran, "Mechanism of hen egg white lysozyme adsorption on a charged solid surface", Langmuir **26**, 15954–15965 (2010), pMID: 20873744.

[86] K. Rezwan, L. Meier, and L. Gauckler, "Lysozyme and bovine serum albumin adsorption on uncoated silica and alooh-coated silica particles: The influence of positively and negatively charged oxide surface coatings", Biomaterials **26**, 4351–7 (2005).

[87] Y. Wang and C. Tang, "Fouling of nanofiltration, reverse osmosis, and ultrafiltration membranes by protein mixtures: The role of inter-foulant-species interaction", Environmental science technology **45**, 6373–9 (2011).

[88] W. Burton, K. Nugent, T. Slattery, B. Summers, and L. Snyder, "Separation of proteins by reversed-phase high-performance liquid chromatography: I. optimizing the column", Journal of Chromatography A **443**, 363 – 379 (1988), seventh international symposium on high-performance liquid.

[89] J. D. Ritchie and E. Perdue, "Proton-binding study of standard and reference fulvic acids, humic acids, and natural organic matter", Geochimica et Cosmochimica Acta **67**, 85 – 96 (2003).

[90] K. Queiroz, V. Medeiros, L. Queiroz, L. Abreu, H. Rocha, C. Ferreira, M. Jucá, H. Aoyama, and E. Leite, "Inhibition of reverse transcriptase activity of hiv by polysaccharides of brown algae", Biomedicine Pharmacotherapy **62**, 303 – 307 (2008).

[91] K. L. Chen, S. E. Mylon, and M. Elimelech, "Enhanced aggregation of alginate-coated iron oxide (hematite) nanoparticles in the presence of calcium, strontium, and barium cations", Langmuir **23**, 5920–5928 (2007), pMID: 17469860.

[92] X. Jin, X. Huang, and E. M. Hoek, "Role of specific ion interactions in seawater ro membrane fouling by alginic acid", Environmental Science & Technology **43**, 3580–3587 (2009), pMID: 19544858.

[93] K. Ishihara, H. Nomura, T. Mihara, K. Kurita, Y. Iwasaki, and N. Nakabayashi, "Why do phospholipid polymers reduce protein adsorption?", Journal of Biomedical Materials Research **39**, 323–330 (1998).

[94] K. W. Trzaskus, W. M. de Vos, A. Kemperman, and K. Nijmeijer, "Towards controlled fouling and rejection in dead-end microfiltration of nanoparticles role of electrostatic interactions", Journal of Membrane Science **496**, 174 – 184 (2015).

[95] J. E. Wong, F. Rehfeldt, P. Hänni, M. Tanaka, and R. v. Klitzing, "Swelling behavior of polyelectrolyte multilayers in saturated water vapor", Macromolecules **37**, 7285–7289 (2004).

[96] R. Fabris, E. K. Lee, C. W. Chow, V. Chen, and M. Drikas, "Pre-treatments to reduce fouling of low pressure micro-filtration (mf) membranes", Journal of Membrane Science **289**, 231 – 240 (2007).

[97] A. Zularisam, A. Ismail, and R. Salim, "Behaviours of natural organic matter in membrane filtration for surface water treatment a review", Desalination **194**, 211 – 231 (2006).

[98] G.-R. Xu, J.-M. Xu, H.-J. Feng, H.-L. Zhao, and S.-B. Wu, "Tailoring structures and performance of polyamide thin film composite (pa-tfc) desalination membranes via sublayers adjustment-a review", Desalination **417**, 19 – 35 (2017).

[99] W. Lau, S. Gray, T. Matsuura, D. Emadzadeh, J. Paul Chen, and A. Ismail, "A review on polyamide thin film nanocomposite (tfn) membranes:

History, applications, challenges and approaches", Water Research **80**, 306 – 324 (2015).

[100] J. M. Gohil and P. Ray, "A review on semi-aromatic polyamide tfc membranes prepared by interfacial polymerization: Potential for water treatment and desalination", Separation and Purification Technology **181**, 159 – 182 (2017).

[101] G. Hurwitz, G. R. Guillen, and E. M. Hoek, "Probing polyamide membrane surface charge, zeta potential, wettability, and hydrophilicity with contact angle measurements", Journal of Membrane Science **349**, 349 – 357 (2010).

[102] E. M. Vrijenhoek, S. Hong, and M. Elimelech, "Influence of membrane surface properties on initial rate of colloidal fouling of reverse osmosis and nanofiltration membranes", Journal of Membrane Science **188**, 115 – 128 (2001).

[103] W. Lau, A. Ismail, N. Misdan, and M. Kassim, "A recent progress in thin film composite membrane: A review", Desalination **287**, 190 – 199 (2012), special Issue in honour of Professor Takeshi Matsuura on his 75th Birthday.

7

Fouling of Polyelectrolyte Multilayer based Nanofiltration Membranes during Produced Water Treatment: The Role of Surfactant Size and Chemistry°

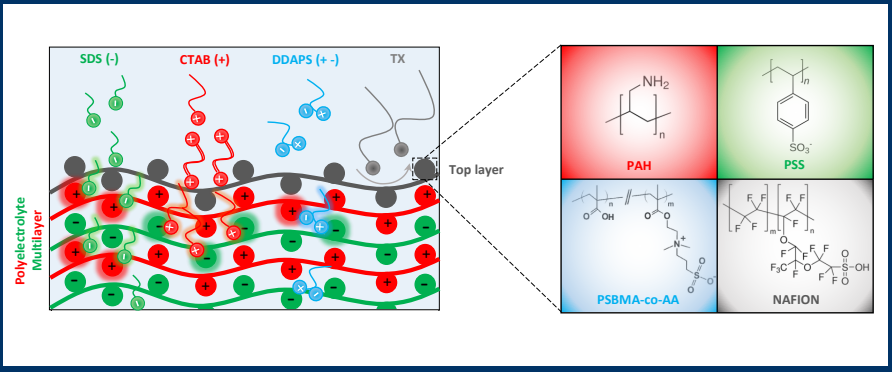

°Published as: **Ettore Virga**, Mario A. Parra, and Wiebe M. de Vos, *Fouling of Polyelectrolyte Multilayer based Nanofiltration Membranes during Produced Water Treatment: The Role of Surfactant Size and Chemistry*, Journal of Colloid and Interface Science **2021**, *594*, 9-19.

Abstract

Large volumes of water become contaminated with hydrocarbons, surfactants, salts and other chemical agents during Oil & Gas exploration activities, resulting in a complex wastewater stream known as produced water (PW). Nanofiltration (NF) membranes are a promising alternative for the treatment of PW to facilitate its re-use. Unfortunately, membrane fouling still represents a major obstacle. In the present work, we investigate the effect of surface chemistry on fouling of NF membranes based on polyelectrolyte multilayers (PEM), during the treatment of artificial produced water. To this end, oil-in-water (O/W) emulsions stabilized with four different surfactants (anionic, cationic, zwitterionic and non-ionic) were treated with PEM-based NF membranes having the same multilayer, but different top layer polymer chemistry: crosslinked poly(allylamine hydrochloride) (PAH, nearly uncharged), poly(sodium 4-styrene sulfonate) (PSS, strongly negative), poly(sulfobetaine methacrylate-co-acrylic acid) (PSBMA-co-AA, zwitterionic) and Nafion (negative and hydrophobic). First, we study the adsorption of the four surfactants for the four different surfaces on model interfaces. Second, we study fouling by artificial produced water stabilized by the same surfactants on PEM-based hollow fiber NF membranes characterized by the same multilayer of our model surfaces. Third, we study fouling of the same surfactants solution but without oil. Very high oil retention ($>$99%) was observed when filtering all the O/W emulsions, while the physicochemical interactions between the multilayer and the surfactants determined the extent of fouling as well as the surfactant retention. Unexpectedly, our results show that fouling of PEM-based NF membranes, during PW treatment, is mainly due to membrane active layer fouling caused by surfactant uptake inside of the PEM coating, rather than due to cake layer formation. Indeed, it is not the surface chemistry of the membrane that determines the extent of fouling, but the surfactant interaction with the bulk of the PEM. A denser multilayer, that would stop these molecules, would benefit PW treatment by decreasing fouling issues, as would the use of slightly more bulky surfactants that cannot penetrate the PEM.

An achemso demo] Fouling of Polyelectrolyte Multilayer based Nanofiltration Membranes during Produced Water Treatment: The Role of Surfactant Size and Chemistry

7.1 Introduction

One of the main environmental challenges in the Oil & Gas (O&G) field is the sustainable management of produced water (PW). This wastewater consists of water already present in the drilled geological formation together with an aqueous solution of chemical agents that is injected into the formation during the hydrocarbon recovery process [1]. PW is the largest waste stream formed during oil and gas recovery, representing in some cases more than 90% of the O&G liquid waste [2]. The volume of PW generated is expected to increase further in the future due to the growing share of hydrocarbons that are recovered using water-intensive methods. Moreover, as older O&G fields get depleted, larger volumes of injected water will be required to extract the remaining resources [3].

PW can be considered an oil-in-water (O/W) emulsion in which different molecules (corrosion inhibitors, biocides and extraction enhancers) act as surfactants, stabilizing the oily-phase and keeping it dispersed [4]. The amount and type of compounds present in PW will differ depending on the well from which the hydrocarbons are extracted, as well as on the chemical agents added to the water during the recovery process. After treatment, PW could be reinjected to extract further resources, reducing the freshwater demand of the O&G industry. Ideally, if higher quality standards are met, treated PW could also be reused in other sectors such as agriculture, livestock raising and industrial processes [2].

Conventional treatment of PW mainly includes physical processes, as for example adsorption, media filtration and cyclones, and chemical methods, such as de-emulsification and chemical precipitation [5]. Even though it is possible to remove most of the contaminants present in PW by a combination of conventional treatment methods, these processes often involve the use of large volumes of chemical agents, require a large installation space and can be energy-intensive [6]. Consequently, the development of novel, energy and resource-efficient technologies is needed to ensure that treated PW complies with increasingly strict water quality standards for its reuse [7].

Over the past decades, researchers have shown the potential of membranes to effectively treat O/W emulsions [8, 9]. Although conventional physical,

chemical and biological treatment processes can remove free-floating oil as well as oil present in unstable emulsions, these methods are not sufficiently effective in separating well-stabilized emulsified oil droplets from water, mainly due to their small size (<10 ţm) and high stability [9, 10]. Membranes, ranging from microfiltration (MF) to nanofiltration (NF), have been proven to be extremely effective in the removal of such small and stable droplets, providing higher quality effluents with a series of advantages in terms of environmental impacts, space requirements and easy to automate operation when compared to traditional methods [11]. Here, NF membranes have an array of added advantages as they can be used at acceptable permeability for de-oiling while simultaneously removing multivalent ions, dissolved organics and part of the monovalent salts [12, 13], providing higher quality effluents than MF and ultrafiltration (UF) with lower use of energy than reverse osmosis (RO).

Several studies have obtained promising results for the use of NF in PW treatment. Muppalla *et al.* tested the performance of a NF membrane prepared by applying a pentablock copolymer (PBC) active layer on top of a polysulphone UF membrane and obtained high oil rejection (∼99.5%) from oil-water emulsions [14]. Xu & Drewes observed high permeability, salt and total organic content (TOC) removal when treating PW with commercially available NF membranes on a bench-scale [15], while Visvanathan *et al.*, after conducting a pilot-scale experiment, concluded that NF was a suitable option for the pre-treatment of PW before applying a reverse osmosis (RO) step, thanks to its stable efficiency and low-fouling performance [16]. Besides, Alzahrani & Mohammad reviewed the application of membrane technologies, including NF, for the treatment of PW [12]. Despite the favorable outcomes, previously mentioned, they stressed the need of considering NF as part of a PW treatment train, consisting of several steps. The complexity of PW makes single-step solutions impossible [5], especially if the quality of the effluent is expected to meet strict beneficial reuse standards. Further research and development is required on several aspects of NF application [17], including the important topic of membrane fouling [4, 18].

Fouling is a major drawback common to all filtration technologies, leading to a decrease in permeate quantity and quality over time, which in turn translates into lost operation periods and higher costs due to membrane cleaning or even replacement [19]. Several of the organic compounds present in PW, such as oil, dissolved organics and surfactants, can easily lead to fouling [10, 12]. Physicochemical interactions between organic molecules and membrane surface lead to adsorption, which is considered the main mechanism for organic

membrane fouling [20]. Surfactants are a type of organic foulant that requires special attention in the case of PW treatment by NF since they are responsible for the stability of the emulsion and can interact in several ways with the membrane [4]. While the extent of fouling for charged surfactants is mainly related to electrostatic interactions [21], for nonionic surfactants it seems to be related to the membrane hydrophilicity and pore size [22]. Researchers have therefore suggested that in order to minimize fouling it is recommended to use membranes with a more hydrophilic, smoother surface, and same charge as the fouling agents [23, 24]. As membrane charge and surface chemistry are believed to be the main parameters able to affect fouling [25], a zwitterionic top layer could prevent fouling by decreasing the interaction between membrane surface and foulants [26]. However, the role of membrane charge and surfactant chemistry remains still unclear, especially in PW treatment, and needs further investigation.

In the past decade, we have seen a major breakthrough in the production of polyelectrolyte multilayer (PEM) based hollow fiber (HF) nanofiltration membranes. The excellent separation properties of these systems, coupled with very good chemical stability, has led to many publications [17, 27–30], but also to very rapid commercialization [31]. Additionally, PEM-based NF membranes have a key advantage over commonly used thin film composite (TFC) NF membranes. As TFC membranes are still commercially available only as flat sheets, as it is quite difficult to make TFC membranes via IP in a hollow fiber configuration [32]. Here, our PEM based membranes have the advantage that hollow fiber manufacturing is very straightforward and HF-based membrane modules do not require a spacer, in contrast to spiral wound modules, where spacer fouling is a much bigger problem than membrane fouling [33]. However, a rather unexplored area of PEM based membranes is their fouling behavior. This is worth mentioning since the chemistry of these systems very naturally lends itself to a large deal of control over the membrane surface chemistry [34–36]. As such, PEM based HF membranes could easily be designed with good separation properties, combined with anti-fouling properties optimized towards PW treatment.

In this manuscript, we study the effect of top layer polymer chemistry, as well as surfactant type, on fouling by PW for PEM-based nanofiltration membranes. As surface chemistry is believed to be the main factor that regulates the interactions between membrane and foulants, it is ideal to investigate such effects on PEM, where we can create very similar membrane active layers, and apply a different top layer to change the membrane surface

chemistry. First, we focus on surfactant adsorption on PEM coated model interfaces to investigate the effect of different top layer polymer chemistry (nearly uncharged crosslinked poly(allylamine hydrochloride) (PAH), strongly negative poly(sodium 4-styrene sulfonate) (PSS), zwitterionic poly(sulfobetaine methacrylate-co-acrylic acid) (PSBMA-co-AA) and negative hydrophobic Nafion) on the adsoption of four different surfactants (anionic SDS, cationic CTAB, zwitterionic DDAPS and nonionic TX). Subsequently, we study fouling by artificial PW (prepared with various surfactants) on NF membranes having the same multilayer chemistry of the model interfaces. The same experiments are also carried out with aqueous solutions of just the surfactant to better understand the underlying fouling mechanisms. While we expected the top layer chemistry to play a major role in membrane fouling by surfactants, our experiments surprisingly demonstrate that it is not the top layer chemistry that determines the degree of fouling, but rather the surfactant size and type and their interaction with the inner part of the PEM. These results indicate clear pathways to reduce fouling of PEM based NF membranes during PW treatment.

7.2 Materials and Methods

7.2.1 Chemicals

O/W emulsions were prepared by mixing N-hexadecane (Merck Schuchardt 99.0%) in a solution containing one out of four surfactants, namely sodium dodecyl sulfate (SDS, Sigma-Aldrich, ACS reagent, 99.0%), hexadecyltrimethylammonium bromide (CTAB, Sigma-Aldrich, for molecular biology, 99%), Ndodecyl-N, N-dimethyl-3-ammonio-1-propanesulfonate (DDAPS, Sigma-Aldrich, 97.0% (dried material, CHN)) and Triton^{TM} X-100 (TX, Sigma-Aldrich, laboratory grade). Figure 7.1 shows the chemical structure of the surfactants used in this work as well as their molecular weight (MW, Da).

PEM-based NF membranes were prepared by coating sulfonated poly(ether sulfone) (SPES) UF-HF membranes (inner diameter of 0.7 mm, molecular weight cut-off (MWCO) of 7.5 kDa, and water permeability of 150 LMH/bar [13]) with four types of polyelectrolytes: PAH (Mw = 50 kDa), PSS (Mw = 70 kDa), Nafion (75wt.% of 1100 EW Nafion) and PSBMA-co-AA. All of the polyelectrolytes used for membrane coating were purchased from Sigma Aldrich except for PSBMA-co-AA, which was synthetized by following the procedure described by de Grooth *et al.* [37]. Using ^{1}H-NMR (spectra reported in Figure

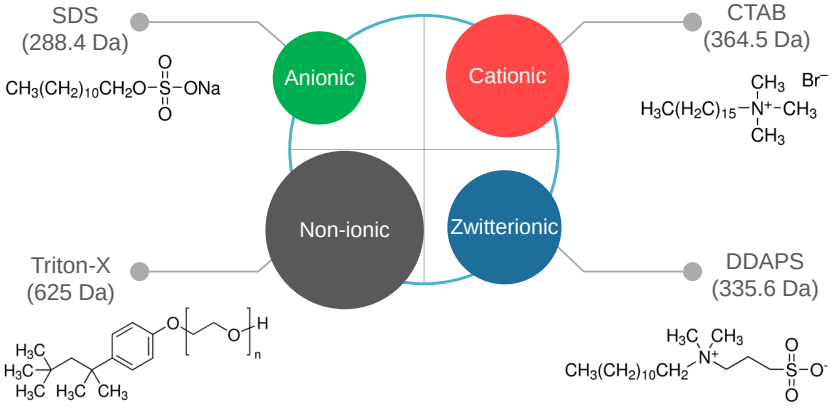

Figure 7.1: Surfactants tested in this work and their characteristics: anionic SDS (288.4 Da), cationic CTAB (364.5 Da), nonionic TX (625 Da) and zwitterionic DDAPS (335.6 Da).

E.1, Appendix E), the monomer distribution of PSBMA-co-AA was estimated to be approximately 10:1 molar ratio of SBMA/AA. For the crosslinking of the PEM, a 25% aqueous solution of glutaraldehyde was purchased from Sigma-Aldrich. Coumarin 6/ Neeliglow Yellow 196 (Neelikon) fluorescent dye was used to measure oil content by means of fluorometry. Silicon wafers were purchased from WaferNet Inc. (San Jose, CA, USA). We purchased all other chemicals from VWR, the Netherlands. All chemicals were used without further purification steps.

7.2.2 Model surface coating with PEM

Polyelectrolyte coating solutions were prepared by dissolving 0.1 g/L polyelectrolyte in a 50 mM NaCl solution without adjusting pH (with pH∼5.5). All the steps (coating, rinsing and crosslinking) step were performed at room temperature and each of them lasted 15 min. First, negatively charged Silica (SiO_2) wafers were cleaned with piranha solution (3:1 mixture of concentrated sulfuric acid (H_2SO_4) with hydrogen peroxide (H_2O_2)) to remove possible organic contaminants. Then, the wafers were dipped in a polycation (PAH) solution (50 mM NaCl) and subsequently rinsed with an aqueous solution

containing only NaCl (50 mM). The model interfaces were then immersed in a polyanion (PSS) solution (50 mM NaCl), followed by another rinsing step, to finally complete the fist bilayer. A crosslinking step, in which the model surfaces were immersed in a 7.5 mM glutaraldehyde solution (50 mM NaCl), was applied after coating each PAH layer to guarantee layer stability in surfactant solutions [13]. The procedure was repeated until 4.5 and 5 bilayers, respectively for PAH and the other top layers (i.e. negative PSS, zwitterionic PSBMA-co-AA and negative hydrophobic Nafion), were coated on top of the wafers. While PSS and PSBMA-co-AA coating solutions contained 50 mM NaCl and 0.1 $g{\cdot}L^{-1}$ of the respective polyelectrolyte, the Nafion coating solution consisted of 0.1 $g{\cdot}L^{-1}$ Nafion dispersed in ethanol 70%. The same coating procedure is applied on hollow fiber membranes (Section 2.4).

7.2.3 Surfactant adsorption on model interfaces via reflectometry

PW can be considered an oil-in-water emulsion in which different molecules (corrosion inhibitors, biocides and extraction enhancers) act as surfactants, stabilizing the oily-phase and keeping it dispersed. Surfactants are a type of organic foulant that requires special attention in the case of PW treatment by NF since they are responsible for the stability of the emulsion and can adsorb at the membrane interface [21, 38].

We initially investigated the adsorption of four different surfactants on model interfaces via reflectometry [39]. To quantify the adsorbed amount of surfactant at the interface, we flushed the surfactant solutions (0.1 times the critical micelle concentration (CMC) of the surfactant and 100 mM NaCl) to the silica wafers, previously coated with PEMs (above described). For simplicity we have taken the CMC value in absence of salt, being aware that especially for the charged surfactants the CMC will decrease at higher salinities. When we reach steady state in surfactant adsorption, we rinse our interfaces with a simple salt solution (100 mM NaCl). The use of a stagnation point flow cell allows to study the surfactant adsorption under well controlled hydrodynamic conditions. We calculate the amount of surfactant, Γ (mg/m^2), adsorbed on the model interface as follows

$$\Gamma = \frac{\Delta S}{S_0} Q. \tag{7.1}$$

where ΔS is the change in the ratio (S (-)) between the two polarized components originated from the reflection and splitting of the monochromatic light

Surfactant	dn/dc (mL/g)	Q (mg/m^2)
SDS	0.108 [40]	45
CTAB	0.150 [40]	35
DDAPS	0.146	30
TX	0.154 [41]	30

Table 7.1: Refractive index increments (dn/dc) and sensitivity factors for the surfactant solutions.

(HeNe laser, 632.8 nm) used in the system, S_0 is the initial output signal of the model interface (-), and Q is the sensitivity factor (mg/m^2). The last parameter (Q) is calculated by using an optical model based on the following system parameters: θ=71°, n_{SiO_2}=1.46, $\tilde{n}_{Si}$=(3.85, 0.02), n_{H_2O}=1.33, δ_{SiO_2}=90 nm and refractive index increment dn/dc (mL/g) for every surfactant (reported in Table 7.1). The refractive index increment of DDAPS was calculated after measuring the refractive index (at 20°C and 590 nm) of different DDAPS solutions (50, 500, 1000, 5000, 10000, 50000 mg/L) with an ATR-BR Schmidt Haensch refractometer. We calculate and report the sensitivity factor Q for each surfactant in Table 7.1. We performed all experiments at least in duplicate.

7.2.4 Membrane coating and characterization

The UF support membranes were coated following the same procedure adopted for the model surfaces (Section 2.2). Initially we coated the UF membranes with one PAH-PSS bilayer by submerging the fibers in a solution (50 mM NaCl) containing 0.1 $g{\cdot}L^{-1}$ PAH, then moving them into a rinsing solution (50 mM NaCl) and finally into a solution (50 mM NaCl) with 0.1 $g{\cdot}L^{-1}$ PSS. Three additional bilayers were added to the membrane by repeating this process, including crosslinking steps in which the membranes were immersed, after adding each PAH layer, in a 7.5 mM glutaraldehyde solution with 50 mM NaCl. Once the first four PAH-PSS bilayers were added to the fibers, an additional PAH coating was performed followed by a final crosslinking step. After this, the membranes were split into four groups. One of these groups was not coated any further, leaving it with a 4.5 bilayer PEM terminated with a PAH top layer. The other three groups were each coated with a different top layer, namely PSS, PSBMA-co-AA and Nafion, for a total of 5 bilayers. For the case of PSS and PSBMA-co-AA, the coating solutions contained 50

mM NaCl and 0.1 $g \cdot L^{-1}$ of the respective polyelectrolyte, while the Nafion coating solution consisted of 0.1 $g \cdot L^{-1}$ Nafion dispersed in ethanol 70%. Every step (coating, rinsing and crosslinking) lasted 15 minutes and was carried out at room temperature. After all the desired layers were coated, the membranes were rinsed in demineralized water, and then stored for 4 hours in a glycerol-water solution (15/85 wt%). Finally, the membrane fibers were left to dry overnight at room temperature. We refer from this point onwards to the coated membranes according to their terminating layer, namely PAH, PSS, PZWT (PSBMA-co-AA) and NAF (Nafion). Individual modules were prepared by assembling single PEM-coated fibers into transparent plastic tubes of 8 mm diameter and approximately 170 mm length. For the evaluation of the membranes permeability, the clean water flux (CWF) was determined by pumping demineralized water through the fibers in a cross-flow configuration for 1 hour, at room temperature and constant transmembrane pressure (TMP) of 3 bar. The cross-flow velocity through the fibers was maintained at approximately 1.7 $m \cdot s^{-1}$ (Reynolds number around 1200) in order to minimize the effects of concentration polarization. Figure 7.2 shows a schematic of the experimental set-up used in this study. Water permeability was then calculated in terms of LMH/bar with the measured CWF and TMP values (Figure S2, SI). All our PEM-based NF membranes have a negative zeta potential. Specifically, we find the zeta potentials for PAH, PSS, PSBMA-co-AA and Nafion polymer coatings to be respectively -10.9, -22.9, -25.8 and -14.6 mV (Figure S3, SI). Ion retention was determined by performing 1-hour crossflow experiments, at the same TMP and temperature conditions as water permeability experiments, with 5 mM solutions of four different salts: NaCl, $CaCl_2$, Na_2SO_4 and $MgSO_4$. The results are reported in Figure S4 (SI).

Conductivity was measured in the feed and permeate samples using a Mettler Toledo SevenExcellence^{TM} pH/Conductivity meter. Ion retention was calculated based on the obtained data as a ratio between conductivity measured in the permeate samples and the feed solution. Since the concentrate outflow was recirculated into the feed solution while permeate volumes were collected as samples, the conductivity of the feed was measured before and after the ion retention experiments in order to detect changes in the feed composition. These changes in feed composition were negligible since the collected permeate volume was much smaller than the total feed volume. Four fibers were tested in every experiment to obtain at least a triplicate set of results for each set of experiments.

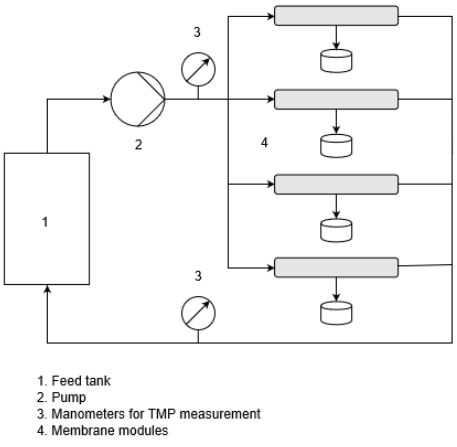

Figure 7.2: Schematic of the experimental set-up for membrane filtration experiments.

7.2.5 Artificial Produced Water preparation and filtration

Fouling experiments were performed on PEM-coated fibers using O/W emulsions (artificial PW) prepared by mixing 1 g·L^{-1} of N-hexadecane in a solution containing 100 mM NaCl and an amount of surfactant equivalent to 1/10 of its critical micelle concentration at 0 salt (CMC), which corresponds to 34.6 mg/L for CTAB, 239.1 mg/L for SDS, 100.6 mg/L for DDAPS and 14.4 mg/L for Triton-X. Each emulsion contained only one type of surfactant. The procedure followed to prepare the artificial PW was the same as described in previous works [13, 42, 43]. In order to measure oil retention, N-hexadecane was first energetically mixed with the fluorescent dye in 15 mL sample tubes. The resulting mixture was then filtered through a Millipore 0.45 ţm filter to remove any solid residuals. The dyed oil was then injected with a long syringe needle into a 1L Schott-Duran bottle in a solution containing 100 mM NaCl and 1/10 CMC of surfactant, and mixed using a IKA® T25 digital Ultra-Turrax® with S25N 18G element element for 10 minutes at 14000 rpm. In this work no zeta potentials were obtained for the emulsions. For similar surfactant concentrations and ionic strength, O/W emulsions are known to be strongly negatively charged for SDS (zeta potentials of -110 to -120 mV [44, 45]), strongly positively charged for CTAB (∼+85 mV [45, 46]), slightly negative for TX (from -20 to -5 mV [47]) and negatively charged for DDAPS (from -35 to -45 mV [48]).

Before each fouling experiment, the water permeability of clean membranes was measured as described in Section 7.2.4. Afterwards, the residual water

remaining in the tested modules was removed and the same cross-flow configuration was used to run the fouling experiments with artificial PW. Pressure and temperature conditions were kept the same as during the water permeability tests (3 bar TMP and room temperature), while the flow velocity was set to 0.43 $m \cdot s^{-1}$ (Reynolds number ~ 300) to enhance fouling. The artificial PW was treated by the membranes for 3 hours. Permeate volumes were collected from each fiber after the first 2 hours of the experiment to estimate permeate flux in terms of LMH/bar. After running each fouling experiment, pH of the filtered PW was measured using a Mettler Toledo SevenExcellence^{TM} pH/Conductivity meter. The fibers were then rinsed by running a solution containing 100 mM NaCl and the respective 1/10 CMC of surfactant, same concentrations of the artificial PW but without oil. The rinsing step lasted 15 minutes and was performed without applied pressure at 1.7 $m \cdot s^{-1}$ crossflow velocity. Finally, the water permeability through the fiber was measured to assess the residual fouling. The ratio between the permeability measured during PW filtration and the initial clean water permeability was used to estimate the flux decline due to irreversible and reversible fouling. We refer to the ratio between the water permeability after cleaning and water permeability for clean membrane (before fouling experiments) as "flux recovery. This term is an indication of the extent of irreversible fouling on the fibers.

The feed and permeate composition during the filtration of PW were analyzed in terms of ion retention and TOC content by means of ion chromatography (Metrohm Compact IC 761) and a TOC analyzer (Shimadzu TOC-L), respectively. Oil retention was determined by using a Perkin Elmer Victor3^{TM} V 1420 Multilabel Counter spectrophotometer to measure the fluorescence of different dilutions of the feed solution with known oil concentration. Given that the artificial PW used in the experiments contains two main fouling agents, namely oil droplets and surfactant molecules, additional fouling experiments were conducted by running solutions containing 1/10 CMC of surfactant and 100 mM NaCl without oil to show the relative contribution of free surfactants to membrane fouling. The fouling tests with these surfactant solutions were performed under the same conditions as the ones performed with PW, with no flushing step and 30 min experiment instead of 2 hours. Indeed, while fouling by oil-in-water emulsions for NF membranes can take up to few hours to reach steady-state [49], in our experiments we noticed that, for PEM-based NF membrane, fouling by surfactants is a fast process, reaching already the steady state in 30 min. Flux ratio and flux recovery after fouling were also measured for all top layers and surfactants in the same way as in the fouling

experiments with O/W emulsions. In order to assess the extent of fouling due to the adsorption of oil droplets, we compared flux recovery measured after fouling with PW with the results after fouling with surfactant solutions. For each type of surfactant and top layer, the difference between the average flux recovery after filtering surfactant solutions and PW is an indicator of the flux decrease related to oil adhesion on the membrane.

7.3 Results and Discussion

The Results and Discussion of this manuscript is divided into three major sections. In the first section, we investigate the adsorption of different surfactants (i.e. anionic, cationic, zwitterionic and nonionic) on model interfaces coated with the same PEM but with different top layer charge and chemistry. In the second section, we study fouling from simple surfactant solutions and from the corresponding artificial PWs on HF membranes coated with same PEM. Based on the results from both sections we finally discuss the expected fouling mechanisms, with a focus on the role of surfactant size and chemistry.

7.3.1 Surfactant adsorption on model interfaces

Membrane fouling during the filtration of O/W emulsions, such as PW, is highly affected by the chemistry and charge of the surfactant that stabilizes the emulsion [42, 43, 50–52]. Surfactants do not only affect fouling by giving charge and stability to the oil droplets of the emulsion but additionally adsorb at the membrane surface [21, 38].

The adsorption of surfactant at the membrane surface is expected to be influenced by both membrane surface chemistry and charge, as well as by multilayer composition. In order to study the interactions that take place at the feed-membrane interface, here we investigated the adsorption of the four different surfactants (anionic SDS, cationic CTAB, zwitterionic DDAPS and nonionic TX) on model PEM surfaces.

Optical reflectometry allowed us to study the adsorption of surfactant on model interfaces, previously prepared with same multilayer ($(PAH/PSS)_{4.5}$), but terminating with four different polymer chemistries. Even if the water content, and therefore water permeability, of PEM can change according to the applied top layer [53], chemical crosslinking allowed for very similar multilayers with similar water permeability (see Figure S2, SI). Every model interface was flushed with a surfactant solution until its adsorption reached steady state.

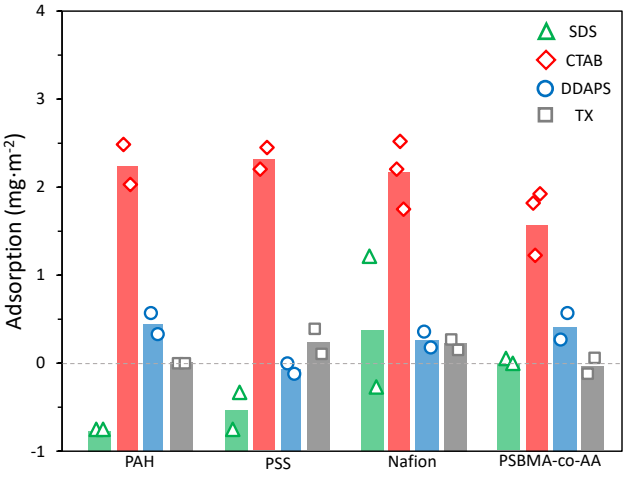

Figure 7.3: Adsorption (mg/m^2) of surfactants on model surfaces coated with PAH, PSS, Nafion and PSBMA-co-AA top layers. Results obtained via reflectometry. Points represent single data points, while bars represent the average of these points. Negative values correspond to multilayer desorption caused by surfactant complexation. All the experiments were performed at least in duplicate, as shown.

The steady state value represents the total amount of surfactant adsorbed on the PEM. We also evaluated the fraction of reversible (and irreversible) adsorption, for each surfactant, by flushing the coated model interfaces with a rinsing solution having same pH and salinity of the surfactant solution. We report the irreversibility of surfactant adsorption on model interfaces in Appendix E (Table E.1).

Figure 7.3 shows the adsorption of the four surfactants on multilayer coated with different polymer chemistry (nearly uncharged crosslinked PAH, negatively charged PSS, hydrophobic Nafion and zwitterionic PSBMA-co-AA). However, changes caused by concentration polarization that can occur in the vicinity of the membrane surface during filtration are not taken into account by Figure 7.3. As a consequence, changes in steady-state adsorption values may occur during filtration, as shown by our adsorption isotherms (see Figure S5, SI).

On all our PEM model surfaces, we observed relatively high adsorption values (2-2.5 mg/m^2) for the cationic CTAB. This is in agreement with literature, as the adsorption of CTAB on negative surfaces, with formation of a monolayer or bilayer, has been widely corroborated [54, 55]. CTAB is positively charged

while all the multilayers we investigated have a net negative charge mainly due to chemical crosslinking (via GA) [56]. The observed behavior is thus due to electrostatic interaction, responsible at first for CTAB adsorption, but also hydrophobic interactions, which lead to attraction between the hydrophobic surfactant tails and the formation of surfactant micelles or a bilayer on top of the negative surface [55]. Slightly lower values of adsorption are observed for PSBMA-co-AA surfaces [57–59]. A reduced amount of DDAPS ($\sim$0.5 mg/^{2}) adsorbed on PAH, Nafion and PSBMA-co-AA surfaces but not on PSS. This is an unexpected result as DDAPS was previously found to interact more with anionic moieties rather than cationic moieities, similarly to nonionic surfactants containing polyoxyetylene units, such as TX [60]. As expected, TX adsorbed on PSS and Nafion, which are more negatively charged than PAH, with almost no adsorption observed for PAH and PSBMA-co-AA top layers [24].

Differently, SDS in our studies adsorbed on all the top layers and, in some cases (like for PAH and PSS), partially removed the multilayer from the substrate, as we can observe from the negative values. This is in agreement with our previous study [13]. If this phenomenon occurs also on membranes, we should notice worse performances and higher water and salt permeability during filtration (see Section 7.3.2 for further details).

7.3.2 Membrane fouling during produced water treatment

As already mentioned, surfactants play a crucial role in membrane fouling not only because they adsorb at the membrane surface but also because they stabilize the oil droplets of PW, determining this way the charge of the stabilized droplets.

In the previous section, we studied surfactant adsorption on model interfaces via reflectometry, but membrane fouling is certainly not only determined by surface adsorption. In this section, we investigate fouling by monitoring the flux decline of our membranes during filtration. The procedure is carefully described in Section 7.2.5. Sodium chloride, TOC and n-hexadecane (oil) retention are measured in each of the experiments. In all the cases, NaCl retention was found 5-15%, oil retention >99% and the pH did not change during filtration.

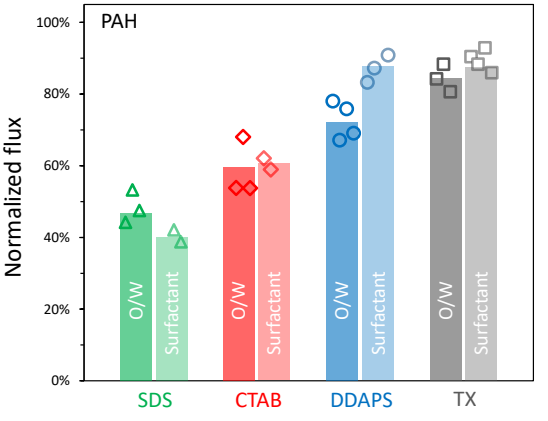

Figure 7.4: Normalized membrane flux of PAH membranes after fouling with O/W emulsions (dark columns) and surfactant solutions (light columns) stabilized by different surfactants (SDS, CTAB, DDAPS and TX). O/W emulsions were made of 100 mM NaCl, 1000 mg/L of n-hexadecane (oil) and surfactant at 1/10 CMC (239.1 mg/L for SDS, 34.6 mg/L for CTAB, 100.6 mg/L for DDAPS and 14.4 mg/L for TX). Surfactant solutions had same salt and surfactant composition of O/W emulsions but did not contain oil. Marks represent single data points while bars their average. All the experiments were performed at least in triplicate, as shown.

7.3.2.1 Fouling of crosslinked PAH terminated membranes

In Figure 7.4, we show the normalized flux for nearly uncharged PAH membranes after fouling with O/W emulsion and only surfactant solutions. The degree of fouling is clearly affected by the surfactant used in the emulsion or solution filtrated. In particular, the magnitude of fouling follows the order SDS > CTAB > DDAPS > TX.

Although for negatively charged membranes one might not expect fouling by anionic surfactants [21], the presence of a multilayer makes this more complex. Anionic surfactants were previously found to easily complex with the cationic polyelectrolyte (PAH) of the multilayer [13, 61], and this effect could lead to the observed fouling.

On the other side, the cationic CTAB also induces a relevant flux decline, probably due to the fact that CTAB can easily complex with the anionic polyelectrolyte (PSS) and adsorb inside the multilayer (see Figure 7.3). DDAPS and TX, probably due to their charge and size respectively, foul less, in agreement with our adsorption studies (see Figure 7.3).

7.3.2.2 Fouling of PSS,PSBMA-co-AA and Nafion terminated membranes

Figure 7.5 shows the normalized flux for negative PSS, zwitterionic PSBMA-co-AA (PZWT) and negative hydrophobic Nafion terminated membranes after fouling with O/W emulsion and only surfactant solutions. The results are quite surprising, as for all surface chemistries, the degree of fouling is determined mainly by the surfactant used in the emulsion or solution filtrated, with SDS > CTAB > DDAPS > TX. If the membranes surface chemistry would be responsible for foulant-membrane interactions, we should have expected big differences between the four top layers. But, fouling follows the same trends for all the top layers with only small differences between them. The only differences we can actually attribute to the different top layer chemistry are the ones we do see in absolute values.

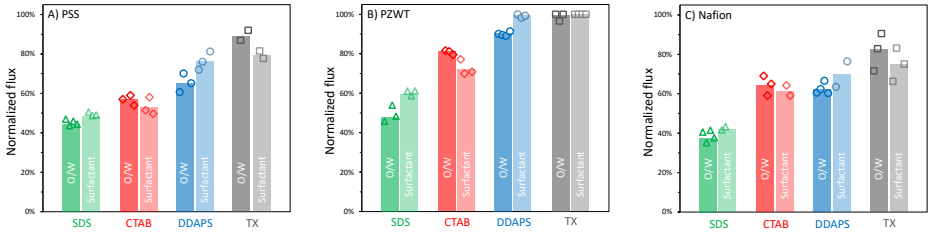

Figure 7.5: Normalized membrane flux of membranes with A) PSS, B) PZWT and C) Nafion top layers after fouling with O/W emulsions (dark columns) and surfactant solutions (light columns) stabilized by different surfactants (SDS, CTAB, DDAPS and TX). O/W emulsions were made of 100 mM NaCl, 1000 mg/L of n-hexadecane (oil) and surfactant at 1/10 CMC (239.1 mg/L for SDS, 34.6 mg/L for CTAB, 100.6 mg/L for DDAPS and 14.4 mg/L for TX). Surfactant solutions had same salt and surfactant composition of O/W emulsions but did not contain oil. Marks represent single data points while bars their average. All the experiments were performed at least in triplicate, as shown.

In our previous work, we studied the fouling of PEM based membranes with three similar surface chemistries with relevance to surface water treatment [26]. For the tested foulants, including BSA, LUDOX, Lysozyme, humic acids and alginates, a very clear effect of membrane surface chemistry was observed. In that case especially the zwitterionic surfaces were demonstrated to be very low-fouling [26]. So why is such an effect not observed for the fouling of artificial produced water as studied here? The key difference lays on the size of the foulants that here seems to completely dominate the fouling behaviour.

Surfactants molecules are much smaller and cannot just adsorb on top of the PEM, but also inside of it.

7.3.3 Effect of surfactant size and chemistry on PEM membrane fouling

As mentioned in the previous section, surfactant chemistry and size seem to be determinant in multilayer fouling. It has been observed in the filtration of pharmaceuticals that NF membranes with bigger pore size suffer more from fouling [62]. Adsorption plays an important role in pore blocking, especially when the pores of the membrane are already restricted due to adsorption of a foulant which is small enough to penetrate into the pores (pore narrowing) [19]. In this case, the size of the surfactant plays a crucial role. Surfactants, especially SDS and CTAB, can easily diffuse in the $(PAH/PSS)_{4.5}$ multilayer and even adsorb in it.

Interestingly, surfactants are typically used as model foulants for ion exchange (IEX) membranes [63–65]. In those systems it is well established that negative surfactant molecules can bind to positively charged sites in an anion exchange membrane (AEM), thereby replacing the anionic counter-ion such as Cl^- or OH^-. The adsorbed surfactants densify the membrane and block transport pathways, leading to reduced membrane performance.

Our results demonstrate that surfactant fouling is a big issue also for PEM based NF membranes. This fits well with the internal chemistry of the PEM separation layers. Similarly to IEX membranes described above, the PEM separation layers will contain charged moieties bound to an oppositely charged counter-ion (extrinsically compensated charges [66]). But in contrast to the IEX membranes, the PEM separation layer will contain both anionic and cationic charges. In particular, anionic SDS and cationic CTAB were the surfactants that fouled the most, independently of the chemistry of the outer layer. If surfactants are small enough to diffuse in the multilayer, they can locally adsorb, by complexing with the free charges in the PEM layer, densifying the layer and increasing the resistance to water permeation.

7.3.3.1 To the roots of PEM based NF membranes fouling during filtration of PW

Even if cake layer build-up is typically considered one of the main causes of membrane fouling, especially for PW treatment, our work shows that for these NF membrane internal multilayer fouling is dominant. In this context,

Figures 7.4-7.5 allow us to discriminate between multilayer fouling and cake layer fouling. The first, as mentioned above, can be mainly attributed to surfactant adsorption in the membrane active layer, which causes increased resistance to the water transport. The second, is due to the build-up of a cake layer of oil droplets on top of the membrane surface [4]. While we should be able to see both effects of fouling when filtering O/W emulsions, we see only multilayer fouling when filtering surfactant solution. The contribution of the cake layer resistance should therefore be observed in the difference between normalized flux due to fouling by surfactant solutions and fouling by O/W emulsions. The cake layer resistance is generally low for TX, while quite relevant for DDAPS. On the other side, for SDS and CTAB we do observe more fouling when filtering only surfactant, which could appear unexpected. Here, the build-up of a cake layer on top of the membrane could slow down, via electrostatic repulsion, the diffusion of SDS and CTAB molecules into the membrane. Moreover, the free surfactant concentration in the oil-in-water emulsion may be lower, as many surfactant molecules are bound to the oil-water interface.

One may think that if the retention of salt during filtration drastically increases due to the layer densification caused by the surfactant interaction with the multilayer, we could observe a reduced flux because of an increased osmotic pressure at the membrane interface and therefore misinterpret fouling. However, we did observe low rejection of NaCl retention during O/W emulsion filtration and report these values in tables E.2-E.5 of SI.

Figure 7.6 shows the TOC retention of our PEM membranes for the different surfactants tested. The observed retention values (lower than 100%) demonstrate that our surfactants can indeed penetrate the multilayer. Two factors, the size of the surfactant and its specific interaction with the multilayer, are expected to affect their retention during filtration as well their fouling behaviour. Previously, Figure 7.3 showed that cationic CTAB and anionic SDS interact the most with the multilayer, and Figures 7.4-7.5 showed that they foul it the most. Contrarily, DDAPS and TX interact less with the multilayer and even foul it less. On the other hand, smaller surfactants (SDS (288.4 Da) < DDAPS (335.6 Da) < CTAB (364.5 Da) < TX (625 Da)) are expected to diffuse easier through the multilayer.

In Figure 7.7 we show the flux recovery for both experiments, with and without oil, in presence of surfactant for all our membranes. High flux recoveries are found, as would be expected if the surfactant adsorption indeed dominates the fouling, since surfactant adsorption is highly reversible. We can

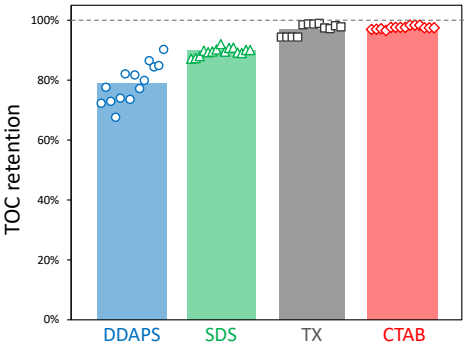

Figure 7.6: TOC retention of PEM hollow fiber (nearly uncharged PAH, negatively PSS, zwitterionic PSBMA-co-AA and negatively hydrophobic Nafion) membranes during experiments with O/W emulsions stabilized by DDAPS, SDS, TX and CTAB. Marks represent single data points while bars their average.

conclude that fouling was mostly reversible for all the solutions tested.

From our results, we can easily conclude that fouling is highly affected by not only specific interactions but also size of the surfactant. While TX gave the most severe fouling issues in UF [42], in NF it is the surfactant that fouls the least as, due to its size, it cannot easily penetrate into the membrane to cause internal fouling. In addition, in contrast with recent interpretations from literature findings [49], in NF, cake layer fouling is not found to be a big issue. The oil droplet cake layer is likely so open that the main resistance to water permeation stems from the PEM separation layer, especially when densified by internal uptake of surfactants. The fouling of our PEM base NF membranes is schematically illustrated in Figure 7.8.

SDS is the smallest surfactant, and its negative charge can easily interact with free cationic groups in the PEM. For that reason, it is SDS that fouls our PEM membranes the most. DDAPS has a slightly lower size than CTAB, but it does not give extremely high fouling issues in our filtration experiments, as the zwitterionic surfactant interacts less strongly with internal charges of the PEM. At steady-state, CTAB hardly permeates into the PEM separation layer, probably because of its strong interaction with free anionic groups which could cause a significant layer densification. Finally, the uncharged and largest surfactant, TX, hardly fouls the membrane as it does not permeate into it and lacks interaction with the internal charges. These observations provide clear directions on how to improve PEM based NF membranes for the treatment of

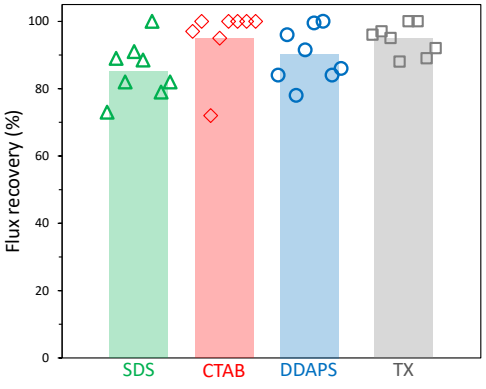

Figure 7.7: Average of flux recovery (%) of nearly uncharged PAH, negatively PSS, zwitterionic PSBMA-co-AA and negatively hydrophobic Nafion membranes for every different set of fouling experiments (with O/W emulsions and only surfactant solutions for SDS, CTAB, DDAPS and TX). Single data points values and SD are reported in tables E.6-E.7.

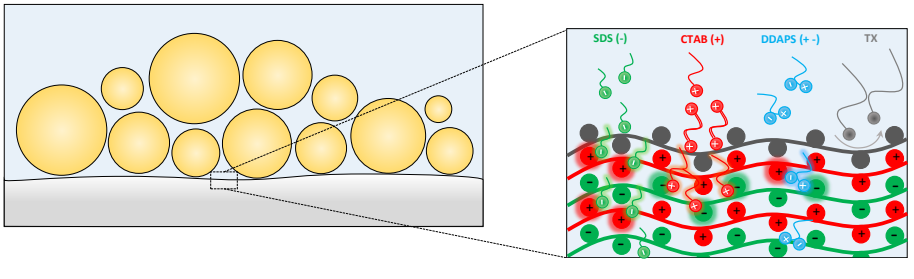

Figure 7.8: Illustration of NF fouling by surfactant stabilized oil-in-water emulsions.

PW. For example, a denser multilayer would be beneficial for PW treatment, as it could stop even the smallest surfactant molecules, preventing the possibility of internal fouling. Another opportunity is to select more bulky and uncharged surfactant molecules such as TX for enhanced oil recovery and more bulky cationic surfactants as corrosion inhibitors to further decrease the negative impact of fouling.

7.4 Conclusions

The sustainable management of produced water is one of the main environmental challenges in the Oil & Gas field. Membrane technology can tackle such a challenge, but fouling still remains a major issue and its causes are not yet well understood. In this work, we highlight surfactants as the dominant fouling species when treating produced water with PEM based NF membranes. We prepared HF NF membranes based on PEMs and studied membrane fouling by only surfactant as well as the corresponding O/W emulsions. Our membranes exhibited high oil retention (>99%), while the physico-chemical interactions between the multilayer and the surfactants determined the extent of fouling, as well as the surfactant retention. While surfactants in MF and UF mainly affect fouling by conferring chemistry to the oil cake-layer, our results prove that in PEM based NF surfactant adsorption into the active layer should be considered as the main cause of fouling in PW treatment. In addition, while we expected different top layers applied on top of the same multilayer to show a different fouling behaviour, it was instead really similar, clearly indicating that for small molecules such as SDS, CTAB and DDAPS, it is not the outer layer chemistry that determines the extent of fouling but the active layer, i.e. the internal multilayer, chemistry. A denser multilayer [67, 68], able to stop these surfactant molecules, would highly benefit PW treatment by decreasing fouling issues of NF membrane modules, while allowing de-oiling and organic molecules removal in one-step process. Alternatively, the use of larger, and preferentially uncharged, surfactant molecules [69], or even polymers [70, 71], in enhanced oil recovery would also substantially reduce the impact on membrane fouling. Finally, as the presence of surfactants can affect the rejection of divalent ions [13], future research should also focus on the interplay between surfactants and divalent ions in membrane fouling and ions retention.

References

[1] J. Neff, K. Lee, and E. M. DeBlois, *Produced Water: Overview of Composition, Fates, and Effects*, 3–54 (Springer New York, New York, NY) (2011).

[2] J. Veil, M. Puder, D. Elcock, and R. Jr, "A white paper describing produced water from production of crude oil, natural gas, and coal bed methane", U.S. Department of energy, National Energy Technology Laboratory. Prepared by Argonne National Laboratory (2004).

[3] J. A. Veil, *Produced Water Management Options and Technologies*, 537–571 (Springer New York, New York, NY) (2011).

[4] J. Dickhout, J. Moreno, P. Biesheuvel, L. Boels, R. Lammertink, and W. de Vos, "Produced water treatment by membranes: A review from a colloidal perspective", Journal of Colloid and Interface Science **487**, 523 – 534 (2017).

[5] A. Fakhrul-Razi, A. Pendashteh, L. C. Abdullah, D. R. A. Biak, S. S. Madaeni, and Z. Z. Abidin, "Review of technologies for oil and gas produced water treatment", Journal of Hazardous Materials **170**, 530 – 551 (2009).

[6] S. Mondal and S. R. Wickramasinghe, "Produced water treatment by nanofiltration and reverse osmosis membranes", Journal of Membrane Science **322**, 162 – 170 (2008).

[7] T. Whalenn, "The challenges of reusing produced water", Society of Petroleum Engineers **64**, 18–20 (2012).

[8] E. Park and S. M. Barnett, "Oil/water separation using nanofiltration membrane technology", Separation Science and Technology **36**, 1527–1542 (2001).

[9] M. Cheryan and N. Rajagopalan, "Membrane processing of oily streams. wastewater treatment and waste reduction", Journal of Membrane Science **151**, 13 – 28 (1998).

[10] E. Tummons, Q. Han, H. J. Tanudjaja, C. A. Hejase, J. W. Chew, and V. V. Tarabara, "Membrane fouling by emulsified oil: A review", Separation and Purification Technology **248**, 116919 (2020).

[11] H. J. Tanudjaja, C. A. Hejase, V. V. Tarabara, A. G. Fane, and J. W. Chew, "Membrane-based separation for oily wastewater: A practical perspective", Water Research **156**, 347 – 365 (2019).

[12] S. Alzahrani and A. W. Mohammad, "Challenges and trends in membrane technology implementation for produced water treatment: A review", Journal of Water Process Engineering **4**, 107 – 133 (2014).

[13] E. Virga, J. de Grooth, K. vab, and W. M. de Vos, "Stable polyelectrolyte multilayer-based hollow fiber nanofiltration membranes for produced water treatment", ACS Applied Polymer Materials **1**, 2230–2239 (2019).

[14] R. Muppalla, S. K. Jewrajka, and A. Reddy, "Fouling resistant nanofiltration membranes for the separation of oilwater emulsion and micropollutants from water", Separation and Purification Technology **143**, 125 – 134 (2015).

[15] P. Xu and J. E. Drewes, "Viability of nanofiltration and ultra-low pressure reverse osmosis membranes for multi-beneficial use of methane produced water", Separation and Purification Technology **52**, 67 – 76 (2006).

[16] C. Visvanathan, P. Svenstrup, and P. Ariyamethee, "Volume reduction of produced water generated from natural gas production process using membrane technology", Water Science and Technology **41**, 117–123 (2000).

[17] A. Mohammad, Y. Teow, W. Ang, Y. Chung, D. Oatley-Radcliffe, and N. Hilal, "Nanofiltration membranes review: Recent advances and future prospects", Desalination **356**, 226 – 254 (2015), state-of-the-Art Reviews in Desalination.

[18] S. P. Nunes, "Can fouling in membranes be ever defeated?", Current Opinion in Chemical Engineering **28**, 90 – 95 (2020).

[19] A. Schaefer, N. Andritsos, A. Karabelas, E. Hoek, R. Schneider, and M. Nyström, *Nanofiltration Principles and Applications 1 Chapter 8 Fouling in Nanofiltration* (2004).

[20] L. Braeken, B. Van der Bruggen, and C. Vandecasteele, "Flux decline in nanofiltration due to adsorption of dissolved organic compounds: model prediction of time dependency", The Journal of Physical Chemistry B **110**, 2957–2962 (2006), pMID: 16471907.

[21] K. Boussu, C. Kindts, C. Vandecasteele, and B. Van der Bruggen, "Surfactant fouling of nanofiltration membranes: Measurements and mechanisms", ChemPhysChem **8**, 1836–1845 (2007).

[22] G. Cornelis, K. Boussu, B. Van der Bruggen, I. Devreese, and C. Vandecasteele, "Nanofiltration of nonionic surfactants: effect of the molecular weight cutoff and contact angle on flux behavior", Industrial & Engineering Chemistry Research **44**, 7652–7658 (2005).

[23] B. Van der Bruggen, M. Mänttäri, and M. Nyström, "Drawbacks of applying nanofiltration and how to avoid them: A review", Separation and Purification Technology **63**, 251–263 (2008).

[24] D. Zhao and S. Yu, "A review of recent advance in fouling mitigation of nf/ro membranes in water treatment: pretreatment, membrane modification, and chemical cleaning", Desalination and Water Treatment **55**, 870–891 (2015).

[25] E. N. Tummons, C. A. Hejase, Z. Yang, J. W. Chew, M. L. Bruening, and V. V. Tarabara, "Oil droplet behavior on model nanofiltration membrane surfaces under conditions of hydrodynamic shear and salinity", Journal of Colloid and Interface Science **560**, 247 – 259 (2020).

[26] E. Virga, K. vab, and W. M. de Vos, "Fouling of nanofiltration membranes based on polyelectrolyte multilayers: The effect of a zwitterionic final layer", Journal of Membrane Science 118793 (2020).

[27] L. Y. Ng, A. W. Mohammad, and C. Y. Ng, "A review on nanofiltration membrane fabrication and modification using polyelectrolytes: Effective ways to develop membrane selective barriers and rejection capability", Advances in Colloid and Interface Science **197-198**, 85 – 107 (2013).

[28] S. T. Muntha, A. Kausar, and M. Siddiq, "Advances in polymeric nanofiltration membrane: A review", Polymer-Plastics Technology and Engineering **56**, 841–856 (2017).

[29] E. Evdochenko, J. Kamp, R. Femmer, Y. Xu, V. Nikonenko, and M. Wessling, "Unraveling the effect of charge distribution in a polyelectrolyte multilayer nanofiltration membrane on its ion transport properties", Journal of Membrane Science 118045 (2020).

[30] S. P. Nunes, P. Z. Culfaz-Emecen, G. Z. Ramon, T. Visser, G. H. Koops, W. Jin, and M. Ulbricht, "Thinking the future of membranes: Perspectives for advanced and new membrane materials and manufacturing processes", Journal of Membrane Science **598**, 117761 (2020).

[31] J. de Grooth, M. G. Elshof, and H. D. W. Roesink, "Polyelectrolyte multilayer (pem) membranes and their use", (2020).

[32] W. Lau, A. Ismail, N. Misdan, and M. Kassim, "A recent progress in thin film composite membrane: A review", Desalination **287**, 190 – 199 (2012), special Issue in honour of Professor Takeshi Matsuura on his 75th Birthday.

[33] J. Vrouwenvelder, D. Graf von der Schulenburg, J. Kruithof, M. Johns, and M. van Loosdrecht, "Biofouling of spiral-wound nanofiltration and reverse osmosis membranes: A feed spacer problem", Water Research **43**, 583 – 594 (2009).

[34] W. Shan, P. Bacchin, P. Aimar, M. L. Bruening, and V. V. Tarabara, "Polyelectrolyte multilayer films as backflushable nanofiltration membranes with tunable hydrophilicity and surface charge", Journal of Membrane Science **349**, 268 – 278 (2010).

[35] J. de Grooth, R. Oborný, J. Potreck, K. Nijmeijer, and W. M. de Vos, "The role of ionic strength and oddeven effects on the properties of polyelectrolyte multilayer nanofiltration membranes", Journal of Membrane Science **475**, 311 – 319 (2015).

[36] J. J. Richardson, M. Björnmalm, and F. Caruso, "Technology-driven layer-by-layer assembly of nanofilms", Science **348** (2015).

[37] J. de Grooth, "A tale of two charges: zwitterionic polyelectrolyte multilayer membranes", Ph.D. thesis, University of Twente (2015).

[38] A. E. Childress and M. Elimelech, "Effect of solution chemistry on the surface charge of polymeric reverse osmosis and nanofiltration membranes", Journal of Membrane Science **119**, 253 – 268 (1996).

[39] J. Dijt, M. Stuart, and G. Fleer, "Reflectometry as a tool for adsorption studies", Advances in Colloid and Interface Science **50**, 79 – 101 (1994).

[40] T. Tumolo, L. Angnes, and M. S. Baptista, "Determination of the refractive index increment (dn/dc) of molecule and macromolecule solutions by surface plasmon resonance", Analytical Biochemistry **333**, 273 – 279 (2004).

[41] G. Csúcs and J. J. Ramsden, "Solubilization of planar bilayers with detergent", Biochimica et Biophysica Acta (BBA) - Biomembranes **1369**, 304 – 308 (1998).

[42] J. M. Dickhout, E. Virga, R. G. Lammertink, and W. M. de Vos, "Surfactant specific ionic strength effects on membrane fouling during produced water treatment", Journal of Colloid and Interface Science **556**, 12 – 23 (2019).

[43] E. Virga, B. Bos, P. Biesheuvel, A. Nijmeijer, and W. M. de Vos, "Surfactant-dependent critical interfacial tension in silicon carbide membranes for produced water treatment", Journal of Colloid and Interface Science **571**, 222 – 231 (2020).

[44] J. Li, D. Mcclements, and L. Mclandsborough, "Interaction between emulsion droplets and escherichia coli cells", Journal of Food Science **66**, 570–657 (2006).

[45] R. Vácha, S. W. Rick, P. Jungwirth, A. G. F. de Beer, H. B. de Aguiar, J.-S. Samson, and S. Roke, "The orientation and charge of water at the hydrophobic oil dropletwater interface", Journal of the American Chemical Society **133**, 10204–10210 (2011), pMID: 21568343.

[46] K. B. Medrzycka, "The effect of particle concentration on zeta potential in extremely dilute solutions", Colloid and Polymer Science **269**, 85–90 (1991).

[47] H. Zhong, L. Yang, G. Zeng, M. L. Brusseau, Y. Wang, Y. Li, Z. Liu, X. Yuan, and F. Tan, "Aggregate-based sub-cmc solubilization of hexadecane by surfactants", RSC Adv. **5**, 78142–78149 (2015).

[48] S. R. Varade and P. Ghosh, "Foaming in aqueous solutions of zwitterionic surfactant: Effects of oil and salts", Journal of Dispersion Science and Technology **38**, 1770–1784 (2017).

[49] C. A. Hejase and V. V. Tarabara, "Nanofiltration of saline oil-water emulsions: Combined and individual effects of salt concentration polarization and fouling by oil", Journal of Membrane Science **617**, 118607 (2021).

[50] D. Lu, T. Zhang, and J. Ma, "Ceramic membrane fouling during ultrafiltration of oil/water emulsions: Roles played by stabilization surfactants of oil droplets", Environmental Science & Technology **49**, 4235–4244 (2015), pMID: 25730119.

[51] X. Zhu, A. Dudchenko, X. Gu, and D. Jassby, "Surfactant-stabilized oil separation from water using ultrafiltration and nanofiltration", Journal of Membrane Science **529**, 159 – 169 (2017).

[52] T. A. Trinh, Q. Han, Y. Ma, and J. W. Chew, "Microfiltration of oil emulsions stabilized by different surfactants", Journal of Membrane Science **579**, 199 – 209 (2019).

[53] D. M. Reurink, E. te Brinke, I. Achterhuis, H. D. W. Roesink, and W. M. de Vos, "Nafion-based low-hydration polyelectrolyte multilayer membranes for enhanced water purification", ACS Applied Polymer Materials **1**, 2543–2551 (2019).

[54] Z. Bi, W. Liao, and L. Qi, "Wettability alteration by ctab adsorption at surfaces of sio2 film or silica gel powder and mimic oil recovery", Applied Surface Science **221**, 25 – 31 (2004).

[55] S. B. Velegol and R. D. Tilton, "Specific counterion effects on the competitive co-adsorption of polyelectrolytes and ionic surfactants", Journal of Colloid and Interface Science **249**, 282 – 289 (2002).

[56] K. L. Cho, A. J. Hill, F. Caruso, and S. E. Kentish, "Chlorine resistant glutaraldehyde crosslinked polyelectrolyte multilayer membranes for desalination", Advanced Materials **27**, 2791–2796 (2015).

[57] Y. Zhang, Z. Wang, W. Lin, H. Sun, L. Wu, and S. Chen, "A facile method for polyamide membrane modification by poly(sulfobetaine methacrylate) to improve fouling resistance", Journal of Membrane Science **446**, 164 – 170 (2013).

[58] T. Xiang, C.-D. Luo, R. Wang, Z.-Y. Han, S.-D. Sun, and C.-S. Zhao, "Ionic-strength-sensitive polyethersulfone membrane with improved antifouling property modified by zwitterionic polymer via in situ cross-linked polymerization", Journal of Membrane Science **476**, 234 – 242 (2015).

[59] C. Liu, J. Lee, C. Small, J. Ma, and M. Elimelech, "Comparison of organic fouling resistance of thin-film composite membranes modified by

hydrophilic silica nanoparticles and zwitterionic polymer brushes", Journal of Membrane Science **544**, 135 – 142 (2017).

[60] P. Wydro and M. Paluch, "A study of the interaction of dodecyl sulfobetaine with cationic and anionic surfactant in mixed micelles and monolayers at the air/water interface", Journal of Colloid and Interface Science **286**, 387 – 391 (2005).

[61] M. Antonietti, J. Conrad, and A. Thuenemann, "Polyelectrolyte-surfactant complexes: A new type of solid, mesomorphous material", Macromolecules **27**, 6007–6011 (1994).

[62] L. D. Nghiem and S. Hawkes, "Effects of membrane fouling on the nanofiltration of pharmaceutically active compounds (phacs): Mechanisms and role of membrane pore size", Separation and Purification Technology **57**, 176 – 184 (2007).

[63] V. Lindstrand, G. Sundström, and A.-S. Jönsson, "Fouling of electrodialysis membranes by organic substances", Desalination **128**, 91 – 102 (2000).

[64] H.-J. Lee, M.-K. Hong, S.-D. Han, J. Shim, and S.-H. Moon, "Analysis of fouling potential in the electrodialysis process in the presence of an anionic surfactant foulant", Journal of Membrane Science **325**, 719 – 726 (2008).

[65] S. Mikhaylin and L. Bazinet, "Fouling on ion-exchange membranes: Classification, characterization and strategies of prevention and control", Advances in Colloid and Interface Science **229**, 34 – 56 (2016).

[66] J. B. Schlenoff and S. T. Dubas, "Mechanism of polyelectrolyte multilayer growth: charge overcompensation and distribution", Macromolecules **34**, 592–598 (2001).

[67] E. te Brinke, D. M. Reurink, I. Achterhuis, J. de Grooth, and W. M. de Vos, "Asymmetric polyelectrolyte multilayer membranes with ultrathin separation layers for highly efficient micropollutant removal", Applied Materials Today **18**, 100471 (2020).

[68] J. Kamp, S. Emonds, and M. Wessling, "Designing tubular composite membranes of polyelectrolyte multilayer on ceramic supports with nanofiltration and reverse osmosis transport properties", Journal of Membrane Science **620**, 118851 (2021).

[69] P. SWPU, "Most common surfactants employed in chemical enhanced oil recovery", Petroleum **3**, 197211 (2017).

[70] A. Abidin, T. Puspasari, and W. Nugroho, "Polymers for enhanced oil recovery technology", Procedia Chemistry **4**, 11 – 16 (2012), the International Conference on Innovation in Polymer Science and Technology.

[71] P. Raffa, A. A. Broekhuis, and F. Picchioni, "Polymeric surfactants for enhanced oil recovery: A review", Journal of Petroleum Science and Engineering **145**, 723 – 733 (2016).

Part III

Interfacial Phenomena

8

Nanofiltration of Complex Mixtures: The Effect of the Adsorption of Divalent Ions on Membrane Retention°

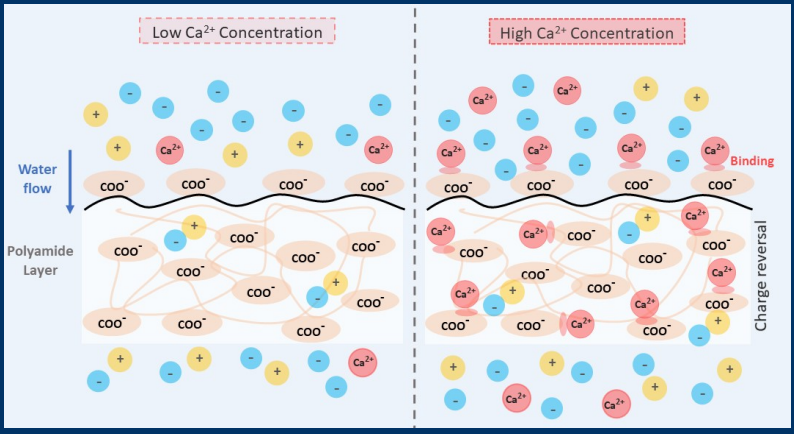

°Submitted as: Sebastian C. Osorio, Jouke E. Dykstra, P. M. Biesheuvel, and **Ettore Virga**, *Nanofiltration of Complex Mixtures: The Effect of the Adsorption of Divalent Ions on Membrane Retention*, Desalination **2021**.

Abstract

Nanofiltration (NF) is nowadays used in a wide range of commercial applications in water desalination, especially to separate divalent from monovalent ions (e.g., in water softening, water reclamation, etc.). The interaction between ions in multi-component electrolyte solutions and the membrane is important and must be studied. In NF, the solution and membrane chemistry determine the charge of the membrane, and therefore the electrostatic repulsion of ions. Membrane charge reversal can take place when divalent ions bind to the membrane and modify its surface charge, which may explain some puzzling results, where the rejection of divalent ions increases with higher concentration in the feed. To model charge reversal and accurately predict the rejection of ions with NF membranes a recent study argued against the suitability of conventional mean-field theory. However, our work emphasizes the suitability of conventional mean-field models which can be extended to account for the interaction between the membrane and divalent counterions. By using a Langmuir equation with two model parameters, we consider the adsorption of divalent ions (e.g. Ca^{2+} and Mg^{2+}) in the polyamide (PA) active layer of the membrane and describe how this adsorption process affects membrane charge. Based on experimental data from two different studies we show that mean-field theory can predict the rejection of all types of ions in a multi-component electrolyte solution when the effect of divalent counterions on the membrane charge is included. These results provide evidence that adsorption of counterions plays a fundamental role in the performance of nanofiltration.

8.1 Introduction

Nowadays, membrane technologies, such as nanofiltration (NF), play a vital role in providing solutions to complex problems in water treatment [1]. Particularly, in the last decade, the technological interest in NF has increased [2], with NF being widely used in numerous applications. To mention some examples, reclamation of wastewater from textile industries [3–5], resource recovery and re-use in agro-food industry [6], removal of harmful pollutants, such as pesticides and arsenic, in the production of drinking water [7, 8], and pretreatment for desalination processes [9–12].

In NF, a pressure gradient is the main driving force and a semi-permeable membrane acts as a barrier for solutes [13]. In terms of rejection, NF is in between ultrafiltration (UF) and reverse osmosis (RO) [12, 14]. In some applications, such as desalination pretreatment, NF presents several advantages. For instance, lower operating pressure, higher water permeability, and lower energy consumption than RO. Despite the lower pressure applied, NF can still achieve high retention of multivalent ions and dissolved organic matter [15]. In addition, using NF as pre-treatment for RO improves overall desalination performance because the frequency of chemical cleaning can be reduced, water recovery increased, and energy consumption decreased [16].

In desalination, polyamide (PA) thin-film composite (TFC) membranes are the most commonly used because of their high selectivity and permeability [17]. PA-TFC membranes consist typically of a low resistance support layer and a functionally active top layer, which plays the main role in the separation and rejection of ions [18]. The top polyamide layer in these membranes contains carboxylic and amine groups that normally, at neutral or alkaline pH, give a strong negative surface charge to the membrane [19], which also serves to reduce organic fouling [20].

During NF operation, the removal of contaminants and ions from water is the consequence of a combination of phenomena, such as steric and Donnan exclusion. Donnan exclusion is the main reason why the net charge, resulting from the dissociation of functional groups in the membrane, strongly influences filtration performance [20, 21]. In addition, other transport effects, such as hindered diffusion in the pores of the membrane, play an important role [22].

We next provide a brief overview of literature on transport of mixed solutions in NF. Mean-field theories such as the extended Nernst-Planck (ENP) equation, which include diffusion, advection, and electromigration [23], have been widely used [24–27]. For instance, Peters *et al.* used the extended Nernst-Planck equation to study the rejection of different single salts and compared

their prediction with experimental data [28]. Moreover, models based on the ENP equation can be easily extended to include, besides ion transport, physical and chemical phenomena, such as chemical equilibrium of amphoteric ions [29] and acid-base reactions inside the membrane [13, 30].

Besides the mean-field theory, phenomenological models that are based on the Nernst-planck equation have been proposed. For instance, Fridman *et al.*[31] studied and theoretically described the rejection of ions prevalent in seawater (Cl^-, Na^+, Ca^{2+}), and concluded that, to accurately predict ion concentrations in the permeate, one has to account for the presence of divalent ions [31]. Bason *et al.* found that ion adsorption and binding of counterions to the charged groups of an NF membrane can radically affect ion retention, and suggested that it needs to be included for accurate model predictions [32]. Recently, from these phenomenological approaches, objections were raised to the applicability of mean-field theory to describe transport in NF membranes and include ion binding or association to the membrane [33]. However, we believe these objections can be resolved. Therefore it is the aim of the present study to show that mean-field theory (ENP) together with suitable models for ion adsorption, can accurately predict ion retention by NF membranes from multi-ionic solutions that contain both monovalent and divalent cations. We compare our theoretical model with experimental data by Fridman *et al.*[34] and by Deon *et al.* [35].

In NF with PA-TFC membranes, it is important to consider the interaction between counterions (cations for negatively charged membranes) and functional groups of the membrane. This interaction can be an important factor affecting the membrane charge, especially when multivalent ions, such as Ca^{2+} and Mg^{2+}, are present in solution [36–39]. Such interactions can even lead to reversal of the membrane charge and influence the transport properties of each individual ion [21, 40].

The binding mechanism between polyamide functional groups and multivalent ions has previously been studied [41]. For instance, Tangara *et al.* already described how cations adsorb on polyamide resins and how PA acts as a polymeric chelate, adsorbing metal ions through a covalent bond [42]. Bruni *et al.* developed a model for single salt solutions to describe competitive adsorption and site-binding of counterions in NF [38]. Similarly, Hall *et al.* studied and modeled a reverse osmosis process for a multi-electrolyte solution considering the adsorption of cations and their effect on the membrane charge [40].

In Figure 8.1, we illustrate the model problem of a multi-component electrolyte solution with three ions, Ca^{2+}, Na^+, and Cl^-, where Ca^{2+}-ions bind

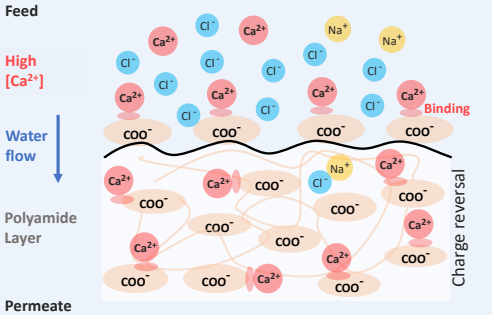

Figure 8.1: General illustration of binding between Ca^{2+} and the carboxylic groups in a PA top layer of a nanofiltration (NF) membrane. With high enough Ca^{2+} concentration, the net charge of the membrane is reversed from negative to positive.

to negative carboxylic groups of the membrane. Therefore, when the concentration of Ca^{2+} is high enough, the surface charge of the membrane becomes positive (charge reversal), as we also show in Figure 8.2.

In our model we include the adsorption of cations in the membrane by describing the membrane charge as function of the local cation concentration. We assume that only Ca^{2+}- or Mg^{2+}-ions can affect the membrane charge. In addition, hindrance, membrane porosity, and pore tortuosity, are all included in a reduction factor for diffusion. We will show how we can include in an ENP-based transport model the adsorption of counterions and arrive at a very good model fit to experimental data from literature. Besides, with the proposed model, we can explain some puzzling results, such as rejection of ions increasing with concentration or controlled by counter-ions, in such experiments that previous models could not predict [33, 34].

8.2 Theory

In the present section, we describe general theory, based on the extended Donnan Steric Partitioning Pore model (ext-DSP model), to calculate the concentration difference that develops between the feed (influent solution) and the permeate (treated water) in NF. The ext-DSP model is based on the ENP equation, which includes advection, diffusion and migration, and in addition describes the partitioning of ions, Φ_i, between solution and membrane pores. Within this model, a Donnan balance applies at both edges of the membrane to include effects of steric hindrance and electric potential on the partitioning of ions. In the one-dimensional model proposed in this study, we only consider

three types of ions, Cl^-, Na^+ and a divalent cation, either Ca^{2+} or Mg^{2+}, and neglect reactions between them [43] while we also neglect any involvement of H^+ or OH^-. We include in the model how the local membrane charge is dependent on the adsorption of Ca^{2+} or Mg^{2+}. Only divalent cations are considered to adsorb to the negatively charged membrane groups, because they have a much stronger binding energy than monovalent cations.

The transport theory makes use of the ENP equation to describe the transport of ions through the membrane

$$J_i = v_{\mathrm{F}} K_{c,i} c_i - K_{d,i} \epsilon D_i \left(\frac{\partial c_i}{\partial x} + z_i c_i \frac{\partial \phi}{\partial x} \right) \tag{8.1}$$

where the ionic flux through the membrane, J_i, is a function of advection, diffusion and migration, respectively. The factor $K_{c,i}$ accounts for a hindrance effect by which advection is reduced, and likewise $K_{d,i}$ is a reduction factor for diffusion and migration. The water velocity through the membrane is given by v_{F}, c_i is ion concentration in the membrane pores, D_i is the diffusion coefficient in bulk solution, ϵ is a reduction factor due to membrane porosity and tortuosity, and x is the coordinate across the membrane.

Inside the membrane, mass conservation of every ion, without chemical reactions, is given by

$$\frac{\partial c_i}{\partial t} = -\frac{\partial J_i}{\partial x} \tag{8.2}$$

which for steady-state can be combined with Eq. (9.1) to arrive at

$$0 = v_{\mathrm{F}} K_{c,i} \frac{\partial c_i}{\partial x} - \zeta_i D_i \frac{\partial}{\partial x} \left(\frac{\partial c_i}{\partial x} + z_i c_i \frac{\partial \phi}{\partial x} \right) \tag{8.3}$$

where the reduction factor ζ_i is given by $\zeta_i = K_{c,i} \cdot \epsilon$. We solve Eq. (8.3) at each position x in the membrane, from the membrane-feed solution boundary, $x = 0$, to the membrane-permeate boundary, $x = \delta$, where δ refers to the thickness of the PA top layer.

At both membrane-solution interfaces, we apply the Donnan equilibrium for each ion

$$c_i^* = c_{\mathrm{out},i} \Phi_i e^{-z_i \Delta \phi_{\mathrm{D}}} \tag{8.4}$$

where c_i^* is the ion concentration in the membrane at the membrane-feed solution boundary, or on the membrane-permeate boundary, and $c_{\mathrm{out},i}$ is the corresponding concentration in solution just outside the membrane. The ion partitioning coefficient, Φ_i, accounts for a steric hindrance effect at the edges of the membrane [44], and $\Delta\phi_{\mathrm{D}}$ is the Donnan potential. In this study, for

simplicity, we assume the steric effect Φ_i of all ions to be the same, which reduces the number of parameters in the model.

We consider local electroneutrality and zero electric current at all positions in the membrane, according to

$$\sum_i z_i c_i + X = 0 \tag{8.5}$$

and

$$\sum_i z_i J_i = 0 \tag{8.6}$$

where X is the charge density in the membrane, which can be constant, or can be variable, in that second case dependent on local concentrations, chemical interactions between ions and membrane material, and on acid-base reactions [30]. In this study, we make X a function of the local Ca^{2+}- or Mg^{2+}-concentration using the equations reported by Hall *et al.* [40], without including a direct effect of other ions. Even though Na^+ might also interact with the negative carboxylic groups of the membrane, divalent cations have a stronger interaction and higher site-binding constant [45], which translates into a larger impact on the membrane charge. Therefore, the membrane charge is defined as function of the local concentration of divalent cations, c^{2+}, according to

$$X = -X_0 \frac{1 - K_b \cdot c^{2+}}{1 + K_b \cdot c^{2+}} \tag{8.7}$$

with K_b the membrane-c^{2+} binding constant, and X_0 the bare membrane charge, i.e., the charge in absence of divalent cations in solution. The derivation of this adsorption model is explained in section F.1 of Appendix F. In the adsorption model, we assume that divalent cations bind to a single membrane group (1:1 interaction). This model allows the membrane charge to flip sign, from negative, in the absence of divalent cations, to positive when sufficient numbers of divalent cations are present. An alternative membrane charging model is discussed in Appendix F (Figure F.1), where we present results for the case when divalent cations bind to two membrane groups at the same time (1:2 interaction).

Another important variable is the rejection of ions, R_i, which is given by

$$R_i = 1 - \frac{c_{\mathrm{p},i}}{c_{\mathrm{f},i}} \tag{8.8}$$

where $c_{\mathrm{p},i}$ and $c_{\mathrm{f},i}$ are the concentration of ions in permeate and in feed. In the model, we define a reference Peclet number, $\mathrm{Pe}_{\mathrm{ref}}$. The Peclet number is

the ratio between convective and diffusive transport, and shows how the same model results are obtained for different combinations of δ and v_F values. The Peclet number is defined as

$$\mathrm{Pe}_{\mathrm{ref}} = \frac{v_F \delta}{D_{\mathrm{ref}}}. \tag{8.9}$$

8.3 Results and Discussion

8.3.1 Membrane charge

In this section, we study the effect of divalent cation adsorption on membrane charge. Generally, polyamide composite membranes have a negative surface charge when the solution pH is above pH 5 [46]. However, a high enough concentration of divalent counterions in the feed solution leads to charge reversal [34]. In Figure 8.2, we show how membrane charge is affected by the feed Ca^{2+} concentration. We present results of calculations for two solutions with constant $[Na^+]_{\mathrm{feed}}$ of 100 and 500 mM, while changing $[Ca^{2+}]_{\mathrm{feed}}$. Other parameters used to obtain the results in Figure 8.2 are given in Table 8.2, Case I.

Results in Figure 8.2 show that the membrane charge density ranges from -400 to 400 mM. For a solution with low $[Ca^{2+}]_{\mathrm{feed}}$ the membrane is negatively charged (as low as X = -400 mM) but it becomes positively charged at a higher $[Ca^{2+}]_{\mathrm{feed}}$. Outside the point of zero membrane charge, $[Na^+]_{\mathrm{feed}}$ also influences membrane charge.

In Figure 8.2, for 100 mM and 500 mM $[Na^+]_{\mathrm{feed}}$, the curve of charge vs divalent cation concentration becomes quite steep when $[Ca^{2+}]_{\mathrm{feed}}$ increases to beyond 2.0 or 25 μM respectively, showing in that range a pronounced effect of the adsorption of counterions on the membrane charge. For both solutions, 100 mM and 500 mM $[Na^+]_{\mathrm{feed}}$, at a concentration of 8 and 9 mM $[Ca^{2+}]_{\mathrm{feed}}$ respectively, the membrane charge is zero (point of zero charge). These concentrations are often reached in practice, and are sometimes even higher [47, 48], and thus membrane charge reversal must certainly be considered. Above the point of zero charge (8 or 9 mM), the charge reversal takes place, with membrane charge ultimately reaching X = 400 mM. The value of the binding constant, K_b, that we find in our study by fitting theory to the data, is comparable to values reported in literature [42].

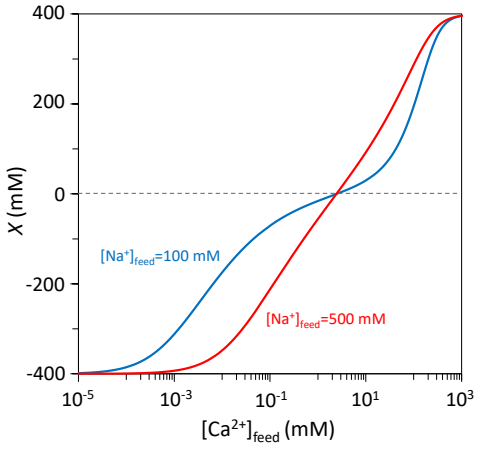

Figure 8.2: Membrane charge as a function of $[Ca^{2+}]_{feed}$ for two solutions with different $[Na^{+}]_{feed}$, 100 mM (blue) and 500 mM (red). Model parameters are given in Table 8.2, Case I.

8.3.2 Model predictions

In this section we show results of comparing our model with experimental data. In Table 8.1, the general transport parameters used are reported. The Nelder-Mead method [49] was used to find model parameters that make the theory fit closely to data from two studies [34, 35]. Detailed information about the Nelder-Mead procedure is given in section F.3 of SI. The Nelder-Mead procedure was successful and gave us a good fit of the theory to experimental data, and provided realistic parameter settings that we report in Table 8.2.

D_{ref}=1·10^{-9} m^2/s	$D_{Mg^{2+}}/D_{ref}$ =0.706
D_{Na^+}/D_{ref} =1.334	δ_{ref}=100 nm
D_{Cl^-}/D_{ref} =2.031	Pe_{ref}=0.0015
$D_{Ca^{2+}}/D_{ref}$ =0.791	$K_{c,i}$=1 for all ions

Table 8.1: Transport parameters used in theory. Diffusion coefficients from Ref. [30]

The data from Fridman *et al.* [34] was the first set of data used to develop and evaluate the model. The description of the experimental protocol is summarized in SI. These data correspond to two solutions with a total feed Cl^- concentration, $[Cl^-]_{tot}$, of 100 mM and of 500 mM, while the concentration of

Case I		Case II	
X_0	400 mM	X_0	36 mM
K_b	2.28 mM^{-1}	K_b	1.57 mM^{-1}
Φ_{Cl^-}, Φ_{Na^+}, $\Phi_{Ca^{2+}}$	0.19	Φ_{Cl^-}, Φ_{Na^+}, $\Phi_{Mg^{2+}}$	0.13
ζ_{Cl^-}/ζ_{ref}	0.46	ζ_{Cl^-}/ζ_{ref}	0.77
ζ_{Na^+}/ζ_{ref}	3.14	ζ_{Na^+}/ζ_{ref}	2.77
$\zeta_{Ca^{2+}}/\zeta_{ref}$	1.43	$\zeta_{Mg^{2+}}/\zeta_{ref}$	0.14

Table 8.2: Model parameters calculated to fit the experimental data for Case I based on Fridman *et al.* [34], and for Case II based on Déon *et al.* [35], with the reference value of reduction factor for diffusion $\zeta_{ref} = 1{\cdot}10^{-2}$

cations was varied. The equivalent Na^+ fraction in the feed, θ, is defined as

$$\theta = \frac{[NaCl]_{feed}}{[Cl^-]_{tot}} = \frac{[NaCl]_{feed}}{[NaCl]_{feed} + 2 \cdot [CaCl_2]_{feed}}. \tag{8.10}$$

In Figure 8.3 we show experimental data and model predictions for the rejection of Na^+ (Figure 8.3a) and Ca^{2+} (Figure 8.3b) as function of feed composition, θ. Blue and red lines are our model predictions that considers Ca^{2+} adsorption on the membrane. The grey dashed line shows an earlier calculation result by Fridman *et al.* for $[Cl^-]_{tot} = 100$ mM [34], in which adsorption of Ca^{2+}-ions to the membrane was not considered. In Figure 8.3a, we can observe how Na^+ rejection decreases to negative values, when its concentration in the feed is less than $\theta \sim 0.4$. This special situation will be discussed in section 8.3.3.1. In contrast, Figure 8.3b shows how Ca^{2+} rejection is relatively stable and only at very low $[Ca^{2+}]_{feed}$, i.e., high θ, drops off, in agreement with the findings of C. Mazzoni *et al.*[50]. This steep decay in rejection of Ca^{2+} at high θ is found both in theory and experiments. As expected for NF, the rejection of divalent ions is much higher than of monovalent ions. Comparing this result with the model prediction by Fridman *et al.*[34] (grey dashed line) shows that including the adsorption of Ca^{2+}-ions to the membrane significantly improves the prediction of ion rejection. Therefore, contrary to what is reported in literature [33], in this study we conclusively demonstrate that it is possible to rationalize the puzzling behavior, such as rejection of ions increasing with concentration or controlled by counter-ions, of three ions in solution by using an extended Nernst-Planck model (mean-field theory) in which the adsorption of counterions in the membrane is included.

In a second exercise we analyzed experimental data from a second study to further validate our model [35]. In this second study, ternary ion mixtures were

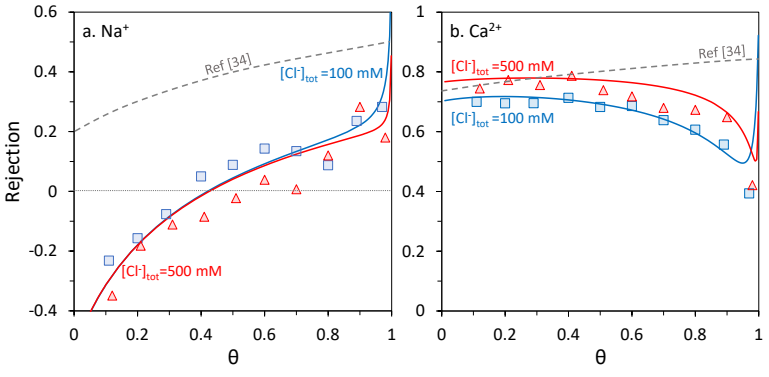

Figure 8.3: Rejection of a) Na^+ and b) Ca^{2+} by NF membranes. Lines are theory, and symbols are experimental data from Fridman *et al.* as function of feed compositions, θ, and $[Cl^-]_{tot}$ [34]. Model parameters in Table 8.2, Case I.

tested with different membranes and experimental conditions. We analyze their data for one membrane (AFC40), tested with a ternary salt mixture of Na^+, Mg^{2+} and Cl^-. We used data reported for a solution of 50 mM Na^+ and 25 mM Mg^{2+} feed concentration. Despite the different membranes and the use of Mg^{2+} instead of Ca^{2+}, the principle of cation binding to the carboxylic groups of the polyamide layer is expected to be the same.

By using the membrane charge reported by Déon *et al.* [35]. and by slightly adapting the values of the reduction factors for diffusion, ζ_i, for each ion, we can again reproduce the data for rejection of ions. For this case, the general transport parameters are given in Table 8.1, and the values of the model parameters are reported in Table 8.2, Case II. In Figure 8.4, we present experimental data [35] and model predictions for the rejection of Mg^{2+} and Na^+ as function of the permeate flux J_v, which is equivalent to the water velocity through the membrane, v_F.

The gradual increase of ion rejection with water flux is clearly shown. In this data set again negative rejections for Na^+ are observed, now at low water flux, which are perfectly reproduced by our model. Indeed, the accurate reproduction of these experimental data with our model shows again that adsorption of divalent cations in the membrane is an important element in theoretical descriptions of NF.

8.3.3 Analysis

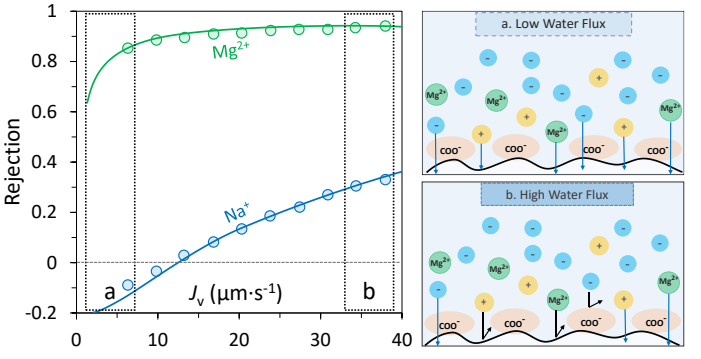

Figure 8.4: Ion rejection by NF membranes from solution with monovalent and divalent cations as function of transmembrane water flow rate, J_v. Lines are theory and symbols are experimental data from Déon *et al.* ($[Cl^-]_{tot}$=100 mM). Further data in main text [35].

8.3.3.1 Limiting Cases

There are two interesting situations in the limits of $\theta \sim 0$ and $\theta \sim 1$ in Figures 8.3a and 8.3b. In the first region, when $\theta \sim 0$, the model and the experimental data show a rejection below zero, $R_{Na^+} < 0$, which can be considered a quite unexpected result. However, this situation has already been reported in literature, especially for multi-component electrolyte solutions in the presence of multivalent ions [39, 51–55]. Yaroshchuk *et al.* studied the different cases and reasons behind the negative rejection [56]. The membrane properties (e.g., charge and material), the ions in the solution and the operating conditions are some of the parameters that can lead to $R_i < 0$. In this particular case, when a counterion with lower valence (Na^+) is a trace ion and a highly charged membrane is used, the electroneutrality principle is the main reason for $R_i < 0$. When multiple counterions with different mobilities and valencies are in solution, due to the electric field, the counterion with a single charge is accelerated, especially when there is a low passage of multivalent ions through the membrane.

The second limit is in the region close to $\theta = 1$. This limit is illustrated in Figure 8.5, which is a magnification of Figures 8.3a and 8.3b. Blue and red lines represent the case for $[Cl^-]_{tot}$ of 100 mM and 500 mM, respectively. In this region, there is a sharp increase in the rejection of both ions, R_{Na^+} and $R_{Ca^{2+}}$. To explain the increase in $R_{Ca^{2+}}$, we need to consider that, in this region, Ca^{2+} is present as a trace ion. When a trace ion has a higher charge,

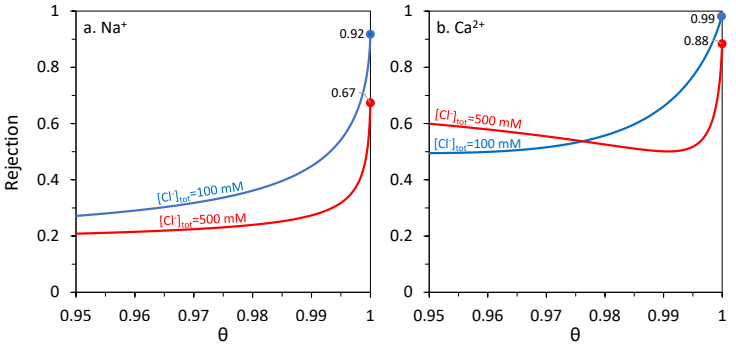

Figure 8.5: Close-up of theoretical results of Figure 3 in the limit close to $\theta = 1$.

and its sign is the same as the faster dominant ion, there is an increase in the rejection of the trace ion [57].

On the other hand, there are no effects of the trace ion on the membrane characteristics and on the transport mechanisms of the dominant ions [58]. Thus, the membrane charge is not affected and the co-ion, in this case Cl^-, determines the rejection. The lower the Ca^{2+} concentration in the feed, the more negative the membrane charge and the lower the Cl^- concentration inside the membrane, which limits the transport of both Cl^- and Na^+ due to the zero current principle as summarized in Eq. (8.5).

8.3.3.2 Concentration profiles across the membrane

Now, we present and discuss the concentrations of Na^+ and Ca^{2+}, and the membrane charge, X, just inside the membrane, at both membrane interfaces, as function of θ, for $[Cl^-]_{tot} = 100$ mM, see Figure 8.6.

Figure 8.6 shows that the concentrations of ions, and the membrane charge, are different between the two sides of the membrane. For instance, the concentration of Ca^{2+} gradually decreases across the membrane, from the feed to the permeate side, and this has the expected effect to lower the membrane charge. On the other hand, the concentration of Na^+ increases across the membrane. For both cations, the difference in concentration across the membrane is largest for low values of θ (Na^+ trace condition). This result agrees with the analysis of negative rejections of Na^+ given in Section 8.3.3.1.

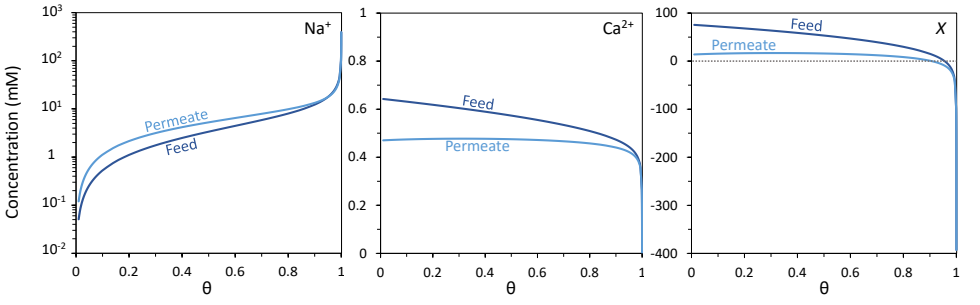

Figure 8.6: Predicted concentration of Na^+ and Ca^{2+}, in the membrane, at the two interfaces, as well as membrane charge, X, at these two locations.

8.4 Conclusions

The ability to better reject divalent ions over monovalent ions makes NF suitable for interesting engineering and environmental science applications, including water reclamation, water softening, and desalination. The wide range of NF applications makes it quite relevant to be able to accurately predict ion rejection. In this study, we focused on multi-component electrolyte solution with three ions: Na^+, Ca^{2+} (or Mg^{2+}), and Cl^-. Such a multi-component electrolyte solution is expected to show discrepancies between theory and experimental data and unexpected behaviors compared to single salt solutions. In this study, we used the extended Nernst-Planck equation, which is a mean-field approach, in combination with a Langmuir isotherm for the adsorption of divalent cations, to come to a substantially improved fit of theory to experimental data. This study demonstrates that mean-field theory can be easily adapted to reliably predict ion rejection in multi-component solutions. Results of our study highlight how the charge of an NF membrane can be considerably affected by the adsorption of divalent counterions, which can even lead to complete charge reversal. This work opens up the possibility for future studies to consider interactions between ions (e.g. Na^+, Ca^{2+} and Mg^{2+}) and the active layer of the membrane.

References

[1] A. Figoli and A. Criscuoli, *Sustainable membrane technology for water and wastewater treatment* (Springer) (2017).

[2] D. L. Oatley-Radcliffe, M. Walters, T. J. Ainscough, P. M. Williams, A. W. Mohammad, and N. Hilal, "Nanofiltration membranes and processes: A review of research trends over the past decade", Journal of Water Process Engineering **19**, 164–171 (2017).

[3] B. Van der Bruggen, I. De Vreese, and C. Vandecasteele, "Water reclamation in the textile industry: nanofiltration of dye baths for wool dyeing", Industrial & engineering chemistry research **40**, 3973–3978 (2001).

[4] E. Sahinkaya, N. Uzal, U. Yetis, and F. B. Dilek, "Biological treatment and nanofiltration of denim textile wastewater for reuse", Journal of hazardous materials **153**, 1142–1148 (2008).

[5] Y. K. Ong, F. Y. Li, S.-P. Sun, B.-W. Zhao, C.-Z. Liang, and T.-S. Chung, "Nanofiltration hollow fiber membranes for textile wastewater treatment: Lab-scale and pilot-scale studies", Chemical engineering science **114**, 51–57 (2014).

[6] R. Castro-Muñoz, "Pressure-driven membrane processes involved in waste management in agro-food industries: A viewpoint", AIMS Energy **6**, 1025–1031 (2018).

[7] B. Van der Bruggen and C. Vandecasteele, "Removal of pollutants from surface water and groundwater by nanofiltration: overview of possible applications in the drinking water industry", Environmental pollution **122**, 435–445 (2003).

[8] K. Košutić, L. Furač, L. Sipos, and B. Kunst, "Removal of arsenic and pesticides from drinking water by nanofiltration membranes", Separation and Purification Technology **42**, 137–144 (2005).

[9] K. Pan, Q. Song, L. Wang, and B. Cao, "A study of demineralization of whey by nanofiltration membrane", Desalination **267**, 217–221 (2011).

[10] P. Chen, X. Ma, Z. Zhong, F. Zhang, W. Xing, and Y. Fan, "Performance of ceramic nanofiltration membrane for desalination of dye solutions containing nacl and na_2so_4", Desalination **404**, 102–111 (2017).

[11] M. Park, J. Park, E. Lee, J. Khim, and J. Cho, "Application of nanofiltration pretreatment to remove divalent ions for economical seawater reverse osmosis desalination", Desalination and water treatment **57**, 20661–20670 (2016).

[12] L. Llenas, X. Martínez-Lladó, A. Yaroshchuk, M. Rovira, and J. de Pablo, "Nanofiltration as pretreatment for scale prevention in seawater reverse osmosis desalination", Desalination and water treatment **36**, 310–318 (2011).

[13] P. M. Biesheuvel and J. E. Dykstra, *Physics of Electrochemical Processes* (2020).

[14] N. Hilal, H. Al-Zoubi, A. W. Mohammad, and N. Darwish, "Nanofiltration of highly concentrated salt solutions up to seawater salinity", Desalination **184**, 315–326 (2005).

[15] E. Virga, J. de Grooth, K. Zvab, and W. M. de Vos, "Stable polyelectrolyte multilayer-based hollow fiber nanofiltration membranes for produced water treatment", ACS Applied Polymer Materials **1**, 2230–2239 (2019).

[16] A. M. Hassan *et al.*, "A new approach to membrane and thermal seawater desalination processes using nanofiltration membranes (part 1)", Desalination **118**, 35–51 (1998).

[17] A. F. Ismail, M. Padaki, N. Hilal, T. Matsuura, and W. J. Lau, "Thin film composite membranerecent development and future potential", Desalination **356**, 140–148 (2015).

[18] D. L. Oatley, L. Llenas, R. Pérez, P. M. Williams, X. Martínez-Lladó, and M. Rovira, "Review of the dielectric properties of nanofiltration membranes and verification of the single oriented layer approximation", Advances in colloid and interface science **173**, 1–11 (2012).

[19] M. Mänttäri, A. Pihlajamäki, and M. Nyström, "Effect of ph on hydrophilicity and charge and their effect on the filtration efficiency of nf membranes at different ph", Journal of Membrane Science **280**, 311–320 (2006).

[20] A. Schaefer, A. G. Fane, and T. D. Waite, *Nanofiltration: principles and applications* (Elsevier) (2005).

[21] M. R. Teixeira, M. J. Rosa, and M. Nyström, "The role of membrane charge on nanofiltration performance", Journal of Membrane Science **265**, 160–166 (2005).

[22] A. W. Mohammad, Y. H. Teow, W. L. Ang, Y. T. Chung, D. L. Oatley-Radcliffe, and N. Hilal, "Nanofiltration membranes review: Recent advances and future prospects", Desalination **356**, 226–254 (2015).

[23] L. Dresner, "Stability of the extended nernst-planck equations in the description of hyperfiltration through ion-exchange membranes", The Journal of Physical Chemistry **76**, 2256–2267 (1972).

[24] A. Yaroshchuk, M. L. Bruening, and E. Zholkovskiy, "Modelling nanofiltration of electrolyte solutions", Advances in Colloid and Interface Science **268**, 39–63 (2019).

[25] R. Wang and S. Lin, "Pore model for nanofiltration: History, theoretical framework, key predictions, limitations, and prospects", Journal of Membrane Science 118809 (2020).

[26] J. Schaep, C. Vandecasteele, A. W. Mohammad, and W. R. Bowen, "Modelling the retention of ionic components for different nanofiltration membranes", Separation and purification Technology **22**, 169–179 (2001).

[27] B. Saliha, F. Patrick, and S. Anthony, "Investigating nanofiltration of multi-ionic solutions using the steric, electric and dielectric exclusion model", Chemical Engineering Science **64**, 3789–3798 (2009).

[28] J. M. M. Peeters, J. P. Boom, M. H. V. Mulder, and H. Strathmann, "Retention measurements of nanofiltration membranes with electrolyte solutions", Journal of membrane science **145**, 199–209 (1998).

[29] T. Urase, J.-i. Oh, and K. Yamamoto, "Effect of ph on rejection of different species of arsenic by nanofiltration", Desalination **117**, 11–18 (1998).

[30] P. M. Biesheuvel, L. Zhang, P. Gasquet, B. Blankert, M. Elimelech, and W. G. J. van der Meer, "Ion selectivity in brackish water desalination by reverse osmosis: Theory, measurements, and implications", Environmental Science & Technology Letters **7**, 42–47 (2019).

[31] N. Fridman-Bishop, O. Nir, O. Lahav, and V. Freger, "Predicting the rejection of major seawater ions by spiral-wound nanofiltration membranes", Environmental science & technology **49**, 8631–8638 (2015).

[32] S. Bason and V. Freger, "Phenomenological analysis of transport of mono- and divalent ions in nanofiltration", Journal of Membrane Science **360**, 389–396 (2010).

[33] V. Freger, "Ion partitioning and permeation in charged low-t^* membranes", Advances in Colloid and Interface Science **277**, 102107 (2020).

[34] N. Fridman-Bishop, K. A. Tankus, and V. Freger, "Permeation mechanism and interplay between ions in nanofiltration", Journal of Membrane Science **548**, 449–458 (2018).

[35] S. Déon, A. Escoda, P. Fievet, P. Dutournié, and P. Bourseau, "How to use a multi-ionic transport model to fully predict rejection of mineral salts by nanofiltration membranes", Chemical Engineering Journal **189**, 24–31 (2012).

[36] J. Schaep, C. Vandecasteele, A. W. Mohammad, and W. R. Bowen, "Analysis of the salt retention of nanofiltration membranes using the donnan–steric partitioning pore model", Separation science and Technology **34**, 3009–3030 (1999).

[37] S. Déon, A. Escoda, and P. Fievet, "A transport model considering charge adsorption inside pores to describe salts rejection by nanofiltration membranes", Chemical Engineering Science **66**, 2823–2832 (2011).

[38] L. Bruni and S. Bandini, "Studies on the role of site-binding and competitive adsorption in determining the charge of nanofiltration membranes", Desalination **241**, 315–330 (2009).

[39] J. Garcia-Aleman and J. M. Dickson, "Permeation of mixed-salt solutions with commercial and pore-filled nanofiltration membranes: membrane charge inversion phenomena", Journal of Membrane Science **239**, 163–172 (2004).

[40] M. S. Hall, V. M. Starov, and D. R. Lloyd, "Reverse osmosis of multicomponent electrolyte solutions part i. theoretical development", Journal of membrane science **128**, 23–37 (1997).

[41] W. M. de Vos and S. Lindhoud, "Overcharging and charge inversion: Finding the correct explanation(s)", Advances in colloid and interface science **274**, 102040 (2019).

[42] V. Thangaraj, K. Aravamudan, R. Lingam, and S. Subramanian, "Individual and simultaneous adsorption of Ni (ii), Cd (ii), and Zn (ii) ions over polyamide resin: Equilibrium, kinetic and thermodynamic studies", Environmental Progress & Sustainable Energy **38**, S340–S351 (2019).

[43] E. M. Kimani, A. J. B. Kemperman, W. G. J. van der Meer, and P. M. Biesheuvel, "Multicomponent mass transport modeling of water desalination by reverse osmosis including ion pair formation", The Journal of Chemical Physics **154**, 124501 (2021).

[44] Y. S. Oren and P. M. Biesheuvel, "Theory of ion and water transport in reverse-osmosis membranes", Physical Review Applied **9**, 024034 (2018).

[45] L. Bruni and S. Bandini, "The role of the electrolyte on the mechanism of charge formation in polyamide nanofiltration membranes", Journal of membrane science **308**, 136–151 (2008).

[46] G. Hurwitz, G. R. Guillen, and E. M. Hoek, "Probing polyamide membrane surface charge, zeta potential, wettability, and hydrophilicity with contact angle measurements", Journal of Membrane Science **349**, 349–357 (2010).

[47] M. Vourch, B. Balannec, B. Chaufer, and G. Dorange, "Treatment of dairy industry wastewater by reverse osmosis for water reuse", Desalination **219**, 190–202 (2008).

[48] Y. A. Le Gouellec and M. Elimelech, "Calcium sulfate (gypsum) scaling in nanofiltration of agricultural drainage water", Journal of membrane science **205**, 279–291 (2002).

[49] J. A. Nelder and R. Mead, "A simplex method for function minimization", The computer journal **7**, 308–313 (1965).

[50] C. Mazzoni and S. Bandini, "On nanofiltration Desal-5 DK performances with calcium chloride–water solutions", Separation and purification technology **52**, 232–240 (2006).

[51] G. Hagmeyer and R. Gimbel, "Modelling the salt rejection of nanofiltration membranes for ternary ion mixtures and for single salts at different pH values", Desalination **117**, 247–256 (1998).

[52] K. Linde and A.-S. Jönsson, "Nanofiltration of salt solutions and landfill leachate", Desalination **103**, 223–232 (1995).

[53] J. Tanninen and M. Nyström, "Separation of ions in acidic conditions using NF", Desalination **147**, 295–299 (2002).

[54] T. Tsuru, M. Urairi, S. Nakao, and S. Kimura, "Reverse osmosis of single and mixed electrolytes with charged membranes: experiment and analysis", Journal of chemical engineering of Japan **24**, 518–524 (1991).

[55] N. Pagès, M. Reig, O. Gibert, and J. L. Cortina, "Trace ions rejection tunning in NF by selecting solution composition: Ion permeances estimation", Chemical Engineering Journal **308**, 126–134 (2017).

[56] A. E. Yaroshchuk, "Negative rejection of ions in pressure-driven membrane processes", Advances in colloid and interface science **139**, 150–173 (2008).

[57] A. Yaroshchuk, X. Martínez-Lladó, L. Llenas, M. Rovira, and J. de Pablo, "Solution-diffusion-film model for the description of pressure-driven transmembrane transfer of electrolyte mixtures: One dominant salt and trace ions", Journal of Membrane Science **368**, 192–201 (2011).

[58] N. Pages, A. Yaroshchuk, O. Gibert, and J. L. Cortina, "Rejection of trace ionic solutes in nanofiltration: Influence of aqueous phase composition", Chemical Engineering Science **104**, 1107–1115 (2013).

9

Wettability of Amphoteric Surfaces: the Effect of pH and Ionic Strength on Surface Ionization and Wetting°

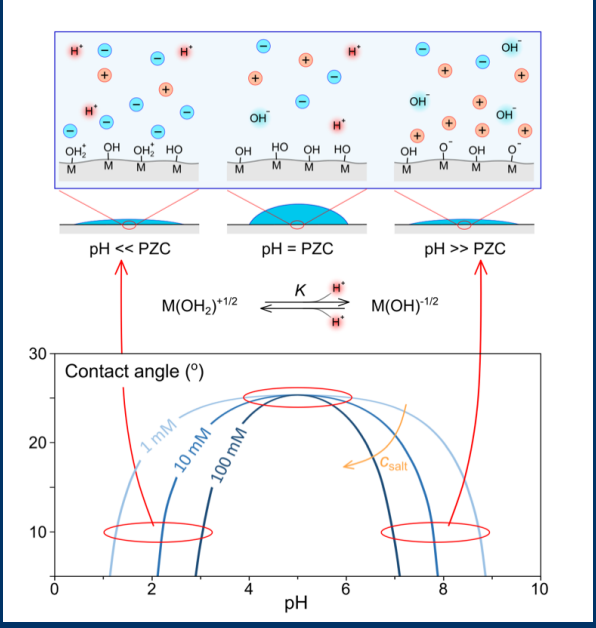

°Published as: **Ettore Virga**, Evan Spruijt, Wiebe M. de Vos, and P. M. Biesheuvel, *Wettability of amphoteric surfaces: the effect of pH and ionic strength on surface ionization and wetting*, Langmuir **2018**, *34*, 15174-15180.

Abstract

We present a novel theory to predict the contact angle of water on amphoteric surfaces, as a function of pH and ionic strength. To validate our theory, experiments were performed on two commonly used amphoteric materials, alumina (Al_2O_3) and titania (TiO_2). We find good agreement at all pH values, and at different salt concentrations. With increasing salt concentration, the theory predicts the contact angle-pH curve to get steeper, while keeping the same contact angle at pH $=$ PZC (point of zero charge), in agreement with data. Our model is based on the amphoteric 1-pK model and includes the electrostatic free energy of an aqueous system as well as the surface energy of a droplet in contact with the surface. In addition, we show how our theory suggests the possibility of a novel responsive membrane design, based on amphoteric groups. At pH $\sim$ PZC, this membrane resists flow of water but at slightly more acidic or basic conditions the wettability of the membrane pores may change sufficiently to allow passage of water and solutes. Moreover, these membranes could act as active sensors that only allow solutions of high ionic strength to flow through in waste water treatment.

9.1 Introduction

Surface wettability is of key relevance in many applications in daily life [1–3] and industry [4–6]. The wettability of a surface results from a dynamic equilibrium between interaction forces taking place at solid-gas, solid-liquid, and gas-liquid interfaces [1, 7]. By far the most common liquid involved in this balance is water. This balance can be shifted in many different ways [8]. For example, by changing pH, surfaces can be switched from hydrophilic to hydrophobic and back [9], as demonstrated by various applications [10, 11], including new smart membranes with antifouling properties [12], sponges for oil water separation [13] and advanced drug delivery systems [14]. The possibility of switching results from weakly basic or acidic groups, of which the degree of ionization depends on solution pH [15, 16]. Rios *et al.* exploit these material properties by developing membranes that are impermeable at neutral and basic conditions because of their hydrophobicity, but are opened to a flux of aqueous solutions at slightly acidic pH because of protonation of amino groups, and subsequently wetting of the membrane pores [17].

Within the class of ionizable materials, amphoteric surfaces are especially interesting. Amphoteric materials can be both positively and negatively charged, depending on pH in solution relative to their point of zero charge (PZC) (see Fig. 9.1). The effects of pH and ionic strength on the wettability of amphoteric surfaces have already been experimentally investigated for titania (TiO_2) surfaces, coated with a thin silane layer (octadecyltryhydrosilane, OTHS), in a wide range of pH values around PZC [18]. For unmodified amphoteric surfaces, the effect of pH on wettability has only been investigated qualitatively for alumina (Al_2O_3) in order to determine PZC [19]. However, the role of the electrical double layer (EDL) on the wettability of amphoteric surfaces is not yet fully understood [18]. The salt concentration influences the diffuse part of the EDL, which in turn affects the surface charge and thereby the surface wettability. A quantitative understanding of the impact of the characteristics of the EDL on the surface energy of amphoteric solids is still missing.

In addition to theoretical challenges, earlier experimental work may not have chosen the best possible method to measure contact angle. Indeed, when contact angle (CA) measurements are based on the sessile drop technique [20], the effect of a change in droplet pH during measurements may have been underestimated. Because when a droplet of water is placed on a solid surface, the ionization of the surface groups in such a small liquid volume can easily lead to a change of droplet pH. We advocate to work with the captive bubble

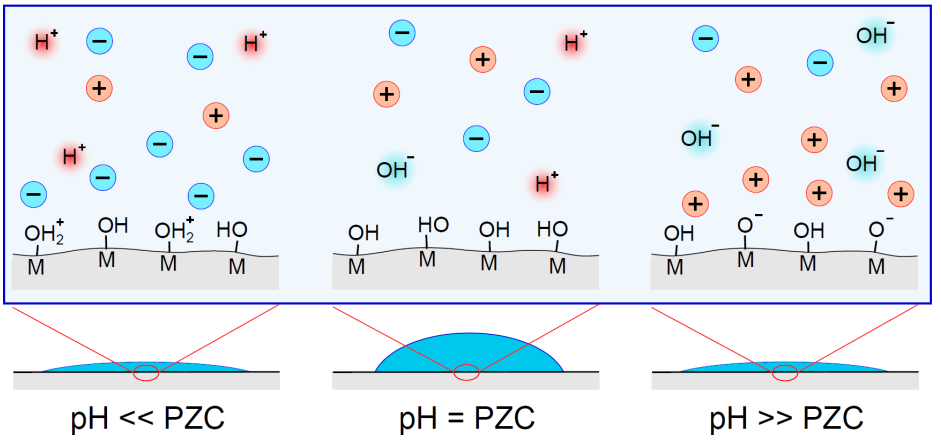

Figure 9.1: Illustration of the wettability of amphoteric materials in response to pH relative to the point of zero charge (PZC).

technique, in which small volume effects can safely be neglected, as water constitutes the continuous phase with a large volume.

In this paper, we present a novel theory to predict the contact angle of water on amphoteric surfaces, as function of pH and ionic strength. To validate our theory, we performed experiments on two commonly used amphoteric materials, alumina (Al_2O_3) and titania (TiO_2).

9.2 Theory

In this section, starting from general expressions for isolated ionizable surfaces [21], we derive an equation that relates the water contact angle to the sum of surface and diffuse electrostatic free energies. Free energies discussed in this work have an electrical origin, due to the formation of the EDL, as well as a chemical origin, due to the adsorption/desorption of protons and ions to/from the surface. A possible Stern layer [22] is neglected in this work. Our system consists of a liquid interacting with a solid ionizable surface that is not soluble in that liquid. Since the Gibbs energy and Helmholtz energy are identical for a system in which the redistribution of ions (which is required for the formation of EDLs) does not affect the volume, the general term free energy is used here. The equations below are derived for an electrolyte with monovalent ions only. The electrostatic free energy, scaled with kT, of an aqueous system containing

a ionizable surface is given by [21]

$$F_{el} = F_S + F_D \tag{9.1}$$

where F_S and F_D are the surface and the diffuse contributions to the electrostatic free energy.

The diffuse contribution for an isolated surface is given by [23]

$$F_D = -16\, n_\infty \lambda_D \sinh^2\left(\frac{1}{4} y_s\right) \tag{9.2}$$

where n_∞ is the salt concentration expressed in m^{-3} ($n_\infty = N_{av}\, c_\infty$, with c_∞ in $\mathrm{mol/m^3}$ = mM and N_{av} Avogadro's number), and the Debye length λ_D is given by

$$\lambda_D = \sqrt{\frac{\varepsilon kT}{2e^2 n_\infty}} \tag{9.3}$$

with e the elementary charge, ε the dielectric constant ($= \varepsilon_r \varepsilon_0 = 78 \cdot 8.854 \times 10^{-12}$ C/(V m) in water), k the Boltzmann constant, and T temperature.

In order to calculate F_{el}, we also need to know the surface contribution, F_S. The expression for F_S depends on the surface chemistry [21]. For an acidic or basic material, the ionization degree α is a number in between 0 and 1 and is given by [21]

$$\alpha = \frac{1}{1 + e^{z(y_N - y_s)}} \tag{9.4}$$

where z is the charge sign of the surface groups (for an acidic site, $z = -1$, and for a basic site, $z = +1$), y_s is the dimensionless electrostatic potential at the surface ($= e\psi_s/kT$, with ψ_s the electrostatic potential at the surface), and where y_N is given by [21]

$$y_N = \ln 10 \cdot (\mathrm{p}K - \mathrm{pH}). \tag{9.5}$$

For an acidic/basic material for which ionization is described by Eq.(9.4), the surface part of the free energy, F_S, is given by [21]

$$F_S = N \cdot \ln(1 - \alpha) \tag{9.6}$$

where N is the number density of ionizable groups on the surface (m^{-2}). One class of amphoteric materials consists of a mixture of acidic and basic surface groups. In that case, the above theory applies with Eqs. (9.4)-(9.6) evaluated

for each group separately (and added up). This approach can be applied to various biological materials, such as protein molecules, the surface of which consists of an assembly of basic and acidic groups [24].

In the present work, we focus on a second class of amphoteric materials, that includes as examples titania and alumina. For these materials, it is known that they have a fractional charge which goes from a number below zero, to above. For alumina, applying the 1-pK model, the surface consists of $OH^{-1/2}$ groups that can be protonated to $OH_2^{+1/2}$ groups [25, 26]. In this case the pK of this material is the pH at which the surface is globally uncharged. The effective surface charge, α ($-\frac{1}{2} < \alpha < +\frac{1}{2}$), is obtained from

$$\alpha = \frac{1}{2} - \frac{1}{1 + e^{y_N - y_s}} \tag{9.7}$$

and, as shown in ref. 10, the surface contribution to the free energy in this case is

$$F_S = {}^1\!/_2 N \ln\left((1+2\alpha)\,(1-2\alpha)\right). \tag{9.8}$$

Combining Eq. (9.2) and Eq. (9.8), we can now rewrite Eq. (9.1) for this amphoteric material to

$$F_{el} = {}^1\!/_2 N \ln\left((1+2\alpha)\,(1-2\alpha)\right) - 16 n_\infty \lambda_D \sinh^2\left(\frac{1}{4} y_s\right). \tag{9.9}$$

According to Hiemstra *et al.* [26], titania is different from alumina, because titania has two ionizable groups, one that goes from $-2/3$ to $+1/3$ in charge, the other from $-1/3$ to $+2/3$. However, because the pK value of both groups can be assumed to be the same, and the number of groups can also be assumed to be the same [26], after adding up these groups we obtain the same equations for α and F_S as for alumina (i.e., Eqs. (9.7)-(9.8)). Eq. (9.8) was derived in ref. 10 but not tested experimentally before, and this test is one of the objectives of the present work.

In order to calculate F_{el}, the value of surface potential y_s is needed. To that end, we solve the 1D Poisson Boltzmann equation for a planar surface,

$$\frac{\partial^2 y}{\partial x^2} = \frac{\sinh y}{\lambda_D^2}, \tag{9.10}$$

with the boundary condition

$$\left.\frac{\partial y}{\partial x}\right|_s = -\frac{e^2 \sigma}{\varepsilon k T} \tag{9.11}$$

where the number density of charged groups σ in m^{-2} is given by $\sigma{=}\alpha N$. For isolated surfaces the solution of Eq. (9.10) is well known to be [27]

$$\sigma = n_{\infty}\lambda_D\sqrt{8\,(\cosh y_s - 1)}. \tag{9.12}$$

By solving Eq. (9.12) with an expression for α, such as Eq. (9.7), both y_s and α are obtained.

F_{el} can be seen as an electrostatic contribution to the free energy per unit of surface area, or the solid-liquid surface energy, which has units mN/m when multiplied by kT. From this point onward, we refer to it as the electrostatic contribution to the surface energy, γ_{el}.

For smooth surfaces, the different surface energies are related to the static contact angle by Youngs equation,

$$\gamma_{lg}\cdot\cos\theta = \gamma_{sg} - \gamma_{sl} \tag{9.13}$$

where γ_{sl}, γ_{sg} and γ_{lg} refer to the surface energy of the solid-liquid, solid-gas and liquid gas interface, respectively. In particular, we can think of γ_{sl} as sum of an electrostatic term, γ_{el}, and a non-electrostatic term, γ_{sl}^{pzc} (value of γ_{sl} when the material is uncharged, i.e., when pH=PZC),

$$\gamma_{sl} = \gamma_{sl}^{pzc} + \gamma_{el}. \tag{9.14}$$

Thus, Eq. (9.13) can be rewritten to

$$\gamma_{lg}\cdot\cos\theta = \Delta\gamma - \gamma_{el} \tag{9.15}$$

where $\Delta\gamma = \gamma_{sg} - \gamma_{sl}^{pzc}$. The value of γ_{lg}, the surface energy of the water-air (liquid-gas) interface, has been fixed in our study to a value of to $\gamma_{lg} = 73$ mN/m [28]. The term $\Delta\gamma$ is independent of pH and salt concentration and can be obtained by experimental data fitting. This means that, if the contact angle at the point of zero charge is known, the model allows us to predict values of contact angle for every other value of pH and ionic strength. This is correct only if these parameters (pH and ionic strength) have a reversible effect on the surface chemistry, hence on the dissociation of surface groups.

9.3 Materials and methods

Chemicals For preparation of the solutions at different ionic strength, we used Milli-Q water and NaCl. We added small quantities of 1 M NaOH or HCl

(37 %) in order to obtain the desired solution pH. We tested two materials, alumina and titania, supplied respectively as sapphire and rutile. Sapphire (1ALO 402E, Al_2O_3 substrate (0001)) and rutile (1TIO 109E, TiO_2 substrate (100)) were supplied by Crystal GmbH (Berlin, Germany). These substrates are polished (on one side, R_a <0.5 nm) and have dimensions $10\times10\times0.5$ mm^3. To improve the measurement of the contact angle, a customized sample holder was designed and constructed (PLA, 3D printing, Ultimaker^{2+}, Geldermalsen, The Netherlands) (see Fig. 9.2), as discussed next.

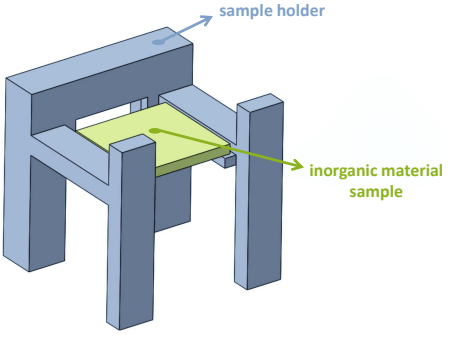

Figure 9.2: Illustration of 3D printed sample holder (blue) containing a sample of inorganic material ($10 \times 10 \times 0.5$ mm^3) (green).

Contact Angle Measurements In order to obtain a higher control on the water solution properties, the static contact angle was measured using the captive bubble approach. The advantage of this technique compared to the more common sessile drop method, is that the volume of the surrounding aqueous solution is much larger than that of a single droplet, and thus pH and salt concentration will be much more stable. Another important advantage of the captive bubble method, relatively to the method where a droplet is placed on top of the material (sessile drop), is that in the captive bubble approach, the gas phase humidity is well-controlled.

The sample surface was first flushed with ethanol (70%) and then with Milli-Q water before every measurement. Then, the sample was placed into the 3D printed sample holder with its polished side facing downwards, and submerged in an aqueous solution of predetermined ionic strength and pH. Before measuring the contact angle, the sample was left in contact with the solution for at least 5 minutes, and only then we injected a gas bubble from

below, displacing water from part of the surface.

The measurements were performed with an instrument for contact angle and contour analysis (OCA 35, Dataphysics, Filderstadt, Germany) used to measure the static contact angle. A clean stainless steel needle was used to produce a bubble of $\sim$ 3 mm in diameter on the surface, and the bubble contour, measured through the aqueous phase, was recorded. At least five measurements were taken for every condition. Image analysis of the shapes of the air bubbles were performed with the software provided with the instrument by using the method of Young-Laplace fitting.

9.4 Results and discussion

In this section we compare our model predictions to experimental data from literature, and compare to data obtained in our own experiments. Subsequently, we will discuss more detailed predictions on how amphoteric surfaces can inspire the design of a responsive membrane that acts as a sensor for the quality of the water in waste water treatment plants, allowing, streams at high ionic strength to flow through and go directly to appropriate disposal units. In this design the membrane would thus act as both a sensor and a valve, with the ability to react to a change in water chemistry automatically and in an autonomic fashion.

Our model prediction are compared with experimental data found in literature [18] for a silanized titania surface (54% OTHS), and are shown in Fig. 9.3.

According to our model fit, the contact angle (CA) has a maximum for pH= 4.4 (PZC of titania [18]), while CA decreases when pH moves away from PZC. Indeed, when we move pH away from PZC, the surface becomes more charged due to the ionization of surface groups, thus it becomes more hydrophilic. We also observe that when the salt concentration is increased, from 1 mM (Fig. 9.3A) to 100 mM (Fig. 9.3B), the steepness of the curve of contact angle versus pH increases considerably. This can be explained by the influence of salt concentration on the Debye length λ_D, thus on the EDL thickness. An increase in ionic strength leads to a reduction in EDL thickness, which translates into a concentration of H^+ or OH^- at the surface that is much closer to the one in the bulk. Thus, for an amphoteric material, if we increase the ionic strength, keeping the pH constant, the ionization of the surface groups will increase.

It is possible to note a plateau at high pH in the experimental results col-

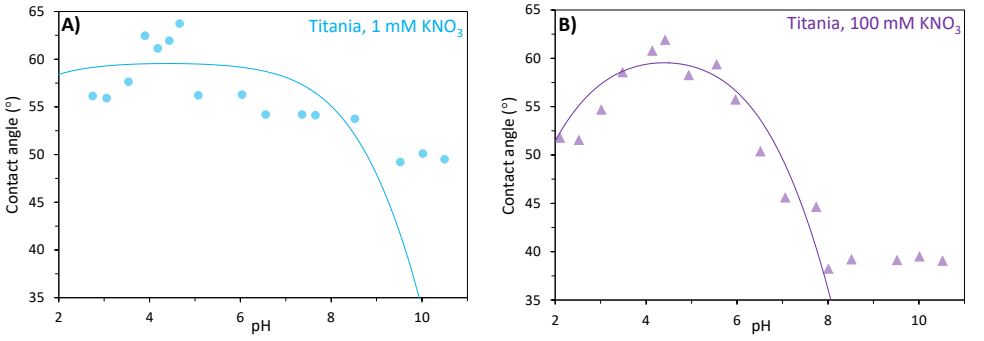

Figure 9.3: Contact angle of water on a partially silanized titania wafer in c_∞=1 mM (A) and 100 mM (B) KNO_3 as a function of pH. Experiments [18] (symbols) and theory (lines) based on Eqs. (9.5), (9.7), (9.9), (9.12) and (9.15). Input model parameters: N=3.0 nm^{-2} [18], pK=4.4 [18], $\Delta\gamma$= 37 mN/m.

lected by Hanly *et al.* (CA$\sim 50°$ in Fig. 9.3A and CA$\sim 40°$ in Fig. 9.3B). This behavior differs from our predictions at high pH. It can possibly be explained by looking at the composition of the surfaces studied by Hanly *et al.*, namely titania partially covered with OTHS (54%). The hydrophobic interactions, due to the silane coverage of titania, are not taken into account in our model and these may be responsible for the observed plateau at high pH.

To validate our model against data for amphoteric surfaces without hydrophobic modifications, we collected experimental data for the CA of two surfaces, titania and alumina, at different values of pH and ionic strength. Model predictions and experimental data are shown in fig. 9.4 for a concentration of NaCl equal to c_∞=1 mM. As can be observed in Fig. 9.4A, also in this case, the contact angle has a maximum for titania at pH$\cong$ 4.4, while for alumina, Fig. 9.4B, the maximum is at pH$\cong$ 8.7 (PZC of alumina [19]), and in both cases the contact angle decreases when the pH moves away from PZC.

In fig. 9.4B, we also show data collected by Cuddy *et al.* [19] (triangles) for alumina. Cuddy *et al.* used the sessile drop technique and worked initially with deionized water. Thus, as discussed previously, the exact salt concentration of their aqueous phase (after contacting the surface) is unknown. Their data overlap with our data (see Fig. 9.4B) and therefore, our model calculations, based on $c_\infty = 1$ mM, fit their data well.

In our model, for an amphoteric material, the contact angle has a maximum for a value of pH equal to pK, which is the point where the surface is on average uncharged (for these materials), i.e. the PZC. When we move pH

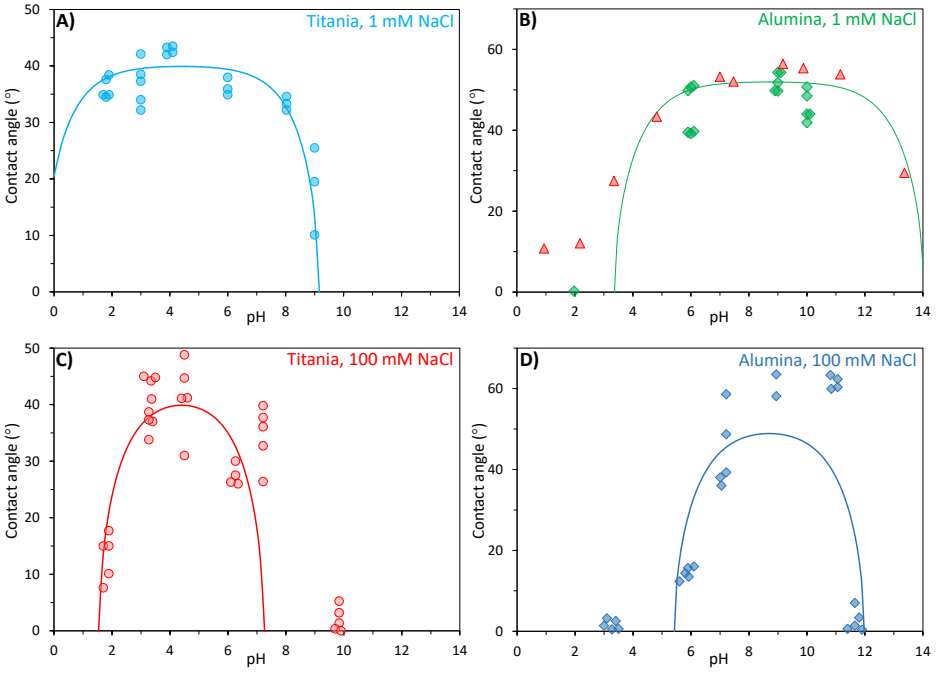

Figure 9.4: Contact angle of water on titania, in c_∞=1 mM (A) and 100 mM (B), and alumina, in c_∞=1 mM (C) and 100 mM (D), substrates as a function of pH. Experiments (circles and diamonds [this work], and triangles [Cuddy *et al.*]) and theory (lines). Input model parameters for titania: N=8.0 nm^{-2} [18], pK=4.4 [18], $\Delta\gamma$= 56 mN/m. Input model parameters for alumina: N=7.25 nm^{-2} [29], pK=8.7 [19], $\Delta\gamma$= 45 mN/m.

away from PZC, the surface becomes more charged due to the ionization of surface groups, thus it becomes more hydrophilic and CA decreases. Next, in Fig. 9.5A, we show how water contact angle changes if both pH and ionic strength are varied. When salt concentration is increased, the contact angle at the PZC is expected to be unchanged, in line with literature data reported for titania (see Fig. 9.3). Shifting pH away from PZC, our model predicts that the influence of ionic strength on contact angle becomes increasingly prominent. One may, indeed, observe an increased curves steepness when ionic strength is increased. Indeed, an increase in ionic strength leads to a reduction in EDL thickness, that translates into a concentration of H^+ or OH^- at the surface closer to the one in the bulk. Thus, if we increase ionic strength, keeping pH constant, the ionization of the surface groups will increase.

These trends of the dependence of CA on salt concentration are confirmed by Hanly *et al.* [18] and by our own experiments at 100 mM salinity (see Fig. 9.4C and Fig. 9.4D). The experimental data show an increase in steepness of the curve for CA, if compared to low salt concentration, such as 1 mM (see Fig. 9.4). This is in line with the theory, where we can observe a decrease of the pH region delimited by our theoretical lines.

As already mentioned above, our theory shows that, if we keep pH constant, away from PZC, an increase in ionic strength leads to an increase in surface hydrophilicity (see Fig. 9.5A). Based on that prediction, we can now think of the possibility of a membrane, where the ionic strength determines the permeability. These membranes will be analogous to the ones already developed by Rios *et al.* [17], but also more versatile. Their modified membranes are dry at neutral and basic conditions because of their hydrophobicity but open to flux of aqueous solutions at slightly acidic pH because of the protonation of amino groups. The same response is expected by switching the ionic strength at constant pH (away from the PZC). Thus, the corresponding membranes will perform as ionic strength-dependent switchable valves. If an intrinsically hydrophobic membrane with amphoteric groups is employed, it will resist flow of water through the pores of the membrane at pH $\sim$ PZC, but at slightly more acidic or basic conditions, the wettability of the membrane pores may change sufficiently to allow passage of water and ions. As explained in ref. [30], the boundary between an open and closed configuration is at value of CA=90° for ideal surfaces. Indeed, by varying the contact angle (when CA $>$ 90°) we are able to show in theory that the critical pressure needed to push the water through a membrane can be varied. But, when CA $<$ 90° we ideally do not need any difference in pressure between the two sides of the membrane in order

to make water pass through it [30]. Thus, operating below the critical pressure, it is possible to open and close ideal membrane pores by shifting the surface from hydrophobic to hydrophilic. These membranes will be able to work in a much larger range of pH (Fig. 9.5A), then the membranes described by Rios *et al*. Our model predicts that these membranes could possibly act as active sensors that only allow solutions of high ionic strength to flow through. This would be especially useful for waste water treatment, when the ionic strength and/or pH of the water vary strongly in time. Streams with a more extreme pH or a high salt concentration would permeate through the membrane and be treated, while low salinity streams with moderate pH could simply be disposed. If we look at Fig. 9.5B, we can see the effect of salt concentration when pH is kept constant. For pH values too close to the PZC, such as pH=6 and pH=7, this shift from hydrophobic to hydrophilic is not possible. But when pH is sufficiently far away from PZC, by changing the ionic strength it becomes possible to switch the membrane surface from hydrophobic to hydrophilic. This effect increases when pH is increasingly different from the PZC of the membrane, that we fixed to PZC=pK=6.5 in this calculation. The high contrast between the open and closed states, as well as high fluxes in the open state because of a large pore size [17] can be useful in different applications for ionic strength/pH switchable membranes.

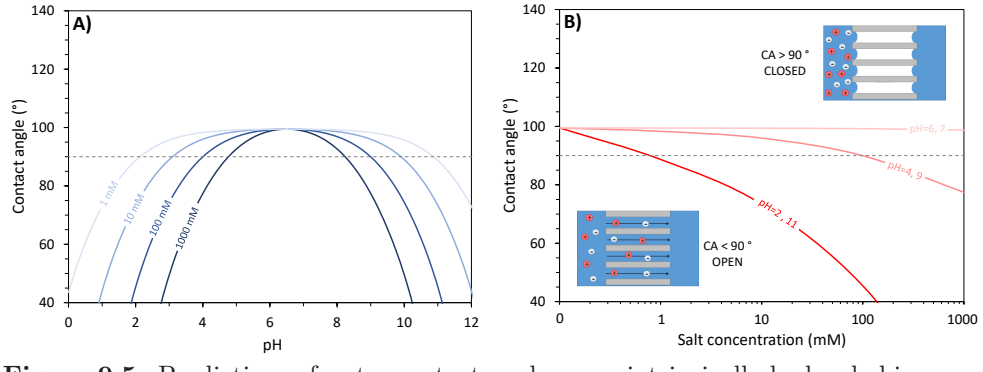

Figure 9.5: Predictions of water contact angle on an intrinsically hydrophobic membrane with amphoteric groups as a function of pH and ionic strength. Input model parameters: N=8.0 nm^{-2}, pK=6.5, $\Delta\gamma$= −12 mN/m.

9.5 Conclusions

This study focused on the effects of pH and ionic strength on the wettability of amphoteric metal oxide surfaces. We studied the contact angle of water on two oxidic (inorganic) materials: alumina (Al_2O_3) and titania (TiO_2). We present a novel theory that is able to predict the contact angle for these materials as function of both ionic strength and pH. This theory is based on the amphoteric 1-pK model. Experimentally, we work with the captive bubble technique which gives a better control over solution and air properties. Data were very well described by the new theory for the lowest salt concentration tested (1 mM NaCl) and their trend confirmed also at high salt concentration (100 mM). For higher salt concentration, the theory predicts the contact angle-pH curve to get steeper, while keeping the same contact angle at pH = PZC. Both literature data and our own experiments do show this effect, thus in line with our theory. Indeed, our theory shows that, if we keep pH constant, away from PZC, an increase in ionic strength leads to an increase in hydrophilicity. Thus, if an intrinsically hydrophobic membrane with amphoteric groups is employed, it will resist the flow of water through the membrane at pH $\sim$ PZC but at slightly more acidic or basic conditions the wettability of the membrane pores may change sufficiently to allow passage water and ions. These membranes could also act as valves that only allow solutions of high ionic strength to flow through. The high contrast between the open and closed states can be particularly useful for water treatment.

References

[1] A. Kondyurin and M. Bilek, *5 - Wetting*, 129 – 143, second edition edition (Elsevier) (2015).

[2] L. Feng, S. Li, Y. Li, H. Li, L. Zhang, J. Zhai, Y. Song, B. Liu, L. Jiang, and D. Zhu, "Super-hydrophobic surfaces: From natural to artificial", Advanced Materials **14**, 1857–1860 (2002).

[3] W. Barthlott, M. Mail, and C. Neinhuis, "Superhydrophobic hierarchically structured surfaces in biology: evolution, structural principles and biomimetic applications", Phil. Trans. R. Soc. A **374**, 20160191 (2016).

[4] R. A. Salathiel, "Oil recovery by surface film drainage in mixed-wettability rocks", JPT **255**, 1216–1224 (1973).

[5] T. Tanaka, J. Lee, and P. R. Scheller, *Chapter 1.5 - Interfacial Free Energy and Wettability*, 61 – 77 (Elsevier) (2014).

[6] Y.-N. Zhou, J.-J. Li, and Z.-H. Luo, "Toward efficient water/oil separation material: Effect of copolymer composition on ph-responsive wettability and separation performance", AIChE Journal **62**, 1758–1771 (2016).

[7] S.-J. Park and M.-K. Seo, *Chapter 3 - Solid-Liquid Interface*, volume 18 of *Interface Science and Technology*, 147–252 (Elsevier) (2011).

[8] N. Verplanck, Y. Coffinier, V. Thomy, and R. Boukherroub, "Wettability switching techniques on superhydrophobic surfaces", Nanoscale Research Letters **2**, 577–596 (2007).

[9] F. Xia, Y. Zhu, L. Feng, and L. Jiang, "Smart responsive surfaces switching reversibly between super-hydrophobicity and super-hydrophilicity", Soft Matter **5**, 275–281 (2009).

[10] S. P. Nunes, A. R. Behzad, B. Hooghan, R. Sougrat, M. Karunakaran, N. Pradeep, U. Vainio, and K.-V. Peinemann, "Switchable ph-responsive polymeric membranes prepared via block copolymer micelle assembly", ACS Nano **5**, 3516–3522 (2011).

[11] X. Chen, J. Gao, B. Song, S. Mario, and X. Zhang, "Stimuli-responsive wettability of nonplanar substrates: ph-controlled floatation and supporting force", Langmuir **26**, 104–108 (2009).

[12] Y. Cai, D. Chen, N. Li, Q. Xu, H. Li, J. He, and J. Lu, "A smart membrane with antifouling capability and switchable oil wettability for high-efficiency oil/water emulsions separation", Journal of Membrane Science **555**, 69 – 77 (2018).

[13] J. Guo, J. Wang, Y. Gao, J. Wang, W. Chang, S. Liao, Z. Qian, and Y. Liu, "ph-responsive sponges fabricated by ags ligands possess smart double-transformed superhydrophilicsuperhydrophobicsuperhydrophilic wettability for oilwater separation", ACS Sustainable Chemistry & Engineering **5**, 10772–10782 (2017).

[14] Y. Salinas, A. M. Castilla, and M. Resmini, "An l-proline based thermoresponsive and ph-switchable nanogel as a drug delivery vehicle", Polym. Chem. **9**, 2271–2280 (2018).

[15] M. R. Aguilar and J. S. Román, "3 - ph-responsive polymers: properties, synthesis and applications", Woodhead Publishing **1**, 45–92 (2014).

[16] G. Kocak, C. Tuncer, and V. Butun, "ph-responsive polymers", Polym. Chem. **8**, 144–176 (2017).

[17] F. Rios and S. N. Smirnov, "ph valve based on hydrophobicity switching", Chemistry of Materials **23**, 3601–3605 (2011).

[18] G. Hanly, D. Fornasiero, J. Ralston, and R. Sedev, "Electrostatics and Metal Oxide Wettability", The Journal of Physical Chemistry C **115**, 14914–14921 (2011).

[19] M. F. Cuddy, A. R. Poda, and L. N. Brantley, "Determination of isoelectric points and the role of ph for common quartz crystal microbalance sensors", ACS Applied Materials & Interfaces **5**, 3514–3518 (2013).

[20] N. Shahidzadeh, M. F. L. Schut, J. Desarnaud, M. Prat, and D. Bonn, "Salt stains from evaporating droplets", Scientific Reports **5**, 10335 (2015).

[21] P. M. Biesheuvel, "Electrostatic free energy of interacting ionizable double layers", Journal of Colloid and Interface Science **2**, 514–522 (2004).

[22] A. Travesset and S. Vangaveti, "Electrostatic correlations at the stern layer: physics or chemistry?", J. Phys. Chem. **131**, 185102 (2009).

[23] D. Y. C. Chan and D. Mitchell, "The free energy of an electrical double layer", Journal of Colloid and Interface Science **95**, 193–197 (1983).

[24] W. M. de Vos, P. M. Biesheuvel, A. de Keizer, J. M. Kleijn, and M. A. Cohen Stuart, "Adsorption of the protein bovine serum albumin in a planar poly(acrylic acid) brush layer as measured by optical reflectometry", Langmuir **24**, 6575–6584 (2008).

[25] T. A. J. Koopal, "Ionized monolayers", Philips Res. Rep. **10**, 425–481 (1955).

[26] T. Hiemstra, J. De Wit, and W. Van Riemsdijk, "Multisite proton adsorption modeling at the solid/solution interface of (hydr)oxides: A new approach: Ii. application to various important (hydr)oxides", Journal of Colloid and Interface Science **133**, 105 – 117 (1989).

[27] E. Virga, W. M. De Vos, and P. M. Biesheuvel, "Theory of gel expansion to generate electrical energy", EPL **120**, 46002–p1–p6 (2018).

[28] I. M. Hauner, A. Deblais, J. K. Beattie, H. Kellay, and D. Bonn, "The dynamic surface tension of water", The Journal of Physical Chemistry Letters **8**, 1599–1603 (2017).

[29] P. M. Biesheuvel and F. F. Lange, "Application of the charge regulation model to the colloidal processing of ceramics", Langmuir **17**, 3557–3562 (2001).

[30] B.-S. Kim and P. Harriott, "Critical entry pressure for liquids in hydrophobic membranes", Journal of Colloid and Interface Science **115**, 1–8 (1987).

10

Theory of Gel Expansion to Generate Electrical Energy°

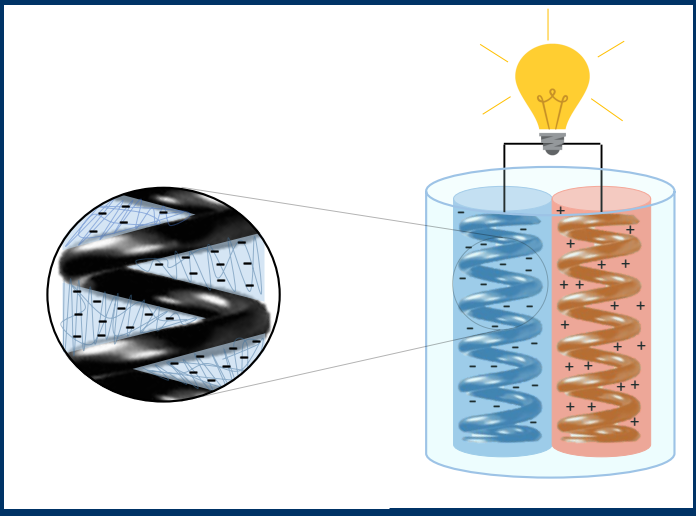

°Published as: **Ettore Virga**, Wiebe M. de Vos, and P. M. Biesheuvel, *Theory of gel expansion to generate electrical energy*, EPL **2017**, *120*, 46002.

Abstract

Mechanical energy harvesters based on coiled carbon nanotube yarns are promising materials for sustainable energy generation. In this work, we present a novel mechanism to harvest energy from mechanical fluctuations by using coiled carbon nanotube yarns coated with polyelectrolyte gel. We developed a theory to explain how this new kind of energy harvesting is possible. The gel fills up all space between the coils and expands when the yarn is stretched. This translates into a change in electrical double layer configuration, hence into a change in electrical potential. This makes it possible to electrochemically convert tensile or torsional mechanical energy into electrical energy. The influence of the yarn surface charge, polyelectrolyte charge density and salt concentration is analyzed, giving directions for optimum process design. We show calculation results for the generated power of a system consisting of two yarns coated with positive and negative polyelectrolyte gel.

10.1 Introduction

Present day research to harvest energy by exploiting small amplitude oscillations shows great potential for sustainable generation and recovery of energy [1–3]. Mechanical vibration sources are ubiquitous since every step and action of a living being results in a release of kinetic energy that is partially dissipated. Converting this vibrational energy into electric energy may provide an alternative to batteries or chargers in portable electronic devices [1, 4, 5]. This conversion can be used for self-powered wireless sensors, structural and human health monitoring systems, extraction of energy from ocean waves [3] and from wind [6]. Different systems based on induction or piezo-electricity have been proposed in the past years in order to recover this mechanical energy but the generated power is still too low [7]. Furthermore, interesting nanogenerators were also introduced to harvest human energy from walking, breathing, typing and more, utilizing piezo-electricity and triboelectricity [8, 9]. Recently, a promising alternative, based on carbon nanotube (CNT) yarns, was developed to convert mechanical energy into electrical energy from both torsional and tensile motion [3]. Kim *et al.* [3] in their mechanical energy harvester employed CNT yarns that are so highly twisted that they completely coil. The yarns they tested are dipped in a liquid electrolyte bath or coated with a gel made of 10 wt% polyvinyl alcohol in 0.1 M HCl.

In our work, we propose an alternative version where the coiled CNT yarn is coated with charged polyelectrolyte (PE) gel. The gel fills up all space between the coils and at the gel-yarn surface it expands when the yarn is stretched, translating into a change in electrical double layer (EDL) configuration. This change brings about a change in electrical potential. Hence, the external mechanical energy input is exploited to create a change in EDL configuration that translates into a different electric potential profile. It has been demonstrated that polymer brushes can reversibly bend cantilevers due to conformational changes of the brush in response to changes in environmental conditions [10, 11], while polyelectrolyte gels were recently used to convert chemical into electrical energy [12], and into mechanical energy [13]. Inspired by these promising recent studies, we theoretically investigated the possibility to use polymer gels to convert external mechanical oscillations into electrical energy. For a more complete and clear picture of our system, it is useful first to describe the model of the PE gel, coated on the coiled twisted yarn (Fig. F.1). We can think of the PE gel as a charged polymer network with positive or negative charges fixed on its chains, and free counterions (and co-ions) localized in the network. PE gels are able to absorb a significant amount (up to

$\sim$ 2000 times the polymer weight) of water within its network structure [14], but do not dissolve in water [15]. A PE gel is characterized by a molar concentration of fixed charges, that we define as X. The yarn surface charge as well as the gel fixed charge density are responsible for the salt ions distribution in the EDL, hence for the profile in the dimensionless potential, that we call y, see Fig. F.1. As depicted in Fig. F.1, it is possible that the potential, y (relative to bulk solution) can flip sign. For a positively charged gel, we can then have an excess of cations at the yarn surface, even though in the gel bulk phase we mainly have free anions. One may think that, because the gel volume will remain constant during stretching, the fixed charge concentration X will not change. This is indeed correct in the bulk of the gel (away from any surface). However, it is likely that directly at any (yarn) surface, stretching a gel can lead to a lowering of X, because the polymer chains are at some points connected to the yarn, and because the gel has to follow the contours of the yarn. Thus, even though a gel bulk may not be diluted upon stretching, near the surface, the polymer fixed charge X can be expected to go down.

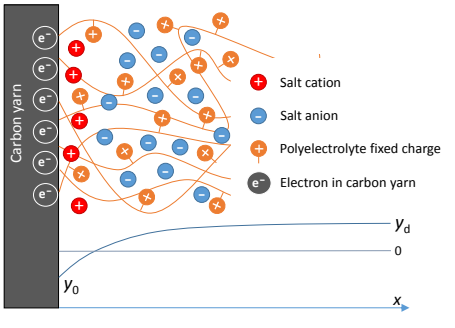

Figure 10.1: The carbon yarn is coated with a positively charged polyelectrolyte gel which holds free ions. The carbon yarn surface and the gel fixed charge density are responsible for the free ions distribution in the EDL, hence for the profile of the dimensionless potential, y, from the gel-yarn interface into the gel bulk. In this case it is possible that the while the gel bulk mainly holds anions, right near the surface there is an excess of cations.

10.2 Theory

In this section, we explain EDL theory of a charged surface coated with a polyelectrolyte gel. In a later section the model of energy harvesting from a system containing two electrodes made of carbon nanotube yarns in a coiled

configuration is presented. We start the derivation describing the equilibrium EDL profile for potential and ion concentration near a charged surface covered with a polyelectrolyte charged gel. Since the EDL around the yarn is thin, we can use the one-dimensional planar form of the Poisson equation

$$\frac{\partial^2 \Psi}{\partial x^2} = -\frac{\rho_e}{\varepsilon} \tag{10.1}$$

where Ψ is the electric potential, x is the direction perpendicular to the gel-yarn interface, ε is the absolute permittivity, and ρ_e is the local electric charge density. We define the dimensionless potential, y, as

$$y = \frac{F\Psi}{RT} \tag{10.2}$$

where F is Faraday's constant, R is the gas constant and T is the temperature. At chemical equilibrium, for the EDL in a charged gel, the local electric charge density is given by

$$\rho_e = F\left(c_\infty\left(e^{-y} - e^{y}\right) + \omega X\right) \tag{10.3}$$

where ω is the sign of the fixed membrane charge ($\omega = +1$ for positive charges and $\omega = -1$ for negative ones). Eq. (10.2) was obtained for a monovalent salt, with bulk concentration (outside the gel) c_∞, in mol/m^3.

Combining Eqs. (10.1)-(10.3), we obtain the modified Poisson-Boltzmann equation,

$$\frac{\partial^2 y}{\partial x^2} = -\frac{F^2}{\varepsilon RT}\left(2c_\infty \sinh\left(y\right) + \omega X\right). \tag{10.4}$$

Multiplying each side of Eq. (10.4) by $\frac{\partial y}{\partial x}$, we obtain

$$\frac{1}{2}\frac{d\left(\frac{\partial y}{\partial x}\right)^2}{dx} = \frac{F^2}{\varepsilon RT}\left(2c_\infty\left(\frac{\partial \cosh\left(y\right)}{\partial x}\right) - \omega X\frac{\partial y}{\partial x}\right) \tag{10.5}$$

which, with boundary conditions $\frac{\partial y}{\partial x} = 0 \wedge y = y_D$ for $x \to +\infty$, $y = y_0$ for $x = 0$, can be integrated to the modified Gouy-Chapman equation

$$\frac{1}{2}\frac{\varepsilon RT}{F^2}\left(\left.\frac{\partial y}{\partial x}\right|_s\right)^2 = 2c_\infty\left(\cosh\left(y_0\right) - \cosh\left(y_D\right)\right) - \omega X\left(y_0 - y_D\right) \tag{10.6}$$

where $y_D = \sinh\left(\omega X/2c_\infty\right)$ is the Donnan potential, which is the potential in the gel far from the EDL at the yarn surface relative to that in free electrolyte outside the gel [16, 17]. Eq. (10.6) is also given in ref. [18] but the boundary

condition far away from the surface is given as $y_D = 0$. Eq. (10.6) is similar to Eq. (13) in ref. [19], which assumes the presence of only counterions, an equation which was earlier presented in ref. [20]. Note that this equation for the counterions-only case cannot predict the change in sign in potential as depicted in Fig. F.1, but our Eq. (6) can. We also define y_0 as the dimensionless potential at the start of the diffuse layer. For $X = 0$, Eq. (10.6) simplifies to the classical Gouy-Chapman equation for a charged surface in contact with an electrolyte.

Making use of Gauss' law

$$\Sigma = -\frac{\varepsilon RT}{F} \left.\frac{\partial y}{\partial x}\right|_s \tag{10.7}$$

where Σ is the yarn surface charge in $\mathrm{C/m^2}$, it is possible to obtain

$$\frac{\Sigma^2}{2\varepsilon RT} = 2c_\infty \left(\cosh\left(y_0\right) - \cosh\left(y_D\right)\right) - \omega X \left(y_0 - y_D\right) \tag{10.8}$$

which we rewrite to

$$B^2 = \cosh\left(y_0\right) - \cosh\left(y_D\right) - A\left(y_0 - y_D\right) \tag{10.9}$$

where $A = \omega X / 2c_\infty$, $B = \Sigma / \sqrt{4c_\infty \varepsilon RT}$ and $y_D = \sinh^{-1}\left(A\right)$. We can think of A as a dimensionless gel fixed charge density and B as a dimensionless yarn surface charge. These parameters will be shown to have a significant influence on system performance. Furthermore, by looking at Fig. E.2 it is possible to understand what are the effects of the two parameters A and B on the dimensionless potential at the yarn surface. Increasing the yarn surface charge, represented by B, leads to an increase in surface potential. For $A = 0$, hence for a gel with no fixed charges, the surface potential equals the potential in the salt solution bulk (hence it is zero) when $B = 0$. Increasing the value of A, the value of B at which the surface potential is zero, shifts towards negative values. Starting from that point, the potential at the surface is positive for higher values of B and negative for lower values of B. Hence, A and B signs and values are of fundamental importance to describe the structure of the EDL near a PE-coated yarn.

It is also interesting for our purpose to define a novel parameter γ, which is a measure of the change of electrical energy upon expanding the gel, while the surface charge B is constant, given by

$$\gamma = -BA\frac{\partial y_0}{\partial A}. \tag{10.10}$$

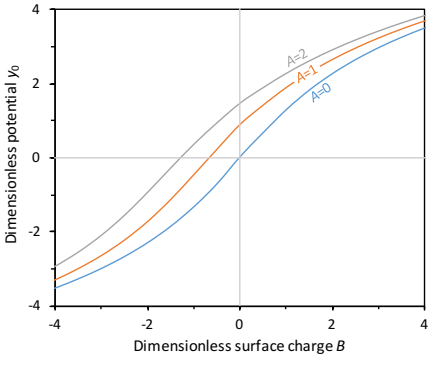

Figure 10.2: Dimensionless potential at the yarn surface, y_0, as a function of the dimensionless yarn surface charge, B, for different values of the dimensionless gel fixed charge density, A.

The parameter γ allows us to identify, for a given value of A, the optimal value of B. Taking the derivative of Eq. (10.9) with respect to the variable A,

$$0 = \sinh(y_0)\frac{\partial y_0}{\partial A} - \frac{A}{\sqrt{A^2+1}} - A\frac{\partial y_0}{\partial A} + A\frac{1}{\sqrt{A^2+1}} - (y_0 - y_D)\,, \qquad (10.11)$$

our γ can be easily obtained as

$$\gamma = -\frac{BA\,(y_0 - y_D)}{\sinh(y_0) - A}. \qquad (10.12)$$

To better understand the influence of A and B on γ, it useful to consider the iso-lines for γ (Fig. E.3). These iso-lines were obtained by numerically solving Eq. (10.9) for a chosen range of A and B, and then using the output values, y_0 and y_D, to calculate γ using Eq. (10.12).

Fig. E.3 is used in the next section, in order to identify the optimal values of fixed gel charge density, salt concentration and yarn surface charge. Given that A can not be increased indefinitely (in our case study we use a value of $A = 50$ which we think could not easily be made higher in practice), it is possible to observe that the highest value of γ can be achieved for a certain optimal value of B. Notice that γ is dimensionless, and must be multiplied by $RT/F \cdot \sqrt{4c_\infty \varepsilon RT}$ to obtain an energy sensitivity with unit J/m^2.

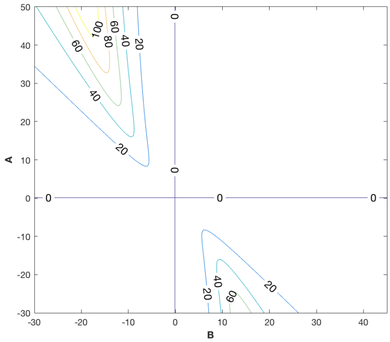

Figure 10.3: Iso-lines of the dimensionless sensitivity, γ, as function of the dimensionless gel fixed charge density, A, and the dimensionless yarn surface charge, B.

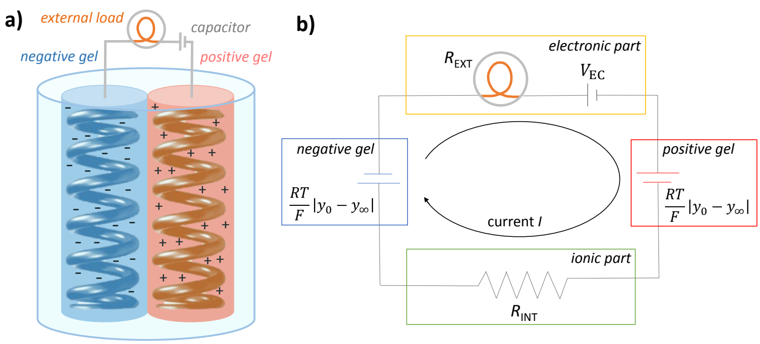

Figure 10.4: a) Schematic picture of an electrochemical cell consisting of two yarns coated with positive and negative polyelectrolyte gel. b) Electrical circuit diagram of the same system, indicating also the salt solution with resistance R_{INT} in which the two yarns are dipped, the load to harvest energy, and the external capacitor.

10.3 Results and Discussion

It is possible to build a system in which two coated coiled yarns, one with positive fixed charges and one with negative charges, are dipped in a salt solution of given concentration c_∞, to produce energy, see Fig. E.4a. In order to reach this objective an external load is placed into the system (Fig. E.4b). The external load, R_{EXT}, is taken as a free parameter in our calculations in Fig. E.5 and Fig. D.6, while in Fig. D.7 results are shown as function of R_{EXT}. The value of R_{EXT} gives some information about the external device that captures the energy, e.g., a battery or other storage system, or direct use in an appliance. Furthermore, an external capacitor is also placed in the circuit in order to charge the yarn surface, similar to the external battery used in the dynamic circuit for harvesting energy from water salinity differences [21]. During a working cycle, we assume that each coiled yarn is stretched with the same frequency, that we define as β. For this reason the polymer fixed charge density X oscillates with the same frequency β, which we describe by

$$\omega X = \omega X_0 - \Delta(\omega X)\left(1 - \cos\left(2\pi\beta t\right)\right) \tag{10.13}$$

where X_0 is the fixed charge density of both gels at $t = 0$, when the yarn is in its equilibrium position, while $\Delta(\omega X)$ is the maximum variation in gel charge density during the cycle.

For the system described above, it is possible to write Kirchhoff's voltage law as

$$V_{cell} + V_{EC} + 2\frac{RT}{F}|y_0 - y_\infty| + V_{INT} = 0 \tag{10.14}$$

where y_∞ (assumed as reference, hence zero) is the dimensionless potential in the solution bulk, while V_{cell}, V_{EC} and V_{INT} are the cell voltage, the voltage across the external capacitor and across the ionic solution. Eq. (10.14) is based on two perfectly symmetric gel electrodes (with only the fixed charge density of opposite sign), and y_0 used in Eq. (10.14) is evaluated in one of the electrodes. Assuming Ohmic behavior for the external load, and for the ionic transport in the gel and solution, we have

$$V_{cell} = I \cdot R_{EXT} \quad , \quad V_{INT} = I \cdot R_{INT} \tag{10.15}$$

where I is the current density ($\mathrm{A/m^2}$), while R_{EXT} and R_{INT} are respectively the external load, and the internal resistance in the gel and solution, in $\Omega \cdot \mathrm{m^2}$.

The current density, I, relates to the surface charge, Σ, by

$$\frac{\partial \Sigma}{\partial t} = -I. \tag{10.16}$$

Combining the above equations, it is possible to obtain the unknown variables of our system. Thus, it is possible to calculate the electrical power generated per unit area, P_d, by

$$P_d = V_{cell} \cdot I. \tag{10.17}$$

Now we can proceed with the analysis of a cycle in which the two coiled NC yarns are stretched with a certain frequency β in order to produce energy. Before starting, some parameters values characterizing our system must be given: $\omega X_0 = 500$ mol/m^3, $\Delta(\omega X) = 100$ mol/m^3, $\beta = 1$ s^{-1}, $c_\infty = 5$ mM, $\Sigma_0 = -110$ mC/m^2, $\varepsilon_r = 78$, $R_{EXT} = 1\ \Omega{\cdot}$m^2 where ε_r is the medium's relative permittivity. In our case study, we set R_{INT} to zero. At time zero, for the given value of A, reading from the graph (Fig. E.3) and maximizing γ, the B value, hence the initial surface charge density, Σ_0, was obtained. A value for V_{EC} by using Eq. (10.14), with the condition $I = 0$ at $t = 0$, was then calculated ($V_{EC} = 165$ mV). Optimal conditions for γ, as can be identified in Fig. E.3, are obtained when A is positive and B is negative. This situation is represented in Fig. F.1, where we observe a flip in the sign of the potential, y, from $y_D > 0$ far away from the yarn surface to $y_0 < 0$ at that surface. In particular, we can distinguish two regions, one near the yarn surface rich in cations and one away from the surface that is rich in anions. The optimum sensitivity is found when B and A have opposite sign.

In Fig. E.5a, we show the trend of ωX versus time. One notices that every minimum in ωX corresponds to the instant in which the maximum stretch of the gel, that we defined as $\Delta(\omega X)$, is reached. It is possible to notice that a similar oscillating trend with respect to time is present in the cell voltage, V_{cell}, and generated power, P_d, see Fig. E.5b and Fig. E.5c. Instead of plotting voltage V_{cell} versus time, we can also plot cell voltage versus charge Σ , as shown in Fig. D.6. The area enclosed by the ellipse shown represents the energy density in μJ/m^2 obtained during a cycle.

Finally, we show result as function of the external load, R_{EXT}, and present in Fig. D.7 results for the average generated power $P_{d,av}$ and the time shift, TS. Indeed, if we compare Fig. E.5b and Fig. E.5c with Fig. E.5a, we can observe that the moments when ωX is not changing, do not coincide with the moments when the cell voltage and power density are zero. Instead, a time shift occurs and its value depends on the value of R_{EXT} as shown in Fig. D.7a.

With increasing R_{EXT}, the time shift, TS, increases until a value of $\text{TS}_{max} = 0.22$ s is reached, where it is possible to notice a plateau. The trend of cycle-averaged power density, $P_{d,av}$, with respect to the external resistance R_{EXT}

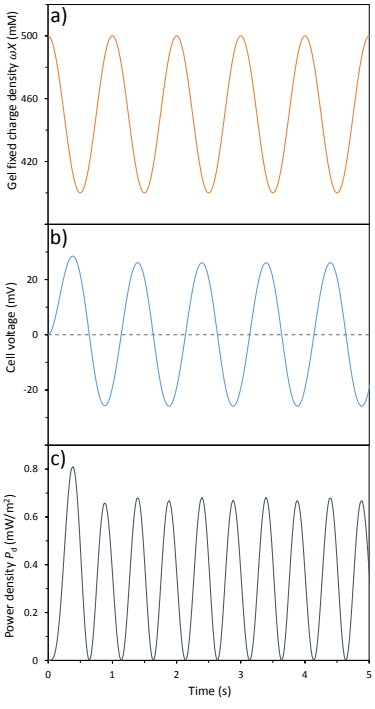

Figure 10.5: Gel fixed charge density ωX (mM), cell voltage, V_{cell} (mV), and power density P_d (mW/m^2) as a function of time (s) for our case study.

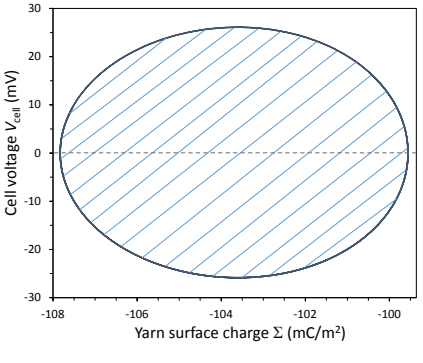

Figure 10.6: Cell voltage, V_{cell}, in mV, as a function of the yarn surface charge Σ (mC/m^2) during the limit cycle for our case study. The area enclosed in the diagram equals the energy harvested in one cycle.

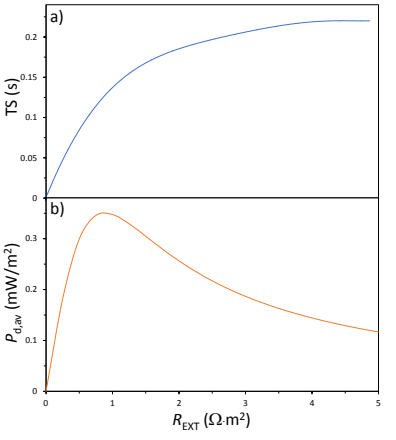

Figure 10.7: Time shift, TS, and average power density, $P_{d,av}$, versus external resistance, R_{EXT}, for our case study.

is shown in Fig. D.7b. We observe that a maximum for $P_{d,av}$ is obtained for $R_{EXT} = 0.9\ \Omega \cdot \mathrm{m}^2$. This represents the optimal condition for power generation.

If we assume a yarn having a 50 μm diameter, constituted of 5.0 nm diameter close-packed nanotubes with 24 kg/m^3 of bulk density [22], we obtain a yarn surface area of 4.4 m^2/g. Hence, we can calculate the achievable average power, that amounts to $\sim$ 770 mW/kg of yarn. This value is similar to the values obtained by Kim *et al.* in their experiments where yarns are stretched by ocean waves [3].

10.4 Conclusions

Motivated by recent experimental work on energy harvesting using coiled nanocarbon twisted yarns [3], we have reported a novel mechanism to harvest energy from mechanical oscillations by using coiled carbon nanotube yarns coated with polyelectrolyte gel. We have developed a model for the change in the electrical double layer structure when a gel, coated on a charged surface, is stretched. Our approach is mathematically simple while it is able to explain the scientific basis behind a hypothetical mechanical energy harvester made of coiled yarn coated with polyelectrolyte gel. The effects of gel fixed charge density, yarn surface charge, and salt concentration were studied. These results represent a helpful guide for future process improvement and development.

The analyzed case study and the calculations performed show the achievable power in a system made of two yarns, where one is coated with a positive polyelectrolyte gel, and the other is coated with a negative gel layer.

References

[1] S. Roundy, "On the effectiveness of vibration-based energy harvesting", Journal of Intelligent Material Systems and Structures **16**, 809–823 (2005).

[2] M. Janssen, B. Werkhoven, and R. van Roij, "Harvesting vibrational energy with liquid-bridged electrodes: thermodynamics in mechanically and electrically driven rc-circuits", RSC Adv. **6**, 20485–20491 (2016).

[3] S. H. Kim, C. S. Haines, N. Li, K. J. Kim, T. J. Mun, C. Choi, J. Di, Y. J. Oh, J. P. Oviedo, J. Bykova, S. Fang, N. Jiang, Z. Liu, R. Wang, P. Kumar, R. Qiao, S. Priya, K. Cho, M. Kim, M. S. Lucas, L. F. Drummy, B. Maruyama, D. Y. Lee, X. Lepró, E. Gao, D. Albarq, R. Ovalle-Robles, S. J. Kim, and R. H. Baughman, "Harvesting electrical energy from carbon nanotube yarn twist", Science **357**, 773–778 (2017).

[4] A. B. Kolomeisky and A. A. Kornyshev, "Corrigendum: Current-generating 'double layer shoe' with a porous sole (2016 j. phys.: Condens. matter 28 464009)", Journal of Physics: Condensed Matter **29**, 049501 (2016).

[5] A. A. Kornyshev, R. M. Twidale, and A. B. Kolomeisky, "Current-generating double-layer shoe with a porous sole: Ion transport matters", The Journal of Physical Chemistry C **121**, 7584–7595 (2017).

[6] G. Zhu, J. Chen, T. Zhang, Q. Jing, and Z. L. Wang, "Radial-arrayed rotary electrification for high performance triboelectric generator", Nature communications **5**, 3426 (2014).

[7] T. Krupenkin and J. Taylor, "Reverse electrowetting as a new approach to high-power energy harvesting", Nature communications **2**, 448 (2011).

[8] Z. L. Wang, J. Chen, and L. Lin, "Progress in triboelectric nanogenerators as a new energy technology and self-powered sensors", Energy Environ. Sci. **8**, 2250–2282 (2015).

[9] Z. L. Wang, "Triboelectric nanogenerators as new energy technology for self-powered systems and as active mechanical and chemical sensors", ACS Nano **7**, 9533–9557 (2013), pMID: 24079963.

[10] G.-G. Bumbu, M. Wolkenhauer, G. Kircher, J. S. Gutmann, and R. Berger, "Micromechanical cantilever technique: A tool for investigating the swelling of polymer brushes", Langmuir **23**, 2203–2207 (2007), pMID: 17279715.

[11] F. Zhou, P. M. Biesheuvel, E.-Y. Choi, W. Shu, R. Poetes, U. Steiner, and W. T. S. Huck, "Polyelectrolyte brush amplified electroactuation of microcantilevers", Nano Letters **8**, 725–730 (2008), pMID: 18269260.

[12] T. Schroeder, A. Guha, A. Lamoureux, G. VanRenterghem, D. Sept, M. Shtein, J. Yang, and M. Mayer, "An electric-eel-inspired soft power source from stacked hydrogels", Nature **552**, 214–218 (2017).

[13] L. Arens, F. WeiSSenfeld, C. O. Klein, K. Schlag, and M. Wilhelm, "Osmotic engine: Translating osmotic pressure into macroscopic mechanical force via poly(acrylic acid) based hydrogels", Advanced Science **4**, 1700112 (2017).

[14] H. Kwon, Y. Osada, and J. Gong, "Polyelectrolyte gels-fundamentals and applications", Polymer Journal **38**, 1211–1219 (2006).

[15] Y. Osada and J.-P. Gong, "Soft and wet materials: Polymer gels", Advanced Materials **10**, 827–837 (1998).

[16] M. Tedesco, H. Hamelers, and P. Biesheuvel, "Nernst-planck transport theory for (reverse) electrodialysis: Ii. effect of water transport through ion-exchange membranes", Journal of Membrane Science **531**, 172–182 (2017).

[17] J. Zhang, Y. Zhao, C.-G. Yuan, L.-N. Ji, X.-D. Yu, F.-B. Wang, K. Wang, and X.-H. Xia, "Donnan potential caused by polyelectrolyte monolayers", Langmuir **30**, 10127–10132 (2014), pMID: 25083596.

[18] G. Shen, N. Tercero, M. A. Gaspar, B. Varughese, K. Shepard, and R. Levicky, "Charging behavior of single-stranded dna polyelectrolyte brushes", Journal of the American Chemical Society **128**, 8427–8433 (2006), pMID: 16802807.

[19] P. M. Biesheuvel, A. A. Franco, and M. Z. Bazant, "Diffuse charge effects in fuel cell membranes", Journal of The Electrochemical Society **156**, B225 (2009).

[20] A. Kornyshev and M. Vorotyntsev, "Conductivity and space charge phenomena in solid electrolytes with one mobile charge carrier species, a review with original material", Electrochimica Acta **26**, 303–323 (1981).

[21] D. Brogioli, "Extracting renewable energy from a salinity difference using a capacitor", Phys. Rev. Lett. **103**, 058501 (2009).

[22] J. H. Lehman, M. Terrones, E. Mansfield, K. E. Hurst, and V. Meunier, "Evaluating the characteristics of multiwall carbon nanotubes", Carbon **49**, 2581–2602 (2011).

11

Outlook and Perspectives

11.1 Tuning surface chemistry to control membrane fouling and performance

In this thesis, we have shown that by carefully selecting the surface chemistry of both foulant and membrane we can achieve a better understanding of the fouling mechanisms that take place at the water-membrane interface, providing clear approaches to alleviate membrane fouling and to control permeate quality. Here, we find zwitterionic surfactants and polymers extremely interesting because of their intrinsic "anti-fouling" tendency, even at high salinities. The hydration shell surrounding zwitterionic molecules has been hypothesized to be the basis of their anti-fouling properties, as this hydration shell formed via ionic solvation constitutes an energy barrier that the foulant must overcome to interact with the zwitterion [1]. The application of zwitterions in both added chemicals for oil extraction and membrane surface materials could be highly beneficial for the field of PW treatment.

11.1.1 Zwitterionic surfactants for enhanced oil recovery

In Chapters 2-3, we demonstrated that zwitterionic surfactants are especially promising for successful treatment of oily waste waters at high salinity from a membrane fouling perspective. Unfortunately, these surfactants are not added to help the membrane separation, but rather to achieve efficient enhanced oil recovery (EOR). If we really want to land zwitterionic surfactants in the Oil&Gas market, we should not limit our view to membrane fouling but we must study the relevant aspects of their application, such as tolerance to reservoir salinity, thermal stability at reservoir temperature, capability of substantially reducing the IFT under reservoir conditions, effectiveness at low concentrations (0.10.3%), low adsorption onto reservoir rock ($<$ 1 mg/g rock), and compatibility with other chemical additives for EOR [2]. And indeed, several types of zwitterionic surfactant satisfy all these criteria for both sandstone and carbonate reservoirs [2, 3], therefore showing their promise for chemical EOR applications. This would mean that zwitterionic surfactants could allow effecient EOR processes and subsequently allow effective PW treatment by membranes, a very appealing prospect. An economic aspect, that should now be investigated when looking at industrial application is the commercial availability of zwitterionic surfactants at a reasonable cost. Surfactants tend to be a major factor associated with the cost of an EOR process, and losing surfactants leads to substantial economic losses. At the present moment the relatively high cost of zwitterionic surfactants limits their large-scale applica-

tion in EOR compared to other types of surfactants [4]. However, if membranes are used, the surfactants could potentially be recovered from PW and reused in the field, thereby reducing the quantity and cost of fresh surfactant needed during the extraction process. Finding effective ways to recycle (zwitterionic) surfactants would thus be the next important step to allow more efficient and sustainable EOR.

11.1.2 Zwitterionic chemistry for low-fouling membranes

Modification of membranes surfaces is potentially an effective way to control and limit membrane fouling. As fabricating a completely novel low-fouling membrane from scratch would require several years before being commercialized, one-step process membrane modifications of already existing membranes could be easily adopted by membrane manufacturing companies and therefore translated into low-fouling industrial products and applications [5].

Several works have focused on biomimetic polymers with zwitterionic moieties which bind on various surfaces [6, 7]. As shown in this thesis work, an easy way to control the membrane surface chemistry, and at the same time its separation properties, is the Layer-by-Layer (LbL) technique. LbL allows us to coat a charged membrane with positive and negative polyelectrolytes, but also with zwitterionic polymers (Chapter 6). Our work showed how a bio-inspired zwitterionic phosphatidylcholine surface chemistry exhibits excellent fouling resistance and stable performances during filtration, thereby demonstrating the potential of zwitterionic coated membranes not only for PW treatment but also for surface water treatment, bio-molecule separation, and filtration of other feeds with large fouling potential. However, anti-fouling studies are nearly always performed with model foulants on short time scales. The long-term stability of the grafted molecules or polymers, their uniformity, stability, shelf life and limited adhesion to the membrane surface remain a concern [8]. Therefore it would be important to see these membranes used in real applications, with real feed streams, especially in the challenging field of PW treatment, to study their stability and low-fouling behaviour for relevant systems and over long time scales.

11.1.3 The non-existence of a perfect anti-fouling surface

A perfect anti-fouling membrane would only exist if its surface does not present (or develops) any defects, and if its chemistry is perfectly stable over time, and if it completely prevents adhesion from any foulant. Unfortunately, in the

complex and challenging conditions as described in this thesis, some foulants will always find a place to adhere, then acting as nuclei for more fouling. This soon translates into a higher membrane area affected by fouling and a subsequent change in permeate quantity and quality (at constant pressure). As such, there are no membranes that will be completely free from fouling under any circumstances [9]. To maximize the effectiveness of a modified membrane surface, other factors need to be taken into account, e.g. membrane module design, membrane cleaning and pre-treatment stages [9].

As the foulant chemistry is typically highly diverse, it is difficult and in essence impossible, to develop a universal surface chemistry able to limit all foulant-surface interactions. Using a flow-cell to study surface-droplet interactions, we observed that a nonionic TX-stabilized O/W emulsion led to remarkable fouling on a negative hydrophobic Nafion-coated surface while fouling was limited for the zwitterionic-coated surface stabilized by zwitterionic surfactants (Figure 11.1A). On the other hand, zwitterionic DDAPS-stabilized O/W emulsions do not irreversebly foul the Nafion-coated surface, while they do foul the zwitterionic-coated surface (Figure 11.1B). Our results suggest that surface chemistry will need to be tailored according to specific applications, taking into account the chemistry of the foulants present in the wastewater.

In addition, when foulant-foulant interactions are dominant and lead to the formation of a rather dense cake layer on the membrane surface, even a zwitterionic membrane surface chemistry cannot prevent fouling to occur [10]. However, membrane cleaning would results easier and more effective as the fouling layer is kept separated from the membrane surface by the well hydrated zwitterionic moieties of the membrane. Coatings that enhance membrane clean ability are certainly as relevant as coatings that reduce fouling.

11.1.4 PEM-based membranes for advanced functionalities

In the last 10 years, the knowledge on LbL assembly of polyelectrolyte multilayers (PEMs) on porous supports has been translated into application and the production of very relevant commercial membranes with advanced separation properties and functionalities. Polyelectrolytes are highly promising materials to allow the formation of nextgeneration membranes with advanced functionalities. But in many ways the field is still developing, and much more exciting work on these versatile materials is expected in the near future.

A tailored ion-selectivity is still believed to be the holy grail of membrane filtration processes. Commercial membranes do exhibit high water-salt selectivity, but their ability to discriminate between different types of ion is

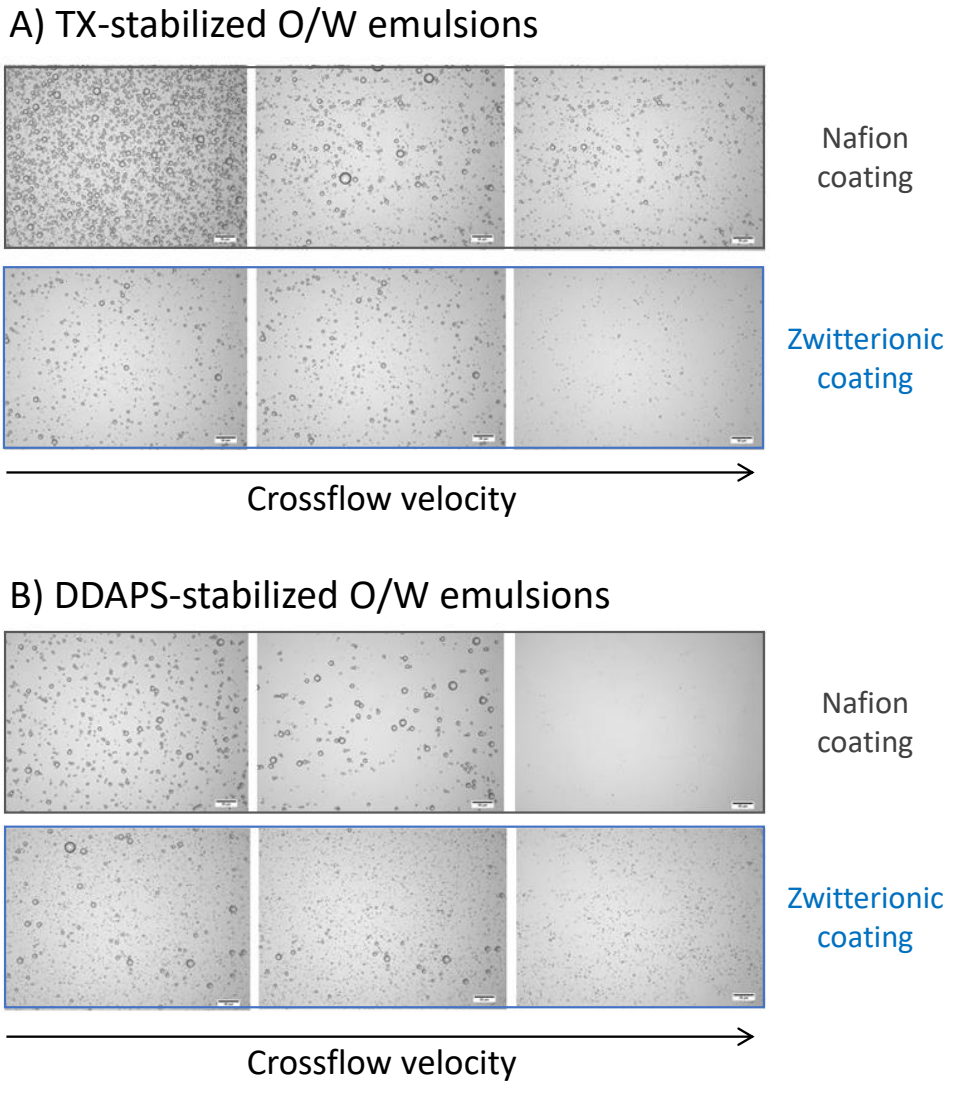

Figure 11.1: Flow-cell images of oil droplets stabilized with A) nonionic TX and B) zwitterionic DDAPS on PEM-coated surfaces with same multilayer but with two different top layers, Nafion and zwitterionic, as a function of 100 mM NaCl solution crossflow velocity. Scale bar of 50 μm.

still limited [11]. Nevertheless, PEM-coated membranes can already tackle challenging separations, including the separation of mono- and divalent (X^{2+}) ions, showing higher Na^+/X^{2+} selectivities than those of commercial NF membranes and even to competing surface modifications, such as polymer grafting, atomic and molecular layer deposition, graphene oxide, and carbon nanotubes incorporation, while retaining good water permeabilities (Figure 11.2A). Experiments that we carried out with PEM-coated membrane show that these membranes are also good for resource recovery, such as Phosphate, compared to commercial membranes (Figure 11.2B), .

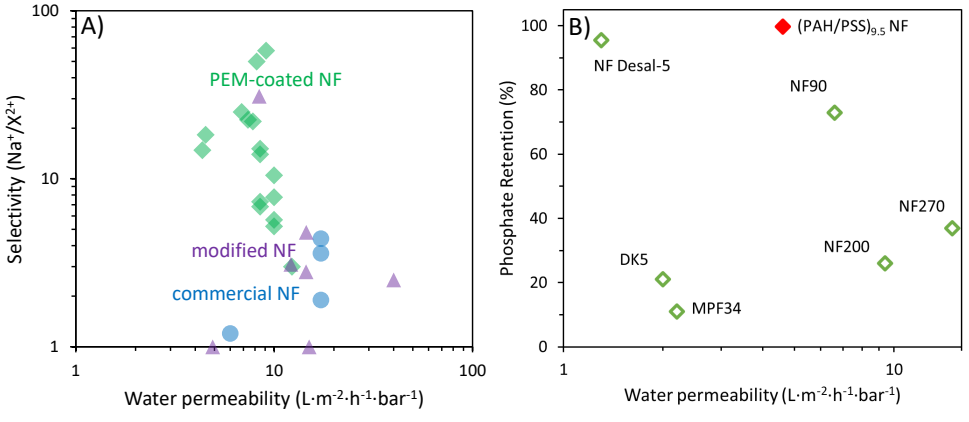

Figure 11.2: A) Comparison of membrane divalent ion-selectivity (Na^+/X^{2+}) and water permeability ($L{\cdot}m^{-2}{\cdot}\ h^{-1}{\cdot}\ bar^{-1}$) as a function of different surface modifications from literature. Green diamonds represent single data points for PEM-coated nanofiltration (NF) membranes [12–15], purple triangles modified NF membranes [16–22], and blue circles commercial NF membranes [4, 16, 17]. B) Comparison of membrane phosphate removal (%) and water permeability ($L{\cdot}m^{-2}{\cdot}\ h^{-1}{\cdot}\ bar^{-1}$) as a function of membrane type [23, 24].

As one other great advantage of PEM-based materials is that additives can easily be incorporated/intercalated to allow additional functionalities and further improvement of membrane properties. The incorporation of ion-selective receptors could make possible the recovery and re-use of specific ions from wastewater. In addition, incorporation of ion-selective groups may allow selectivity between monovalent ions for PEM-based membranes. Additionally, nanoparticles can be incorporated into the multilayer to increase PEM-

based membrane performance (e.g., permeability, selectivity, strength, and hydrophilicity) [25, 26]. Here, future research is expected to focus on membranes with incorporated ion-selective nanoparticles for selective adsorption and recovery (via pH regeneration) of specific resources from wastewater, thereby combining filtration and adsorption in a single step process. Finally, polyelectrolyte multilayers could be combined with functional biological moieties, such as enzymes. Current PEM-based membranes can stop already stop micropollutants (MPs) with a high efficiency. However, future works on stable PEM-based catalytic membranes, i.e. with incorporated catalytic groups, would allow for MP rejection and degradation in a single step process.

11.2 Applying membranes worldwide to treat Produced Water

Membrane technology has been shown to be quite promising for the treatment of produced water. However, some barriers limit membranes to be widely applied for PW treatment: membrane stability and good quality permeate.

11.2.1 Stable membranes for harsh Produced Waters

In this thesis, we have focused on membrane fouling by produced water, but there are other important aspects that limit large scale use of membrane technology. Indeed, produced Water can be quite challenging to treat due to its variable, and sometimes harsh, composition. Most of the challenges that limit the application of especially commercially available polymeric membranes in PW treatment can be attributed to these harsh conditions, such as:

- High contents of total dissolved solids (TDS) ($4x10^5$ ppm) and total suspended solids (TSS) (up to 1000 ppm) [27] that can clog and/or damage the membrane;
- Small organics, such as BTEX compounds, phenol, and naphthalene, which can diffuse into the membrane and compromise the stability of most polymeric supports used in membrane fabrication;
- Extreme salinities [28], able to de-stabilize the emulsion and substantially worsen membrane fouling;
- Biocides (10-200 ppm) [29] used to prevent biofilm growth in the seawater pipelines, that can affect membrane stability;

- High concentration of H_2S [28], which may plasticize the membrane or react with the membrane surface groups and bulk, thereby affecting their stability;
- Relatively high temperatures, in the range 50-65°C.

Given the harsh conditions that can be typical of PW, investigating membrane stability in such conditions becomes key. Here, PEMs allow the production of very stable membranes, which can go beyond that of commercial alternatives. Stable PEM membranes have been prepared to withstand organic solvents [30], extreme pH conditions [31], and high salinity [32]. Furthermore, as cleaning processes can also affect the stability of membranes, different researchers have demonstrated that PEMs based on strong polyelectrolytes such as PDADMAC and PSS can withstand physical (e.g., backwash) [33, 34] and chemical (via hypochlorite) [33] cleaning. However, future work, focused on harsh PW conditions, is needed to further address membrane chemical stability to organic compounds (e.g. BTEX), biocides and H_2S, to finally bring good and stable membrane candidates into the market for PW treatment. We believe that these stable and functionalized membranes could highly benefit the treatment of challenging PWs, separating organics from water to re-use water at lower energy costs, thanks to the thin PEM-based separation layer. Finally, fine-tuning membrane chemistry and polarity could help recovering organics and added chemicals such as surfactants from water, reducing the chemical consumption.

PEM based membranes for PW treatment would thus have benefits that go beyond the possible anti-fouling properties described in this thesis. The high stabilities demonstrated for these systems would be very relevant, even for harshest PW conditions.

11.2.2 Integrated schemes towards a PW reuse

Besides pressure-driven membranes, other technologies are certainly also needed within the larger treatment scheme to effectively clean produced water and facilitate its reuse [35]. The OPUS® II from Veolia Water Solutions & Technologies is an example of one of the most established technologies used in the field of PW treatment. This technology uses ceramic membranes with chemical and ion exchange softening as pretreatment to reverse osmosis (RO), which is operated at high pH. Even tough this treatment system provides high quality water for industrial reuse, it requires a huge amount of chemicals (specifically acids and bases). Additionally, the chemicals added during the

extraction (e.g. surfactants) cannot be recovered and go to the waste stream of the process.

In a world where circular economy becomes an urgent need, the consumption of such huge amount of chemicals cannot be tolerated. Therefore, a system focused on both chemicals and water re-use is much more relevant for PW treatment. Here a system where sand filters are used to remove the bigger particles, NF membranes for divalent ions removal, Electrodialysis (ED) [36, 37] to allow recovery of specific components, and RO for high quality permeate production [38], could allow effective removal and recovery of oil, added chemicals and salts from water, while facilitating water re-use. The recovered water and added chemicals from the NF [39, 40]/ED [37] stage could here be re-used as water for re-injection, lowering the demand for fresh water, while the water coming from the RO permeate, if remineralized, could find application for basic needs, such as water for irrigation [41–43].

11.3 General Conclusion

By good control over the membrane surface chemistry, membrane process conditions and a good understanding of the chemistry of produced water it is certainly possible to substantially alleviate membrane fouling, allowing efficient membrane treatment of PW. But this is just part of a much larger puzzle. It now becomes important to also look in detail at membrane stability, the recycling of added chemicals and the effective integration of membrane technology with other separation technologies. Only by looking carefully at the bigger picture of produced water treatment we can really reduce the environmental impact and re-use the water in the most efficient way. The potential is certainly there, but it is up to scientists, companies and governments to push forward with improving sustainability and limiting worldwide water scarcity.

References

[1] A. Erfani, J. Seaberg, C. P. Aichele, and J. D. Ramsey, “Interactions between biomolecules and zwitterionic moieties: A review”, Biomacromolecules **21**, 2557–2573 (2020), pMID: 32479065.

[2] O. Massarweh and A. S. Abushaikha, “The use of surfactants in enhanced oil recovery: A review of recent advances”, Energy Reports **6**, 3150–3178 (2020).

[3] A. Kumar and A. Mandal, "Critical investigation of zwitterionic surfactant for enhanced oil recovery from both sandstone and carbonate reservoirs: Adsorption, wettability alteration and imbibition studies", Chemical Engineering Science **209**, 115222 (2019).

[4] S. Chen, H. Liu, H. Sun, X. Yan, G. Wang, Y. Zhou, and J. Zhang, "Synthesis and physiochemical performance evaluation of novel sulphobetaine zwitterionic surfactants from lignin for enhanced oil recovery", Journal of Molecular Liquids **249**, 73–82 (2018).

[5] S. P. Nunes, "Can fouling in membranes be ever defeated?", Current Opinion in Chemical Engineering **28**, 90–95 (2020), materials Engineering Separations Engineering.

[6] G. Li, G. Cheng, H. Xue, S. Chen, F. Zhang, and S. Jiang, "Ultra low fouling zwitterionic polymers with a biomimetic adhesive group", Biomaterials **29**, 4592–4597 (2008).

[7] C. Gao, G. Li, H. Xue, W. Yang, F. Zhang, and S. Jiang, "Functionalizable and ultra-low fouling zwitterionic surfaces via adhesive mussel mimetic linkages", Biomaterials **31**, 1486–1492 (2010).

[8] L. Upadhyaya, X. Qian, and S. Ranil Wickramasinghe, "Chemical modification of membrane surfaceoverview", Current Opinion in Chemical Engineering **20**, 13–18 (2018), nanotechnology / Separation Engineering.

[9] D. Rana and T. Matsuura, "Surface modifications for antifouling membranes", Chemical Reviews **110**, 2448–2471 (2010), pMID: 20095575.

[10] W. Zhai, M. Wang, J. Song, L. Zhang, X.-M. Li, and T. He, "Fouling resistance of 3-[[3-(trimethoxysilane)-propyl] amino] propane-1-sulfonic acid zwitterion modified poly (vinylidene fluoride) membranes", Separation and Purification Technology **239**, 116589 (2020).

[11] X. Zhou, Z. Wang, R. Epsztein, C. Zhan, W. Li, J. D. Fortner, T. A. Pham, J.-H. Kim, and M. Elimelech, "Intrapore energy barriers govern ion transport and selectivity of desalination membranes", Science Advances **6** (2020).

[12] C. Liu, L. Shi, and R. Wang, "Crosslinked layer-by-layer polyelectrolyte nanofiltration hollow fiber membrane for low-pressure water softening with the presence of so42 in feed water", Journal of Membrane Science **486**, 169–176 (2015).

[13] W. Cheng, C. Liu, T. Tong, R. Epsztein, M. Sun, R. Verduzco, J. Ma, and M. Elimelech, "Selective removal of divalent cations by polyelectrolyte multilayer nanofiltration membrane: Role of polyelectrolyte charge, ion size, and ionic strength", Journal of Membrane Science **559**, 98–106 (2018).

[14] L. Y. Ng, A. W. Mohammad, C. Y. Ng, C. P. Leo, and R. Rohani, "Development of nanofiltration membrane with high salt selectivity and performance stability using polyelectrolyte multilayers", Desalination **351**, 19–26 (2014).

[15] L. Ouyang, R. Malaisamy, and M. L. Bruening, "Multilayer polyelectrolyte films as nanofiltration membranes for separating monovalent and divalent cations", Journal of Membrane Science **310**, 76–84 (2008).

[16] J. Wang, Z. Wang, Y. Liu, J. Wang, and S. Wang, "Surface modification of nf membrane with zwitterionic polymer to improve anti-biofouling property", Journal of Membrane Science **514**, 407–417 (2016).

[17] S. Chaudhury, E. Wormser, Y. Harari, E. Edri, and O. Nir, "Tuning the ion-selectivity of thin-film composite nanofiltration membranes by molecular layer deposition of alucone", ACS Applied Materials & Interfaces **12**, 53356–53364 (2020), pMID: 33190482.

[18] Z. Song, M. Fathizadeh, Y. Huang, K. H. Chu, Y. Yoon, L. Wang, W. L. Xu, and M. Yu, "Tio2 nanofiltration membranes prepared by molecular layer deposition for water purification", Journal of Membrane Science **510**, 72–78 (2016).

[19] X. Zhou, Y.-Y. Zhao, S.-R. Kim, M. Elimelech, S. Hu, and J.-H. Kim, "Controlled tio2 growth on reverse osmosis and nanofiltration membranes by atomic layer deposition: Mechanisms and potential applications", Environmental Science & Technology **52**, 14311–14320 (2018).

[20] S. Gao, Y. Zhu, Y. Gong, Z. Wang, W. Fang, and J. Jin, "Ultrathin polyamide nanofiltration membrane fabricated on brush-painted single-walled carbon nanotube network support for ion sieving", ACS Nano **13**, 5278–5290 (2019), pMID: 31017384.

[21] R. Hu, Y. He, C. Zhang, R. Zhang, J. Li, and H. Zhu, "Graphene oxide-embedded polyamide nanofiltration membranes for selective ion separation", J. Mater. Chem. A **5**, 25632–25640 (2017).

[22] M. Homayoonfal, A. Akbari, and M. R. Mehrnia, "Preparation of polysulfone nanofiltration membranes by uv-assisted grafting polymerization for water softening", Desalination **263**, 217–225 (2010).

[23] C. Visvanathan and P. K. Roy, "Potential of nanofiltration for phosphate removal from wastewater", Environmental Technology **18**, 551–556 (1997).

[24] C. P. Leo, W. K. Chai, A. W. Mohammad, Y. Qi, A. F. A. Hoedley, and S. P. Chai, "Phosphorus removal using nanofiltration membranes", Water Science and Technology **64**, 199–205 (2011).

[25] Z. Liu, Z. Yan, and L. Bai, "Layer-by-layer assembly of polyelectrolyte and gold nanoparticle for highly reproducible and stable sers substrate", Applied Surface Science **360**, 437–441 (2016).

[26] L. Y. Ng, A. W. Mohammad, C. P. Leo, and N. Hilal, "Polymeric membranes incorporated with metal/metal oxide nanoparticles: A comprehensive review", Desalination **308**, 15–33 (2013), new Directions in Desalination.

[27] M. A. Al-Ghouti, M. A. Al-Kaabi, M. Y. Ashfaq, and D. A. Dana, "Produced water characteristics, treatment and reuse: A review", Journal of Water Process Engineering **28**, 222–239 (2019).

[28] S. Jiménez, M. Micó, M. Arnaldos, F. Medina, and S. Contreras, "State of the art of produced water treatment", Chemosphere **192**, 186–208 (2018).

[29] J. Neff, K. Lee, and E. M. DeBlois, *Produced Water: Overview of Composition, Fates, and Effects*, 3–54 (Springer New York, New York, NY) (2011).

[30] X. Li, W. Goyens, P. Ahmadiannamini, W. Vanderlinden, S. De Feyter, and I. Vankelecom, "Morphology and performance of solvent-resistant nanofiltration membranes based on multilayered polyelectrolytes: Study of preparation conditions", Journal of Membrane Science **358**, 150–157 (2010).

[31] M. Elshof, W. de Vos, J. de Grooth, and N. Benes, "On the long-term ph stability of polyelectrolyte multilayer nanofiltration membranes", Journal of Membrane Science **615**, 118532 (2020).

[32] K. L. Cho, A. J. Hill, F. Caruso, and S. E. Kentish, "Chlorine resistant glutaraldehyde crosslinked polyelectrolyte multilayer membranes for desalination", Advanced Materials **27**, 2791–2796 (2015).

[33] J. de Grooth, B. Haakmeester, C. Wever, J. Potreck, W. M. de Vos, and K. Nijmeijer, "Long term physical and chemical stability of polyelectrolyte multilayer membranes", Journal of Membrane Science **489**, 153–159 (2015).

[34] D. Menne, J. Kamp, J. Erik Wong, and M. Wessling, "Precise tuning of salt retention of backwashable polyelectrolyte multilayer hollow fiber nanofiltration membranes", Journal of Membrane Science **499**, 396–405 (2016).

[35] Siagian, Utjok W.R., Widodo, Setyo, Khoiruddin, Wardani, Anita K., and Wenten, I Gede, "Oilfield produced water reuse and reinjection with membrane", MATEC Web Conf. **156**, 08005 (2018).

[36] T. Sirivedhin, J. McCue, and L. Dallbauman, "Reclaiming produced water for beneficial use: salt removal by electrodialysis", Journal of Membrane Science **243**, 335–343 (2004).

[37] P. Sosa-Fernandez, J. Post, H. Bruning, F. Leermakers, and H. Rijnaarts, "Electrodialysis-based desalination and reuse of sea and brackish polymer-flooding produced water", Desalination **447**, 120–132 (2018).

[38] *Evaluation of Nanofiltration Membranes for Low Salinity Injection Water Flood LSF*, volume Day 3 Thu, September 05, 2019 of *SPE Offshore Europe Conference and Exhibition* (2019), d031S012R004.

[39] S. Zha, J. Yu, G. Zhang, N. Liu, and R. Lee, "Polyethersulfone/Cellulose Acetate Butyrate Hybrid Hollow-Fiber Membranes for Organic-Matter Removal From Produced Water", SPE Journal **22**, 1478–1486 (2017).

[40] R. R. Nair, E. Protasova, T. Bilstad, and S. Strand, "Evaluation of Nanofiltration Membrane Process for Smartwater Production in Carbonate Reservoirs From Deoiled Produced Water and Seawater", SPE Production Operations **34**, 409–420 (2019).

[41] *Chevron San Ardo Facility Unit (SAFU) Beneficial Produced Water Reuse for Irrigation*, volume Day 2 Tue, March 18, 2014 of *SPE International Conference and Exhibition on Health, Safety, Environment, and Sustainability* (2014), d021S021R004.

[42] F. C. Dolan, T. Y. Cath, and T. S. Hogue, "Assessing the feasibility of using produced water for irrigation in colorado", Science of The Total Environment **640-641**, 619–628 (2018).

[43] *Reuse of Produced Water in the Oil and Gas Industry*, volume Day 2 Tue, July 28, 2020 of *SPE International Conference and Exhibition on Health, Safety, Environment, and Sustainability* (2020), d021S004R001.

Appendix A

In this Appendix, we first report the investigation of the SiC membrane structure and pore size. Later, we also prove that in our fouling study no droplets break-up occurs.

A.1 Pore size estimation

We investigated membrane structure and estimate pore size of our Liqtech CoMem© membrane, based on SiC. The membrane structure and pore size of our Liqtech CoMem© SiC membrane were investigated with SEM. Figure A.1 shows the SEM pictures of the analysis performed. Figure A.1A shows the inner surface of one of the 31 channels of the membrane. Figure A.1B and A.1C show the porous support structure and the active layer, while Figure A.1D displays the SiC particles forming the membrane active layer.

We calculated the particle size D_p of the active layer, and it resulted in an average of 670 nm. This calculation was performed by using of manual particle selection to avoid inaccuracy related to a contrast based method. The image used and the particle size distribution are displayed in Figure A.2. With this average particle size and the active layer thickness l_c, which was found to be around 50 μm (Figure A.1B), the porosity ϵ_c of this layer can be calculated by

$$R_m = \frac{150 l_c (1-\epsilon_c)^2}{D_p^2 \epsilon_c^3}. \tag{A.1}$$

This is possible since R_m can be determined from the average permeability J with the corresponding TMP and viscosity μ at the operated temperature

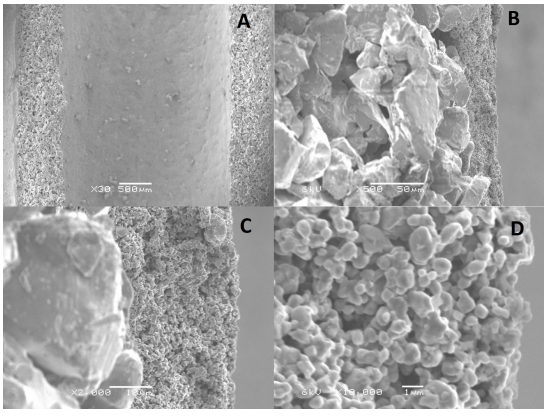

Figure A.1: SEM images of SiC membrane with different magnifications. One of the 31 channels (A), active layer on porous support (B) and (C). Particles forming active layer (D).

as follows

$$J = \frac{TMP}{\mu \cdot R_m} \tag{A.2}$$

The average permeability is 1725 LMH/bar and it was calculated from 35 performed experiments. It results in $R_m = 2.4 \times 10^{11}$ m^{-1}.

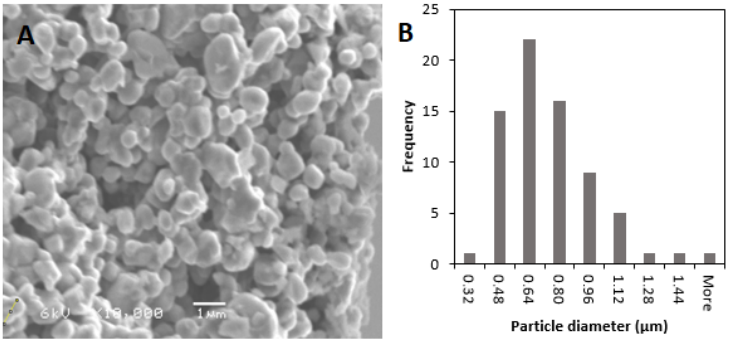

Figure A.2: Used active layer part for pore size calculations (A). Particle sizes from analysis (B).

From Equation A.1 and the R_m value, the porosity ϵ_c was calculated and found to be $\epsilon_c = 0.3185$. This value of porosity is slightly lower than for random close packing for monodisperse spheres, due to the fact that the particle size is here polydisperse. However if we assume three same sized particles, it is

possible to calculate the area between them. This area is schematically shown in Figure A.3, and marked in orange.

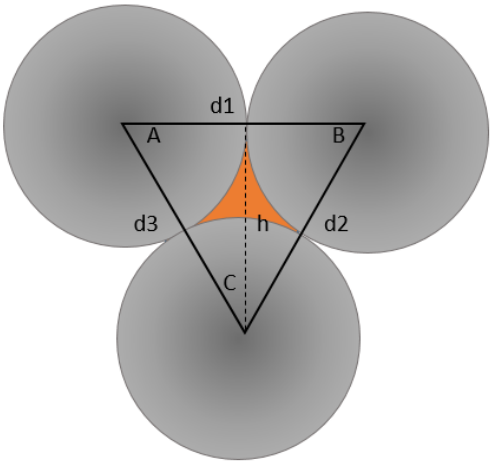

Figure A.3: Pore area calculation of three equally sized particles.

We can estimate the pore area by first calculating the area of the drawn black triangle, which has sides that are equal to the diameter of the particles (d_1=d_2=d_3). From the 60° angles or Pythagoras theorem, the height h can then be calculated, and with that, the area of the triangle

$$h = \sqrt{d_3^2 - r_1^2} = \sqrt{d_1^2 - \frac{1}{4}d_1^2} = \sqrt{\frac{3}{4}d_1^2} \tag{A.3}$$

$$A_{triangle} = \frac{1}{2}d_1 h \tag{A.4}$$

with $r_1 = 1/2d_2$. From this area we can then subtract the parts of the circles A, B, and C. These parts are equal in the case of same sized particles:

$$\frac{1}{2}r_1^2\theta = \frac{1}{2}r_1^2 \arccos\frac{r_1}{d_1} \tag{A.5}$$

With θ being the angle of A, B or C, which again are equal in the case of monodispersed particles. Thus, the pore area can be written as

$$A_{pore} = \frac{1}{2}d_1 h - 3\left(\frac{1}{2}r_1^2 \arccos\frac{r_1}{d_1}1\right) \tag{A.6}$$

If the calculated pore area is then assumed to be spherical, the pore diameter can be easily calculated. For a particle diameter of 0.670 μm, we then find a pore diameter of 0.152 μm. This pore diameter is the value used for the calculations of the critical pressure P_{cr} and critical capillary number Ca_{cr}.

A.2 Capillary number and droplets breakup

If the critical pressure is reached, the oil can almost freely permeate through the membrane and oil retention is diminished. This is not happening in all cases, it is also possible that droplets breakup when they are deformed in the pores at sufficient shear stress and so smaller droplets are created, especially in crossflow filtration.

Indeed, one of the effects of low interfacial tensions is that the deformability of droplets increases. This is what makes it possible to squeeze droplets trough the pores, which would normally be too small to pass. This deformability has a limit though, and the interfacial tension can decrease to such an extent that the droplets become instable leading to its break up [1–3]. This break up is in the case of membrane filtration initiated by shear stress on the droplets. To see which forces are dominant, the shear forces or the interfacial tension forces, the capillary number can be used, which is defined as

$$Ca = \mu_w \dot{\gamma} \frac{r_d}{\gamma} \tag{A.7}$$

Ca can be calculated for each experiment separately and then be compared with a critical capillary number Ca_{cr}. Ca_{cr} was proposed to see if droplet break up can be expected, or if oil permeation is due to complete passing of oil. This Ca_{cr} was defined by Darvishzadeh *et al.* as [3]

$$Ca_{cr} \approx 0.3546 \frac{1}{f_D(\lambda)\overline{r}} \tag{A.8}$$

wherein the 0.3546 is determined from data presented by Darvishzadeh *et al.* as well [3]. Furthermore, this equation uses the ratio between the droplet radius, r_d and the pore radius r_p given by

$$\overline{r} = \frac{r_d}{r_p} = 52.63 \tag{A.9}$$

Alternatively, if the smaller pore size is used, $\overline{r}$ becomes 65.57. The $f_D(\lambda)$ is a function of the viscosity ratio which, in the case of hexadecane in water, is:

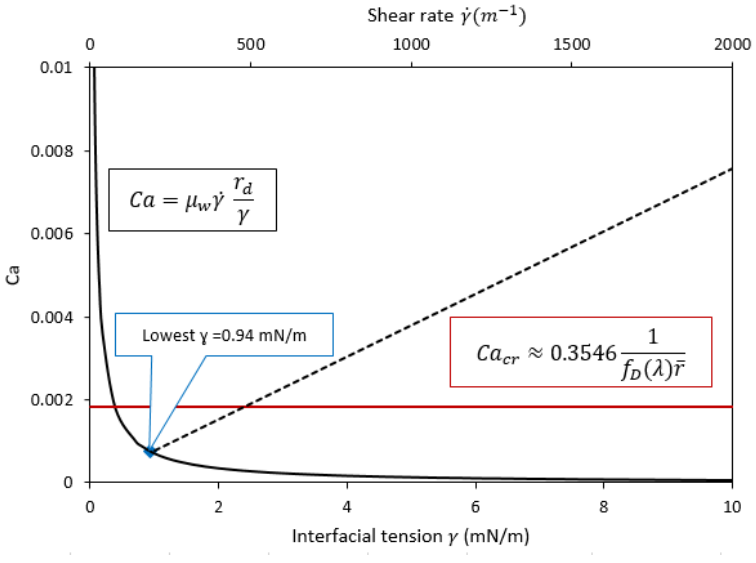

Figure A.4: Ca (solid black), Ca_{cr} (red) for pore size of 0.152 μm, emulsion with lowest γ (blue) and needed shear rate increase (dashed line).

$$= \frac{\mu_o}{\mu_w} = \frac{2.38\times10^{-3}}{8.9\times10^{-4}} = 2.67 \tag{A.10}$$

and $f_D(\lambda)$ was estimated according to Sugiyama for a hemispherical droplet with $\theta = 90°$, to be [1]:

$$f_D(\lambda) \approx \frac{2 + 4.510\lambda}{1 + 1.048\lambda} \approx 3.70 \tag{A.11}$$

Ca as a function of the interfacial tension can then be plotted since the shear rate, droplet size and water viscosity were constant during our experiments. We can compare Ca then with the Ca_{cr} described above, which we show in Figure A.4.

Figure A.4 shows that the emulsion with the lowest interfacial tension is still far below the Cacr for our system, suggesting that droplet break up is not prominent in our system. This also means that if we see oil permeation, it is most likely not due to droplet leakage as described by Darvishzadeh but complete penetration [2]. In Figure A.4, we also present the necessary increase in shear rate to arrive in the break up regime. For the largest pore size, corresponding to $\bar{r} = 52.63$ a needed shear rate of roughly 470 m^{-1} would

correspond to an increase in feed rate from 60 kg/h to 139 kg/h, which is equal to a CFV increase from 0.076 m/s to 0.177 m/s. For $\overline{r} = 65.57$, which comes from the pore size of 0.122 μm, the shear rate should be increased to 386 m^{-1}, equal to an increase in feed rate to 114 kg/h, which is a CFV increase to 0.145 m/s.

A.3 Flux decline and average oil retention: complete set of data

In Figure A.5, A.6, A.7 and A.8, we report the complete data set of flux decline and average oil retention as a function of permeate volume for CTAB, SDS, DDAPS and TX, respectively. The results are discussed in the manuscript.

A.3.1 Filtration of CTAB stabilized emulsions

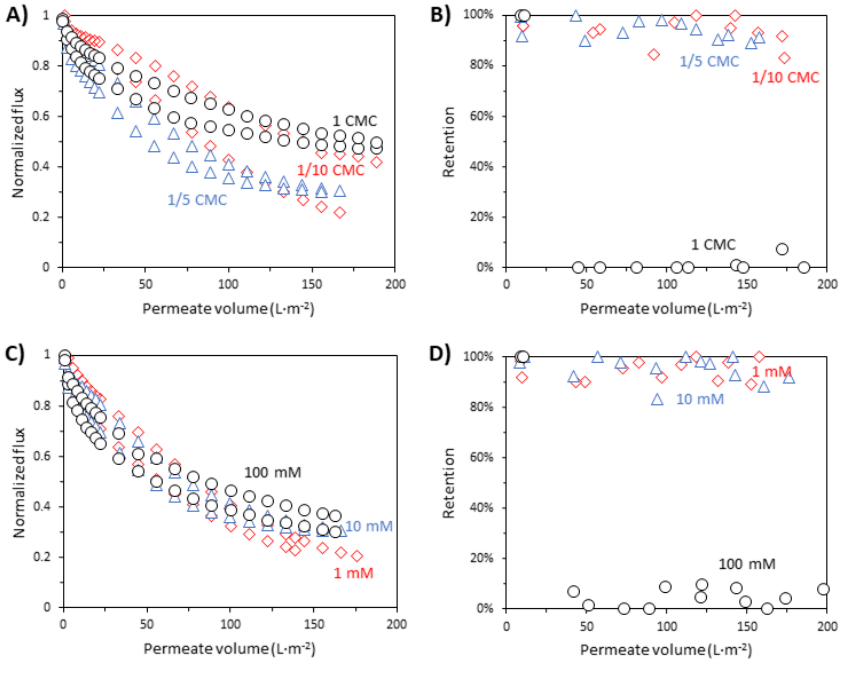

Figure A.5: Flux decline of CTAB stabilized emulsions at a crossflow velocity of 7.6 cm/s and a transmembrane pressure of 0.1 bar. Flux decline (A) and oil retention (B) as a function of surfactant concentration at 1 mM NaCl, flux decline (C) and oil retention (D) as a function of ionic strength at 0.2 CMC (69.2 mg/L CTAB). CMC = 346 mg/L is the critical micelle concentration for CTAB in absence of salt. All the experiments were performed in duplicate, as shown.

A.3.2 Filtration of SDS stabilized emulsions

In Figure A.6B, we can see for permeate volumes higher than 50 L/m^2 an increase in retention over time for the experiments carried out at the two lowest SDS concentrations, 0.1 and 0.2 times CMC. This maybe caused by the build up of a cake layer which, although it reduces the flux, improves the oil retention. This effect is evident at the lowest SDS concentration (0.1 CMC) where the repulsion between droplets is the lowest and the cake layer is expected to be the densest.

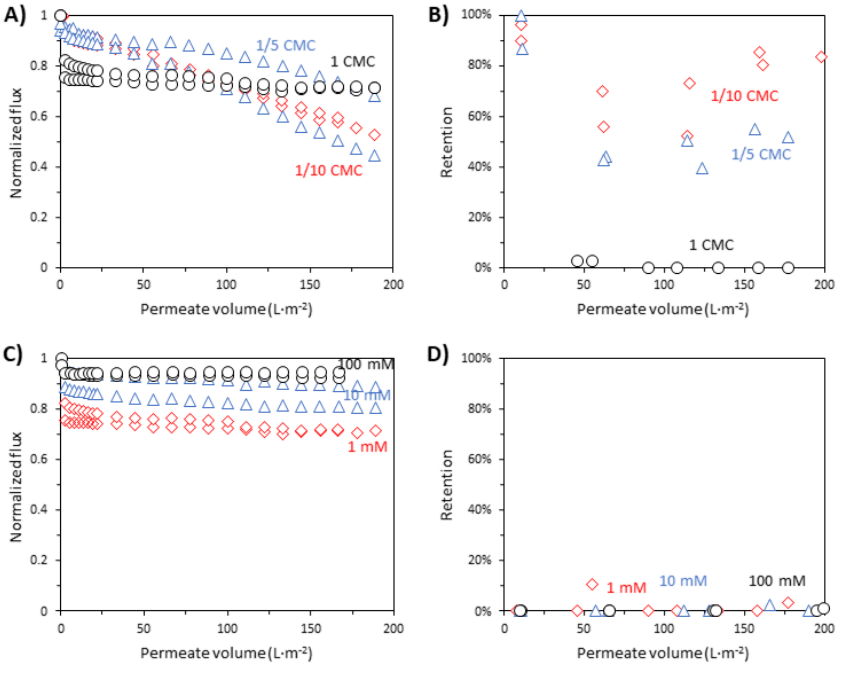

Figure A.6: Flux decline of SDS stabilized emulsions at a crossflow velocity of 7.6 cm/s and a transmembrane pressure of 0.1 bar. Flux decline (A) and oil retention (B) as a function of surfactant concentration at 1 mM NaCl, flux decline (C) and oil retention (D) as a function of ionic strength at CMC (2391 mg/L SDS). CMC = 2391 mg/L is the critical micelle concentration for SDS in absence of salt. All the experiments were performed in duplicate, as shown.

A.3.3 Filtration of DDAPS stabilized emulsions

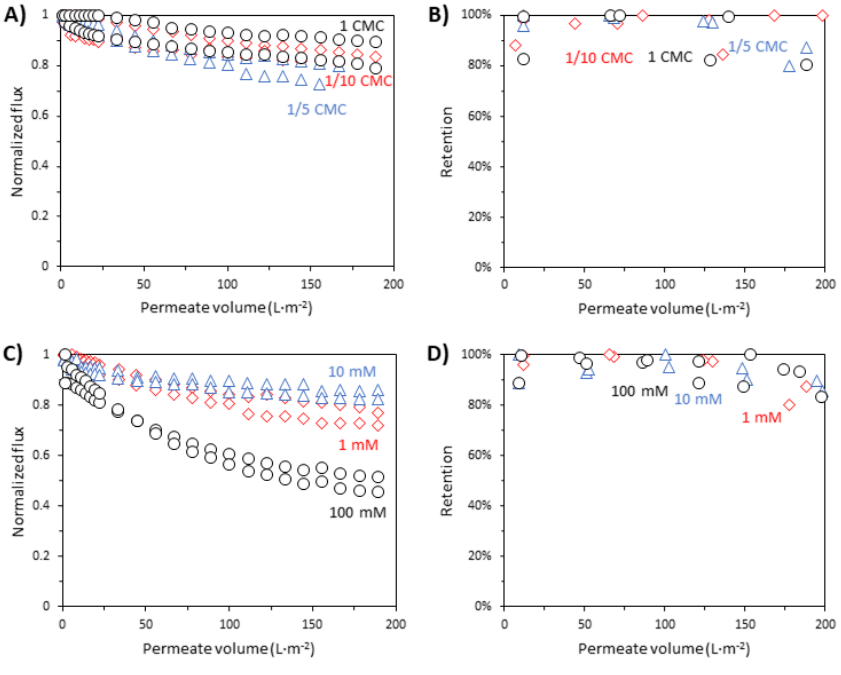

Figure A.7: Flux decline of DDAPS stabilized emulsions at a crossflow velocity of 7.6 cm/s and a transmembrane pressure of 0.1 bar. Flux decline (A) and oil retention (B) as a function of surfactant concentration at 1 mM NaCl, flux decline (C) and oil retention (D) as a function of ionic strength at 0.2 CMC (201.2 mg/L DDAPS). CMC = 1006 mg/L is the critical micelle concentration for DDAPS in absence of salt. All the experiments were performed in duplicate, as shown.

A.3.4 Filtration of TX stabilized emulsions

We do observe a clear effect of the ionic strength on the oil retention. Figure A.8B shows that the membrane seems to behave differently at high ionic strength, showing an increased oil permeation with increasing permeate volumes.

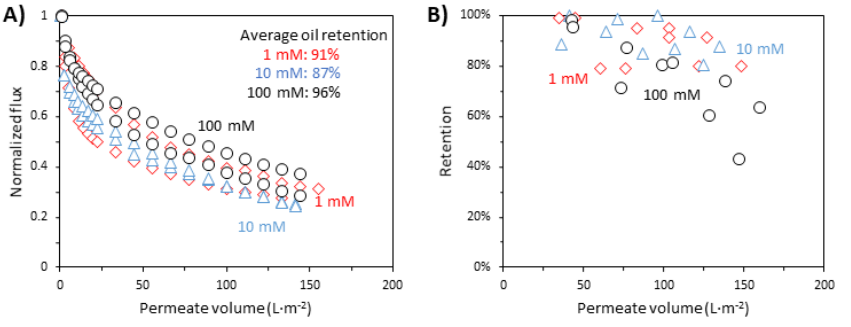

Figure A.8: Flux decline of TX stabilized emulsions at a crossflow velocity of 7.6 cm/s and a transmembrane pressure of 0.1 bar. Flux decline (A) and oil retention (B) as a function of ionic strength at CMC (144 mg/L TX). CMC = 144 mg/L is the critical micelle concentration for SDS in absence of salt. All the experiments were performed in duplicate, as shown.

References

[1] K. Sugiyama and M. Sbragaglia, "Linear shear flow past a hemispherical droplet adhering to a solid surface", Journal of Engineering Mathematics **62**, 35–50 (2008).

[2] T. Darvishzadeh and N. Priezjev, "Effects of crossflow velocity and transmembrane pressure on microfiltration of oil-in-water emulsions", Journal of Membrane Science **423424**, 468–476 (2012).

[3] T. Darvishzadeh, V. Tarabara, and N. Priezjev, "Oil droplet behavior at a pore entrance in the presence of crossflow: Implications for microfiltration of oil-water dispersions", Journal of Membrane Science **447**, 442–451 (2013).

Appendix B

B.1 Model parameters

In table B1, we report the values of the parameters used in the model calculations.

Membrane	Surfactant (mg/L)	Salinity (mM NaCl)	Contact Angle$_{o/m}$ (°)	τ_{pb}	α	β	ϕ_{CL}
SiC	CTAB, 345	1	136	0.15	1	0	0.9
RC	CTAB, 345	1	147.5	0.11	1	0.01	0.965
SiC	SDS, 2390	1	174	1	1	0.0111	0.99
SiC	DDAPS, 1005	1	137.5	0.001	1	0.0002	0.85
SiC	TX, 145	1	150	2	1	0	0.93
RC	SDS, 460	1	150	0.12	1	0	0.94
SiC	SDS, 2390	10	177	5	1	0.0035	0.98
RC	SDS, 460	10	148	10	1	0.00025	0.965
SiC	SDS, 2390	100	165	5	1	0	0.7
RC	SDS, 460	100	141	0	1	0	0.968

Table B.1: Values of the parameters used in the model calculations.

B

Appendix C

C

In this Appendix, we report the scanning electron microscope (SEM) pictures of the SPES hollow fiber (HF) membranes we fabricated (see Figure C.1). These hollow fiber membranes are designed for inside-out filtration, having the smallest pores at the inside of the fiber.

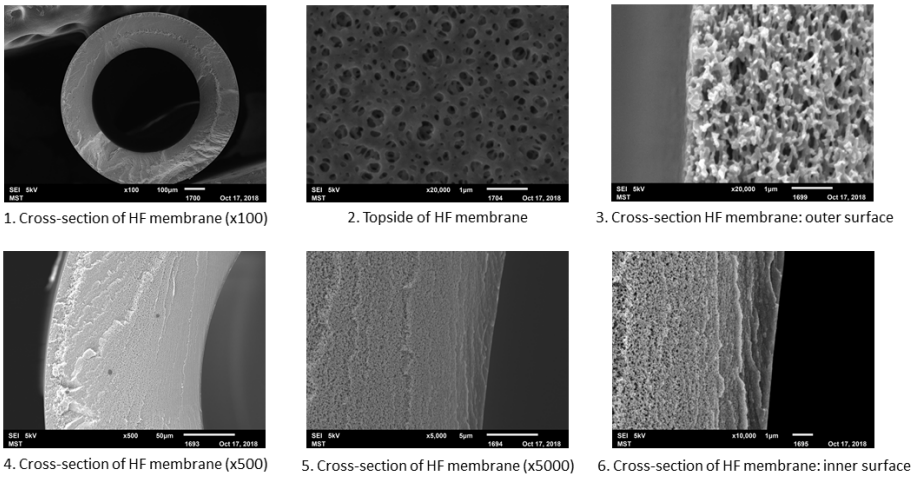

Figure C.1: SEM images showing morphology of the bare SPES HF membranes.

In Figure C.2, we show SEM images of the fiber before and after coating with $(PAH/PSS)_{4.5}$ and crosslinked for 5h in glutaraldehyde.

While some differences in the SEM pictures can be observed, a clear PEM

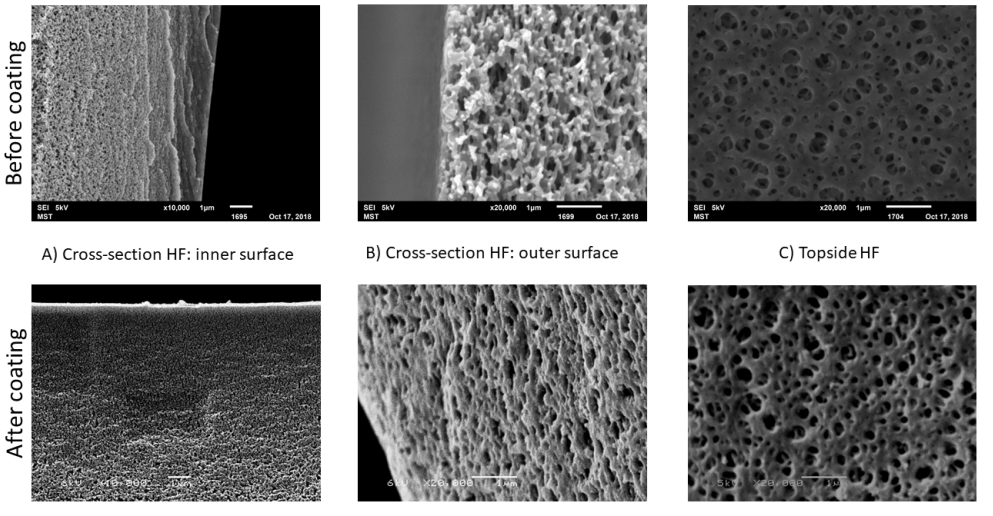

Figure C.2: SEM images showing morphology of the SPES HF membranes before and after coating with crosslinked $(PAH/PSS)_{4.5}$

is not seen. The layer is too thin to be observed in this fashion. Still this is a relevant outcome as the thin coating is exactly why polyelectrolyte multilayers are so promising for membrane applications.

Appendix D

D.1 NMR

In Figure D.1 we show the ^{1}H NMR (400Hz) of poly(2-Methacryloyloxyethyl phosphorylcholine-co-acrylic acid) (PMPC-co-AA) in D_2O. Peak 1 (δ 3.25, 9H), 2 (δ 3.69 2H), and 3 (δ 4.11-4.33, 6H) are part of the MPC side chain, while the peaks at 4 (δ 0.9-2.5, 9H) are part of the backbone. Since D_2O was used a solvent, the proton of the carboxylic acid group could not be observed. Therefore the ratio of MPC:AA was estimated based on the ratio between the MPC side chain and the backbone of the polymer resulting in an approximate ratio of 1:2 MPC:AA.

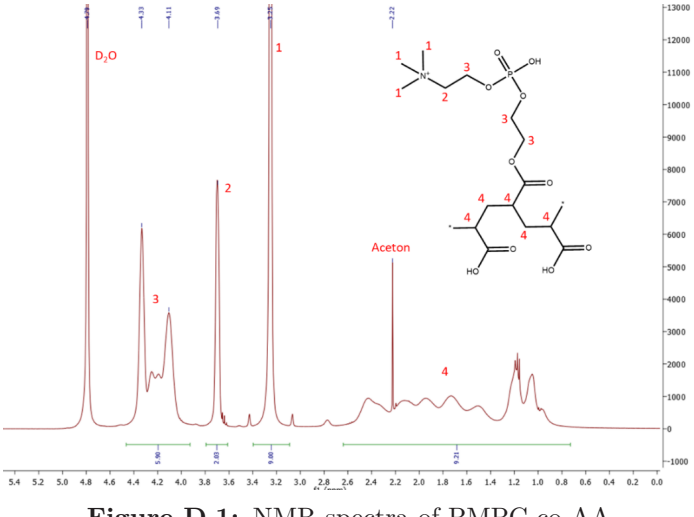

Figure D.1: NMR spectra of PMPC-co-AA.

Figure D.2: Picture of the experimental set-up (front-view).

D.2 Water permeability measurements

For water permeability and ion retention experiments, single PEM-coated fibers were potted in a module with a fiber length of approximately 170 mm and mounted in our crossflow experimental set-up, shown in Figure D.2 and Figure D.3.

The water permeability (LMH/bar) in was calculated by normalizing the measured pure water flux with the transmembrane pressure (TMP). The pure water flux was measured at room temperature with demi water in a cross-flow configuration at a transmembrane pressure of 3 bar. All experiments were performed at least in triplicate. The results of the water permeability measurements are reported in Figure D.4.

D.3 Membrane zeta-potential measurements

For the determination of the membrane zeta-potential, the coated hollow fiber membranes were potted into a module and the zeta potential was measured with an electrokinetic analyzer SurPASS (Anton Paar, Graz Austria). The zeta potential is calculated by measuring the streaming current versus the pressure in a 5 mM KCl solution at room temperature using the following equation

$$\zeta = \frac{dI}{dP} \cdot \frac{\eta}{\epsilon \cdot \epsilon_0} \cdot k_B \cdot R, \tag{D.1}$$

where ζ is de zeta potential (V), I is the streaming current (A), P is the

Figure D.3: Picture of the experimental set-up (top-view).

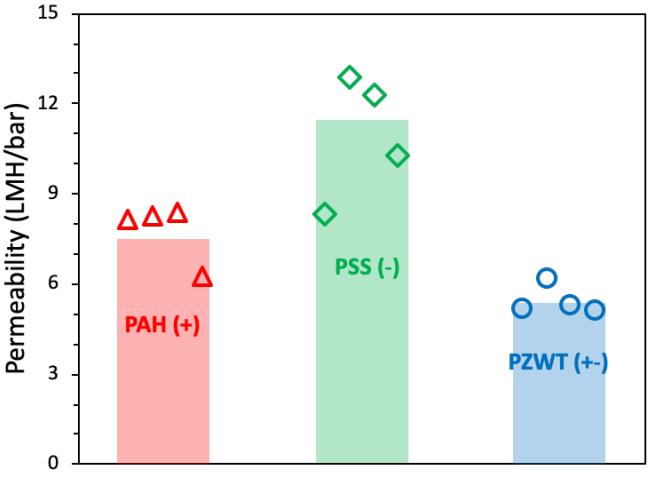

Figure D.4: Membrane permeability (LMH/bar) for hollow fiber membranes based on $(PAH/PSS)_{4.5}$ coated with three different top layers: PAH, PSS and PZWT. Points represent single data points, while bars represent the average of these points.

pressure (Pa), η is the dynamic viscosity of the electrolyte solution (Pa·s), ϵ is the dielectric constant of the electrolyte (-), ϵ_0 is the vacuum permittivity ($F \cdot m^{-1}$), k_B bulk electrolyte conductivity ($S \cdot m^{-1}$), and R is the electrical resistance (Ω) inside the streaming channel. The results of the zeta-potential for the different coatings are shown in Figure D.5.

D.4 Irreversibility in adsorption and membrane fouling

In order to determine the amount of irreversible and reversible fouling for every single fouling agent, both wafers and membranes, when fouled, were flushed with a rinsing solution with the same pH and ionic concentration as the fouling solution. We defined as irreversible fouling the amount of foulant (in percentage) still adsorbed on the PEM and the unrecovered water permeability, after flushing, respectively for reflectometry and membranes experiments. In Figure D6 we show for all the experiments (colloidal silica excluded) carried out in paragraphs 6.3.1 and 6.3.2, the irreversibility in filtration (%), i.e. irreversible flux decline, as a function of irreversibility in adsorption (%) measured via reflectometry. In Table D.1 we show all the results from paragraphs 6.3.1 and 6.3.2.

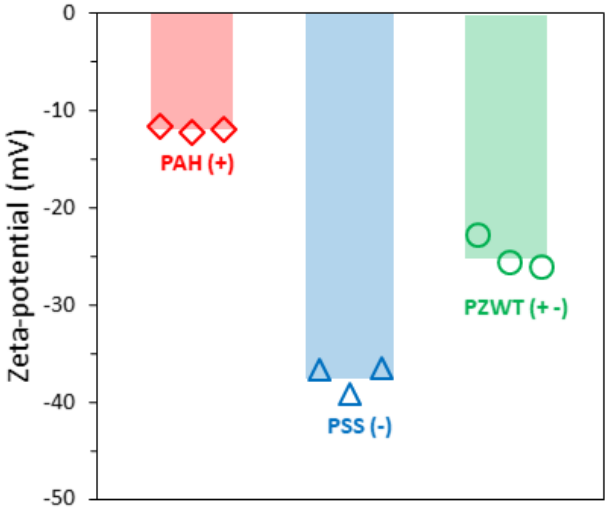

Figure D.5: Membrane zeta-potential (mV) for hollow fiber membranes based on $(PAH/PSS)_{4.5}$ coated with three different top layers: PAH, PSS and PZWT. Points represent single data points, while bars represent the average of these points.

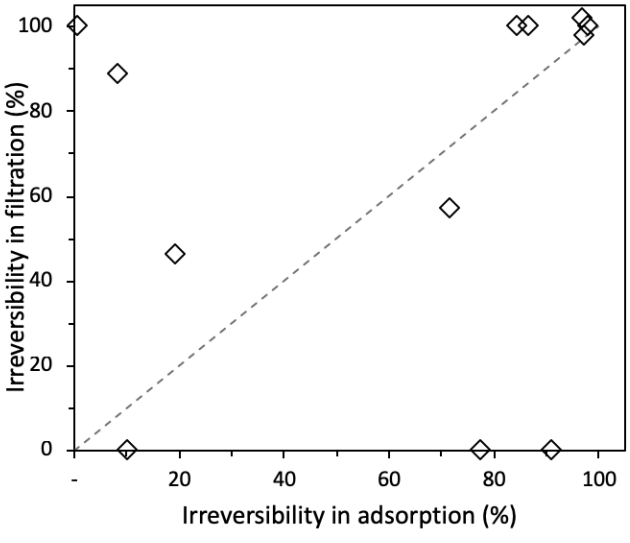

Figure D.6: Irreversibility in filtration (%), i.e. irreversible flux decline, as a function of irreversibility in adsorption (%) measured via reflectometry for different foulants (Alginate, Lysozyme, LUDOX colloidal silica, Humic Acids and BSA) and different final layers (PMPC-co-AA, PAH and PSS).

Foulant	Layer	Reflectometry (%)	Filtration (%)
Alginate	PMPC-co-AA	0.94	100.0
Lysozyme	PAH	8.56	88.6
Lysozyme	PMPC-co-AA	10.38	0.0
Alginate	PSS	19.29	46.1
LUDOX	PSS	38.76	0.0
HA	PAH	71.77	57.2
BSA	PMPC-co-AA	77.63	0.0
HA	PSS	84.59	100.0
Lysozyme	PSS	86.79	100.0
HA	PMPC-co-AA	91.23	0.0
LUDOX	PAH	94.01	0.0
Alginate	PAH	96.83	100.0
BSA	PAH	97.41	100.0
LUDOX	PMPC-co-AA	98.06	0.0
BSA	PSS	98.05	100.0

Table D.1: Data for irreversibility in Reflectometry (adsorption, %) and Filtration (Flux decline) for different foulants (Alginate, Lysozyme, LUDOX colloidal silica, Humic Acids and BSA) and different final layers (PMPC-co-AA, PAH and PSS).

D.5 Filtration of Alginate from Brown Algae

In Figure D.7 we show the results of our filtration experiments with synthetic surface water, where Alginate is the only foulant. In particular,in Figure D.7A, D.7C and D.7E, we show retentions of Ca^{2+}, Na^{+}, Mg^{2+}, SO_4^{2-}, Cl^{-} and Alginate from membranes coated with PAH, PSS and PZWT final layers, respectively. In Figure D.7B, D.7D and D.7F we show the remaining membrane flux after fouling and flux recovery after cleaning PAH, PSS and PZWT, respectively.

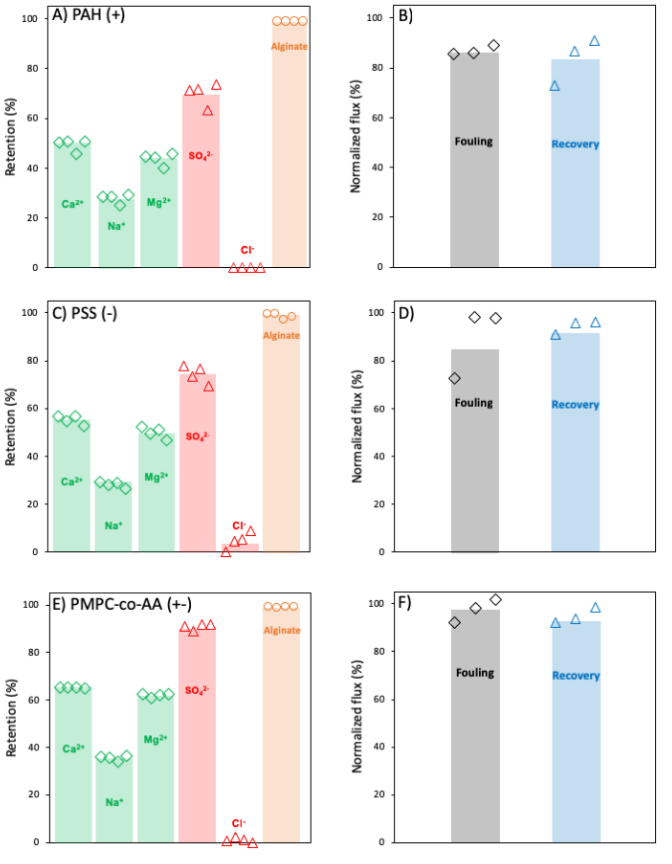

Figure D.7: Retentions of Ca^{2+}, Na^{+}, Mg^{2+}, SO_4^{2-}, Cl^{-} and Alginate from membranes coated with A) PAH, C) PSS and E) PZWT top layers in experiments performed with synthetic surface water. Remaining membrane flux after fouling and flux recovery after cleaning are also shown for B) PAH, D) PSS and F) PZWT. The synthetic surface water was made of 2.92 mM NaCl, 0.57 mM $MgSO_4$, 1.47 mM $CaSO_4$, 0.3 mM $MgCl_2$ and 100 mg/L of Alginate. Points represent single data points, while bars represent the average of these points.

Appendix E

E.1 NMR

In Figure E.1 we show the ^{1}H NMR (400Hz) of of poly(SBMA-co-AA) in D_2O. The ratio of the two monomers, SBMA and AA, was found to be 10:1. This ratio was estimated by comparing the integrals of peak *e* (for SBMA) and peak *a*' (for AA). The ^{1}H NMR also shows that a contamination with ethanol is present (see in particular peak *a*).

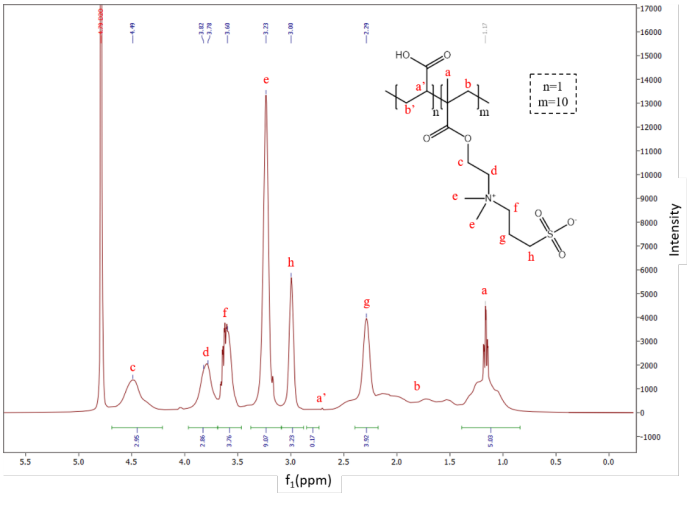

Figure E.1: ^{1}H NMR spectra of PSBMA-co-AA.

E.2 Water permeability measurements

The water permeability (LMH/bar) was calculated by normalizing the measured pure water flux with the transmembrane pressure (TMP). The pure water flux was measured at room temperature with demineralized water in a crossflow configuration at a transmembrane pressure of 3 bar. All experiments were performed at least 15 times. The results of the water permeability measurements are reported in Figure E2.

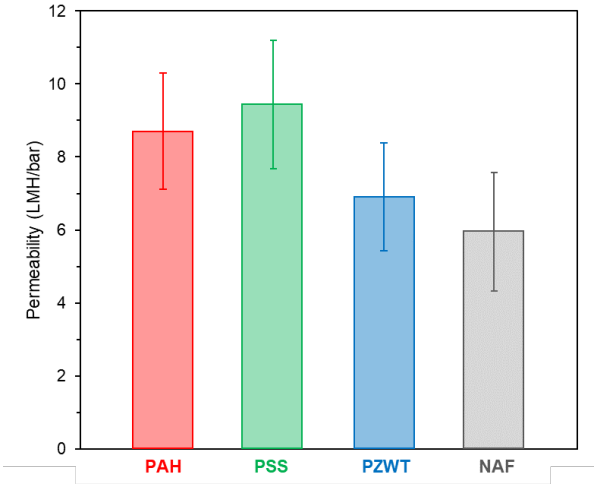

Figure E.2: Membrane permeability (LMH/bar) for hollow fiber membranes based on $(PAH/PSS)_{4.5}$ coated with four different top layers: PAH, PSS, PZWT, and Nafion.

E.3 Membrane zeta-potential measurements

For the determination of the membrane zeta-potential, the coated hollow fiber membranes were potted into a module and the zeta potential was measured with an electrokinetic analyzer SurPASS (Anton Paar, Graz Austria). The zeta potential is calculated by measuring the streaming current versus the pressure in a 5 mM KCl solution at room temperature using the following equation

$$\zeta = \frac{dI}{dP} \cdot \frac{\eta}{\epsilon \cdot \epsilon_0} \cdot k_B \cdot R, \tag{E.1}$$

where ζ is de zeta potential (V), I is the streaming current (A), P is the

pressure (Pa), η is the dynamic viscosity of the electrolyte solution (Pa·s), ϵ is the dielectric constant of the electrolyte (-), ϵ_0 is the vacuum permittivity ($F \cdot m^{-1}$), k_B bulk electrolyte conductivity ($S \cdot m^{-1}$), and R is the electrical resistance (Ω) inside the streaming channel. The results of the zeta-potential for the different coatings are shown in Figure E.3.

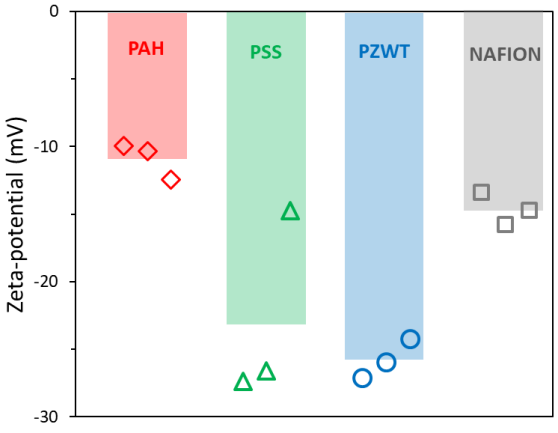

Figure E.3: Membrane zeta-potential (mV) for hollow fiber membranes based on $(PAH/PSS)_{4.5}$ coated with four different top layers: PAH, PSS, PZWT, and Nafion. Markers represent single data points, while bars represent the average of these points.

E.4 Salt retention

Salt retention was determined by performing 1-hour cross-flow experiments at the same TMP and temperature conditions as before with 5 mM solutions of four different salts, namely NaCl, $CaCl_2$, Na_2SO_4, and $MgSO_4$. The results of the retention test are shown in Figure S4 for PAH, PSS, PSBMA-co-AA, and Nafion top layers. Four fibers were tested at a time to obtain at least a triplicate set of results for each experiment.

E.5 Surfactant adsorption: irreversibility and isotherms

To determine the amount of irreversible and reversible fouling for every single fouling agent, wafers, when fouled, were flushed with a rinsing solution with the same pH and ionic concentration as the fouling solution. We defined as

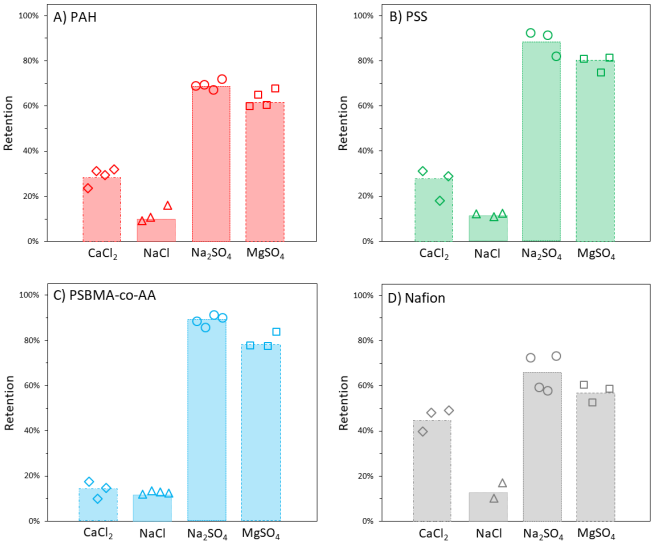

Figure E.4: Retention of $CaCl_2$, NaCl, Na_2SO_4, and $MgSO_4$ for hollow fiber membranes based on $(PAH/PSS)_{4.5}$ coated with A) PAH, B) PSS, C) PSBMA-co-AA and D) Nafion. Markers represent single data points, while bars represent the average of these points

Top layer	Surfactant	Reflectometry (%)
PAH	CTAB	4.3
PAH	SDS	100
PAH	DDAPS	100
PAH	TX	0
PSS	CTAB	12.5
PSS	SDS	100
PSS	DDAPS	0
PSS	TX	62.9
PSBMA-co-AA	CTAB	7.3
PSBMA-co-AA	SDS	100
PSBMA-co-AA	DDAPS	100
PSBMA-co-AA	TX	100
Nafion	CTAB	34.8
Nafion	SDS	100
Nafion	DDAPS	12.5
Nafion	TX	52

Table E.1: Irreversibility in adsorption (%) measured via reflectometry on model surfaces for different surfactants (SDS, CTAB, DDAPS, and TX) and top layers (PAH, PSS, PSBMA-co-AA, and Nafion).

irreversible fouling the amount of foulant (in percentage) still adsorbed on the PEM after flushing. In Table E.1 we show for all the experiments the irreversibility in adsorption (%) measured as a function of the surfactant used for model surfaces coated with different top layers.

Additionally, we measured adsorption isotherms for SDS and CTAB on $(PAH/PSS)_{4.5}$ model surfaces and report the results in Figure E.5. We here report the relative adsorption, in comparison to the value at CMC, for SDS and CTAB at the following concentrations of surfactant: 0.01, 0.1, 0.25, 0.5 and 1 times CMC. The surfactant adsorption was corrected when, in some cases, small amount of PEM was desorbed.

E.6 6. Ions and oil retention during filtration of artificial PW

We measured ions (Na^+ and Cl^-) and oil retention during our fouling experiments with artificial PW, respectively via ion chromatography (Metrohm Compact IC 761) and spectrophotometer (Perkin Elmer Victor3^{TM} V 1420 Multilabel Counter), and reported the values in tables E.2-E.5. The artificial PW filtrated by our PEM-coated fibers was prepared by mixing 1 g/L of n-hexadecane in a solution containing 100 mM NaCl and an amount of surfactant equivalent to 1/10 of its critical micelle concentration at 0 salt (CMC),

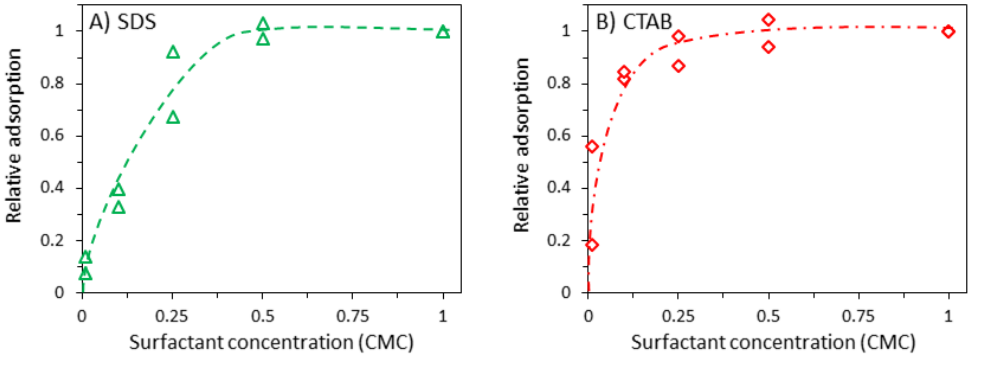

Figure E.5: Isotherms of adsorption of A) SDS and B) CTAB. Markers represent single data points, while lines follow the average of these points.

Top layer	Na^+ retention	Cl^- retention	Oil retention
PAH	12.2 ± 1.1%	11.8 ± 1.1%	99.6 ± 0.1%
PSS	9.9 ± 0.5%	10.1 ± 0.3%	99.0 ± 0.4%
ZWT	11.0 ± 1.0%	10.7 ± 1.7%	99.9 ± 0.1%
NAF	9.8 ± 1.3%	8.0 ± 1.4%	99.7 ± 0.2%

Table E.2: Retention of Na^+, Cl^-, and oil (n-hexadecane) during the filtration of artificial PW (1000 ppm oil, 100 mM NaCl, 239.1 mg/L SDS) for hollow fiber membranes based on $(PAH/PSS)_{4.5}$ coated with PAH, PSS, PSBMA-co-AA and Nafion.

which corresponds to 34.6 mg/L for CTAB, 239.1 mg/L for SDS, 100.6 mg/L for DDAPS and 14.4 mg/L for Triton-X.

Top layer	Na^+ retention	Cl^- retention	Oil retention
PAH	16.6 ± 0.6%	17.4 ± 0.5%	100%
PSS	17.3 ± 0.2%	17.6 ± 0.1%	100%
ZWT	15.2 ± 1.0%	16.2 ± 0.8%	100%
NAF	15.4 ± 0.5%	16.3 ± 0.3%	100%

Table E.3: Retention of Na^+, Cl^-, and oil (n-hexadecane) during the filtration of artificial PW (1000 ppm oil, 100 mM NaCl, 34.6 mg/L CTAB) for hollow fiber membranes based on $(PAH/PSS)_{4.5}$ coated with PAH, PSS, PSBMA-co-AA and Nafion.

Top layer	Na^+ retention	Cl^- retention	Oil retention
PAH	6.3 ± 1.5%	5.0 ± 0.4%	100%
PSS	5.0 ± 0.7%	5.3 ± 0.8%	100%
ZWT	6.3 ± 1.0%	5.4 ± 0.9%	100%
NAF	8.2 ± 1.0%	8.3 ± 1.2%	100%

Table E.4: Retention of Na^+, Cl^-, and oil (n-hexadecane) during the filtration of artificial PW (1000 ppm oil, 100 mM NaCl, 100.6 mg/L DDAPS) for hollow fiber membranes based on $(PAH/PSS)_{4.5}$ coated with PAH, PSS, PSBMA-co-AA and Nafion.

Top layer	Na^+ retention	Cl^- retention	Oil retention
PAH	5.7 ± 0.8%	6.4 ± 0.8%	99.1 ± 0.3%
PSS	5.1 ± 0.7%	6.5 ± 0.7%	99.9 ± 0.1%
ZWT	5.5 ± 1.5%	6.0 ± 0.6%	100%
NAF	8.6 ± 0.3%	9.0 ± 0.6%	99.5 ± 0.4%

Table E.5: Retention of Na^+, Cl^-, and oil (n-hexadecane) during the filtration of artificial PW (1000 ppm oil, 100 mM NaCl, 14.4 mg/L TX) for hollow fiber membranes based on $(PAH/PSS)_{4.5}$ coated with PAH, PSS, PSBMA-co-AA and Nafion.

O/W emulsion	Flux recovery (%)	SD (%)
SDS-PAH	72.9	4.8
CTAB-PAH	97.3	3.8
DDAPS-PAH	84.1	3.6
TX-PAH	95.5	3.5
SDS-PSS	84.0	3.1
CTAB-PSS	71.7	1.7
DDAPS-PSS	78.4	2.1
TX-PSS	95.4	3.8
SDS-PSBMA-co-AA	88.5	1.0
CTAB-PSBMA-co-AA	100.0	0.0
DDAPS-PSBMA-co-AA	99.5	0.8
TX-PSBMA-co-AA	100.0	0.0
SDS-Nafion	78.6	1.5
CTAB-Nafion	100.0	0.0
DDAPS-Nafion	84.0	4.3
TX-Nafion	88.9	7.9

Table E.6: Average of flux recovery (%) and SD (%) of nearly uncharged PAH, negatively PSS, zwitterionic PSBMA-co-AA and negatively hydrophobic Nafion membranes for every different set of fouling experiments with O/W emulsions for SDS, CTAB, DDAPS and TX.

Single Surfactant	Flux recovery (%)	SD
SDS-PAH	88.6	0.9
CTAB-PAH	100.0	0.0
DDAPS-PAH	96.2	2.7
TX-PAH	97.3	2.0
SDS-PSS	90.7	1.1
CTAB-PSS	95.4	2.0
DDAPS-PSS	91.5	2.6
TX-PSS	87.9	4.3
SDS-PSBMA-co-AA	100.0	0.0
CTAB-PSBMA-co-AA	100.0	0.0
DDAPS-PSBMA-co-AA	100.0	0.0
TX-PSBMA-co-AA	100.0	0.0
SDS-Nafion	81.9	0.7
CTAB-Nafion	100.0	0.0
DDAPS-Nafion	86.0	8.4
TX-Nafion	91.6	4.9

Table E.7: Average of flux recovery (%) and SD (%) of nearly uncharged PAH, negatively PSS, zwitterionic PSBMA-co-AA and negatively hydrophobic Nafion membranes for every different set of fouling experiments with only surfactant solutions for SDS, CTAB, DDAPS and TX.

E

Appendix F

F.1 Adsorption model

With the adsorption model, the interaction of divalent cation with the negative functional groups of the polyamide (PA) top layer is considered. The carboxylic groups in the membrane are negatively charged, which allows the positive divalent ions to bind. This binding phenomena influences the net membrane charge. To derive the change of the membrane charge due to cation adsorption, we first consider the stoichiometry

$$R^- + \beta A^{z+} \underset{k_{-1}}{\overset{k_1}{\rightleftharpoons}} RA^{(z\beta-1)} \tag{F.1}$$

where R^- is the concentration of fixed carboxylic groups, A any cation, z the valency, k the rate constants, and β represents the number of cations that bind with each carboxylic group. The only interaction we implemented in our model is the one between the divalent cation, c^{2+}, and the carboxylic groups, and thus $A = c^{2+}$. Assuming chemical equilibrium, we obtain

$$\left[Rc^{(2\beta-1)}\right] = \frac{k_1}{k_{-1}} \left[R^-\right] \left[c^{2+}\right]. \tag{F.2}$$

Now, assuming that the number of carboxylic groups in the membrane is constant, we have

$$X_0 = \left[R^-\right] + \left[Rc^{(2\beta-1)}\right] \tag{F.3}$$

where X_0 is the total initial concentration of carboxylic groups in the membrane. Further, we describe the charge density inside the membrane according

to

$$X = -\left[R^-\right] + (2\beta - 1)\left[Rc^{(2\beta-1)}\right]. \tag{F.4}$$

We also need to define the binding constant

$$K_b = \frac{k_1}{k_{-1}}. \tag{F.5}$$

By substituting Eqs. F.2, F.3 and F.5 into Eq. F.4, the charge density inside the membrane can be derived as

$$X = X_0 \frac{-1 + (2\beta - 1)K_b\left[c^{2+}\right]}{1 + K_b\left[c^{2+}\right]}. \tag{F.6}$$

In Eq. F.6, β is the number of c^{2+} ions interacting with one carboxylic group. If the interaction is 1:1 this equation results in the adsorption model reported in the main text of this study. To compare the effect of β in the model results, we evaluated the model for the case there is a 1:2 adsorption ratio between $c^{2+} = Ca^{2+}$ and the carboxylic groups ($\beta = 0.5$). The results of this case are given in Fig F.1. It is important to mention that with $\beta = 0.5$ there is no charge reversal. Instead, at high enough Ca^{2+} concentration, the membrane closely approaches the zero-charge point.

F

F.2 Experimental data used in the model

In this study, experimental data reported in literature is used to demonstrate that mean field theory is still valid predict the puzzling behavior of complex mixtures, and to stress that counterion adsorption might affect the rejection of ions. Particularly, in this section, we describe the experimental protocol, methods and conditions used to produce and collect the data by Fridman et al.

Two cross-flow cells in series, both containing a flat sheet of NF270 (DOW), were assembled together with a spacer mesh from Toray TM820R-440. The retentate was continuously recirculated to the feed tank. Because the permeate flow was much lower than the feed flow rate, any change in feed composition was neglected. To avoid pH changes due to CO_2 dissolution, the feed was constantly purged with N2 and the temperature of the feed was kept constant at 25°C. The experiments were performed with water velocity through the membrane $v_F = 1.5s^{-1}$ and under two main conditions, both with Cl^-as reference ion. The first set of experiments was conducted with total Cl^-

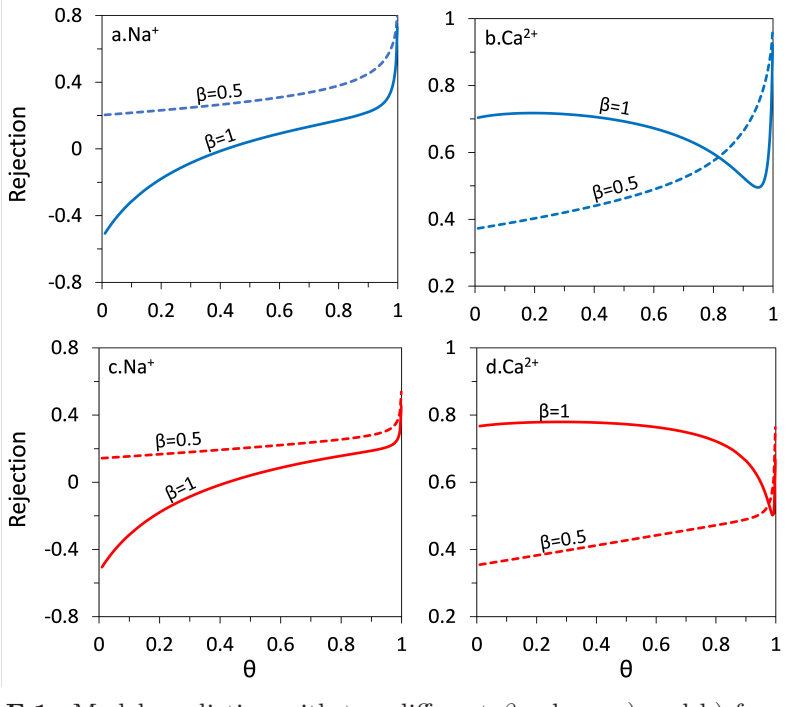

Figure F.1: Model prediction with two different β values, a) and b) for a solution with 100 mM Cl^- ions, c) and d) for a solution with 500 mM Cl^- ions.

concentration of 100 mM while the second one with 500 mM. For each of these solutions, the equivalent Na^+ fraction, θ, was varied.

F.3 Nelder-Mead calculation

Here, we explain the general procedure that we used to obtain the actual fit of our model to the data, as compared in Fig 8.3 of the main text. We used a 1:1 adsorption ratio between Ca^{2+} and the negative fixed charge in the membrane. Different calculation where made during the study, some of them to find initial guesses that could help us to find the final fit.

In the first calculation, we used only four experimental points. The experimental points were taken from the data with 100 mM Cl^- ions and correspond to the Ca^{2+} and Na^+ rejection at high and low θ values (0.8 and 0.2). In this calculation, we found four parameters, the partitioning coefficient Φ, the binding constant that represents the adsorption of Ca^{2+}, and the efficiency factor for diffusion ζ. Note that in this calculation all the ions where assumed to have the same efficiency factor associated with their diffusion coefficients. Finally, the membrane charge density X_0. In the NM procedure, this last parameter tends to decrease gradually (to lower values than 50 mM), and for this reason we fixed its value at X0=400 mM. To make sure realistic values are obtained, the allowable values for Φ were limited to be in the range $0.1 < \Phi < 1$. After trying different guesses and run the Nelder-Mead (NM) code different times, we found that our results predict some of the points and follow the trends of the experimental data. However, we saw the largest discrepancy was in the limits $\theta \approx 0$ and $\theta \approx 1$.

Next, we did a second calculation. In this calculation we removed X_0 from the model parameters and we allowed to code to adjust the parameter ζ_i for each ion separately. Hence, this NM-procedure was used to calculate five model parameters. From this calculation, the fit for the solution with 100 mM Cl^- ions was satisfactory. Nevertheless, for the solution with 500 mM Cl^- ions, the prediction for Ca^{2+} was not sufficiently accurate.

To further improve the fit for the solution with higher Cl^- concentration, we tried to fit both cases, 100 and 500 mM, simultaneously. This implies that eight point were used to fit the same five parameters. Again, the initial guesses came from the previous calculation. With this last NM calculation, we could improve the prediction of the experimental data to an accurate degree. The results from this last calculation are provided in Table 8.2, Case I.

Summary

The effective treatment of complex industrial wastestreams such as produced water (PW) is important to ensure clean water in a world where water scarcity is becoming increasingly problematic. Membranes can play an essential role in this process, but membrane fouling remains a major problem. In **Chapter 1**, we propose that surface chemistry plays a key role in PW treatment, and that control over the surface chemistry of both the emulsion and the membrane can substantially alleviate fouling.

As surface interactions are critical in PW treatment with **Porous Membranes**, it is important to control the surface chemistry of the major fouling agent, the oil droplets, by carefully choosing its stabilizer, i.e. the surfactant. In **Chapter 2**, we study the relation between surfactant type and the effect of the ionic strength on membrane filtration of an artificial produced water emulsion. As surfactants, we use anionic sodium dodecyl sulphate (SDS), cationic hexadecyltrimethylammonium bromide (CTAB), nonionic Triton ™ X-100 (TX) and zwitterionic N-dodecyl-N,N-dimethyl-3-ammonio-1-propanesulfonate (DDAPS), at various ionic strengths (1, 10, 100 mM NaCl). Filtration experiments on a regenerated cellulose ultrafiltration (UF) membrane showed a pronounced effect of the ionic strength for the charged surfactants SDS and CTAB, although the nature of the effect was quite different. For anionic SDS, an increasing ionic strength leads to less droplet-droplet repulsion, allowing a denser cake layer to form, resulting in a much more pronounced flux decline. CTAB, on the other hand leads to a lower interfacial tension than observed for SDS, and thus more deformable oil droplets. At high ionic strength, increased surfactant adsorption leads to such a low oil-water surface tension that the oil droplets can permeate through the much smaller membrane pores. For the nonionic surfactant TX, no clear effect of the ionic strength was observed, but the flux decline is very high compared to the other surfactants. For the zwitterionic surfactant DDAPS, the flux decline was found to be very low and even decreased with increasing ionic strength, suggesting

that membrane fouling decreases with increasing ionic strength. Especially promising is that at lower surfactant concentration (0.1 CMC) and high ionic strength no flux decline was observed, while a high oil retention (85%) was obtained. In **Chapter 3**, membrane fouling and oil retention of synthetic PW stabilized with the same cationic, anionic, zwitterionic and nonionic surfactant of Chapter 2, were studied at various surfactant and salt concentrations for a microfiltration (MF) silicon carbide (SiC) membrane. Here, we discuss our results in the framework of the Young-Laplace (YL) equation, which predicts for a given membrane, pressure and oil-membrane contact angle, a critical interfacial tension (IFT) below which oil permeation should occur. We observe such a transition from high to low oil retention with decreasing IFT for the anionic (SDS), cationic (CTAB) and non-ionic (TX) surfactant, but at significantly higher critical IFTs than predicted by YL. On the other side, for the zwitterionic DDAPS we do not observe a drop in oil retention, even at the lowest IFT. The discrepancy between our findings and the critical IFT predicted by YL can be explained by the difference between the measured contact angle and the effective contact angle at the wall of the membrane pores. This leads to a surfactant-dependent critical IFT. Additionally, our results point out that zwitterionic surfactants even at the lowest IFT did not present a critical IFT and exhibited low fouling and low oil permeation. In **Chapter 4**, we present a quantitative model that describes cake layer formation and pore blocking for the typical situation where emulsion oil droplets are much larger than the membrane pore size. Here the degree of pore blocking is determined by the membrane contact angle and the resulting surface coverage, while the cake layer is described via a mass balance and the presence of a cake erosion flux. The model is validated by comparison to experimental data from Chapters 2 and 3, where membrane type, surfactant type and salinity were varied. Most input parameters could be directly taken from the experimental conditions, while only 4 fitting parameters were required. The experimental data can be well described by the model, using a very limited number of fitting parameters, providing insight into the dominant fouling mechanism. Moreover, where existing models usually assume that pore blocking precedes cake layer formation, here we find that cake layer formation can start and occur while the degree of pore blocking is still increasing, in line with the more dynamic nature of oil droplets.

On the other hand, polyelectrolyte multilayers (PEMs) allow a very nice approach to control the membrane properties of **Dense Membranes**, including the membrane surface chemistry. Unfortunately, the presence of surfactants

in PW can affect the stability of polyelectrolyte multilayers. In **Chapter 5**, we investigate the stability of polyelectrolyte multilayers towards different types of surfactant, initially on model surfaces. We find that chemically stable multilayers, such as Poly(diallyldimethylammonium chloride)(PDADMAC)/Poly(sodium 4-styrene sulfonate)(PSS), based only on electrostatic interactions, are substantially desorbed by charged surfactants. For Poly(allylamine hydrochloride)(PAH)/PSS multilayers, however, we demonstrate that chemical crosslinking by glutaraldehyde, leads to surfactant stable layers. These stable PEM coatings can also be applied on hollow fiber support membranes to create hollow fibre nanofiltration (NF) membranes dedicated for PW treatment. Increased crosslinking time leads to more stable and more selective separation performance. These newly developed membranes were subsequently studied for the treatment of synthetic PW, consisting of freshly prepared oil-in-water emulsions stabilized by cationic CTAB and anionic SDS, in the presence of a mixture of ions. For both types of produced water, the membranes showed excellent oil removal ($\sim 100\%$) and organics removal (TOC reduced up to $\sim 97\%$) as well as good divalent ion retentions ($\sim 75\%$ for Ca^{2+} and up to $\sim 80\%$ for SO_4^{2-}). Moreover, we observed a high flux recovery for both emulsions (100% for CTAB and 80% for SDS), with especially for the CTAB emulsion a very low degree of fouling. In **Chapter 6**, we investigate the effect of membrane surface chemistry on fouling in surface water treatment for polyelectrolyte multilayer based NF membranes. The polyelectrolyte multilayer approach allows us to prepare three membranes with the same active separation layer, apart from a difference in surface chemistry: nearly uncharged crosslinked PAH, strongly negative PSS and zwitterionic poly(2-methacryloyloxyethyl phosphorylcholine-co-acrylic acid) (PMPC-co-AA). Initially, we studied foulant adsorption for the three different surfaces (on model interfaces), to demonstrate how a different surface chemistry of the top layer affects the subsequent adsorption of five different model foulants (Humic Acids, Alginates, Silica Nanoparticles, negatively and positively charged Proteins). Subsequently, we study fouling of the same model foulants on our polyelectrolyte multilayer based hollow fiber NF membranes with identical surface chemistry to the model surfaces. Our results show that the nearly uncharged crosslinked PAH surface generally fouls more than the strongly negatively charged PSS surface. Overall, fouling was mainly driven by electrostatic and acid-base interactions, which led, for both PAH and PSS terminated membranes, to flux decline and changes in selectivity. In contrast, we demonstrate through filtration experiments carried out with synthetic and real surface wa-

ter, that the bio-inspired zwitterionic phosphatidylcholine surface chemistry exhibits excellent fouling resistance and thus stable performance during filtration. Then, in **Chapter 7**, we investigate the effect of surface chemistry on fouling of PEM-based NF membranes, during the treatment of artificial produced water. To this end, oil-in-water (O/W) emulsions stabilized with four different surfactants (anionic, cationic, zwitterionic and non-ionic) were treated with PEM-based NF membranes having the same multilayer, but different top layer polymer chemistry: PAH (nearly uncharged), PSS (strongly negative), poly(sulfobetaine methacrylate-co-acrylic acid) (PSBMA-co-AA, zwitterionic) and Nafion (negative and hydrophobic). Very high oil retention (>99%) was observed when filtering all the O/W emulsions, while the physicochemical interactions between the multilayer and the surfactants determined the extent of fouling as well as the surfactant retention. Unexpectedly, our results show that fouling of PEM-based NF membranes, during PW treatment, is mainly due to membrane active layer fouling caused by surfactant uptake inside of the PEM coating, rather than due to cake layer formation. Indeed, it is not the surface chemistry of the membrane that determines the extent of fouling, but the surfactant interaction with the bulk of the PEM.

Interfacial Phenomena play a critical role in many different fields, from membrane filtration to the design of energy harvesters. In NF, the solution and membrane chemistry determine the charge of the membrane, and therefore the electrostatic repulsion of ions. Membrane charge reversal can take place when divalent ions bind to the membrane and modify its surface charge, which may explain some puzzling results, where the rejection of divalent ions increases with higher concentration in the feed. In **Chapter 8**, by using a Langmuir equation with two model parameters, we consider the adsorption of divalent ions (e.g. Ca^{2+} and Mg^{2+}) in the polyamide (PA) active layer of the membrane and describe how this adsorption process affects membrane charge. Based on experimental data from two different studies we show that mean-field theory can predict the rejection of all types of ions in a multi-component electrolyte solution when the effect of divalent counterions on the membrane charge is included. These results provide evidence that adsorption of counterions plays a fundamental role in the performance of nanofiltration. In **Chapter 9**, we present a novel theory to predict the contact angle of water on amphoteric surfaces, as a function of pH and ionic strength. To validate our theory, experiments were performed on two commonly used amphoteric materials, alumina (Al_2O_3) and titania (TiO_2). We find good agreement at all pH values, and at different salt concentrations. With increasing salt concentration, the

theory predicts the contact angle-pH curve to get steeper, while keeping the same contact angle at pH = PZC (point of zero charge), in agreement with data. Our model is based on the amphoteric 1-pK model and includes the electrostatic free energy of an aqueous system as well as the surface energy of a droplet in contact with the surface. In addition, we show how our theory suggests the possibility of a novel responsive membrane design, based on amphoteric groups. At pH $\sim$ PZC, this membrane resists flow of water but at slightly more acidic or basic conditions the wettability of the membrane pores may change sufficiently to allow passage of water and solutes. Moreover, these membranes could act as active sensors that only allow solutions of high ionic strength to flow through in waste water treatment. In **Chapter 10**, we work on a novel mechanism to harvest energy from mechanical fluctuations by using coiled carbon nanotube yarns coated with polyelectrolyte gel. We develop a new theory and present a theoretical framework to explain how this new kind of energy harvesting is possible. The gel fills up all space between the coils and expands when the yarn is stretched. This translates into a change in electrical double layer configuration, hence into a change in electrical potential. This makes it possible to electrochemically convert tensile or torsional mechanical energy into electrical energy. The influence of the yarn surface charge, polyelectrolyte charge density and salt concentration was analyzed, giving directions for optimum process design. We analyzed the generated power of a system consisting of two yarns coated with positive and negative polyelectrolyte gel.

To conclude, in **Chapter 11**, with the obtained knowledge from the different chapters, the main outcomes of this thesis are revisited, and the future challenges of PEM-based membranes for PW treatment and other applications are addressed.

Samenvatting

De effectieve behandeling van complexe industriële afvalstromen zoals geproduceerd water (GW) is belangrijk om te zorgen voor schoon water in een wereld waar waterschaarste steeds problematischer wordt. Membranen kunnen een essentiële rol spelen in dit proces, maar membraanvervuiling blijft een groot probleem. In **Hoofdstuk 1** stellen we voor dat oppervlaktechemie een sleutelrol speelt bij de behandeling van GW, en dat controle over de oppervlaktechemie van zowel de emulsie als het membraan vervuiling aanzienlijk kan verminderen.

Aangezien oppervlakte-interacties van cruciaal belang zijn bij de behandeling van GW met **Poreuze Membranen**, is het belangrijk om de oppervlaktechemie van het belangrijkste vervuilingsmiddel, de oliedruppeltjes, te beheersen door zorgvuldig de stabilisator, d.w.z. de oppervlakteactieve stof, te kiezen. In **Hoofdstuk 2** bestuderen we de relatie tussen het type oppervlakteactieve stof en het effect van de ionsterkte op membraanfiltratie van een kunstmatig geproduceerde wateremulsie. Als oppervlakteactieve stoffen gebruiken we anionisch natriumdodecylsulfaat (SDS), kationisch hexadecyltrimethylammoniumbromide (CTAB), niet-ionisch Triton ™ X-100 (TX) en zwitterionisch N-dodecyl-N,N-dimethyl-3-ammonio-1-propaansulfonaat (DDAPS), bij verschillende ionsterkten (1, 10, 100 mM NaCl). Filtratie-experimenten op een ultrafiltratiemembraan van geregenereerde cellulose (UF) toonden een uitgesproken effect van de ionsterkte voor de geladen oppervlakteactieve stoffen SDS en CTAB, hoewel de aard van het effect nogal verschillend was. Voor anionische SDS leidt een toenemende ionsterkte tot minder druppel-druppel afstoting, waardoor een dichtere cakelaag kan worden gevormd, wat resulteert in een veel meer uitgesproken afname van de flux. CTAB leidt daarentegen tot een lagere grensvlakspanning dan waargenomen voor SDS, en dus tot meer vervormbare oliedruppeltjes. Bij een hoge ionsterkte leidt een verhoogde adsorptie van oppervlakteactieve stoffen tot een zo lage olie-wateroppervlaktespanning dat de oliedruppeltjes door de veel kleinere mem-

braanporiën kunnen dringen. Voor de niet-ionische oppervlakteactieve stof TX werd geen duidelijk effect van de ionsterkte waargenomen, maar de fluxdaling is zeer hoog in vergelijking met de andere oppervlakteactieve stoffen. Voor de zwitterionische oppervlakteactieve stof DDAPS bleek de fluxdaling erg laag te zijn en zelfs af te nemen met toenemende ionsterkte, wat suggereert dat membraanvervuiling afneemt met toenemende ionsterkte. Vooral veelbelovend is dat bij lagere concentratie oppervlakteactieve stof (0,1 CMC) en hoge ionsterkte geen fluxdaling werd waargenomen, terwijl een hoge olieretentie (85%) werd verkregen. In **Hoofdstuk 3** werden membraanvervuiling en olieretentie van synthetisch GW gestabiliseerd met dezelfde kationische, anionische, zwitterionische en niet-ionische surfactant van Hoofdstuk 2 bestudeerd bij verschillende surfactant- en zoutconcentraties voor een microfiltratie (MF) siliciumcarbide (SiC)) membraan. Hier bespreken we onze resultaten in het kader van de Young-Laplace (YL) -vergelijking, die voor een bepaald membraan, druk en olie-membraancontacthoek een kritische grensvlakspanning (IFT) voorspelt waaronder oliepermeatie zou moeten optreden. We zien een dergelijke overgang van hoge naar lage olieretentie met afnemende IFT voor de anionische (SDS), kationische (CTAB) en niet-ionische (TX) oppervlakteactieve stof, maar bij significant hogere kritische IFT's dan voorspeld door YL. Aan de andere kant zien we voor de zwitterionische DDAPS geen daling van de olieretentie, zelfs niet bij de laagste IFT. De discrepantie tussen onze bevindingen en de kritische IFT die door YL voorspeld wordt kan worden verklaard door het verschil tussen de gemeten contacthoek en de effectieve contacthoek aan de wand van de membraanporiën. Dit leidt tot een oppervlakteactieve stof-afhankelijke kritische IFT. Bovendien wijzen onze resultaten erop dat zwitterionische oppervlakteactieve stoffen zelfs bij de laagste IFT geen kritische IFT vertoonden en een lage vervuiling en lage oliepermeatie vertoonden. In **Hoofdstuk 4** presenteren we een kwantitatief model dat cakelaagvorming en poriënblokkering beschrijft voor de typische situatie waarin emulsieoliedruppeltjes veel groter zijn dan de poriëngrootte van het membraan. Hier wordt de mate van porieblokkering bepaald door de membraancontacthoek en de resulterende oppervlaktedekking, terwijl de cakelaag wordt beschreven via een massabalans en de aanwezigheid van een cakeerosieflux. Het model is gevalideerd door vergelijking met experimentele gegevens uit Hoofdstukken 2 en 3, waar membraantype, oppervlakteactieve stof en zoutgehalte werden gevarieerd. De meeste invoerparameters konden direct uit de experimentele omstandigheden worden gehaald, terwijl slechts 4 fitparameters nodig waren. De experimentele gegevens kunnen goed worden beschreven door het model,

met behulp van een zeer beperkt aantal fitparameters, wat inzicht geeft in het dominante vervuilingsmechanisme. Bovendien, waar bestaande modellen gewoonlijk aannemen dat porieblokkering voorafgaat aan de vorming van een cakelaag, vinden we hier dat de vorming van een cakelaag kan beginnen en optreden terwijl de mate van porieblokkering nog steeds toeneemt, in overeenstemming met de meer dynamische aard van oliedruppeltjes.

Aan de andere kant maken polyelektrolyt multilagen (PEM's) een zeer mooie benadering mogelijk om de membraaneigenschappen van **Dichte Membranen** te controleren, inclusief de membraanoppervlakchemie. Helaas kan de aanwezigheid van oppervlakteactieve stoffen in GW de stabiliteit van polyelektrolyt-multilagen beïnvloeden. In **Hoofdstuk 5** onderzoeken we de stabiliteit van polyelektrolyt multilagen ten opzichte van verschillende soorten oppervlakteactieve stoffen, in eerste instantie op modeloppervlakken. We vinden dat chemisch stabiele meerlagen, zoals poly(diallyldimethylammoniumchloride)(PDADMAC)/poly(natrium-4-styreensulfonaat)(PSS), alleen gebaseerd op elektrostatische interacties, in hoofdzaak worden gedesorbeerd door geladen oppervlakteactieve stoffen. Voor poly(allylamine hydrochloride)(PAH)/PSS multilayers tonen we echter aan dat chemische verknoping door glutaaraldehyde leidt tot stabiele lagen voor oppervlakteactieve stoffen. Deze stabiele PEM-coatings kunnen ook worden aangebracht op holle-vezel-ondersteuningsmembranen om holle-vezel-nanofiltratie (NF)-membranen te creëren die speciaal zijn bedoeld voor GW-behandeling. Verhoogde verknopingstijd leidt tot stabielere en selectievere scheidingsprestaties. Deze nieuw ontwikkelde membranen zijn vervolgens onderzocht voor de behandeling van synthetisch GW, bestaande uit vers bereide olie-in-water emulsies gestabiliseerd door kationisch CTAB en anionisch SDS, in aanwezigheid van een mengsel van ionen. Voor beide soorten geproduceerd water vertoonden de membranen een uitstekende verwijdering van olie ($\sim$ 100%) en verwijdering van organische stoffen (TOC verlaagd tot $\sim$ 97%) evenals goede retentie van tweewaardige ionen ($\sim$ 75% voor Ca^{2+} en tot $\sim$ 80% voor SO_4^{2-}). Bovendien zagen we een hoge flux recovery voor beide emulsies (100% voor CTAB en 80% voor SDS), met vooral voor de CTAB-emulsie een zeer lage vervuilingsgraad. In **Hoofdstuk 6** onderzoeken we het effect van membraanoppervlaktechemie op vervuiling in oppervlaktewaterbehandeling voor op polyelektrolyt gebaseerde meerlaagse NF-membranen. De polyelektrolyt meerlaagse benadering stelt ons in staat om drie membranen te maken met dezelfde actieve scheidingslaag, afgezien van een verschil in oppervlaktechemie: bijna ongeladen verknoopte PAK, sterk negatieve PSS en zwitterion-

isch poly(2-methacryloyloxyethylfosforycholine-co-acrylzuur) (PMPC- mede-AA). In eerste instantie hebben we de adsorptie van vuile stoffen voor de drie verschillende oppervlakken (op modelinterfaces) bestudeerd om aan te tonen hoe een verschillende oppervlaktechemie van de toplaag de daaropvolgende adsorptie van vijf verschillende modelverontreinigingen (humuszuren, alginaten, silica-nanodeeltjes, negatief en positief geladen) beïnvloedt. eiwitten). Vervolgens bestuderen we vervuiling van dezelfde modelvervuilingen op onze op polyelektrolyt meerlaagse holle vezel NF-membranen met identieke oppervlaktechemie als de modeloppervlakken. Onze resultaten laten zien dat het bijna ongeladen verknoopte PAK-oppervlak over het algemeen meer vervuilt dan het sterk negatief geladen PSS-oppervlak. Over het algemeen werd vervuiling voornamelijk veroorzaakt door elektrostatische en zuur-base-interacties, wat leidde, voor zowel PAK- als PSS-getermineerde membranen, tot fluxafname en veranderingen in selectiviteit. Daarentegen demonstreren we door middel van filtratie-experimenten uitgevoerd met synthetisch en echt oppervlaktewater, dat de bio-geïnspireerde zwitterionische fosfatidylcholine-oppervlaktechemie een uitstekende vervuilingsweerstand vertoont en dus stabiele prestaties tijdens filtratie. Vervolgens onderzoeken we in **Hoofdstuk 7** het effect van oppervlaktechemie op vervuiling van op PEM gebaseerde NF-membranen, tijdens de behandeling van kunstmatig geproduceerd water. Hiertoe werden olie-in-water (O/W) emulsies gestabiliseerd met vier verschillende oppervlakteactieve stoffen (anionische, kationische, zwitterionische en niet-ionische) behandeld met PEM-gebaseerde NF-membranen met dezelfde meerlaagse, maar verschillende toplaag polymeerchemie : PAK (bijna ongeladen), PSS (sterk negatief), poly(sulfobetaïnemethacrylaat-co-acrylzuur) (PSBMA-co-AA, zwitterionisch) en Nafion (negatief en hydrofoob). Zeer hoge olieretentie (>99%) werd waargenomen bij het filteren van alle O/W-emulsies, terwijl de fysisch-chemische interacties tussen de meerlaagse en de oppervlakteactieve stoffen de mate van vervuiling en de oppervlakteactieve stofretentie bepaalden. Onverwacht laten onze resultaten zien dat vervuiling van op PEM gebaseerde NF-membranen, tijdens GW-behandeling, voornamelijk te wijten is aan vervuiling van de actieve laag van het membraan veroorzaakt door de opname van oppervlakteactieve stoffen in de PEM-coating, in plaats van door de vorming van een cakelaag. Het is inderdaad niet de oppervlaktechemie van het membraan die de mate van vervuiling bepaalt, maar de interactie van de oppervlakteactieve stof met het grootste deel van het PEM.

Interfacial Phenomena spelen een cruciale rol op veel verschillende gebieden, van membraanfiltratie tot het ontwerp van energieoogsters. In NF

bepalen de oplossing en membraanchemie de lading van het membraan, en daarmee de elektrostatische afstoting van ionen. Omkering van de membraanlading kan plaatsvinden wanneer tweewaardige ionen aan het membraan binden en de oppervlaktelading ervan wijzigen, wat enkele raadselachtige resultaten kan verklaren, waarbij de afstoting van tweewaardige ionen toeneemt met een hogere concentratie in de voeding. In **Hoofdstuk 8** beschouwen we, door gebruik te maken van een Langmuir-vergelijking met twee modelparameters, de adsorptie van tweewaardige ionen (bijv. Ca^{2+} en Mg^{2+}) in het polyamide (PA) actieve laag van het membraan en beschrijven hoe dit adsorptieproces de membraanlading beïnvloedt. Op basis van experimentele gegevens van twee verschillende onderzoeken laten we zien dat de gemiddeldeveldtheorie de afstoting van alle soorten ionen in een meercomponenten elektrolytoplossing kan voorspellen wanneer het effect van tweewaardige tegenionen op de membraanlading wordt meegerekend. Deze resultaten leveren bewijs dat adsorptie van tegenionen een fundamentele rol speelt bij de uitvoering van nanofiltratie. In **Hoofdstuk 9** presenteren we een nieuwe theorie om de contacthoek van water op amfotere oppervlakken te voorspellen als functie van pH en ionsterkte. Om onze theorie te valideren, werden experimenten uitgevoerd op twee veelgebruikte amfotere materialen, aluminiumoxide (Al_2O_3) en titania (TiO_2). We vinden een goede overeenkomst bij alle pH-waarden en bij verschillende zoutconcentraties. Met toenemende zoutconcentratie voorspelt de theorie dat de contacthoek-pH-curve steiler wordt, terwijl dezelfde contacthoek bij pH = PZC (punt van nullading) wordt behouden, in overeenstemming met de gegevens. Ons model is gebaseerd op het amfotere 1-pK-model en omvat zowel de elektrostatische vrije energie van een waterig systeem als de oppervlakte-energie van een druppel in contact met het oppervlak. Daarnaast laten we zien hoe onze theorie de mogelijkheid suggereert van een nieuw responsief membraanontwerp, gebaseerd op amfotere groepen. Bij pH $\sim$ PZC is dit membraan bestand tegen stroming van water, maar bij iets meer zure of basische omstandigheden kan de bevochtiging van de membraanporiën voldoende veranderen om water en opgeloste stoffen door te laten. Bovendien zouden deze membranen kunnen fungeren als actieve sensoren die alleen oplossingen met een hoge ionsterkte doorlaten in de afvalwaterzuivering. In **Hoofdstuk 10** werken we aan een nieuw mechanisme om energie te winnen uit mechanische fluctuaties door gebruik te maken van opgerolde koolstof nanobuisgarens gecoat met polyelektrolytgel. We ontwikkelen een nieuwe theorie en presenteren een theoretisch kader om uit te leggen hoe deze nieuwe vorm van energiewinning mogelijk is. De gel vult alle ruimte tussen de spoe-

len en zet uit wanneer het garen wordt uitgerekt. Dit vertaalt zich in een verandering in elektrische dubbellaagsconfiguratie, dus in een verandering in elektrisch potentiaal. Dit maakt het mogelijk om mechanische trek- of torsie-energie elektrochemisch om te zetten in elektrische energie. De invloed van de oppervlaktelading van het garen, de dichtheid van de polyelektrolytlading en de zoutconcentratie werd geanalyseerd, wat aanwijzingen gaf voor een optimaal procesontwerp. We analyseerden het gegenereerde vermogen van een systeem dat bestaat uit twee garens gecoat met positieve en negatieve polyelektrolytgel.

Om te besluiten, in **Hoofdstuk 11**, worden met de opgedane kennis uit de verschillende hoofdstukken de belangrijkste resultaten van dit proefschrift opnieuw bekeken en worden de toekomstige uitdagingen van op PEM gebaseerde membranen voor PW-behandeling en andere toepassingen besproken.

Acknowledgments

This thesis is the fruit of a deep professional and personal growth, which envelopes not only the experiments and the scientific research discussed in the various chapters of this work but most of all life lessons, personal development steps, meaningful relationships created along the way, and life-changing experiences. All unique pieces of a puzzle which depicts these past four years.

Every person that I met during my four-year path taught me something and inspired me with her/his attitude and unique skills. Here, I would like to thank these unique people, all part of this beautiful puzzle.

Profound thanks to my supervisor and promotor **Wiebe de Vos** who made this PhD-journey and this wonderful research path possible. Wiebe, your positive, supportive, and strategic character inspired me during these four years. Your brilliant research eye and mind taught me to be a patient, precise and organized scientist. Thank you for always being available to email, call or videocall, for believing in my inner potential and support my choices when needed.

To my co-promotor and Wetsus supervisor **(P.) Maarten Biesheuvel**. You motivated me to grow as a scientist by setting clear and large goals for my research path. Your support pushed me to write and publish various manuscripts, already starting from the first months of my Ph.D. at Wetsus, and to take the lead as Theme Coordinator of Concentrates. You taught me to be bold, and to stand up for my value. Thank you for teaching me how to write good-quality theory papers and make outstanding graphics. You and Wiebe are the main actors in my career and scientific growth. Thanks again.

My path and growth as Theme Coordinator at Wetsus would not be possible without the support, trust, and guidance of **Jan Post**, **Bert Hamelers**,

Ingrid Weurman, and **Cees Buisman**. Jan, you are a clear example of how a calm, patient, and clear mind is needed to lead a Team. Thank you for supporting my meetings with the industrial partners of our Theme, as well for the strategic support received in planning the next steps. Bert, your vision and talent-oriented attitude helped and still help me in better recognizing my strong potential and put that into practice. Ingrid, thank you for your personal development training, leadership lessons, and the inspiring talks on society, history, and politics. Thanks for designing and taking care, together with Bert, of the PhD personal development program. Cees, your leadership, determination, long-term vision, and goals are inspiring to me and the whole Wetsus building. Thank you all, and **Johannes Boonstra** as well, for making Wetsus such an inspiring place where to work.

To the members of my committee, **Prof. dr. R.W. Field**, **Prof. dr. ing. A. Van der Wal**, **Dr. ir. D. Fernandez Rivas**, **Dr. S. J. A. de Beer**, and **Prof. dr. ir. H.D.W. Roesink**, thank you very much for reading my thesis and allowing me to defend it. I would also like to thank **the members of the Concentrates Theme** for the discussions, feedback, and cooperation of the past four years.

To all the Wetsus colleagues of the second floor, with special thanks to **Michele**, **Cristina**, **Valentina**, **Doekle**, **Inez**, **Roel**, **Michel**, **Prashanth**, **Henk**, **Lucía**, **Slawomir**, **Pawel**, **Philipp**, **Caroline**, **Tom**, **Leon**, **Martijn**, and **Elmar**. Thank you for your support, enthusiasm and for everyday contributing to the success of Wetsus. Thanks also to **the colleagues of the Membrane Group of The University of Twente** for their kindness, help, and support, in particular to **Dennis**, **Elif**, **Wouter**, **Audrey**, **Heleen**, **Rob**, **Joris**, **Bob**, **Iske**, **Muhammad**, **Özlem** and **Antoine**.

I extend my sincere gratitude to all the students/Wetsus interns who contributed to the accomplishment of this work. **Fabiola**, **Bernard**, **Klara**, **Alejandro**, **Indah** and **Laura**, thank you for the hard work, dedication, and commitment. This thesis is also yours.

For all the practical work of this thesis, I would like to thank the excellent support of the Wetsus technical team, including **Jan Jurjen**, **Wim**, **Jan Willem S.**, **Mieke**, **Lisette**, **Marianne**, **Jelmer**, **Gerrit**, and **Rienk**. Thanks also to **Gerben**, **Riet** and **Katharina** for making of the canteen

such a "gezellig" place. To the administrative, HR and secretarial staff, thank you all for your cooperation, smile, and kindness. In particular, thanks to **Jannie**, **Tineke**, **Marnejaeike**, and **Hester**.

My first and last office as PhD, 1.18E, has seen many people passing by. Many thanks to **Jan Willem**, **Victor T.**, **Gaofeng**, **Janneke D.**, **Sebastian**, and **Elias** for kindly welcoming me in 2017. Special thanks to who came to the office after me and made it unforgettable: **Deepika** (Deeeepikaaaaa), **Carlo** (Carloni, best office mate ever), **XiaoXia** (Queen of patience and hotpot), **Yujia** , **Terica**, **Angel**, **Ruben**, **Olga**, **Vania**, and **Antony**. To the new one, **Nouran**, have a great stay and enjoy your journey at Wetsus!

A big thanks goes also to all the Wetsus people (former PhDs and students included) who made coffee breaks, borrels and hangouts fun and memorable. In particular, thanks to **Hakan**, **Rose**, **Sandra**, **Raquel**, **Beatriz O.**, **Mariana**, **Thomas**, **Chris**, **Rebeca**, **Karine**, **Victor A.**, **Ruizhe**, **Daniele**, **Giulia I.**, **Alessandra**, **Nike**, **Nick**, **Pauline**, **Iñigo**, **Louis**, **Tania**, **Vanessa**, **Andrew**, **Natasha**, **Hector**, **Jaap**, **Paulina**, **Maarten**, **Steffen**, **Sara**, **Caspar**, **Nimmy**, and **Agnieszka**.

Thanks to all the member of the Wetsus Band for the nice evenings playing together: **Stan**, **Steffen**, **Michele**, **Carlo**, **Gonçalo**, **Brazhil**, **Steffen**, **Wokke**, and **Maarten**.

The best memories of my PhD at Wetsus are mainly related to my move into The Castle, house of memorable evenings and parties. There it was possible to create a second family made of trusted lifetime friends. Thanks to **Laura Carcelli** (Court Jester, "blindly" happy on New Year's Eve 2019), **Veronica** (Chef Carbonara, best dinners and funniest entertainment), **Larissa** (Guardian of the goats, amazing crazy party and adventure companion), **Julie** (Princess, concentrate of love and kindness), **Elena** (Warrior, always ready to use her Kung Fu skills), and **Carlo** and **Emad** (together with I, Kings of the Castle). Our moments together are unforgettable. Thanks for being such great friends and for making the effort, space, and time to meet in our crazy and happy reunions all over Europe.

To the greatest paranymphs and friends.

Cristina, guardando indietro a quattro anni fa, chi l'avrebbe mai detto che saresti stata al mio fianco durante questa tanto attesa defense? Grazie per

essermi stata di sostegno ed aiuto fin dai miei primi giorni a Leeuwarden. Ricordo quando ancora non ci conoscevamo e durante il mio primo compleanno a Leeuwarden (al quinto giorno del mio arrivo in Olanda) hai deciso di passare l'intera giornata con un compaesano nostalgico della sua amata Sicilia. Grazie per esserci stata durante tappe importantissime di questi quattro anni, ed anche in momenti meno belli, come in piena pandemia a godere delle splendide giornate di sole al parco, momenti di incertezza che assieme abbiamo trasformato in momenti preziosi ed unici. Grazie per farmi da guida e motivarmi anche in scienza e per fornirmi sempre punti di vista diversi e critici, i quali mi aiutano a vedere certe situazioni in maniera piú oggetiva. Grazie per tutti i pranzi, le cene e gli snacks condivisi con amore, allegria e spensieratezza. Ti voglio bene amica mia.

Carloni, sará difficile condensare in un solo paragrafo tutte le esperienze passate assieme e tutti i bei momenti che mi hai regalato in questi 3 anni e mezzo. Posso dirti chiaramente che dal tuo arrivo in cittá, circa sei mesi dopo il mio di arrivo, la mia vita sociale a Wetsus é cambiata radicalmente. Non dimenticheró mai tutte le feste passate assieme, la ricerca dell casa poi conclusa nel mitico The Castle, le chiacchierate serali, il mitico viaggio in Cina...mamma mia che storie! Grazie per essermi stato vicino in tantissimi dei momenti passati in questi anni, anche nei momenti piú speciali. Grazie ancora per officiare alla grande il mio matrimonio e per essere un amico simpatico, sincero, buono ed unico. Grazie ancora per prendere parte al mio fianco a quest'altro atteso momento.

Muchas gracias a mis otras familias, **Familia Sánchez-Puerta** y **Familia Florindo**. Gracias por recibirme como nieto, sobrino, primo, y hermano. Especialmente gracias a **Ana** y mis hermanas **Laura** y **María**. Os quiero muchísimo.

Ed adesso, un grazie enorme va alla mia famiglia. **Mamma (Antonella)** e **Papá (Rodolfo)**, é grazie a voi che sono qui al mondo ed é grazie a voi che ho potuto realizzare questo cammino. Grazie per avermi potuto sostenere durante la mia crescita ed i miei studi. Grazie per avermi impartito importanti lezioni di vita, e grazie per la grandissima tenacia, dedizione e spirito che mi avete sempre fornito. Senza il vostro sostegno non avrei mai lasciato l'Italia per andar a vivire in Olanda. Grazie per il supporto e per esserci sempre nel momento del bisogno. Un ringraziamento speciale a tutti gli altri membri della mia famiglia che hanno contribuito alla mia crescita,

dandomi amore ed affetto anche negli anni meno felici. Grazie a **Nonna Concetta**, **Zio Nino**, **Zia Annalisa**, **Zia Ornella**, **Zio Sandro**, ed i **cugini Benedetto (grande e piccolo)**, **Cristiana** e **Flaminia**.

Y gracias a Wetsus he conocido a mi compañera de vida. **Elena**, miles de gracias van a ti. En estos años he aprendido mucho, gran parte de mi desarrollo personal viene inspirado por tu camino y nuestra relación. Estos años han significado mucho para nosotrxs: nos hemos conocido, empezado una relación a distancía, vivido juntxs y casado. Gracias por todo el apoyo, la alegría y la espontaneidad que me regalas todos los días. Gracias por ser parte de esta aventura maravillosa que es la vida.

To the new generation that is rising, to the one that is more conscious of how they live, what they buy, and where they work. To all the people busy in making this world a better place by fighting face to face against global threats, such as climate change, inequality, patriarchy and racism. Thanks. I do believe in all of you.

Ettore Virga
September 2021

About the author

Ettore Virga was born on September 9, 1993 in Palermo, main town of Sicily, Italy. After finishing high school in 2012, he enrolled at the University of Palermo to study Chemical Engineering. Ettore finished his Bachelor *cum laude* with a thesis on Reverse Electrodialysis (RED) modelling in closed-loop operation. In 2015, Ettore started his Master in Chemical Process Engineering. His Master project was conducted at FUJIFILM Manufacturing Europe B.V., located in Tilburg, The Netherlands. Ettore obtained his Master in Chemical Process Engineering *cum laude* with a thesis on experimental investigation of closed-loop RED.

In 2017 Ettore started his PhD in the Membrane Science and Technology (MST) group at the University of Twente, in close collaboration with Wetsus, European Centre of Excellence for Sustainable Water Technology, in Leeuwarden, where he carried out most of his research. The research focused on addressing the challenge of produced water (PW) treatment with membrane filtration with a focus on fouling understanding and prevention via membrane surface modification. In 2020, Ettore was awarded with the Marcel Mulder Prize for his research on a novel zwitterionic polymer that can be applied on membranes to make them less prone to fouling. In the same year, Ettore started coordinating the Concentrates Theme of Wetsus while finishing his PhD research.

About the cover

Pictured on the front cover are oil droplets stabilized by surfactant molecules and interacting with a polymeric multilayer. Such a picture emphasizes the complex interaction between three elements that are the main characters of this thesis, i.e. oil emulsion, membrane chemistry, and surfactants.

This thesis is printed by IPSKAMP printing company, Enschede, The Netherlands (www.ipskampprinting.nl).

Scientific output

Publications

- *prepared for submission:* Theory of Oil Fouling for Microfiltration and Ultrafiltration Membranes in Produced Water Treatment
  E. Virga, R. W. Field, P. M. Biesheuvel, W. M. de Vos

- *submitted:* Nanofiltration of Complex Mixtures: The Effect of the Adsorption of Divalent Ions on Membrane Retention
  S. C. Osorio, J. E. Dykstra, P. M. Biesheuvel, and **E. Virga**
  Desalination

- *2021:* Polyelectrolytes as Building Blocks for Next-Generation Membranes with Advanced Functionalities
  E. N. Durmaz* & S. Sahin* & **E. Virga***, S. J. A. de Beer, L. C. P. M. de Smet, W. M. de Vos
  ACS Applied Polymer Materials

- *2021:* Fouling of Polyelectrolyte Multilayer based Nanofiltration Membranes during Produced Water Treatment: The Role of Surfactant Size and Chemistry
  E. Virga, M.A. Parra, W.M. de Vos
  Journal of Colloid and Interface Science, 594, 9-19

- *2021:* Fouling of Nanofiltration Membranes based on Polyelectrolyte Multilayers: The Effect of a Zwitterionic Final Layer
  E. Virga, K. Zvab, W. M. de Vos
  Journal of Membrane Science, 620, 118793

- *2020:* Surfactant-dependent Critical Interfacial Tension in Silicon Carbide Membranes for Produced Water Treatment
  E. Virga, B. Bos, P. M. Biesheuvel, A. Nijmeijer, W. M. de Vos
  Journal of Colloid and Interface Science, 571, 222-231

- *2019:* Stable Polyelectrolyte Multilayer-Based Hollow Fiber Nanofiltration Membranes for Produced Water Treatment
  E. Virga, J. de Grooth, K. Zvab, W. M. de Vos
  ACS Applied Polymer Materials, 1, 2230-2239

- *2019:* Surfactant Specific Ionic Strength Effects on Membrane Fouling during Produced Water Treatment
  J. M.Dickhout* & **E. Virga***, R. G. H. Lammertink, W. M. de Vos
  Journal of Colloid and Interface Science, 556, 12-23

- *2018:* Wettability of Amphoteric Surfaces: the Effect of pH and Ionic Strength on Surface Ionization and Wetting
  E. Virga, E. Spruijt, W. M. de Vos, P. M. Biesheuvel
  Langmuir, 34, 15174-15180

- *2017:* Theory of Gel Expansion to Generate Electrical Energy
  E. Virga, W. M. de Vos, P. M. Biesheuvel
  EPL, 120, 46002

  *These authors contributed equally.

Selected oral presentations in conferences

- *2020:* Stable polyelectrolyte multilayer based hollow fiber nanofiltration membranes for produced water treatment
  International Congress on Membranes & Membrane Processes (ICOM), online

- *2020:* Polyelectrolyte multilayer nanoltration membranes for simultaneous oil and salt removal in produced water treatment
  Environmental Technology for Impact (ETEI), online

- *2020:* Stable polyelectrolyte multilayer based hollow fiber nanofiltration membranes for produced water treatment
  International Membrane Science Technology Conference (IMSTEC), Sydney, Australia

- *2018:* Theory of gel expansion to generate electrical energy
  International Association of Colloid and Interface Scientists (IACIS), Rotterdam, The Netherlands

The effective treatment of complex industrial wastestreams such as PW is important to ensure clean water. Membranes can play a key role in this process, but membrane fouling remains a major problem. We propose that **surface chemistry** plays a key role here, and that control over the surface chemistry of the emulsion and the membrane can substantially alleviate fouling.

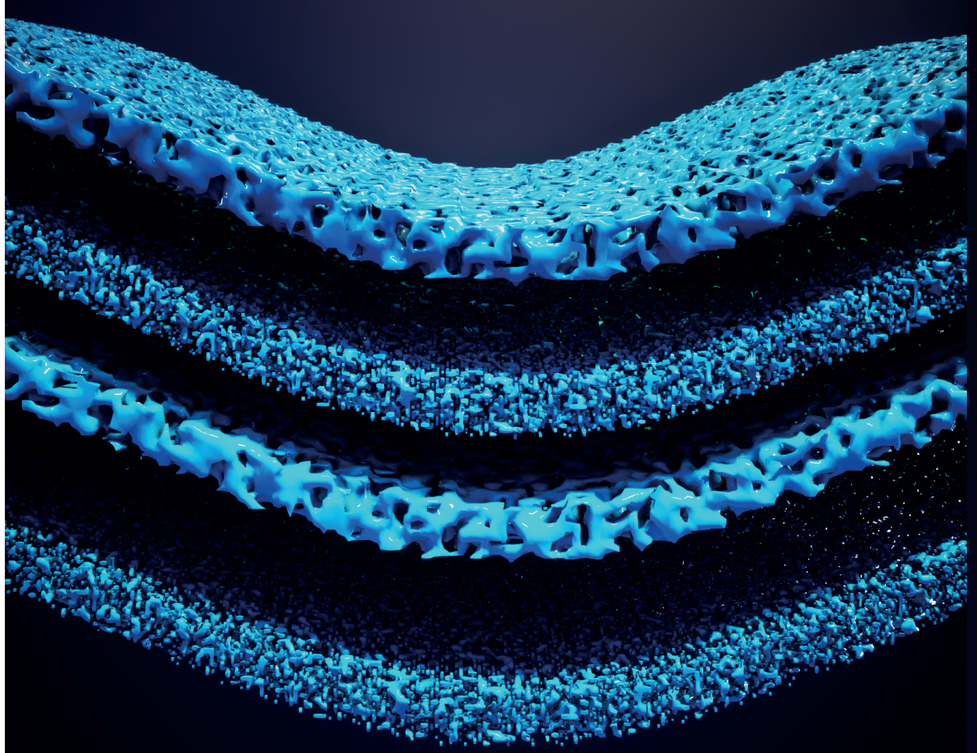

ISBN 978-90-365-5217-2

The Relevance of Surface Chemistry in Complex Filtrations Ettore Virga

The Relevance of Surface Chemistry in Complex Filtrations

Ettore Virga

INVITATION

It is my great pleasure to invite you to attend the public defence of my PhD thesis entitled

The Relevance of Surface Chemistry in Complex Filtrations

Which will be held on Friday 17 September 2021 at 15:00 in 'De Harmonie' (Ruiterskwartier 4, 8911 BP Leeuwarden)

Ettore Virga

Paranymphs

Carlo Belloni
Carlo.belloni@outlook.com

Cristina Gagliano
gaglianomariacristina@gmail.com

NSL

564814-L-os-Virga